

High Valent Osmium Complexes Incorporating a Tetradentate
Tetraanionic Chelating Ligand; Stabilization Modification Resulting from
the Formation of Non-planar Amides

Thesis by
John Tyler Keech

In Partial Fulfillment of the Requirements
for the Degree of
Doctor of Philosophy

California Institute of Technology
Pasadena, California

1987

(Submitted August 8, 1986)

© 1986

John Tyler Keech

All Rights Reserved

Acknowledgments

I would like to thank my advisor, Terry Collins, for his support and encouragement throughout this project. His creativity and enthusiasm attracted me to his group and inspired me continually since then.

I would like to thank Dr. Stephen L. Gipson, formerly of the Anson group, for the collaboration on the isomerization project. Steve performed most of the electrochemistry contained herein. His research was essential in unravelling the isomerization phenomenon and understanding it in detail. Discussions with Steve were both stimulating and insightful. I would also like to thank Geoffrey T. Peake, whose work on a related isomerization system provided useful comparisons.

I would like to thank Tracy T. Furutani for collecting the data for the cis- α isocyanide complex and Dr. Bernard D. Santarsiero for helping me solve the structure. I want to thank Dr. Robert J. Coots, who performed the structure determination of the bipy complex. James D. Meinhart provided useful assistance with my NMR spectroscopy. Dr. B. Jean Westphal assisted with the Cambridge database "N-amido" computer search. I want to thank Debbie Chester, who typed this thesis, and Valerie Purvis, who did the art work.

I want to thank Terry Collins for his financial support, as well as SOHIO, W. R. Grace, and Shell Oil for fellowships. The ability to devote full time to my research expedited bringing this project to fruition. I want to thank the Dreyfus Foundation for the award of a Dreyfus Travelling Fellowship, whereby I had the opportunity to visit and become familiar with industrial laboratories.

I want to thank the Collins group, present and past, for generating an environment conducive to research, but sufficiently distractive to provide necessary diversions. My association with everyone has been an important aspect of my Caltech experience.

Finally, I want to thank my family who has consistently encouraged my pursuit of graduate school and especially Katherine, my wife, who has provided constant support, encouragement, and enthusiasm.

Abstract

A new tetradentate tetraanionic chelating ligand has been synthesized: 1,2-bis(3,5-dichloro-2-hydroxybenzamido)-4,5-dichlorobenzene, $H_4CHBA-DCB$. This ligand is one of a class of polyanionic chelating (PAC) ligands synthesized by the Collins group for stabilizing high valent metal centers. $H_4CHBA-DCB$ has an aromatic framework that is chlorinated for added chemical resistance. Reacting equimolar amounts of $H_4CHBA-DCB$ and $K_2[Os(OH)_4(O)_2]$ coordinates the ligand as *trans*- $K_2[Os(\eta^4-CHBA-DCB)(O)_2]$, **3**. Compound **3** undergoes reversible protonation at an oxo ligand to produce *trans*- $K[Os(\eta^4-CHBA-DCB)(O)(OH)]$, **4**. Compound **4** reacts with solid $MgSO_4$ and forms the square-pyramidal mono-oxo complex $Os(\eta^4-CHBA-DCB)(O)$, **5**. Most oxidizing agents, with the exception of bromine, decompose **3** into a black amorphous material. Bromination of **3** produces a compound similar to **4** and is proposed to be *trans*- $K[Os(\eta^4-CHBA-DCB)(O)(OBr)]$, **6**. Triphenylphosphine readily reduces Os(VI) **3** to a neutral Os(IV) complex, *trans*- $Os(\eta^4-CHBA-DCB)(PPh_3)_2$, **7**. The ancillary phosphine ligands of **7** prove to be substitutionally labile and can be exchanged for other Lewis bases (e.g., py, *t*-Bupy, bipy, dppe, and *t*-BuNC) to produce a series of Os(IV) complexes. Using cyclic voltammetry, the formal potentials of the Os(V/IV), Os(IV/III), and Os(III/II) couples are determined in CH_2Cl_2 . In liquid SO_2 , the formal potentials of the Os(V/IV), Os(2+/+), and Os(3+/2+) couples are measured for three compounds, the highest potential being at +1.70 V vs. Fc^+/Fc or ca. +2.4 V vs. NHE. A fourth irreversible couple is observed at +2.12 to +2.20 V vs. Fc^+/Fc . These osmium complexes display temperature-independent paramagnetism.

Os(IV) complexes with bidentate ligands (e.g., bipy and dppe) and Lewis acid ligands (*t*-BuNC) form *cis* complexes where the (η^4 -CHBA-DCB)⁴⁻ ligand is non-planar, and the auxiliary ligands are *cis* to one another. Two such complexes have been crystallographically characterized: *cis*- β -Os(η^4 -CHBA-DCB)(bipy), 11, and *cis*- α -Os(η^4 -CHBA-DCB)(PPh₃)(*t*-BuNC), 14. Compound 11 crystallizes with 0.5 equiv EtOH solvate in the triclinic space group $P\bar{1}$ with $a = 10.860(3)$ Å, $b = 12.633(3)$ Å, $c = 12.844(4)$ Å, $\alpha = 117.42(2)^\circ$, $\beta = 90.42(3)^\circ$, $\gamma = 95.90(3)^\circ$, $V = 1552.2(7)$ Å³, $Z = 2$, $D_{\text{calc}} = 1.97$ g/cm³, and $R_f = 0.047$ ($I > 0$; 2888 reflections). Compound 14 crystallizes in the orthorhombic space group $Pbca$ with $a = 22.09(2)$ Å, $b = 19.92(2)$ Å, $c = 19.40(2)$ Å, $V = 8537(4)$ Å³, $Z = 8$, $D_{\text{calc}} = 1.69$ g/cm³, and $R_f = 0.063$ ($I > 0$; 1564 reflections). These structures contain novel non-planar amide groups. The amount of deformation in each amide is quantified by a torsion angle analysis. Two bonding changes cause the amide non-planarity: amide C-N bond rotation and pyramidalization of the amide nitrogen atom. Consistent with the presence of non-planar amides, unusually high amide carbonyl stretching frequencies are observed (1650-1695 cm⁻¹), which imply that amide delocalization stabilization has been restricted.

The *cis*- α and *trans* isomers of [Os(η^4 -CHBA-DCB)(*t*-Bupy)₂]⁺ are in equilibrium with one another. From the measured equilibrium constant of 1.3 (in favor of the *trans*) and the formal reduction potentials for each isomer, the equilibrium constants for the interconversion of the neutral (3.4×10^3), anionic (2.4×10^{11}), and dianionic (2.0×10^{15}) species are derived. The trend in equilibrium constants shows that the *cis*- α ligand set is increasingly favored as the metal is oxidized. A linear free energy relationship (LFER) is established between the *cis*- α \rightleftharpoons *trans* equilibrium

constants of $\text{Os}(\eta^4\text{-CHBA-DCB})(p\text{-X-py})_2$ [$X = \text{MeO}, t\text{-Bu}, \text{Et}, \text{Me}, \text{H}, \text{Br}, \text{Cl}, \text{Ac}$] and both Fischer $\bar{\sigma}$ ($\rho = -2.10, r = 0.948$) and Hammett σ_p ($\rho = -1.60, r = 0.949$) substituent parameters. The formal potentials of the $\text{Os}(\text{V/IV})$, (IV/III) , and $\text{Os}(\text{III/II})$ couples of both the *cis- α* and *trans* isomers also correlate with $\bar{\sigma}$ constants, showing that the electron density at the metal center is perturbed in a predictable manner by the pyridine substituents. These LFERs show that the isomerization equilibria are controlled by electronic demand for stabilization at the metal center with the *cis- α* ligand set being more electron-donating than the *trans* set. This difference apparently results from the increased localization of the amide nitrogen lone pair due to restricted amide delocalization in the non-planar amide groups of the *cis- α* isomers. The localized lone pair probably enhances σ - and π -bonding between the amide nitrogen atoms and the osmium center. The balance between the stabilization derived from the *cis- α* isomer and the destabilization incurred from restricted amide delocalization may determine which isomer is thermodynamically most stable.

The mechanism for the interconversion of *cis- α* and *trans* isomers is probed through kinetic rate measurements and ligand exchange studies. Most of the results suggest that an intramolecular "twist" mechanism, T, requiring no ligand dissociation steps, controls the isomerization processes. The mechanism explains why no *cis- β* isomers are detected during the isomerization of *cis- α* and *trans* isomers. The activation parameters are derived for the *cis- α* \rightarrow *trans* isomerizations of three systems: $\text{Os}(\eta^4\text{-CHBA-DCB})(t\text{-Bupy})_2$ ($\Delta H^\ddagger = 21.6(19)$ kcal/mol; $\Delta S^\ddagger = -10(6)$ eu), $\text{Os}(\eta^4\text{-CHBA-DCB})(\text{O}=\text{PPh}_3)_2$ ($\Delta H^\ddagger = 21.6(2)$ kcal/mol; $\Delta S^\ddagger = 0.3(6)$ eu), and $[\text{Os}(\eta^4\text{-CHBA-DCB})(\text{O}=\text{PPh}_3)_2]^+$ ($\Delta H^\ddagger = 23.7(6)$

kcal/mol; $\Delta S^\ddagger = +17(2)$ eu). This suggests that the different rates of isomerization result from entropic differences in the transition state, not enthalpic differences. That is, the *t*-Bupy system has the "tightest" transition state, as evidenced by the most negative ΔS^\ddagger , and consequently the slowest isomerization rate. The rates are observed to be faster in the d^3 Os(V) phosphine oxide system than in its d^4 Os(IV) analog.

Table of Contents

	Page
Acknowledgments	iii
Abstract	v
List of Figures	xi
List of Tables	xiii
List of Schemes	xv
Abbreviations	xvi
Chapter 1.	1
Introduction. Polyanionic Chelating (PAC) Ligands for the Production of New High Valent Inorganic Complexes	
References	13
Chapter 2.	17
H ₄ CHBA-DCB, A New Robust PAC Ligand, and High Valent Osmium Complexes of It	
Introduction	18
Results and Discussion	20
Conclusions	58
Experimental Section	60
References	74
Chapter 3.	80
Non-planar Amide Groups as Ligands	
Introduction	81
Results and Discussion	84
Conclusions	118
Experimental Section	120
References	127

Table of Contents (continued)

	Page
Chapter 4.	141
Thermodynamic and Bonding Differences Between Planar and Non-planar N-amido Ligands	
Introduction	142
Results and Discussion	144
Conclusions	170
Experimental Section	172
References	185
Chapter 5.	190
Kinetics and Mechanism of the Isomerization of cis-α and trans PAC Ligand Complexes	
Introduction	191
Results and Discussion	195
Conclusions	213
Experimental Section	217
References	227

List of Figures

Figure		Page
1.1	PAC ligand (η^4 -CHBA-DCB) $^{4-}$ coordinated as a tetradentate, tetraanionic ligand to metal M.	9
2.1	^{13}C NMR spectrum of 3 .	26
2.2	Superimposed IR spectra of 3 and oxidized 3 .	30
2.3	The three possible isomers of $\text{M}(\eta^4\text{-L}')(\text{L})_2$ compounds.	34
2.4	Different products expected from mixed-pyridine substitutions of 9-<i>t</i>Bu under thermodynamic and kinetic controls.	37
2.5	Rate of mono-phosphine substitution of 7 vs. <i>t</i> -Bupy concentration at 50 °C.	39
2.6	Cyclic voltammogram of 1 mM 10-<i>t</i>Bu in $\text{CH}_2\text{Cl}_2/0.1\text{ M TBAP}$ at 0.17 cm^2 BPG electrode.	44
2.7	Quinoidal resonance forms of the metal-chelate moiety.	47
2.8	Cyclic voltammogram of 1 mM 7 in $\text{SO}_2/0.1\text{ M TBABF}_4$ at -60 °C with 0.02 cm^2 Pt electrode.	50
2.9	Plots of χ_m vs. temperature for Os(IV) complexes 7 , 8 , 10-H , 11 , and 13 .	55
3.1	Organic complexes containing non-planar amide groups: penicillin, polycyclic spirodilactams, and anti-Bredt bridgehead nitrogen complexes.	82
3.2	Ortep of <i>cis</i> - β -Os(η^4 -CHBA-DCB)(bipy), 11 .	85
3.3	Ortep of <i>cis</i> - α -Os(η^4 -CHBA-DCB)(PPh $_3$)(<i>t</i> -BuNC), 14 .	92
3.4	Ortep of 14 viewed down the amide C-N axis.	100
3.5	Parameters for describing non-planarity in N-amido groups.	104
3.6	Plot of $\bar{\tau}$ vs. χ_N for all $\text{RC}(\text{O})\text{NR}'\text{M}$ and $\text{RC}(\text{OM}')\text{NR}'\text{M}$ fragments.	107

List of Figures (continued)

3.7	Plot of $\bar{\tau}$ vs. χ_C for all RC(O)NR'M and RC(OM')NR'M fragments.	108
3.8	Plot of $\bar{\tau}$ vs. χ_N for all RC(O)NR'M fragments where the free base form, RC(O)NR'H, is a secondary amide.	109
3.9	Plot of $\bar{\tau}$ vs. χ_C for all RC(O)NR'M fragments where the free base form, RC(O)NR'H, is a secondary amide.	110
3.10	Plots of amide ν_{CO} vs. $\cos(\bar{\tau})$ for the N-amido groups of 11 and 14.	117
4.1	Cyclic voltammograms of 4.1 mM 10- <i>t</i> Bu in CH ₂ Cl ₂ /0.1 M TBAP at 0.03 cm ² Pt electrode.	145
4.2	Low temperature 400 MHz ¹ H NMR spectra of 19- <i>t</i> Bu showing coalescence of aromatic <i>t</i> -Bupy signals	151
4.3	Plots of formal potentials vs. Fischer $\bar{\sigma}$ substituent parameters of Os(η^4 -CHBA-DCB)-(<i>p</i> -X-py) ₂ .	154
4.4	Linear free energy correlations of $\log K^\circ$ for <i>cis</i> - $\alpha \rightleftharpoons$ <i>trans</i> equilibrium of Os(η^4 -CHBA-DCB)(<i>p</i> -X-py) ₂ and both Hammett σ_p and Fischer $\bar{\sigma}$ constants.	157
4.5	Amide carbonyl IR bands for neutral and cationic forms of both <i>cis</i> - α - and <i>trans</i> -Os(η^4 -CHBA-DCB)L ₂ , where L = <i>t</i> -Bupy and O = PPh ₃ .	160
4.6	Bridgeless complexes of salicylamide ligands.	163
4.7	Cyclic voltammograms of 1.2 mM Os(η^4 -CHBA-DCB)-(<i>t</i> -BuNC) ₂ in CH ₂ Cl ₂ /0.1 M TBAP at 0.03 cm ² Pt electrode.	167
5.1	UV-vis spectral monitoring of [20] ⁺ \rightleftharpoons [8] ⁺ equilibrium in CH ₂ Cl ₂ at 0 °C.	193
5.2	Rate equations and k_{obs} expressions for T and D _L isomerization mechanisms.	196
5.3	van't Hoff plot of [20] ⁺ \rightleftharpoons [8] ⁺ equilibrium data against 1/T(K).	207
5.4	Eyring plots of the variable temperature rate data.	212
5.5	Reaction profile for the isomerization of [20] ^{-0,+} to [8] ^{-0,+} at 22 °C.	216

List of Tables

Table		Page
1.1	Known Os(VII) and Os(VIII) Compounds.	5
1.2	Frequently Employed PAC Ligands.	8
2.1	Mono-oxo and Amide Carbonyl IR Bands of Square-pyramidal Os(VI) Mono-oxo Complexes.	29
2.2	First-order Rate Constants for Substitution of PPh ₃ by <i>t</i> -Bupy in 7 Measured in Toluene Solution.	40
2.3	Formal Potentials of the Os(III/II), Os(IV/III), and Os(V/IV) Couples of the Os(IV) Complexes.	45
2.4	Comparisons of Formal Potentials of 7 with Os(IV) Halide Complexes.	49
2.5	Formal Potentials of Os(η^4 -CHBA-DCB)L ₂ Complexes in SO ₂ .	51
2.6	Magnetic Properties of Os(IV) Complexes Studied.	54
2.7	Magnetic Susceptibilities of the Compounds Studied.	56
2.8	¹ H and ³¹ P NMR Data (ppm).	70
3.1	Selected Bond Distances of 11 .	86
3.2	Selected Bond Angles of 11 .	88
3.3	Selected Bond Distances of 14 .	93
3.4	Selected Bond Angles of 14 .	95
3.5	Best Least-Squares Planes of the PAC Ligand Phenolate Arms and Bridge for 14 .	101
3.6	Selected Amide Torsion Angles and Calculated Non-planarity Parameters for 11 and 14 .	105
3.7	Amide Non-planarity Parameters for RC(O)NR'M and RC(OM')NR'M Fragments where $\bar{\tau} > 25^\circ$.	111
3.8	Summary of Crystal Data and Intensity Collection Information for <i>cis</i> - β -Os(η^4 -CHBA-DCB)(bipy)·0.5 EtOH, 11 , and <i>cis</i> - α -Os(η^4 -CHBA-DCB)(PPh ₃)(<i>t</i> -BuNC), 14 .	123

List of Tables (continued)

3.9	Atomic Coordinates and Gaussian Amplitudes for 11.	125
3.10	Atomic Coordinates and Gaussian Amplitudes for 14.	126
4.1	Formal Potentials and Equilibrium Constants for $\text{Os}(\eta^4\text{-CHBA-DCB})(p\text{-X-py})_2$ Complexes.	153
4.2	Values for Correlation of Formal Potentials with $\bar{\sigma}$ Constants.	155
4.3	Amide Carbonyl IR Bands for Three <i>cis</i> - β - $\text{Os}(\eta^4\text{-CHBA-DCB})\text{L}_2$ Complexes.	169
4.4	Formal Potentials of the Three Isomers of $\text{Os}(\eta^4\text{-CHBA-DCB})(p\text{-Clpy})_2$.	169
4.5	^1H and ^{31}P NMR Data (ppm).	182
5.1	Measured Rate Constants for <i>cis</i> - $\alpha \rightarrow$ <i>trans</i> Isomerization of $\text{Os}(\eta^4\text{-CHBA-DCB})(t\text{-Bupy})_2$.	200
5.2	Measured Rate Constants for <i>cis</i> - $\alpha \rightarrow$ <i>trans</i> Isomerization of $\text{Os}(\eta^4\text{-CHBA-DCB})(\text{O}=\text{PPh}_3)_2$.	204
5.3	Measured Equilibrium Constants for <i>cis</i> - $\alpha \rightleftharpoons$ <i>trans</i> Equilibrium of $[\text{Os}(\eta^4\text{-CHBA-DCB})(\text{O}=\text{PPh}_3)_2]^+$.	208
5.4	Measured Composite Rate Constants for <i>cis</i> - $\alpha \rightleftharpoons$ <i>trans</i> Equilibrium of $[\text{Os}(\eta^4\text{-CHBA-DCB})(\text{O}=\text{PPh}_3)_2]^+$.	209
5.5	Derived Forward (k_1) and Reverse (k_{-1}) Rate Constants for <i>cis</i> - $\alpha \rightleftharpoons$ <i>trans</i> Equilibrium of $[\text{Os}(\eta^4\text{-CHBA-DCB})(\text{O}=\text{PPh}_3)_2]^+$.	211
5.6	Kinetic Rates and Activation Parameters for Investigated Systems.	215
5.7	Extinction Coefficients for All Compounds Studied.	226

List of Schemes

		Page
Scheme		
1.1	Oxidative Decomposition of <i>trans</i> -Os(η^4 -CHBA-Et)L ₂ .	11
2.1	Synthesis of H ₄ CHBA-DCB.	21
2.2	Proposed Mechanism of H ₂ CHP-DCBI Synthesis.	22
2.3	Coordination of H ₄ CHBA-DCB to Osmium.	24
2.4	Synthesis of Os(IV) Complexes.	33
4.1	Thermodynamic Ladder for the <i>cis</i> - $\alpha \rightleftharpoons$ <i>trans</i> Equilibrium of Os(η^4 -CHBA-DCB)(<i>t</i> -Bupy) ₂ at Os(V), Os(IV), Os(III), and Os(II) Oxidation States.	147
4.2	Reduction of <i>cis</i> - α -Os(η^4 -CHBA-DCB)(<i>t</i> -BuNC) ₂ , 15.	166
5.1	Possible Isomerization Mechanisms.	194

Abbreviations

Ac	acetyl
BPG	basal plane pyrolytic graphite
bipy	2,2'-bipyridine
br	broad
<i>t</i> -Bu	<i>tert</i> -butyl
CV	cyclic voltammogram
d	doublet
dppe	1,2-bis(diphenylphosphino)ethane
E ^f	formal potential of a reversible redox couple
Et	ethyl
F	Faraday, 96485 coul/mol
H ₂ CHP-DCBI	1,2-bis(3,5-dichloro-2-hydroxyphenyl)- 5,6-dichlorobenzimidazole
H ₄ CHBA-DCB	1,2-bis(3,5-dichloro-2-hydroxybenzamido)- 4,5-dichlorobenzene
H ₄ CHBA-Et	1,2-bis(3,5-dichloro-2-hydroxybenzamido)ethane
H ₄ HBA-B	1,2-bis(2-hydroxybenzamido)benzene
H ₄ HBA-Et	1,2-bis(2-hydroxybenzamido)ethane
H ₄ HMPA-B	1,2-bis(2-hydroxy-2-methylpropanamido)- benzene
H ₄ HMPA-DMP	1,2-bis(2-hydroxy-2-methylpropanamido)- 2,4-dimethylpentan-3-one
I	current, coul/sec
IR	infrared
L	ligand, usually dative and monodentate
LFER	linear free energy relationship
m	multiplet
Me	methyl
MeO	methoxy
NMR	nuclear magnetic resonance
NO ⁺	nitrosonium
NPV	normal pulse voltammetry

Abbreviations (continued)

O = PPh ₃	triphenylphosphine oxide
O = P(<i>p</i> -tolyl) ₃	tri- <i>p</i> -tolylphosphine oxide
ox	oxalate
PAC	polyanionic chelating ligand
py	pyridine
PPh ₃	triphenylphosphine
P(<i>p</i> -tolyl) ₃	tri- <i>p</i> -tolylphosphine
q	quartet
R	alkyl
s	singlet
SCE	saturated calomel reference electrode
SSCE	saturated sodium chloride reference electrode
t	triplet
TBABF ₄	tetrabutylammonium tetrafluoroborate
TBAP	tetrabutylammonium perchlorate
TBAPF ₆	tetrabutylammonium hexafluorophosphate
THF	tetrahydrofuran
TLC	thin layer chromatography
UV-vis	ultraviolet visible

Chapter 1

Introduction

**Polyanionic Chelating (PAC) Ligands for the Production of New High
Valent Inorganic Complexes**

This thesis encompasses three areas of research: synthetic, physical inorganic, and kinetic studies of high valent osmium complexes stabilized by a polyanionic chelating (PAC) ligand. The stability imparted from the electron-donating PAC ligand makes possible the electro-oxidation of neutral Os(IV) compounds to tricationic species at potentials of up to +1.70 V vs. ferrocinium/ferrocene (Fc^+/Fc) or *ca.* +2.4 V vs. NHE. This chelate usually coordinates to the metal in a planar geometry through phenolate and N-coordinated organic amido (N-amido) linkages. Under oxidizing conditions, however, the ligand coordinatively isomerizes by forming novel non-planar amide moieties. In doing so, the chelate becomes an even stronger electron-donor and reduces the formal potentials of osmium couples by up to 510 mV. A literature search reveals that these are the first examples of non-planar amides bound to a metal center. The final portion of the research probes the thermodynamic driving forces behind this rearrangement and the mechanism through which it proceeds. From these studies, we can discern how a PAC ligand interacts with an oxidized metal center and what factors affect the metal-ligand bonding.

This research is part of a larger effort by the Collins group to produce new PAC ligand complexes and study the chemistries of them.^{6-8,10} To define the reasons for initiating my research, it is necessary to explain the underlying concepts and goals of the overall PAC ligand project.

The objectives of the project are to determine (1) if inorganic complexes of PAC ligands have more selective reaction chemistry than high valent compounds not containing such ligands and (2) if these ligands allow additional modes of reactivity for oxidized metal centers, reactivity which is not possible with existing complexes. Many high valent metal compounds are reagents or catalysts for organic oxidations (e.g., Ce(IV),

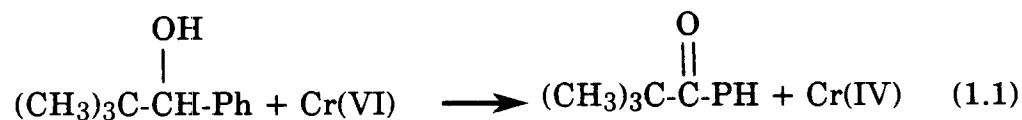
MnO_4^- , OsO_4 , and CrO_3); hence, the ultimate goal of the PAC ligand project is to create more selective inorganic oxidizing agents. Although the project to date is best described as high valent inorganic chemistry, the research pertains to a broader field: oxidation chemistry.

The extensive scope of oxidation chemistry is best revealed by the fundamental processes that the field encompasses: organic hydrogen elimination ($\text{CH}_3\text{CH}_3 \rightarrow \text{H}_2\text{C}=\text{CH}_2 \rightarrow \text{HC}\equiv\text{CH}$), oxygen atom transfer ($\text{CH}_4 \rightarrow \text{CH}_3\text{OH} \rightarrow \text{CH}_2\text{O} \rightarrow \text{HCO}_2\text{H} \rightarrow \text{CO}_2$), and electron abstraction ($\text{Fe(II)} \rightarrow \text{Fe(III)} + e^-$). The numerous substrates and inorganic reagents that react via these processes make oxidation diverse and complicated. Excellent references are available describing oxidation chemistry in more detail.¹ Industrial applications include the epoxidation of ethylene with dioxygen, the Wacker process, the Mid-Century process, and the Oxirane process. Transition metal complexes catalyze all of these processes.

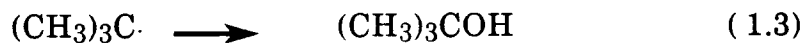
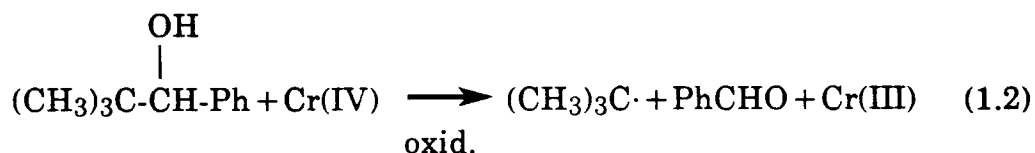
From the number of important oxidation processes, one might assume that metal-based oxidations have been studied in detail and are thoroughly understood. Unfortunately, mechanistic information often is lacking.² Rapid kinetic rates and numerous intermediates obscure reaction steps. Radical reaction paths frequently participate. The role of the inorganic component is rarely established. Its function is usually inferred from product distributions alone. Multiple reaction paths often reduce the chemoselectivity of an oxidation. These pathways include homolytic, heterolytic and disproportionation events that are metal-centered. Shuttling among several valence states simultaneously generates multiple oxidants.

Chromic acid oxidation of α -*tert*-butylbenzyl alcohol is a representative system that contains manifold oxidants.³ Mechanistic

studies reveal that two chromium catalysts of different oxidation states are present and have excellent, but different, chemoselectivities: Cr(VI) and Cr(IV). The alcohol is cleanly oxidized to phenyl *tert*-butyl ketone by Cr(VI) reducing to a Cr(IV) intermediate (eq 1.1).



The Cr(IV) intermediate, however, homolytically oxidizes more alcohol and generates cleavage products: benzaldehyde and *tert*-butanol (eqs 1.2 and 1.3).



Each chromium reagent produces different organic products from the alcohol. The presence of both reagents limits the reaction efficiency.

Solvent, pH and temperature adjustments can marginally improve yields. Controlling the redox changes at the metal center, however, is imperative. Stabilization of the Cr(IV) intermediate discussed above

Table 1.1. Known Os(VII) and Os(VIII) Compounds.

Os(VII)	Ref	Os(VIII)	Ref
OsF ₇	4a	OsO ₄	
OsOF ₅	4b,c	OsO ₃ F ₂	4d
		OsO ₃ F ₃ ⁻	4d
		OsO ₂ N(OH)	4e
		OsO _n (N- <i>t</i> -Bu) _{4-n} (n = 1-3)	4f
		Os(N- <i>t</i> -Bu) ₃ (N-SO ₂ -Ar) (Ar = 2,4,6-Me ₃ Ph; 2,4,6- <i>i</i> -Pr ₃ Ph; 4-MePh)	4g

would confine oxidation to the heterolytic Cr(VI/IV) pathway (eq 1.1); Cr(VI) could then be considered a selective inorganic oxidant. Prudent changes in the ligation of the metal center can control such inorganic redox processes.

Only a limited number of ligands stabilizes high valent metal centers while resisting oxidation. Most well-known examples are monodentate, electronegative species such as F⁻, Cl⁻, Br⁻, O²⁻, and N³⁻. Useful exceptions include dianionic η²-peroxo and η⁴-porphyrinato ligands. This limited number of ligands restricts the number of high valent compounds available. A survey of all known Os(VII) and Os(VIII) complexes illustrates this point. Only twelve Os(VII) and Os(VIII) compounds have been well-characterized (Table 1.1). This number sharply contrasts the thousands of low valent osmium complexes containing phosphine, carbonyl, alkyl, cyclopentadienyl, hydride, and olefinic ligands, among others.⁵

The limited number of ligands makes it difficult to fine-tune the reactivity of high valent compounds; only coarse changes in ligation are possible. Most of these ligands are poorly suited for spectroscopic observation. As a result, monitoring the inorganic reagents *in situ* is difficult, if not impossible. Before new oxidants can be created, a more immediate problem must be solved—designing new ligands for high valent metal centers. Additional ligands must be developed, and the chemistry of complexes containing them must be explored.

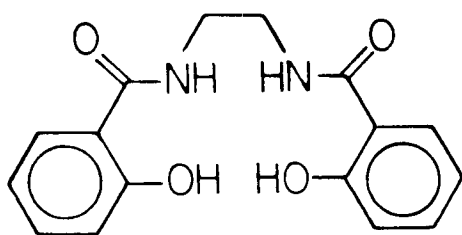
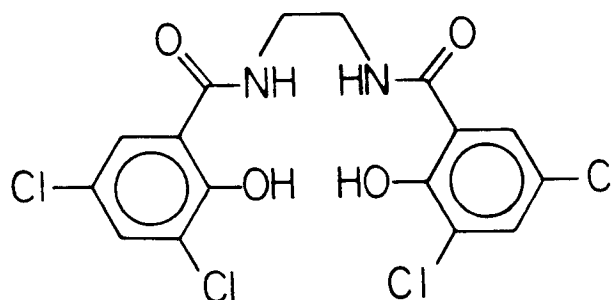
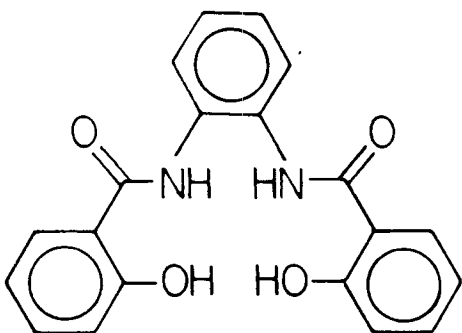
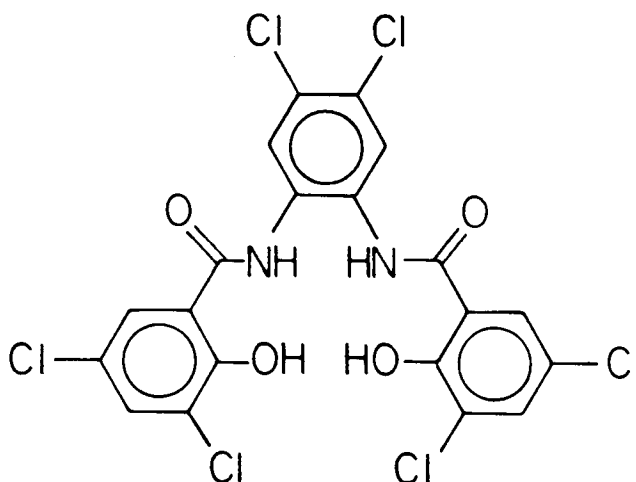
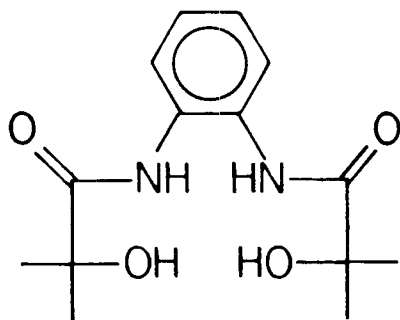
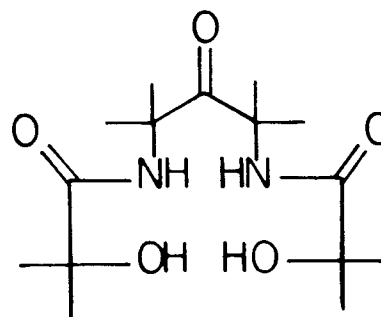
The Collins group has prepared PAC ligands that are capable of forming stable high oxidation state complexes. We consider the following design criteria necessary for producing suitable ligands:

1. Incorporate hard donor atoms that are negatively charged to provide chemically innocent binding sites and strong σ -donation.
2. Provide sufficient negative charge formation upon coordination to compensate for the high positive charge on an oxidized metal center.
3. Build chelating ligands, rather than monodentate ligands, to provide strong binding to the metal and to limit the number of available coordination sites about the metal center.
4. Design ligands that form five- and six-membered metallacycles upon coordination to ensure the formation of monomeric vs. polymeric compounds.

5. Develop PAC ligands that are both oxidation- and hydrolysis-resistant to ensure the integrity of complexes in harsh environments.
6. Include a means of derivatization to vary the steric and electronic properties of the ligand or even to incorporate chiral substituents.
7. Devise simple and economical syntheses.

Several PAC ligands have been designed and coordinated to metal centers. Of these ligands, those in Table 1.2 have been employed often by the Collins group. The ligands in Table 1.2 are presented in the chronological order of their design. H₄HBA-Et was the prototype of the ligand family. Chloride substituents and an aromatic bridge were added to protect the ligand from oxidation (e.g., H₄CHBA-Et, H₄HBA-B, and H₄CHBA-DCB). Recently, the aromatic framework has been replaced by an aliphatic one (e.g., H₄HMPA-B and H₄HMPA-DMP). The aliphatic ligands have greater σ -donating capabilities and greater resistance to oxidation than the former aromatic ligands. Chromium,^{8,10j} cobalt,^{10g,h;11} copper,¹¹ iron,^{8,11} and osmium^{6;7;10a-f,i-k;11} complexes of PAC ligands have been prepared thus far.

The chemistry of osmium complexes incorporating the ligand H₄CHBA-DCB is reported in this thesis. Deprotonation of both phenols and both secondary amides produces a potentially tetradentate, tetraanionic ligand, (η^4 -CHBA-DCB)⁴⁻ (Figure 1.1). The phenolate¹² and

Table 1.2. Frequently Employed PAC Ligands.^a**H₄HBA-Et^b****H₄CHBA-Et^c****H₄HBA-Bd****H₄CHBA-DCB^e****H₄HMPA-B^f****H₄HMPA-DMP^g**

^aRef 9 explains ligand abbreviations. ^b Refs 7,8. ^c Refs 6; 7;8;9a,b,f,i,j,k.
^d Refs 6; 8; 10c,d,e. ^e Refs 10c,e,f,h,i. ^f Refs 10g, 11. ^g Ref 11.

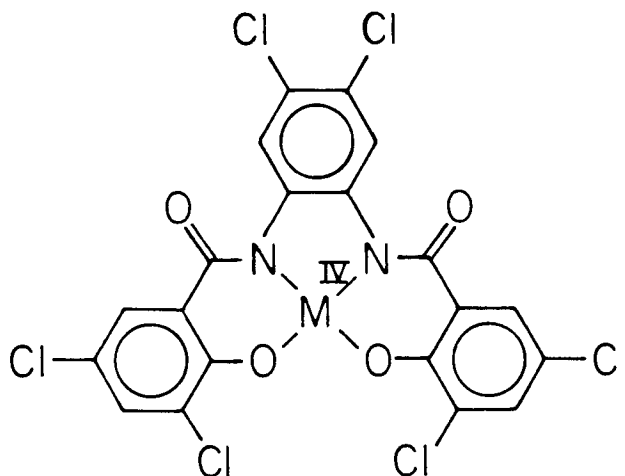


Figure 1.1. PAC ligand (η^4 -CHBA-DCB) $^{4-}$ coordinated as a tetradentate, tetraanionic ligand to metal M.

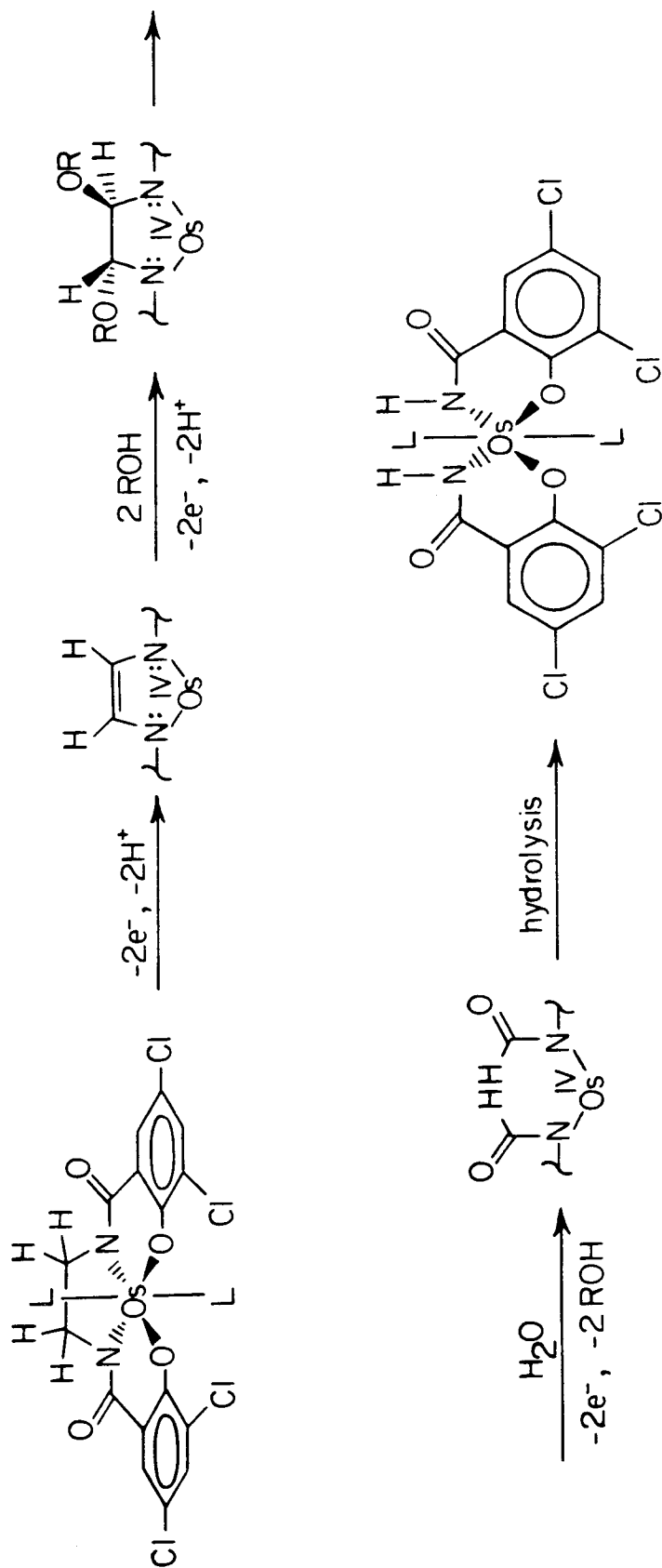
N-amido¹³ moieties are strong σ -donors. Electrochemical studies by Margarum *et al.* of Cu(II) and Ni(II) intercalated in polypeptides reveal that successive coordination of one to three N-amido ligands lowers the formal potentials of the M(III/II) couples by up to 0.43 V.¹⁴ Kimura *et al.* use amide-containing cyclam ligands, such as 1,4,7,10,13-pentaaza-cyclohexadeca-14,16-dione, to produce stable Ni(III) compound.^{15b,c} These ligands render Ni(II) centers sufficiently basic to bind dioxygen.^{15a,b} Nickel complexes of standard cyclam ligands without amide substituents are unstable in the +3 oxidation state and cannot bind dioxygen. The accessibilities of these high valent complexes of copper and nickel are attributed to the exceptional electron-donation from the N-amido moieties.

The motivation for designing H_4 CHBA-DCB came from studies documenting the deficiencies of H_4 CHBA-Et. Drs. Terry E. Krafft and

Stephen L. Gipson showed that osmium complexes of $\text{H}_4\text{CHBA-Et}$ were susceptible to oxidation at the ethylene bridge.^{6;7;10a,b} These were octahedral Os(IV) complexes, *trans*- $\text{Os}(\eta^4\text{-CHBA-Et})\text{L}_2$, where L represents pyridine or 4-*tert*-butylpyridine (Scheme 1.1). Upon electrochemical oxidation of these compounds, successive bridge-localized reactions gave rise to a cascade of degradation products. First, the ethylene bridge underwent dehydrogenation, producing an olefinic bridge. In the presence of alcohol, this unsaturated bridge was further oxidized to a 1,2-diether moiety. Cleavage of the bridging C-C bond followed by hydrolytic loss of the alkoxide groups yielded a complex with two bidentate residues, each binding through phenolate and organic N-imido donors.¹³ Stepwise hydrolysis of the two formyl groups produced a bis-salicylamido complex that was structurally analogous to the initial $(\eta^4\text{-CHBA-Et})^4-$ complex, except for the lack of an ethylene bridge. Protonated forms of the final compound proved to be catalysts for the electrochemical oxidation of alcohols. Although elucidating this cascade was scientifically challenging, and the electrochemical oxidation catalysts warranted characterization and testing, the ligand $\text{H}_4\text{CHBA-Et}$ did not fulfill design criteria #5 requiring PAC ligands to be chemically resistant. An improved ligand was needed. We anticipated that a dichlorophenylene bridge would alleviate the problem of the ethylene bridge oxidation.

Chapter 2 describes the synthesis of $\text{H}_4\text{CHBA-DCB}$ and osmium complexes of it. The osmium complexes of $(\eta^4\text{CHBA-DCB})^4-$ show greater resistance to oxidation than analogous $(\eta^4\text{CHBA-Et})^4-$ compounds do. As previously mentioned, the neutral Os(IV) compounds display reversible $\text{Os(3+}/2+)$ couples at 1.70 V vs. Fc^+/Fc in liquid SO_2 . Measurements of the magnetic susceptibilities of five Os(IV) complexes show temperature-

Scheme 1.1. Oxidative Decomposition of *trans*-Os(η^4 -CHBA-Et) L_2 .



$L = py, \text{ t-Bupy}$

independent paramagnetism. In Chapter 3, complexes containing non-planar N-amido ligands are presented. Two deformations generate non-planar amides: pyramidalization at the amide nitrogen atom and amide C-N bond rotation. X-ray crystallographic characterization of two systems makes possible the quantification of amide non-planarity and an assessment of the contribution from each type of deformation. The changes in metal-ligand bonding induced by each deformation are compared. Reduced delocalization in the non-planar amides is evidenced by high amide carbonyl IR bands and basic amide nitrogen atoms. Chapter 4 includes a thermodynamic analysis of the free energy differences between complexes with planar N-amido ligands and those with non-planar ligands. This suggests that a non-planar N-amido ligand is more electron-donating than its planar analog. A linear free energy correlation confirms this hypothesis and reveals that electronic demands at the metal center trigger these isomerizations. Oxidizing the metal center can induce a planar to non-planar isomerization. In Chapter 5, the mechanism of this isomerization is examined through kinetic rate measurements and ligand exchange studies. An intramolecular twist rearrangement occurs, which requires no bond cleavage prior to isomerization. Unless otherwise noted, Dr. Stephen L. Gipson performed all of the electrochemistry in Chapters 2, 3, and 4.

References

1. (a) Moureu, C.; Dufraisse, C. *Chem. Rev.* **1926**, *3*, 113-162.
 (b) Sheldon, R. A.; Kochi, J. A. "Metal-Catalyzed Oxidations of Organic Compounds"; Academic: New York, 1981. (c) Parshall, G. W. "Homogeneous Catalysis"; John Wiley and Sons: New York, 1980. (d) "Oxidation in Organic Chemistry", Wiberg, K. W., Ed.; Academic: New York, 1965; Part A. (e) *Ibid.* Trahanovsky, W. S., Ed.; Academic: New York, 1973; Part B. (f) *Ibid.* 1978; Part C. (g) Benson, D. "Mechanism of Oxidation by Metal Ions"; Elsevier: New York, 1976. (h) Dumas, T.; Bulani, W. "Oxidation of Petrochemicals: Chemistry and Technology"; John Wiley and Sons: New York, 1974. (i) House, H. O. "Modern Synthetic Reactions"; Benjamin/Cummings: Menlo Park, 1972.
2. Report of the International Workshop on "Activation of Dioxygen Species and Homogeneous Catalytic Oxidations", Collins, T. J., Ed.; Galzignano, Italy, June 28-29, 1984.
3. (a) Doyle, M.; Swedo, R. J.; Rocek, J. *J. Am. Chem. Soc.* **1973**, *95*, 8352-8357. The following references are additional mechanistic investigations of Cr(VI) oxidations. (b) Rocek, J.; Radowski, A. E. *J. Am. Chem. Soc.* **1973**, *95*, 7123-7132. (c) *Ibid.* **1968**, *90*, 2986-2988. (d) Hampton, J.; Leo, A.; Westheimer, F. H. *J. Am. Chem. Soc.* **1956**, *78*, 306-312. (e) Cohen, M.; Westheimer, F. H. *Ibid.* **1952**, *74*, 4387-4391. (f) Westheimer, F. H.; Nicolaides, N. *Ibid.* **1949**, *71*, 25-28. (g) Watanabe, W.; Westheimer, F. H. *J. Chem. Phys.* **1949**, *17*, 61-70.

4. (a) Glemser, O.; Roesky, H. W.; Hellberg, K.-H.; Werther, H.-V. *Chem. Ber.* **1966**, *99*, 2652-2662. (b) Bartlett, N.; Trotter, J. *J. Chem. Soc. (A)* **1968**, 543-547. (c) Bartlett, N.; Jha, N. K. *Ibid.*, 536-543. (d) Hepworth, M. A.; Robinson, P. L. *J. Inorg. Nucl. Chem.* **1957**, *4*, 24-29. (e) Griffith, W. P. *J. Chem. Soc.* **1965**, 3694-3697. (f) Chong, A. O.; Oshima, K.; Sharpless, K. B. *J. Am. Chem. Soc.* **1977**, *99*, 3420-3426. (g) Sharpless, K. B.; Hentges, S.; Stanford University, unpublished results. See the following: Nugent, W. A.; Haymore, B. L. *Coord. Chem. Rev.* **1980**, *31*, 123-175.
5. (a) Cotton, F. A.; Wilkenson, G. "Advanced Inorganic Chemistry", 4th ed.; John Wiley and Sons: New York, 1980; pp 912-933. (b) Adams, R. D.; Selegue, J. P. In "Comprehensive Organometallic Chemistry", 1st ed.; Wilkenson, G.; Stone, F. G. A.; Abel, E. W., Eds.; Pergamon: New York, 1982; Vol. 4, pp 967-1064.
6. Gipson, S. L., Ph.D. Thesis, California Institute of Technology, June 1985.
7. Krafft, T. E., Ph.D. Thesis, California Institute of Technology, February 1985.
8. Spies, G. H., Ph.D. Thesis, California Institute of Technology, October 1984.
9. PAC ligands are abbreviated as follows: 1,2-bis(2-hydroxybenz-amido)-ethane, H₄HBA-Et; 1,2-bis(3,5-dichloro-2-hydroxybenz-amido)-ethane, H₄CHBA-Et; 1,2-bis(2-hydroxybenzamido)-benzene, H₄HBA-B; 1,2-bis(3,5-dichloro-2-hydroxybenzamido)-4,5-dichlorobenzene, H₄CHBA-DCB; 1,2-bis(2-hydroxy-2-methylpro-

panamido)-benzene, H₄HMPA-B; 2,4-bis(2-hydroxy-2-methylpropanamido)-2,4-dimethylpentan-3-one, H₄HMPA-DMP.

10. (a) Anson, F. C.; Collins, T. J.; Gipson, S. L.; Krafft, T. E. *Inorg. Chem.*, submitted for publication. (b) Anson, F. C.; Collins, T. J.; Coots, R. J.; Gipson, S. L.; Krafft, T. E.; Santarsiero, B. D.; Spies, G. H. *Inorg. Chem.*, submitted for publication. (c) Anson, F. C.; Collins, T. J.; Gipson, S. L.; Keech, J. T.; Krafft, T. E.; Peake, G. T. *J. Am. Chem. Soc.*, in press. (d) Barner, C. J.; Collins, T. J.; Mapes, B. E.; Santarsiero, B. D. *Inorg. Chem.*, in press. (e) Collins, T. J.; Coots, R. J.; Furutani, T. T.; Keech, J. T.; Peake, G. T.; Santarsiero, B. D. *J. Am. Chem. Soc.*, in press. (f) Anson, F. C.; Collins, T. J.; Gipson, S. L.; Keech, J. T.; Krafft, T. E. *Inorg. Chem.*, in press. (g) Collins, T. J.; Richmond, T. G.; Santarsiero, B. D.; Treco, B. G. R. T. *J. Am. Chem. Soc.* **1986**, *108*, 2088-2090. (h) Anson, F. C.; Collins, T. J.; Coots, R. J.; Gipson, S. L.; Richmond, T. G. *J. Am. Chem. Soc.* **1984**, *106*, 5037-5038. (i) Anson, F. C.; Christie, J. A.; Collins, T. J.; Coots, R. J.; Furutani, T. T.; Gipson, S. L.; Keech, J. T.; Krafft, T. E.; Santarsiero, B. D.; Spies, G. H. *J. Am. Chem. Soc.* **1984**, *106*, 4460-4472. (j) Christie, J. A.; Collins, T. J.; Krafft, T. E.; Santarsiero, B. D.; Spies, G. H. *J. Chem. Soc., Chem. Commun.* **1984**, 198-199. (k) Collins, T. J.; Santarsiero, B. D.; Spies, G. H. *J. Chem. Soc., Chem. Commun.* **1983**, 681-682.
11. Barner, C. J.; Brewer, J. C.; Peake, G. T.; Richmond, T. G.; Toth, J. E.; Treco, B. G. R. T.; California Institute of Technology, unpublished results.

12. Jones, R. D.; Summerville, D. A.; Basolo, F. *Chem. Rev.* **1979**, *79*, 139-179.
13. Sigel, H.; Martin, R. B. *Chem. Rev.* **1982**, *82*, 385-426. Henceforth, a deprotonated secondary amide group ligated to a metal center through the nitrogen atom will be called an N-amido ligand. An N-imino ligand is of the type $RC(O)N(M)CHO$.
14. (a) Margarum, D. W. *Pure Appl. Chem.* **1983**, *55*, 23-24. (b) Diaddario, L. L.; Robinson, W. R.; Margarum, D. W. *Inorg. Chem.* **1983**, *22*, 1021-1025. (c) Margarum, D. W.; Wong, L. F.; Bossu, F. P.; Chellapa, K. L.; Czarnecki, J. J.; Kirksey, S. T., Jr.; Neubecker, T. A. *Adv. Chem. Ser.* **1977**, *162*, 281-303.
15. (a) Kushi, Y.; Machida, R.; Kimura, E. *J. Chem. Soc., Chem. Commun.* **1985**, 216-218. (b) Kimura, E.; Machida, R.; Kodama, M. *J. Am. Chem. Soc.* **1984**, *106*, 5497-5505. (c) Kimura, E.; Sakonaka, A.; Machida, R.; Kodama, M. *J. Am. Chem. Soc.* **1982**, *104*, 4255-4257.

Chapter 2

H₄CHBA-DCB, A New Robust PAC Ligand, and High Valent Osmium Complexes of It

Introduction

The first task in this project was to synthesize the new PAC ligand H₄CHBA-DCB.¹ Os(IV) complexes of a similar ligand, *trans*-Os(η^4 -CHBA-Et)(py)₂, had been shown to be susceptible to oxidation at the ethylene bridge of the chelating ligand. In designing a more robust PAC ligand, a dichlorophenylene (DCB) bridge was substituted for the ethylene unit in H₄CHBA-Et. This bridge replaces the aliphatic C-C and C-H bonds with stronger aromatic bonds² and is protected from aromatic substitution and oxidation by the chloride substituents. The new ligand was synthesized and coordinated to osmium as *trans*-K₂[Os(η^4 -CHBA-DCB)(O)₂]. Os(IV) complexes were prepared analogous to those containing the ligand (η^4 -CHBA-Et)⁴⁻. These new compounds remain intact under oxidizing conditions; hence, the DCB bridge effectively blocks oxidative decomposition. Complexes of the new ligand undergo unprecedented Os(IV) chemistry: (1) facile ligand substitution reactions, (2) reversible electrochemistry at potentials of +2.00 V vs. ferrocinium/ferrocene (Fc⁺/Fc) in liquid SO₂, and (3) a ligand isomerization process whereby the electron-donation of the chelate varies according to the demand for electron density at the metal center.

The triphenylphosphine complex *trans*-Os(η^4 -CHBA-DCB)(PPh₃)₂ is a useful starting material for producing a series of Os(IV) compounds. Upon gentle heating of this compound, Lewis bases (e.g., py, 4-*t*-Bupy, and *t*-BuNC), L, readily displace one phosphine to produce complexes of the type Os(η^4 -CHBA-DCB)(PPh₃)L, **9-L**. High temperatures usually effect substitution of the second phosphine generating bis-substituted products, Os(η^4 -CHBA-DCB)L₂, **10-L**. Bidentate Lewis bases such as bipy and dppe

displace both phosphines, producing monomeric complexes where the chelate assumes a non-planar geometry. Non-planar chelate geometries were not expected. We thought that the stiff aromatic framework and the planarity of amide groups would necessitate planar coordination of the ligand; this assumption, however, was wrong. Detailed studies demonstrate that changes in chelate planarity cause variations in the electron-donating capabilities of the PAC ligand.

In dichloromethane, the Os(IV) compounds exhibit reversible Os(III/II), Os(IV/III), and Os(V/IV) couples, as observed by cyclic voltammetry. Beyond the Os(V/IV) couple, no anodic activity is observed within the oxidative limit of dichloromethane, about +1.4V vs. Fc⁺/Fc. Recent reports using liquid SO₂ as an electrochemical medium place its anodic limit at about +3.5V vs. Fc⁺/Fc.³ This remote limit prompted an investigation of the Os(IV) electrochemistry in liquid SO₂ to determine the potential limits at which the compounds degraded. For each of these complexes, three reversible couples are observed, the highest of which has a formal potential of +1.7V vs. Fc⁺/Fc. Irreversible oxidation of these complexes occurs at potentials of *ca.* +2.2V vs. Fc⁺/Fc.⁴

The ¹H NMR spectra of the Os(IV) complexes show well-resolved paramagnetic shifts. For example, in the ³¹P NMR spectrum of Os(η⁴-CHBA-DCB)(dppe) the signals of the dppe phosphorus atoms are at -992.9 and -1015.6 ppm relative to an 85% H₃PO₄ reference. To determine the nature of the magnetic influence, variable temperature magnetic susceptibility measurements were done on a number of Os(IV) compounds. Temperature-independent paramagnetism was observed with no detectable Curie-Weiss component for all complexes studied.

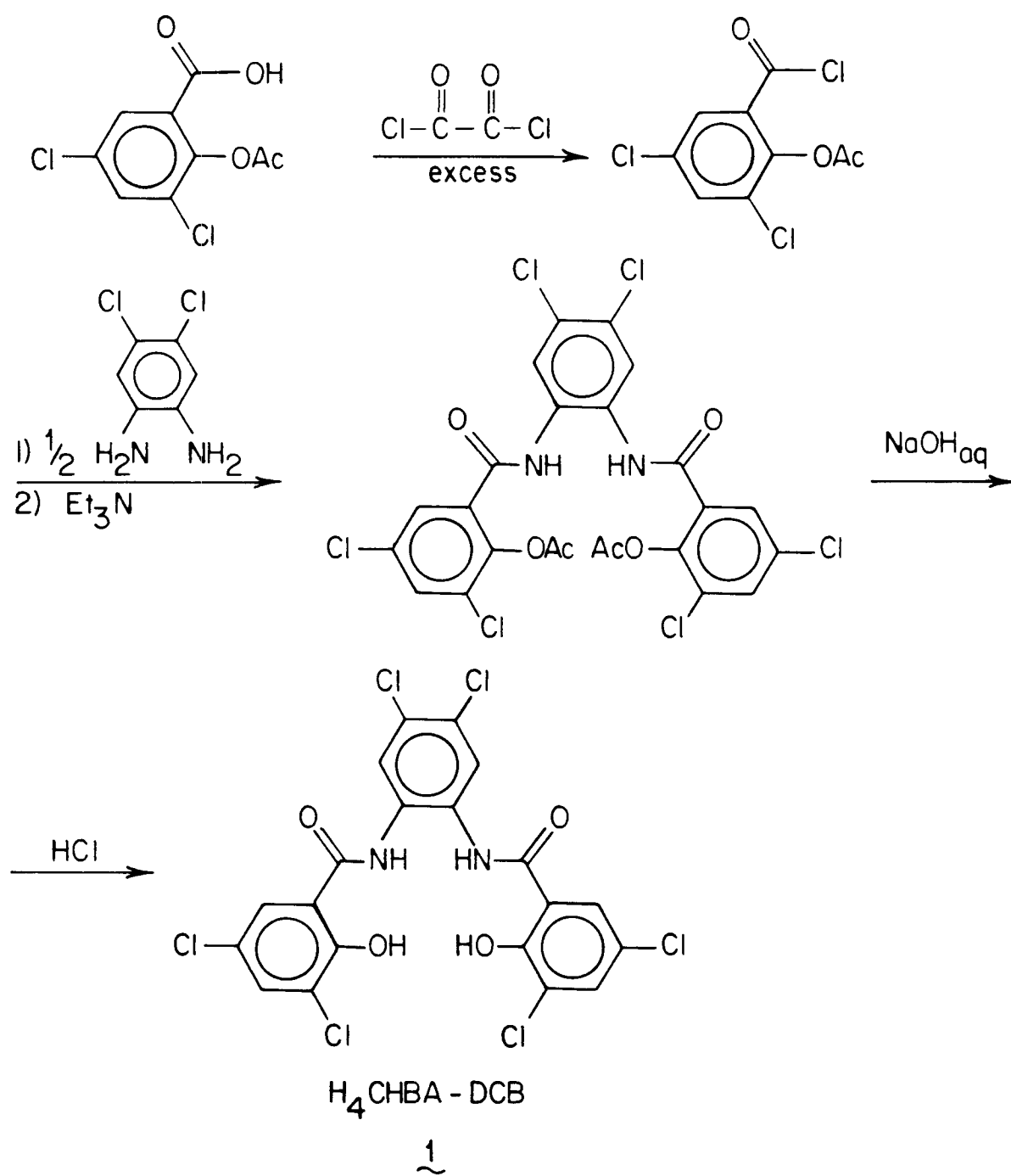
Results and Discussion

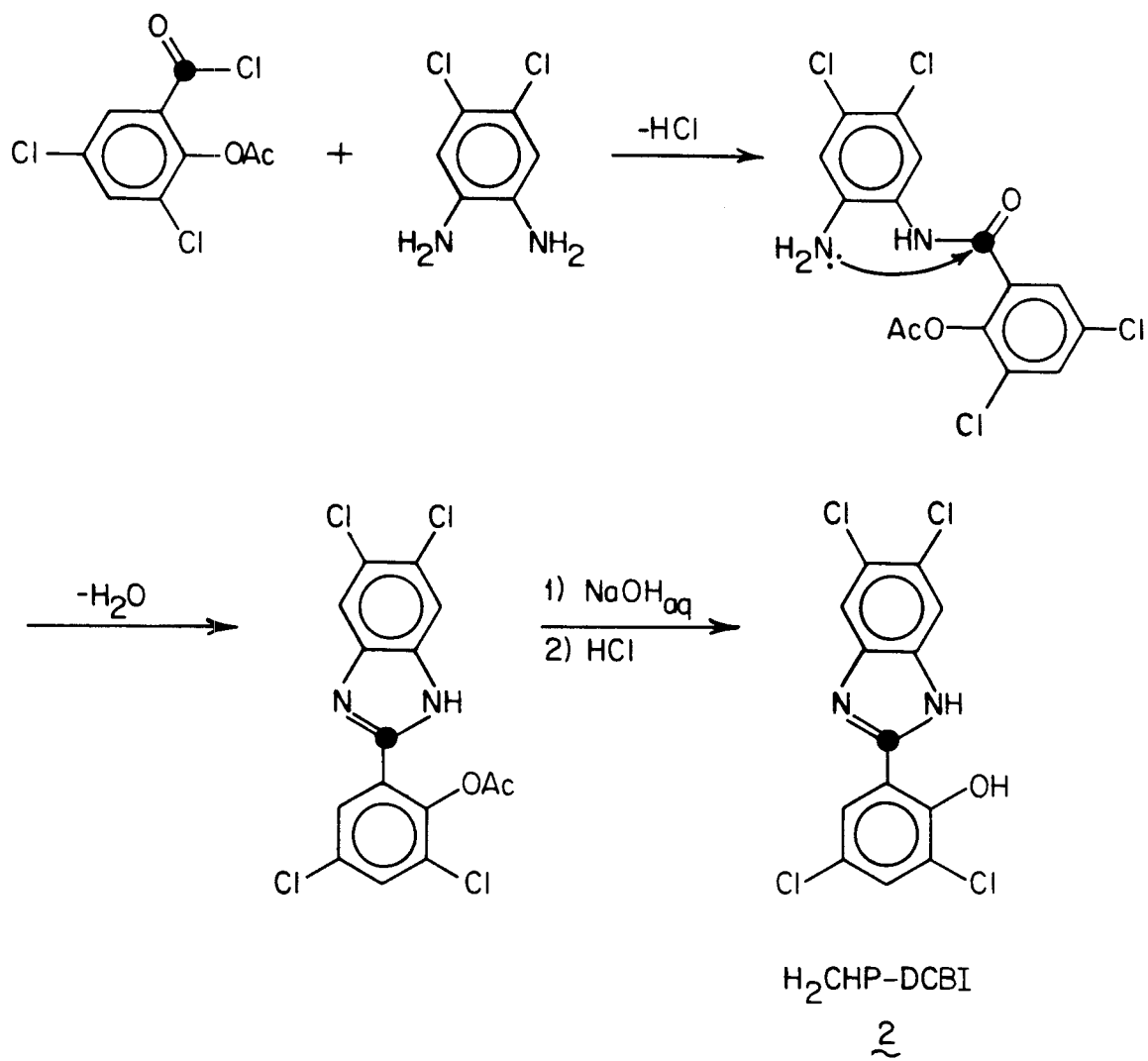
Ligand Synthesis

The synthetic route used to make H₄CHBA-DCB, 1, was originally developed by Dr. George H. Spies⁵ for the production of other PAC ligands (e.g. H₄HBA-Et and H₄HBA-B)¹ (Scheme 2.1). Commercially available 3,5-dichlorosalicylic acid is acetylated with acetylchloride in acetic anhydride and then converted to the acid chloride with oxalyl chloride. 4,5-Dichlorophenylenediamine must be purified prior to use by reduction with either sodium sulphite or triphenylphosphine followed by recrystallization from hexane. Reacting two equivalents of the acid chloride with the diamine produces the acetylated PAC ligand. Hydrolysis removes the acetyl protecting groups. Multiple recrystallizations of the crude product from THF/EtOH (1:1 v/v) are necessary for adequate purification.

The yields of 1 from this synthesis varied between 10 and 60%. These are in contrast with yields routinely attained in the synthesis of other PAC ligands (60-90%).^{5,6} The conditions used for reacting the acid chloride and the diamine were varied in hopes of optimizing the yield. These modifications included heating under reflux (~ 50 °C), cooling with an ice-bath (0 °C), activating the acid chloride with aluminum trichloride,⁷ and using an acid imidazolid reagent in place of the acid chloride.⁸ All of these attempts proved useless.

A recurring impurity was isolated and identified in attempts to understand reaction paths leading to by-products. Characterization of the impurity revealed it to be a condensation product from the synthesis, aryl-substituted benzimidazole, H₂CHP-DCBI (2, Scheme 2.2).¹ Reactions of

Scheme 2.1. Synthesis of H₄CHBA-DCB.

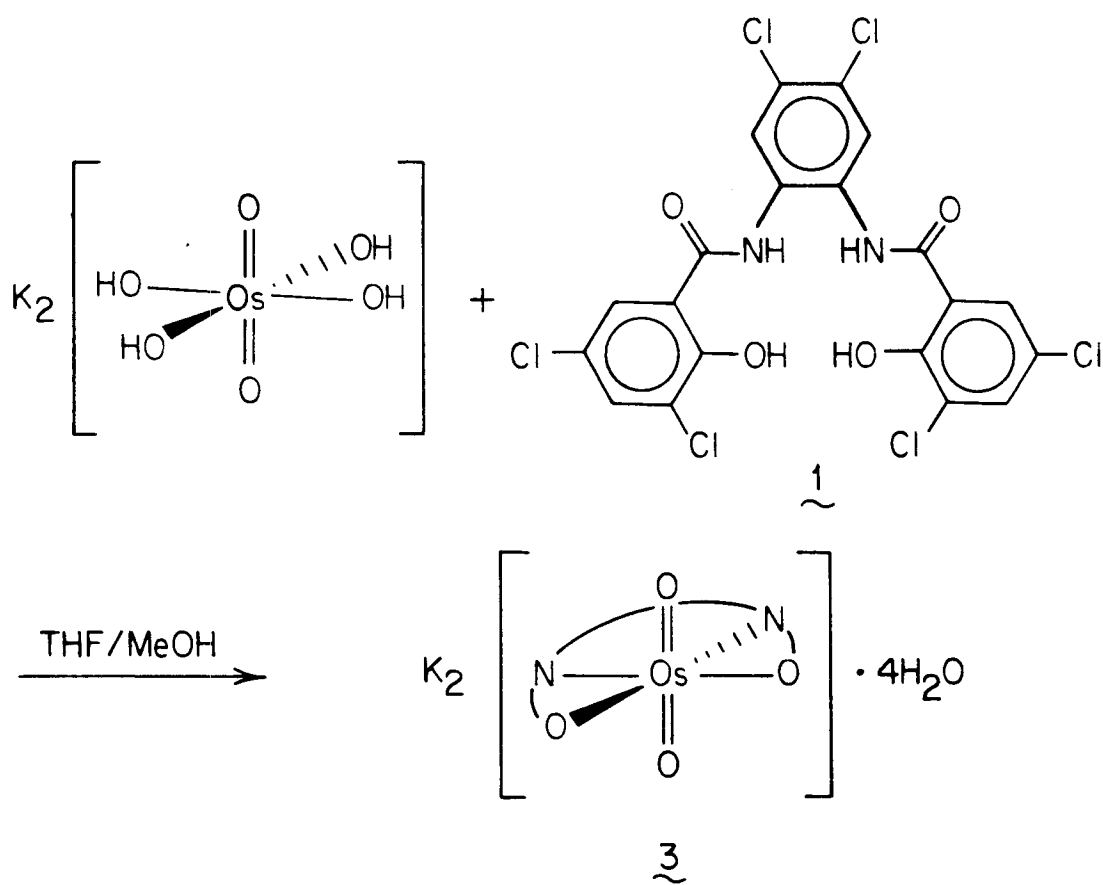
Scheme 2.2. Proposed Mechanism of H₂CHP-DCBI Synthesis.

acylating agents with *o*-phenylenediamine are known to form benzimidazole products.^{9,10} Following the formation of one amide, the free amine group condenses with the amide carbonyl group, producing the benzimidazole heterocycle. Apparently, there are two competitive reactions of the mono-amide intermediate. Simple ring closure leads to **2**, whereas reaction with one equivalent of acid chloride produces acetyl-protected **1**. Syntheses carried out at high temperatures or using impure acid chloride generate high yields of benzimidazole. At 0 °C, negligible **2** is produced, but large amounts of unidentified by-products reduce the yield of isolated **1**. Reacting pure reagents over long reaction times (> 12 h) at ambient temperatures gives the highest yields of **1** ($\geq 50\%$).

H₄CHBA-DCB is soluble only in THF, in DMSO, and sparingly in acetone. It is the least soluble of the PAC ligands, possibly because of the six chloride substituents. It has been characterized by IR and ¹H NMR spectroscopies and elemental analysis. Its IR spectrum displays N-H and O-H absorptions ($\nu_{\text{N-H}} = 3280 \text{ cm}^{-1}$; $\nu_{\text{O-H}} = 3505 \text{ cm}^{-1}$), amide I and II absorptions ($\nu_{\text{amide I}} = 1650 \text{ cm}^{-1}$; $\nu_{\text{amide II}} = 1552 \text{ cm}^{-1}$) and a complicated fingerprint region.¹¹

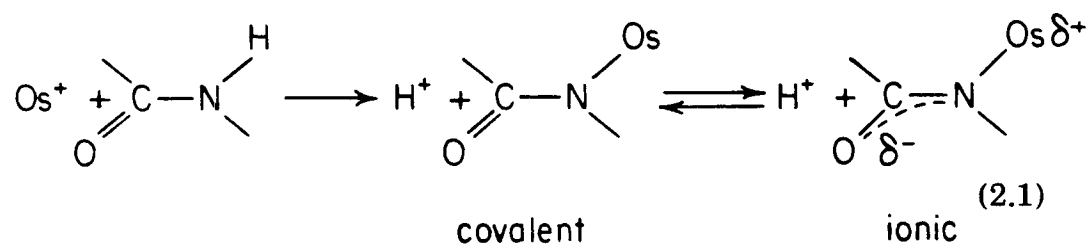
Os(VI) Complexes of (η^4 -CHBA-DCB)⁴⁻

The ligand H₄CHBA-DCB coordinates to osmium if reacted with an equimolar amount of *trans*-K₂[Os(OH)₄(O)₂], potassium osmate.^{6,12} Metathesis of osmate hydroxyl ligands with the donor atoms of **1** proceeds rapidly, producing *trans*-K₂[Os(η^4 -CHBA-DCB)(O)₂], **3**, and eliminating four equivalents of water (Scheme 2.3). This parallels known osmate reactions with excess acid HX where X⁻ substitutes for the hydroxyl

Scheme 2.3. Coordination of H₄CHBA-DCB to Osmium.

groups to produce *trans*-K₂[OsX₄(O)₂] (X⁻ = Cl⁻, Br⁻, CN⁻, C₂O₄²⁻, and NO₂⁻).^{13a} Recrystallization of **3** from butyl ether/THF/MeOH affords an 85% yield of tan microcrystalline product.

Compound **3** has been characterized by IR, ¹H NMR, and ¹³C NMR spectroscopies and elemental analysis. The primary amide IR band decreases from 1650 cm⁻¹ (free ligand) to 1607 cm⁻¹ (**3**) upon coordination. This phenomenon is routinely observed for free vs. metal-bound amide groups¹⁴ and serves as a diagnostic marker for N-amido ligand formation. The drop in ν_{C=O} suggests that the M-N bond is partially ionic, M^{δ+}-N^{δ-}, and that the anionic charge is delocalized through the amide, creating lower C-O bond order (eq 2.1).¹⁴



The single asymmetric dioxo stretch at 820 cm⁻¹ establishes the *trans* relationship of the two oxo ligands. ¹⁸O labelling lowers the dioxo band to 782 cm⁻¹, which confirms the assignment. The 5d² Os(VI) center is diamagnetic, making NMR spectroscopy feasible. The ¹H NMR spectrum of **3** shows three signals for the six protons of the chelate: a singlet (bridge protons) and two doublets (phenolate protons). Together the IR and ¹H NMR spectra require **3** to have C_{2v} symmetry as pictured in Scheme 2.3. Consistent with this symmetry, the 20 carbon atoms of the (η⁴-CHBA-DCB)⁴⁻ ligand exhibit ten ¹³C NMR signals (Figure 2.1, top). An INEPTNON ¹³C NMR spectrum enhances only methyne and methyl

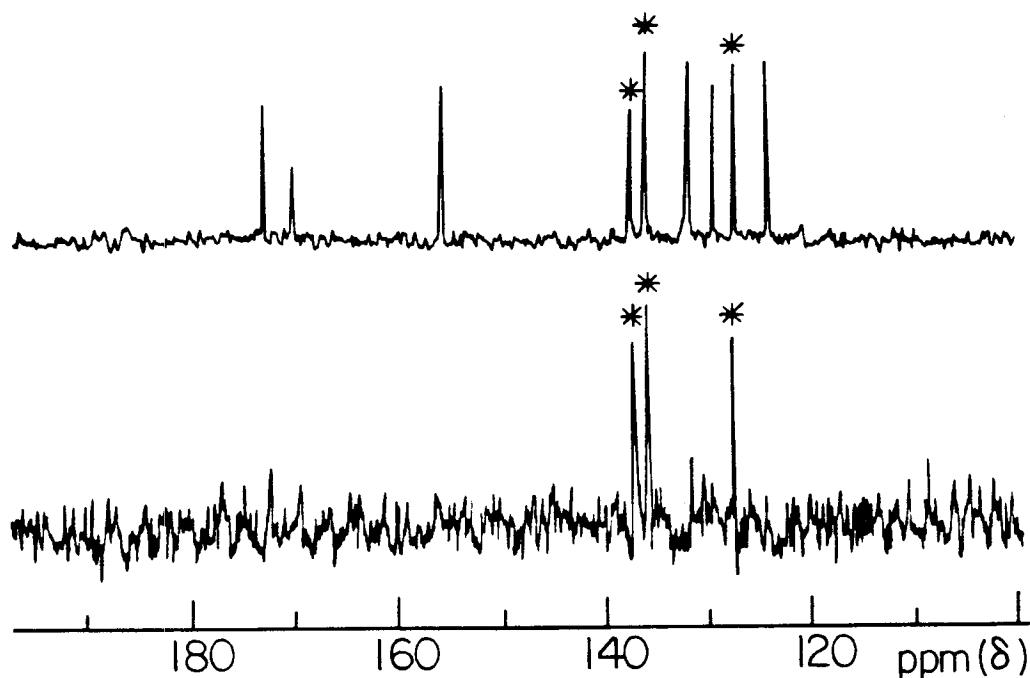


Figure 2.1. Top: ^{13}C NMR spectrum of **3**. Bottom: INEPTNON spectrum of **3**. This pulse sequence enhances only methyne carbon signals. All others are nullified.

carbon signals while nulling all others. This spectrum of **3** makes partial assignment of the ^{13}C NMR spectrum possible.¹⁵

Unlike potassium osmate, none of the PAC ligand complexes shows evidence of either chelate dissociation or amide hydrolysis in acidic, oxidative, or reductive media. Compound **3** undergoes reversible acid-base chemistry that is oxo-localized.

Brønstead acids turn orange solutions of **3** deep blue. The IR spectrum of the blue product, **4**, has PAC ligand bands similar to those recorded for **3** but has no *trans*-dioxo absorption. Furthermore, the

appearance of a broad band in the hydroxyl region (3400-3500 cm^{-1}) suggests that mono-protonation of one oxo ligand has occurred, producing *trans*-K[Os(η^4 -CHBA-DCB)(O)(OH)], **4**. The ^1H NMR spectrum of **4** is almost useless in that it shows the same pattern of chelate signals observed for **3** (one singlet and two doublets), but at new chemical shifts, and does not detect the rapidly exchanging hydroxyl protons. If allowed to remain in solution more than *ca.* 20 min, **4** precipitates and cannot be redissolved. Being an unsaturated 16-electron compound, **4** may polymerize through bridging hydroxyl groups. Hydroxyl-bridged dimers are known for Cu(II), Cr(III), Fe(III), Co(III), and Pb(III) metal centers.¹⁶ An isopiestic molecular weight determination proved unattainable due to the limited solubility of **4**.

The best evidence of **4** being protonated **3** is the efficient reversibility of the reaction. Successive protonation and deprotonation of **3** can be followed by ^1H NMR spectroscopy. Adding one drop conc. HClO_4 to an acetone- d_6 solution of **3** produces **4**. Subsequent addition of two drops triethylamine cleanly regenerates **3** as its triethylammonium salt.

By passing an acetone/THF (1:1 v/v) solution of **4** through anhydrous MgSO_4 , **4** is transformed into neutral square-pyramidal Os(η^4 -CHBA-DCB)(O), **5**. Isostructural complexes with aliphatic PAC ligands (η^4 -HMPA-B) $^{4-}$ and (η^4 -HMPA-DMP) $^{4-}$ have been well-characterized.^{17,18} New ^1H NMR signals characteristic of **5** are observed. The IR spectrum of **5** is the same as that of **3** except for a higher amide carbonyl band and a mono-oxo band in place of the *trans*-dioxo band (Table 2.1). PAC ligand complexes Os-(η^4 -HMPA-B)(O) and Os(η^4 -HMPA-DMP)(O) also exhibit high amide carbonyl bands, indicating that the amides may donate more strongly in mono-oxo compounds than in dianionic *trans*-

dioxo complexes because of more covalent Os-N bonds (eq 2.1). The mono-oxo IR band of **5** is lower than those of either aliphatic PAC ligand or bis-diolato complexes (Table 2.1).¹⁹ This implies that the osmium-oxo bond of **5** has lower bond order and, hence, weaker bond strength than the bonds of these other complexes. That is, **5** may be less stable than other osmium (VI) mono-oxo complexes. Consistent with this, **5** rapidly reverts to **4** upon exposure to traces of water, whereas mono-oxo complexes of aliphatic PAC ligands are impervious to hydrolysis.

An objective of this project has been the one- or two-electron oxidation of **3** to produce either an anionic Os(VII) or a neutral Os(VIII) dioxo complex. These would be exemplary high valent compounds stabilized by a PAC ligand. Unfortunately, most products from oxidation of **3** are difficult to characterize. Most oxidizing conditions (e.g., Cl₂/THF, PhIO, and solid state autoxidation at 130°C) convert **3** into a black amorphous material with only limited solubility. The oxidized product exhibits no NMR spectrum, prompting speculation that it may be paramagnetic Os(VII). The IR spectrum of it is almost able to be superimposed on that of **3** (Figure 2.2), the only differences being the absence of the 820 cm⁻¹ *trans*-dioxo band of **3** and a new absorption at 875 cm⁻¹ for the black material. This product may be the monoanionic Os(VII) analog of **3** or, more likely, oligomers of such complexes linked through μ -peroxo units. The latter explanation is consistent with the limited solubility, the lack of a ¹H NMR spectrum, and the new IR band at 875 cm⁻¹ ($\nu_{O-O(\mu\text{-peroxo})} = 790\text{-}930\text{ cm}^{-1}$)^{13b} of the oxidized product.

Table 2.1. Mono-oxo and Amide Carbonyl IR Bands of Square-pyramidal Os(VI) Mono-oxo Complexes.

Complex	$\nu_{\text{Os}=\text{O}}$ (cm^{-1})	$\nu_{\text{C}=\text{O}}$ (amide) (cm^{-1})
$\text{Os}(\text{O}_2(\text{CH}_2)_2)_2(\text{O})^{\text{b}}$	992	a
$\text{Os}(\text{O}_2(\text{CMe}_2)_2)_2(\text{O})^{\text{b}}$	978	a
$\text{Os}(\eta^4\text{-HMPA-B})(\text{O})^{\text{c}}$	962	1714
$\text{Os}(\eta^4\text{-HMPA-DMP})(\text{O})^{\text{c}}$	962	1710
$\text{Os}(\eta^4\text{-CHBA-DCB})(\text{O})$, 5 ,	939	1670
$\text{K}_2[\text{Os}(\eta^4\text{-CHBA-DCB})(\text{O})_2]$, 3	820 (dioxo)	1607

^a No amide groups. ^b Refs 17, 18. ^c Refs 1, 10.

No evidence for the formation of a neutral Os(VIII) dioxo complex has been obtained. We suspect that OsX_4O_2 species may be inherently unstable; the Os(VIII) fluoride analog of *trans*-Os(η^4 -CHBA-DCB)(O)₂, OsF₄O₂, is an unrealized synthetic target of fluorine chemists. Reactions of osmium metal with oxygen and fluorine gases at ratios varying between 0.5 and 2.0 (P_{O₂}:P_{F₂}) produce osmium complexes with ensuing ratios of oxide to fluoride ligands: OsF₆, OsF₅O, OsF₄O, and OsF₂O₃.²⁰ The formulation OsF₄O₂ is not detected. The investigators speculated that if OsF₄O₂ was formed, then it disproportionated into OsF₄O and O₂.

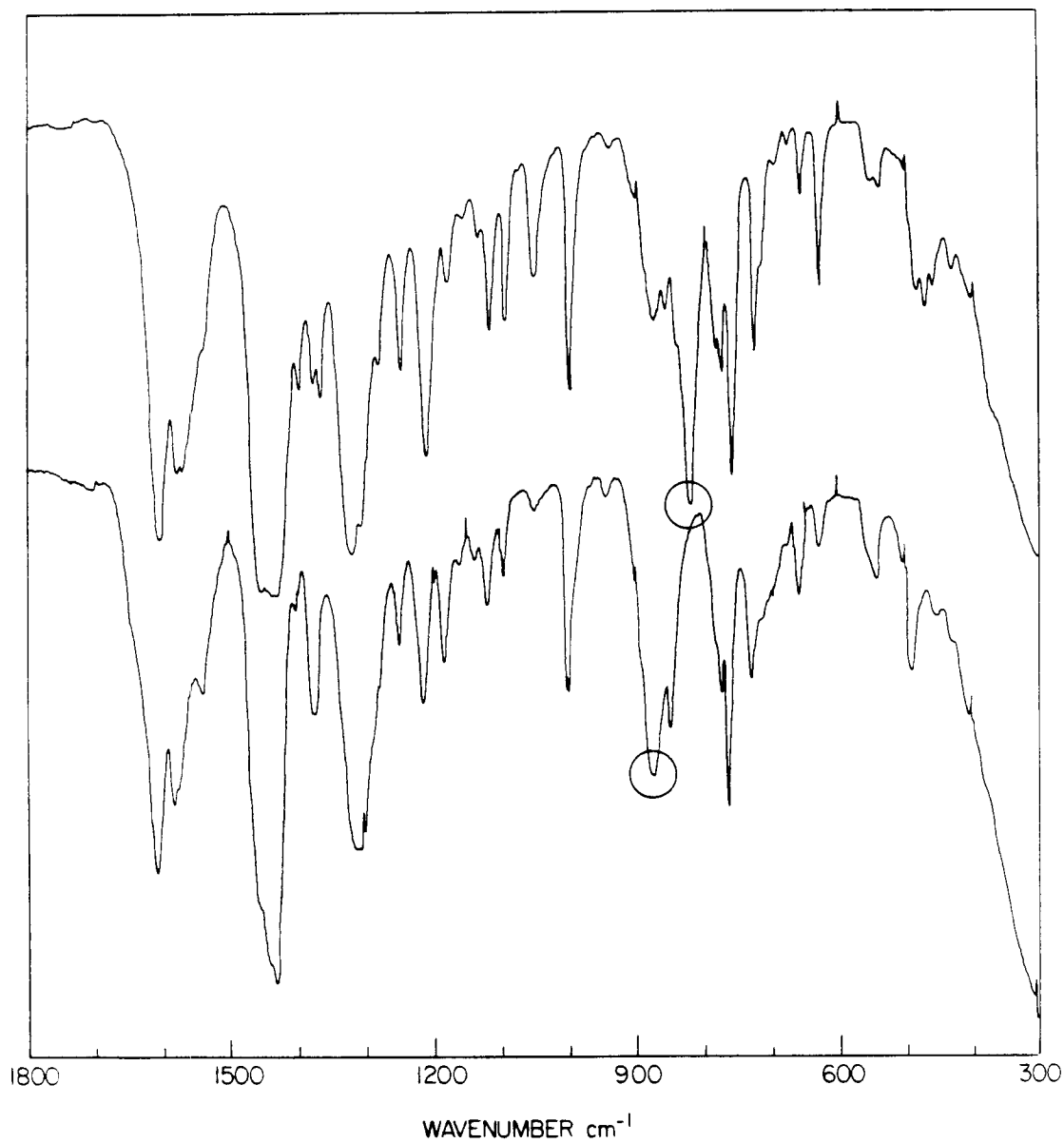


Figure 2.2. Superimposed IR spectra of **3** (top; 820 cm⁻¹ *trans*-dioxo band circled) and oxidized **3** (bottom; 875 cm⁻¹ new band circled).

Bromine is the only oxidant that reacts cleanly with **3**. Treatment of an orange THF solution of **3** with dry bromine produces a new complex, **6**, which has deep blue color and a ^1H NMR spectrum similar to that of protonated *trans*-dioxo, **4**. These similarities between **4** and **6** prompted speculation that they were identical. Trace HBr present in the bromine may have produced **4**. Compound **6**, however, is unaffected by the addition of excess triethylamine, whereas **4** reverts to **3** in the presence of excess triethylamine. Furthermore, **6** is synthesized with a large excess of K_2CO_3 present. The IR spectrum of **6** shows no oxo band and is similar to the spectrum of **4**. The spectrum of **4** shows a strong hydroxyl absorption at $3400\text{--}3500\text{ cm}^{-1}$, whereas **6** shows no activity in that region. The similarities in the NMR and IR spectra of the complexes suggest that they are isostructural. With these results and elemental analysis of **6**, we cautiously regard **6** to be a hypobromide complex, *trans*- $\text{K}[\text{Os}(\eta^4\text{-CHBA-DCB})(\text{O})(\text{OBr})]$. Presumably, treatment of **3** with bromine produces **6** and one equivalent of KBr. The amide carbonyl IR bands for **4** and **6** are strong, and no oxo band is apparent in either spectrum. Thus, the chemical modification that transforms **3** into either **4** or **6** occurs at the oxo ligands. Addition of ethanolic silver nitrate to a THF solution of **6** generates a white precipitate, AgBr, indicative of free bromide in solution. **6** remains unchanged for hours in the presence of Ag(I) but eventually decomposes and precipitates. A UV-vis spectroscopic titration of the bromination of **3** was attempted using THF stock solutions of Br_2 and **3**. Unfortunately, the instability of the bromine concentration precluded the experiment.

The reduction of **3** with a large excess of molten triphenylphosphine (*ca.* $250\text{ }^\circ\text{C}$) and trifluoroacetic acid (TFA) produces a

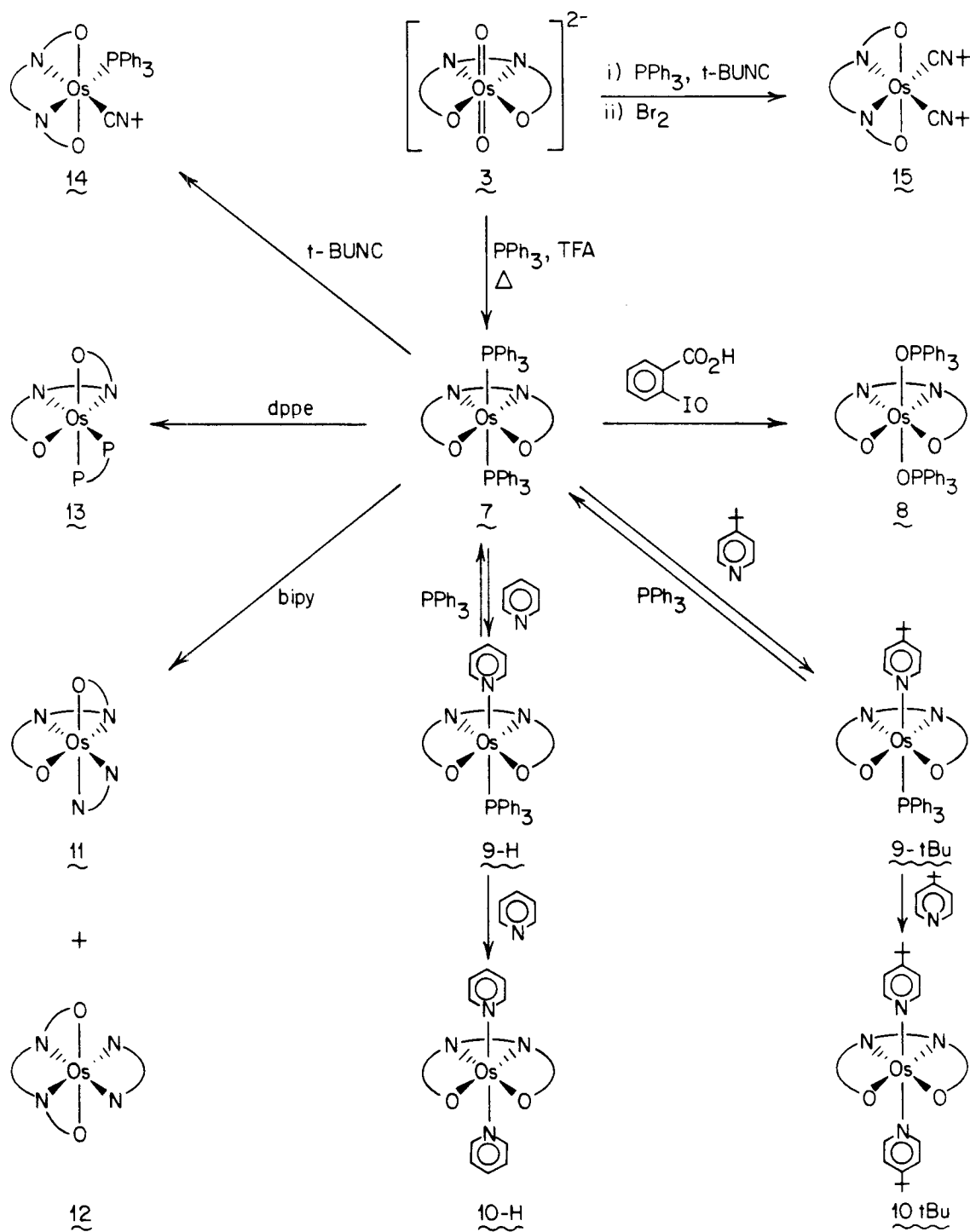
dark green Os(IV) complex, $\text{Os}(\eta^4\text{-CHBA-DCB})(\text{PPh}_3)_2$, **7**. The product is purified by elution with dichloromethane or benzene through silica gel. Recrystallization from hexane affords dark green crystals. Compound **7** is soluble in most solvents, except water, and will even color hexane. The stability of the complexed PAC ligand in the TFA-triphenylphosphine melt demonstrates that the ligand is robust; obviously, the design criterion for PAC ligand chemical resistance is satisfied by $(\eta^4\text{-CHBA-DCB})^{4-}$. No tractable products, much less $\text{Os}(\eta^4\text{-CHBA-Et})(\text{PPh}_3)_2$, can be isolated from reactions of molten triphenylphosphine, TFA, and $\text{K}_2[\text{Os}(\eta^4\text{-CHBA-Et})(\text{O})_2]$.⁶ The lability of the phosphine auxiliary ligands of **7** makes possible the synthesis of a large series of Os(IV) complexes.

Os(IV) Complexes of $(\eta^4\text{-CHBA-DCB})^{4-}$

Compound **7** has two triphenylphosphine ligands capable of ligand exchange chemistry as illustrated in Scheme 2.4. Most compounds in Scheme 2.4 have been characterized by ^1H NMR and IR spectroscopies, elemental analysis, and cyclic voltammetry. This series of Os(IV) complexes gave us the opportunity to examine the stability imparted from the PAC ligand $(\eta^4\text{-CHBA-DCB})^{4-}$ to osmium compounds with various auxiliary ligands and isomeric forms.

Three hypothetical isomers exist for an octahedral complex containing a tetradentate ligand and two identical monodentate ligands; trans, cis- β , and cis- α (Figure 2.3). In trans isomers, a planar chelate coordinates around the metal center, while the auxiliary ligands reside trans to one another.

Scheme 2.4. Synthesis of Os(IV) Complexes.



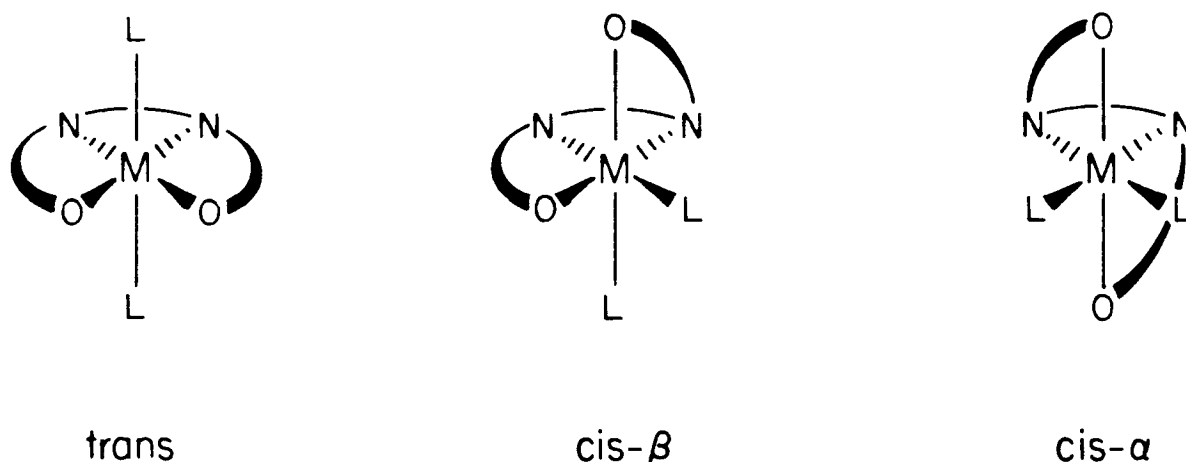


Figure 2.3. The three possible isomers of $M(\eta^4-L')(L)_2$ compounds (ref 21).

Trans isomers are achiral meso complexes with C_{2v} symmetry. As a cis- β isomer, one axial and three equatorial metal sites are occupied by the chelating ligand. The two monodentate ligands bind cis to one another. This isomer has the lowest symmetry of the three possible isomers, C_1 , and is chiral, possessing both D and L forms. As a cis- α isomer, both terminal ends of the chelate occupy axial metal sites, and the remaining ligation occupies equatorial sites. This isomer possesses one C_2 axis and is chiral, having both D and L forms. In the absence of a chiral bias, cis complexes exist as racemic mixtures. All cis compounds reported herein are racemic DL mixtures. This nomenclature was first established by Sargeson *et al.* for describing the Co(III) triethylenetetramine (trien) complexes of the type $[Co(trien)X_2]^+$.²¹ The terminology has since been used to describe complexes of tetradentate Schiff's bases, such as the [N,N'-ethylenebis-(salicylideneimine)] ligand.²² Henceforth, isomeric forms will be included

in naming PAC ligand complexes. For example, **7** is explicitly labelled *trans*-Os(η^4 -CHBA-DCB)(PPh₃)₂.

Reacting **7** with *o*-iodosobenzoic acid oxidizes both phosphine ligands rather than the Os(IV) metal center and produces red-brown *trans*-Os(η^4 -CHBA-DCB)(O=PPh₃)₂, **8**. Stronger oxidants (e.g., peroxides, iodosobenzene and nitrous oxide) transform **7** into **8** but form decomposition by-products also. Because *o*-iodosobenzoic acid is a single oxygen atom source, two equivalences are necessary to produce **8** (although an excess is actually used). Under the conditions to form **8**, no mono-oxidized intermediate, *trans*-Os(η^4 -CHBA-DCB)(PPh₃)(O=PPh₃), is detected by TLC. Slow room temperature reactions of oxidants with **7** produce a transient turquoise product that is absent with additional reaction time or higher reaction temperature. This complex may be the half-oxidized complex. Unlike the phosphine groups of **7**, the phosphine oxide ligands of **8** do not exchange with excess phosphine or pyridine, a somewhat surprising result for what is commonly considered a weak ligand.

Gently warming a methylene chloride solution of **7** with 4-*tert*-butylpyridine induces substitution of one phosphine by *t*-Bupy, forming *trans*-Os(η^4 -CHBA-DCB)(PPh₃)(*t*-Bupy), **9-*t*Bu**. Substitution of the second phosphine is more sluggish than the first. A neat *t*-Bupy solution of **7** is heated under reflux, which generates high reaction temperatures and high concentrations of *t*-Bupy. A 68% isolated yield of *trans*-Os(η^4 -CHBA-DCB), **10-*t*Bu**, can be achieved using this procedure. Using neat pyridine in place of *t*-Bupy produces *trans*-Os(η^4 -CHBA-DCB)(PPh₃)(py), **9-H**, and *trans*-Os(η^4 -CHBA-DCB)(py)₂, **10-H**, substitution products. This synthesis takes 16 hours, whereas production of **10-*t*Bu** requires only 15

minutes. We presume that the lower boiling point of pyridine (115 °C) compared to that of *t*-Bupy (197 °C) necessitates longer reaction time. The first *t*-Bupy substitution reaction is reversible. When added to a heated chloroform solution of PPh₃, **9-*t*Bu** reverts to **7**. Furthermore, if **9-*t*Bu** is heated in the presence of 4-acetylpyridine, then *trans*-Os(η^4 -CHBA-DCB)(PPh₃)(Acpy), **9-Ac**, is produced. Bis-substituted products **10-*t*Bu** and **10-H**, on the other hand, show no propensity towards substitution in the presence of excess phosphine or pyridines. The differences between the **9-L** substitution reactions and the **10-L** reactions suggest that kinetic effects control the substitution processes rather than thermodynamic effects (*vide infra*).

The first substitution proceeds more readily than the second. This may be due to the greater kinetic *trans* effect of phosphine over pyridine ligands.^{23a} A *trans* effect is the through-metal influence of a static ligand upon the substitution kinetics of a ligand *trans* to it; faster or slower kinetic substitution rates can be achieved by changing the static ligand. In the mono-substitution reaction of **7**, the *trans* effect of one phosphine may facilitate substitution of the other. In the conversion of **9-H** to **10-H**, however, the pyridine ligand exerts a weak *trans* effect upon the *trans* phosphine ligand, and forcing conditions are required to carry out secondary substitution. The mixed-pyridine reaction of **9-*t*Bu** and Acpy suggests that the substitutions are under kinetic control (Figure 2.4). The Os-py bond should be stronger than the Os-PPh₃ bond because of better overlap between the osmium orbitals and the nitrogen orbitals. Under

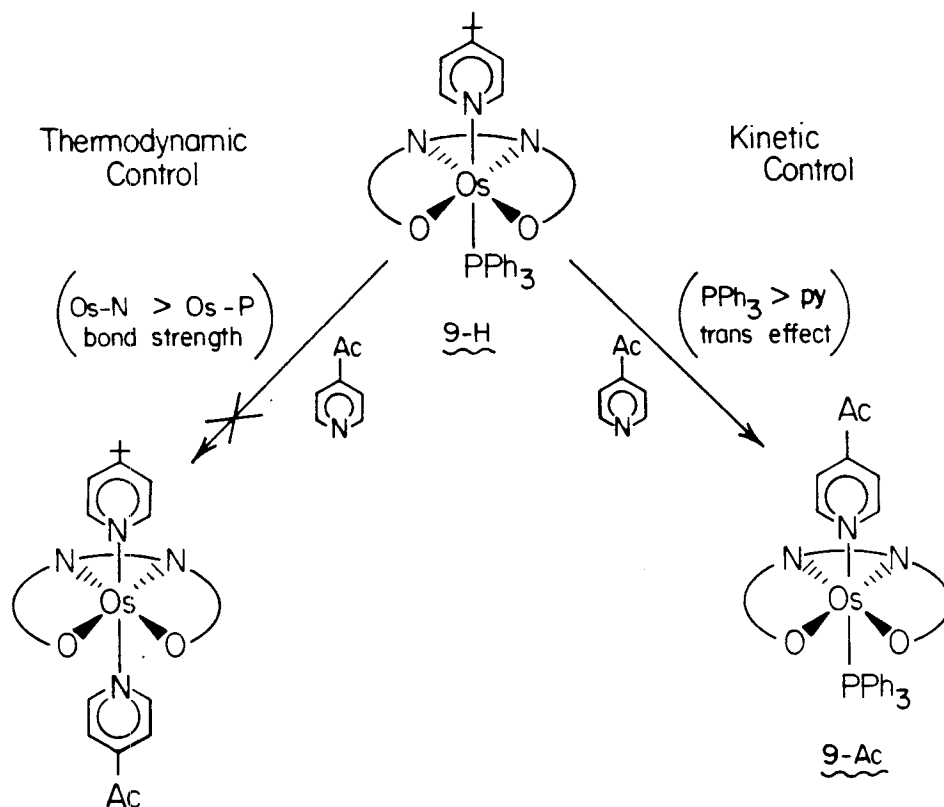


Figure 2.4. Different products expected from mixed-pyridine substitutions of **9-*t*Bu** under thermodynamic and kinetic controls.

strict thermodynamic control, the Acpy should displace the phosphine ligand to produce the most stable product, *trans*-Os(η^4 -CHBA-DCB)(py)(Acpy). Instead, the Acpy exchanges for the *t*-Bupy ligand generating **9-Ac**, the expected product if kinetic control dominates.

The mechanism of the phosphine substitutions has interested us. The kinetics of the initial phosphine substitution of **7** by *t*-Bupy have been studied by Sonny C. Lee, an undergraduate in our group.²⁴ Rates were conveniently measured by UV-vis spectroscopy. The rate equation proved to be first-order in concentration of **7** and independent of *t*-Bupy concentrations over the range of 5 to 113 mM at 50 °C (Figure 2.5).

Substitution products were identical to authentic samples when examined by UV-vis spectroscopy and TLC. The activation parameters were calculated from rates at temperatures of 35 to 65 °C: $\Delta H^\ddagger = 29.7 \pm 0.6$ kcal/mol; $\Delta S^\ddagger = 19 \pm 2$ eu. The large enthalpy factor and positive entropy factor are consistent with a dissociative mechanism, **D**,^{23a} where extrusion of a phosphine ligand precedes *t*-Bupy coordination. This mechanism also explains the apparent zero-order dependence on *t*-Bupy concentration. This mechanistic result surprised us. Predissociation of a phosphine ligand generates a 14-electron, square-pyramidal intermediate of questionable stability. We anticipated an associative mechanism to dominate where *t*-Bupy preassociates to **7** and phosphine is subsequently extruded. Being coordinatively unsaturated, **7** could bind a seventh ligand and produce an 18-electron intermediate. Stable seven-coordinate Os(IV) complexes are known, in fact.²⁵ A concerted displacement where both the incoming and leaving groups are weakly bound to the metal center in the transition state can account for the first-order rate expression without inferring an unreasonable five-coordinate intermediate. Such a mechanism has been termed dissociative interchange, **I_d**, by Langford and Gray.^{23a} An extensive kinetic investigation would be necessary to determine whether **D** or **I_d** mechanisms are responsible for the initial substitution.^{23b-d}

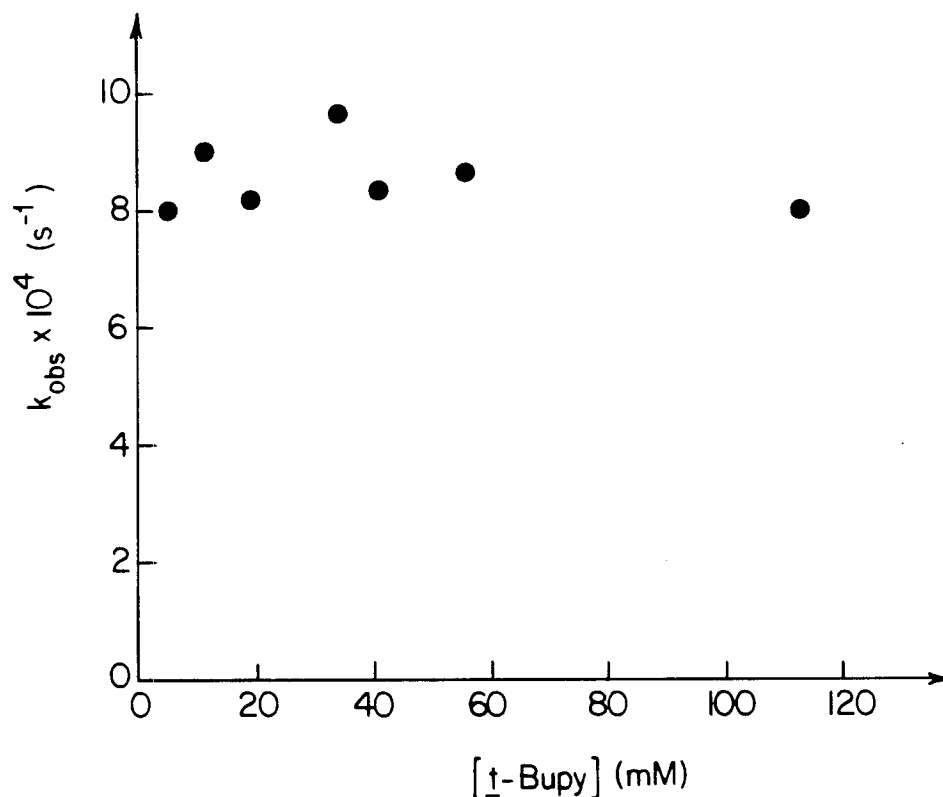


Figure 2.5. Rate of mono-phosphine substitution of **7** vs. *t*-Bupy concentration at 50 °C.

The phosphine lability of **7** is unprecedented in Os(IV) chemistry.^{26,34} When heated in the presence of a Lewis base, L', osmium compounds of the type OsX_4L_2 (X = Br, Cl; L = phosphine ligands) generally form products of the type $[\text{OsXL}_2\text{L}'_3]\text{X}_2$.^{26a} The only analogous example of substitution is dppe exchanging for two $\text{PPh}(i\text{-Bu})_2$ ligands.^{26e} Two reasons may explain the different reactivities of halide and PAC ligand complexes. The chelation of a PAC ligand restricts heterolytic dissociation of it. The only exchangeable ligands are the phosphine ligands. Strong σ -donation of the PAC ligand may labilize the auxiliary ligands by delivering sufficient electron density to the metal center to activate the Os-P bond, a type of cis effect.^{23a} This assertion, however,

Table 2.2. First-order Rate Constants for Substitution of PPh₃ by *t*-Bupy in 7 Measured in Toluene Solution.

T (°C)	[<i>t</i> -Bupy](mM)	$k_{\text{obs}} \times 10^4 \text{ (s}^{-1}\text{)}^{\text{b}}$	T (°C)	[<i>t</i> -Bupy](mM)	$k_{\text{obs}} \times 10^4 \text{ (s}^{-1}\text{)}^{\text{b}}$
50.0	5.0	8.00(1)	35.0	23.0	0.800(1)
50.0	11.0	9.00(1)	40.0	24.0	1.77(1)
50.0	19.0	8.17(1)	45.0	23.0	4.03(1)
50.0	34.0	9.67(1)	50.0	19.0	8.20(1)
50.0	41.0	8.33(1)	55.0	24.0	17.1 (1)
50.0	56.0	8.67(1)	60.0	23.0	33.3 (1)
50.0	113.0	8.00(1)	65.0	23.0	65.2 (1)

^a The estimated error in the temperature of the cell is ± 0.5 °C.^b Figures in parentheses are the standard deviations in the last digit.

may be difficult to prove because *cis* effects are typically small and irregular compared to *trans* effects.

Reacting potentially bidentate Lewis bases with **7** requires the formation of *cis*- β or *cis*- α products. Assuming static structures in solution, ^1H NMR spectroscopy is sufficient to distinguish the isomers. In *cis*- β isomers, all six (η^4 -CHBA-DCB) $^{4-}$ ligand protons are unique, whereas in *cis*- α isomers, the C_2 axis reduces the number to three inequivalent protons.

Three such *cis* complexes have been synthesized using dppe and bipy (Scheme 2.4). Reacting **7** with dppe produces *cis*- β -Os(η^4 -CHBA-DCB)(dppe), **13**, which can be isolated in high yields. The ^1H NMR spectrum of **13** contains the pattern of PAC ligand signals expected for the *cis*- β isomer. The large number of aromatic protons and the low symmetry of **13** makes for a highly congested aromatic region. Selective ^1H decoupling of each signal at 400 MHz is necessary to assign the spectrum. Reacting **7** with bipy produces a mixture of both *cis* isomers: *cis*- β -Os(η^4 -CHBA-DCB)(bipy), **11**, and *cis*- α -Os(η^4 -CHBA-DCB)(bipy), **12**. Column chromatography with silica gel adequately separates the isomers, which are subsequently recrystallized from CH_2Cl_2 /hexane. As with **13**, ^1H NMR spectroscopy unambiguously identifies each isomer. In the spectrum of **11**, all of the bipy protons are inequivalent, yet well-separated. A 2-D COSY spectrum was used to fully assign the spectrum in lieu of multiple spin decoupling experiments.^{15,27} Compound **11** has been structurally characterized by X-ray crystallography (see Chapter 2).

Two neutral Os(IV) complexes with monodentate ligands form stable *cis*- α isomers. Mono-substitution of *t*-BuNC for a phosphine ligand in **7** generates *cis*- α -Os(η^4 -CHBA-DCB)(PPh₃)(*t*-BuNC), **14**. The ^1H NMR

spectrum shows six inequivalent PAC ligand protons, indicating that **14** is a cis isomer. Structural characterization of **14** was necessary to prove its cis- α geometry (see Chapter 2). In the IR spectrum, the C \equiv N band at 2160 cm⁻¹ is low for bound isocyanide ligands and suggests that back-bonding is occurring. This implies that the Os(IV) metal center is electron-rich. The amide carbonyl band of **14** at 1650 cm⁻¹ is higher than those of trans Os(IV) complexes (1590-1620 cm⁻¹), which indicates that more covalent Os-N bonding is present (eq 2.1) and that there is stronger donation from the N-amido ligands to the osmium metal center in the cis- α isomer than in trans isomers.

Besides the substitution of phosphine ligands of **7**, a second route into neutral Os(IV) complexes exists that starts with *trans*-dioxo **3**. Reducing **3** with triphenylphosphine in the presence of an excess of the desired ligand L produces an Os(III) intermediate, [Os(η^4 -CHBA-DCB)L₂]⁻. Oxidizing this with either bromine or hydrogen peroxide cleanly converts it to the neutral Os(IV) complex Os(η^4 -CHBA-DCB)L₂. This route was developed and optimized by Dr. Terry E. Krafft for producing *trans*-Os(η^4 -CHBA-Et)(py)₂.⁶ Direct reduction of **7** with phosphine in the presence of excess *t*-BuNC generates the red Os(III) intermediate [Os(η^4 -CHBA-DCB)(*t*-BuNC)₂]⁻. After bromine oxidation of this intermediate, moderate yields of neutral *trans*-Os(η^4 -CHBA-DCB)(*t*-BuNC)₂, **15**, can be isolated. The ¹H NMR spectrum of **15** reveals equivalent *tert*-butyl groups and three chelate resonances. Initially, we thought **15** was trans, but its IR spectrum shows two $\nu_{\text{N}\equiv\text{C}}$ bands at 2209 cm⁻¹ and 2183 cm⁻¹ (in both solid state and solution IR spectra), indicating cis isocyanide ligands; **15** is actually a cis- α isomer, not trans. The replacement of either one or both phosphines of **7** with π -acidic *t*-BuNC

ligands generates cis- α isomer products. One might assume that the incorporation of electron-withdrawing isocyanide ligands triggers the formation of cis- α isomers. The enhanced donation to the metal from the N-amido ligands of the cis- α isomers could compensate for the effects of the π -acids. Electrochemistry has proven a useful tool for characterizing compounds and determining the relative donating abilities of different ligands and different isomeric forms.

Electrochemistry of Os(IV) Compounds

The electrochemistry of the Os(IV) (η^4 -CHBA-DCB) $^{4-}$ complexes was examined, and, as we had hoped, it showed reversible oxidations of Os(IV) to Os(V). In 0.1 M TBAP in CH₂Cl₂, the complexes show reversible Os(III/II), Os (IV/III), and Os(V/IV) couples by cyclic voltammetry. The cyclic voltammogram (CV) of **10-*t*Bu** is exemplary both in appearance and in simplicity of the electrochemistry of these Os(IV) compounds (Figure 2.6). Thus, the replacement of the ethylene bridge in (η^4 -CHBA-Et) $^{4-}$ with a dichlorophenylene bridge to produce (η^4 -CHBA-DCB) $^{4-}$ eliminates undesirable oxidative degradation reactions. This initial objective of the (η^4 -CHBA-DCB) $^{4-}$ project was fulfilled. The electrochemical data for the Os(IV) complexes described previously are summarized in Table 2.3.

The formal potentials of the Os(III/II), Os(IV/III), and Os(V/IV) couples vary substantially depending upon the auxiliary ligands. For example, the potential for the Os(V/IV) couple of **10-H** is at +0.72 V, whereas that of **8** is at + 0.47 V. This variation suggests that the electrochemical couples are metal-centered rather than chelate-centered. Thus, the oxidations are Os(V/IV) couples. Being stable to bulk electrolysis, stable solutions of cationic Os(V) complexes have been

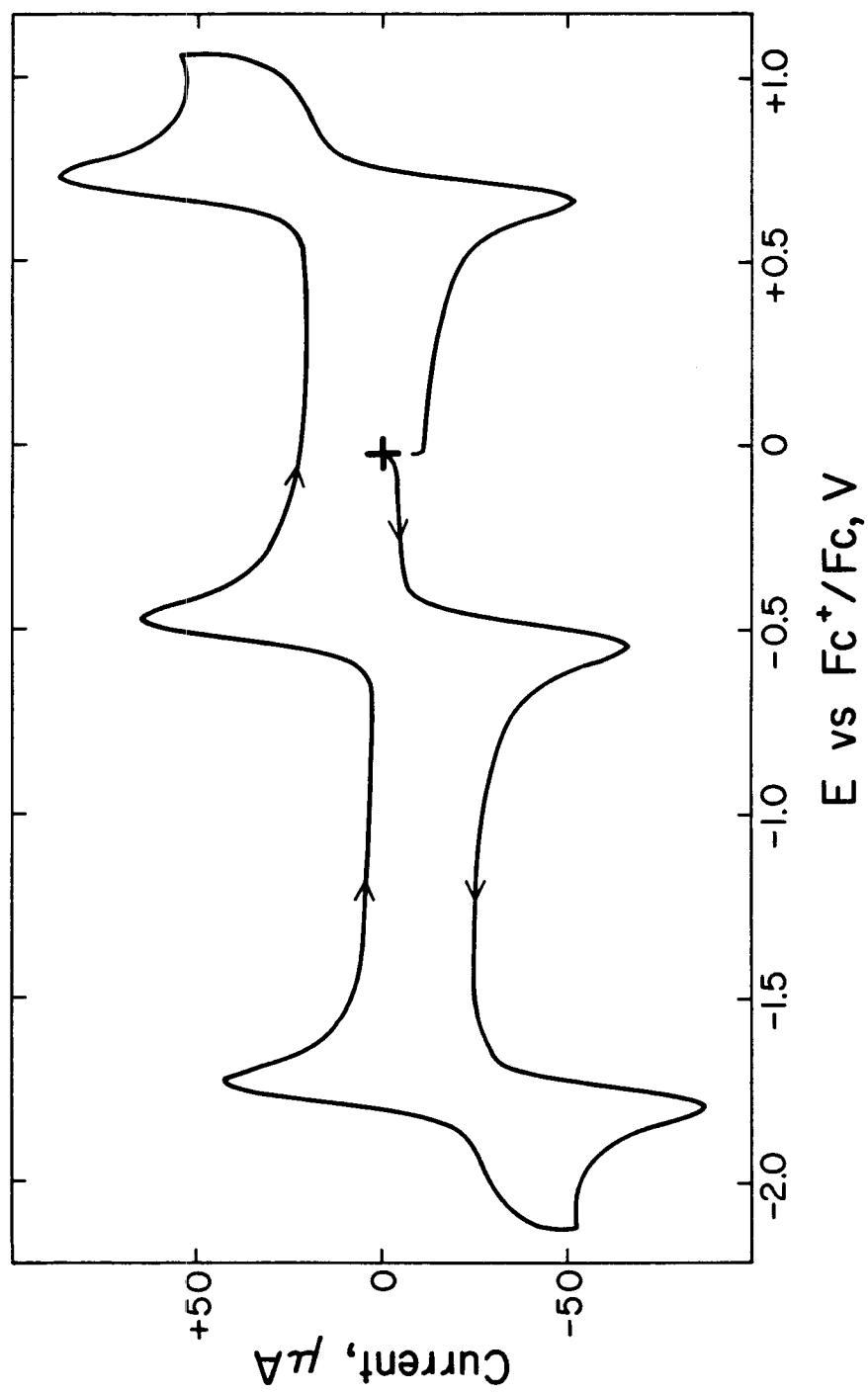


Figure 2.6. Cyclic voltammogram of 1 mM 10-*t*Bu in $\text{CH}_2\text{Cl}_2/0.1$ M TBAP at 0.17 cm^2 BPG electrode.

Scan rate = 200 mV/s.

Table 2.3. Formal Potentials of the Os(III/II), Os(IV/III), and Os(V/IV) Couples of the Os(IV) Complexes.

	Os(η^4 -CHBA-DCB) L_2 $L_2 =$	Isomer	Formal Potentials (V) ^a		
			Os(III/II)	Os(IV/III)	Os(V/IV)
7	(PPh ₃) ₂	trans	(-1.72) ^b	-0.46	+0.59
8	(O=PPh ₃) ₂	trans	c	-1.05	+0.47
10-<i>t</i>Bu	(<i>t</i> -Bupy) ₂	trans	-1.77	-0.51	+0.70
10-H	(py) ₂	trans	-1.68	-0.44	+0.72
11	(bipy)	cis- β	-1.37	-0.49	+0.50
12	(bipy)	cis- α	-1.45	-0.86	+0.49
13	(dppe)	cis- β	-1.22	-0.37	+0.55
14	(PPh ₃)(<i>t</i> -BuNC)	cis- α	-1.25	-0.64	+0.74
15	(<i>t</i> -BuNC) ₂	cis- α	-1.05	-0.57	+0.92

^a Measured in CH₂Cl₂/0.1 M TBAP and referenced to Fc⁺/Fc internal standard. ^b Peak potential of irreversible reduction to Os(II). ^c Not observed at $E < -2.3$ V.

produced. Compounds at the Os(V) oxidation state were previously thought to be unstable.²⁸ This has been commonly attributed to a characteristic instability of osmium at that oxidation state. The powerful electron-donation of the (η^4 -CHBA-DCB)⁴⁻ ligand stabilizes this valence state making possible the production of solution-stable Os(V) complexes. When the Os(V/IV) couple is considered, however, quinoidal resonance forms of the PAC ligand may contribute at the higher Os(V) oxidation state affecting the formal oxidation state assignment. These resonance forms, shown in Figure 2.7, can be both bridge-localized (benzoquinonediimine, A, and semibenzoquinonediimine, B) and arm-localized (quininoid, C). Crystal structure data of compounds 11 and 14 show little foreshortening of either the bridge C-N bonds or the phenolate C-O bonds, which would be expected if structures A, B, or D contributed significantly. (See Tables 3.1 and 3.3 for bond length data.) These resonance forms cannot contribute to the dianionic Os(II) complexes without violating the 18-electron rule for transition metal complexes. No structural data are yet available for an Os(V) complex where bond length changes should be most pronounced. The formal potential for the oxidation of *trans*-Os(η^4 -CHBA-Et)(py)₂ in liquid SO₂, + 0.86 V, is only slightly higher than that of 10-H, +0.82 V. Because structures A and B do not exist for the aliphatic-bridged (η^4 -CHBA-Et)⁴⁻ ligand, a larger difference would be anticipated if the resonance forms contributed to [10-H]⁺. Although structural and electrochemical evidence suggests that quinoidal resonance structures do not contribute, the oxidation states of the cationic complexes are cautiously regarded as Os(V).

The extraordinary stabilization derived from the PAC ligand is demonstrated by comparing the formal oxidation potentials of 7, *trans*-

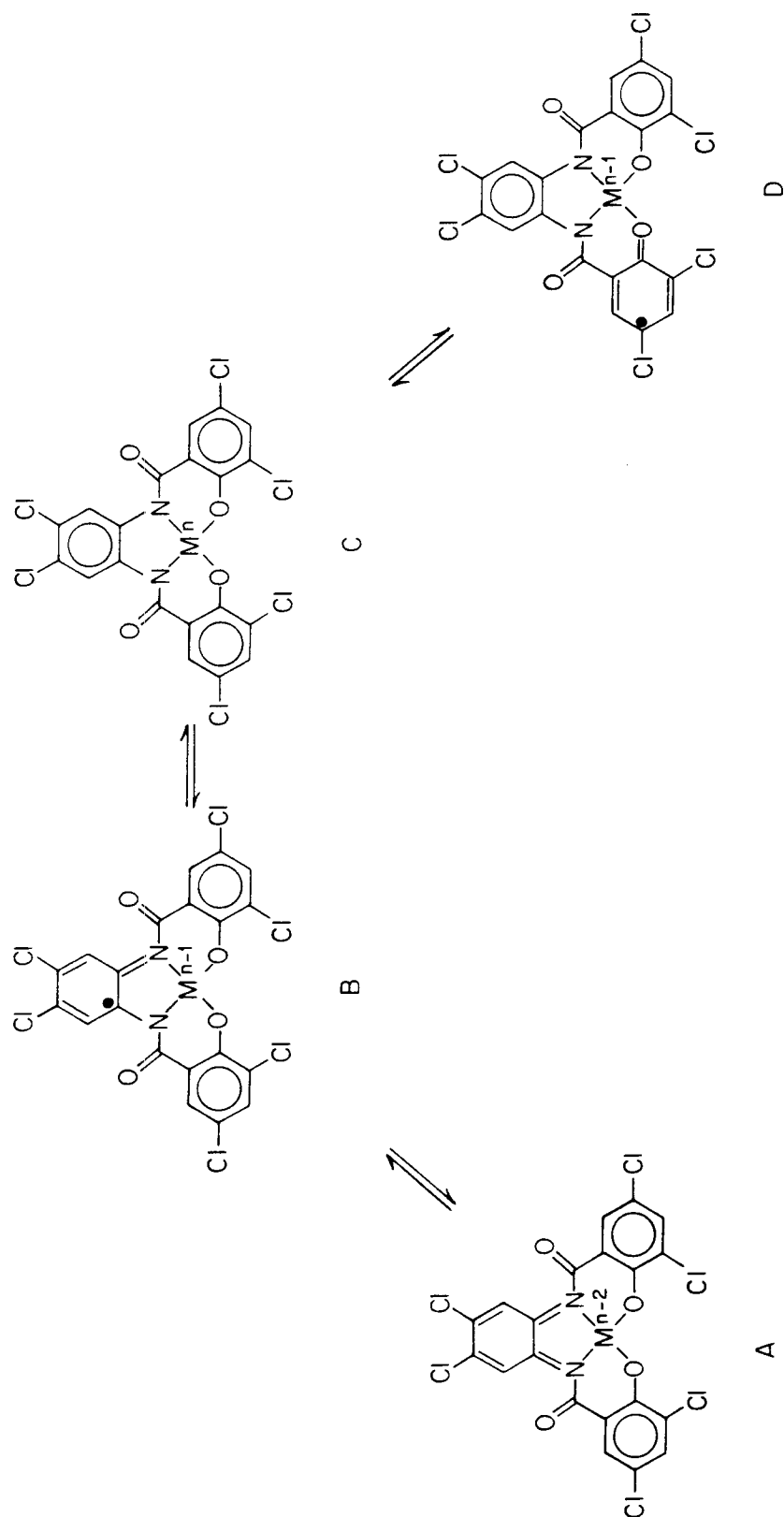


Figure 2.7. Quinoidal resonance forms of the metal-chelate moiety.

OsCl₄(PPh₃)₂, and [OsCl₆]²⁻ (Table 2.4). The oxidation of *trans*-OsCl₄(PPh₃)₂ occurs at a potential 750 mV higher than that of **7**. The cationic product is not stable as evidenced by the irreversibility of the couple. Because the oxidation of *trans*-OsCl₄(PPh₃)₂ is irreversible, its formal potential cannot be measured. The subsequent chemical reaction causing the irreversibility lowers the anodic peak potential; hence, the 750 mV estimated difference in formal potentials is a lower limit. The PAC ligand is more inert to oxidation and a better electron-donor to the metal center than simple chloride ligands. The formal potential of the Os(V/IV) couple of **7** is also lower than that of dianionic hexachloroosmate. The Os(III/II) formal potential of **7** is 340 mV lower than that of *trans*-OsCl₄(PPh₃)₂. We cite these systematic differences between the formal potentials of the oxidation and reduction couples of **7** and those of related halide complexes as unambiguous evidence that PAC ligands are more powerful electron-donors to a metal center than traditional halide ligands.

Electro-oxidation of the Os(IV) complexes in CH₂Cl₂ is limited by the oxidative limit of the solvent, *ca.* +1.4 V vs. Fc⁺/Fc. Up to this threshold, no anodic activity past the Os(V/IV) couple can be observed. A solvent with a higher anodic range was required to probe the higher oxidations of the osmium compounds. Liquid SO₂ provides sufficient anodic range for these experiments. It is an aprotic, dipolar solvent (dielectric constant of 24.9 at -69 °C) with a wide liquid range (-75 to -10 °C).³⁰ Recent reports in the literature by Bard *et al.* have documented its

Table 2.4. Comparisons of Formal Potentials of **7** with Os(IV) Halide Complexes.

Compound	Formal Potential (V) ^a	
	Os(IV/III)	Os(V/IV)
<i>trans</i> -Os(η^4 -CHBA-DCB)(PPh ₃) ₂ , 7	-0.46	+0.59
<i>trans</i> -OsCl ₄ (PPh ₃) ₂ ^b	-0.12	(+1.34) ^c
[OsCl ₆] ²⁻ ^d	-1.19	+0.74

^a Measured in CH₂Cl₂/0.1 M TBAP and referenced to Fc⁺/Fc internal standard. ^b Ref 29. ^c Peak potential of irreversible oxidation to Os(V). ^d Ref 28g.

use as an electrochemical solvent.³ With TBAP as the supporting electrolyte, the anodic limit of liquid SO₂ is about +3.0 V vs. Fc⁺/Fc, and with TBABF₄ or TBAPF₆ as the supporting electrolyte, about 3.5 V vs. Fc⁺/Fc.

The CV of **7** in liquid SO₂ is shown in Figure 2.8. The Os(IV/III) couple is seen at $E_f = -0.14$ V vs. Fc⁺/Fc, and three reversible oxidations are seen at +0.72, +1.29, and +1.71 V. Following the third reversible oxidation, irreversible anodic activity begins. An almost identical CV was recorded for **10-H** in liquid SO₂. The second and third oxidations of **15** are not completely reversible. All of the data from the liquid SO₂ electrochemistry of **7**, **10-H**, and **15** are summarized in Table 2.5.

Large variations in the formal potentials for oxidation and reduction couples with different auxiliary ligands, which are cited as evidence for metal-centered activity, are not observed in the Os(2+/+), Os(3+/2+), and irreversible Os(4+/3+) oxidations of **7** and **10-H**. The

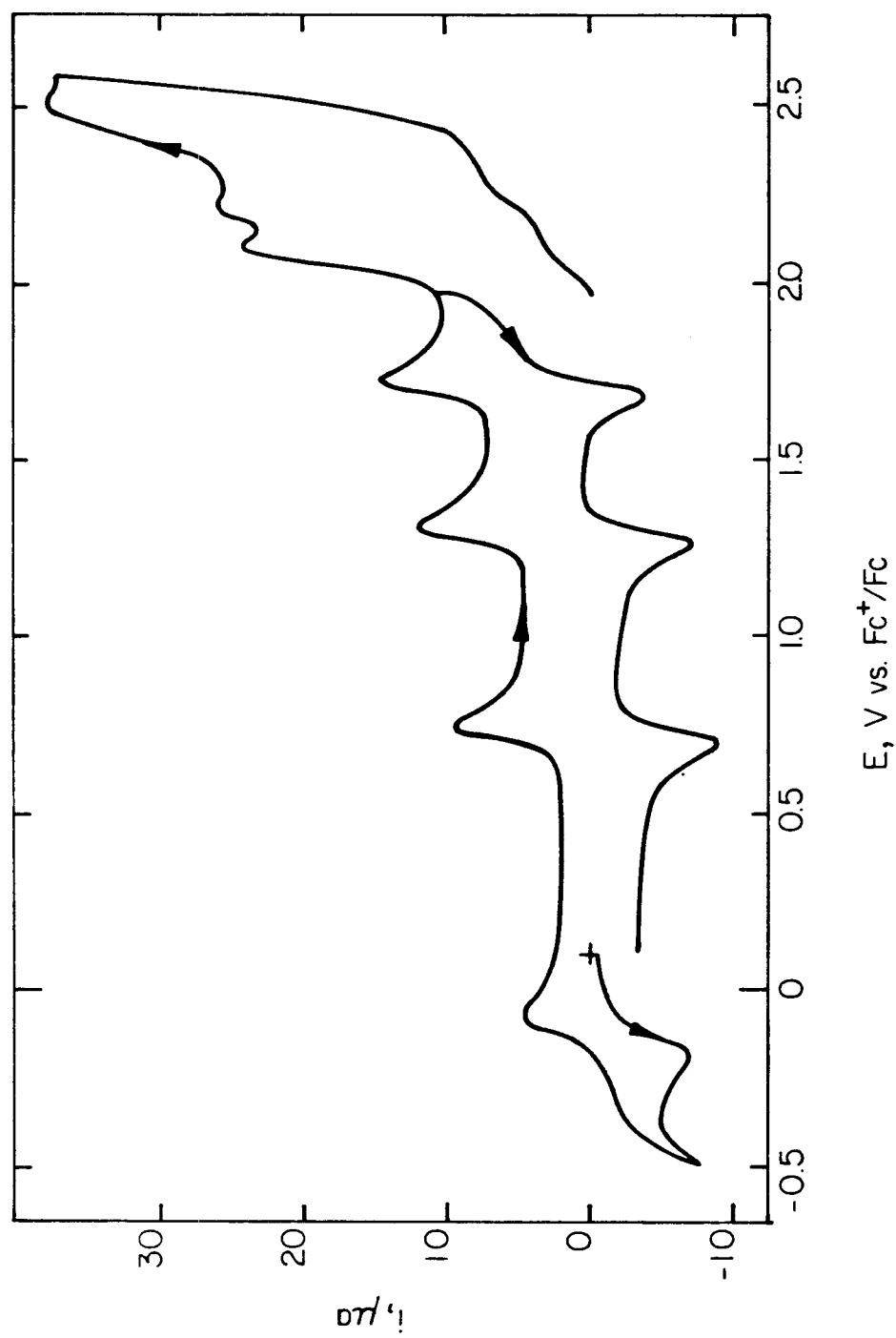


Figure 2.8. Cyclic voltammogram of 1 mM **7** in $\text{SO}_2/0.1 \text{ M TBABF}_4$ at -60°C with $0.02 \text{ cm}^2 \text{ Pt}$ electrode. Scan rate = 200 mV/s .

Table 2.5. Formal Potentials of Os(η^4 -CHBA-DCB)L₂ Complexes in SO₂

Os(η^4 -CHBA-DCB)L ₂	Formal Potentials (V) ^a				
	Os(IV/III)	Os(V/IV)	2 ⁺ / ⁺	3 ⁺ /2 ⁺	4 ⁺ /3 ⁺ + b
L ₂ = (PPh ₃) ₂ ^c , 7	-0.14	+0.72	+1.29	+1.71	(+2.16)
(py) ₂ ^c , 10-H	-0.15	+0.82	+1.29	+1.69	(+2.12)
(<i>t</i> -BuNC) ₂ ^d , 15	-0.30	+0.98	+1.48 ^e	+1.70 ^e	(+2.20)

^a Formal potential measured in SO₂/0.1 M TBABF₄ and referenced to Fc⁺/Fc internal standard. ^b Peak potential of irreversible oxidation. ^c Trans isomer. ^d Cis- α isomer. ^e Oxidations not completely reversible.

formal potentials for oxidation of **15** are less certain due to the problems with electrochemical reversibility. The similarity in the formal potentials of the second, third, and fourth oxidations of **7** and **10-H** indicates that these oxidations may be ligand-localized and do not represent Os(VI/V), Os(VII/VI), and Os(VIII/VII) couples.

The stabilities of the second and third oxidation products of **7** and **10-H** were investigated by controlled-potential electrolysis experiments. As observed in CH₂Cl₂ solvent, the first oxidation product of each compound is stable with only occasional minor impurities detectable in the CVs following electrolysis. Several attempts at isolating [10-H]⁺ by precipitating it from SO₂ with benzene or chlorobenzene had only limited success. Dicationic [10-H]²⁺ is stable in solution or as a solid under vacuum at -40 °C . When the solid is warmed to room temperature, it rapidly decomposes to a brown material having no reversible electrochemistry. Reactions using a solution of [10-H]²⁺ to oxidize a substrate at -40 °C are feasible but have not been conducted. The third oxidation product, [10-H]³⁺, decomposes in solution at -40 °C. The second and third oxidation products of **7** are even less stable than those of **10-H**. The marginal stability of [7]³⁺, [10-H]²⁺, and [10-H]³⁺ will hinder potential application of them as oxidants. These results have prompted efforts to synthesize new PAC ligands with protected aliphatic frameworks that may be more stable in highly oxidizing conditions.¹⁰

Magnetic Properties of Os(IV) Complexes

All of the trans and cis- β complexes exhibit well-resolved, paramagnetically shifted NMR spectra. For example, in the ^1H NMR spectrum of 10-H, the ortho pyridine protons appear upfield of TMS at -7.15 ppm, whereas the meta protons appear at +8.30 ppm in the normal region for aromatic protons. The ^{31}P NMR signals for the dppe ligand of 13 are measured at -992.9 and -1015.6 relative to an 85% H_3PO_4 standard.^{27b} Spectra of this type have been observed previously for Os(IV) complexes.³⁴ Though trans and cis- β isomers are paramagnetic, cis- α isomers 14 and 15 are diamagnetic. Changes in the energy levels and relative order of the osmium molecular orbitals (MOs) resulting from isomerization may account for the diamagnetism of the cis- α isomers. We wanted to investigate the magnetic properties of the osmium in order to understand the effects seen in NMR spectra and ultimately to ascertain the molecular orbital configuration at the metal center. If Curie-Weiss behavior dominated or if a triplet-singlet state equilibrium existed, information could be derived concerning orbital energy splittings.

The magnetic susceptibilities of complexes 7, 8, 10-H, 11, and 13 were measured between 6 and 300 K on the SQUID susceptometer at the University of Southern California. All of the compounds exhibited temperature-independent paramagnetism, TIP, of between 303×10^{-6} and 1400×10^{-6} cgs/mol and magnetic moments at 300 K of 0.85 to $1.80 \mu_{\text{B}}$, all below the spin-only value of $2.83 \mu_{\text{B}}$ for a triplet state (Figure 2.9, Table 2.6). No Curie-Weiss component to the magnetic susceptibility was detected. Thus, no information could be derived from the magnetic study concerning the metal MOs. Other Os(IV) complexes have similar magnetic

moments. Hexahalogenoosmates, $[\text{OsX}_6]^{2-}$ ($\text{X} = \text{F}, \text{Br}, \text{I}$), have magnetic moments at 300 K of 1.21 to 1.76 μ_{B} ³⁵ and tetrachloro-bis-phosphine complexes, $\text{OsCl}_4(\text{PR}_3)_2$, between 1.5 and 1.6 μ_{B} at 300 K.^{26d,e} TIP results from the large spin-orbit coupling commonly associated with osmium metal centers.^{35b}

Table 2.6. Magnetic Properties of Os(IV) Complexes Studied.

$\text{Os}(\eta^4\text{-CHBA-DCB})\text{L}_2$ $\text{L}_2 =$	$\chi_{\text{m}} \times 10^6$ (cgs/mol) ^a	μ_{eff} (μ_{B}) ^b
(PPh_3) ₂ , 7 ^c	952	1.51
($\text{O}=\text{PPh}_3$) ₂ 8 ^c	1030	1.56
(py) ₂ , 10-H ^c	1400	1.80
(bipy), 11 ^d	877	1.44
(dppe), 13 ^d	303	0.85

^a Average of χ_{m} values between 100 and 300 K. ^b μ_{eff} calculated from χ_{m} value at 300 K. ^c Trans isomers. ^d Cis- α isomers.

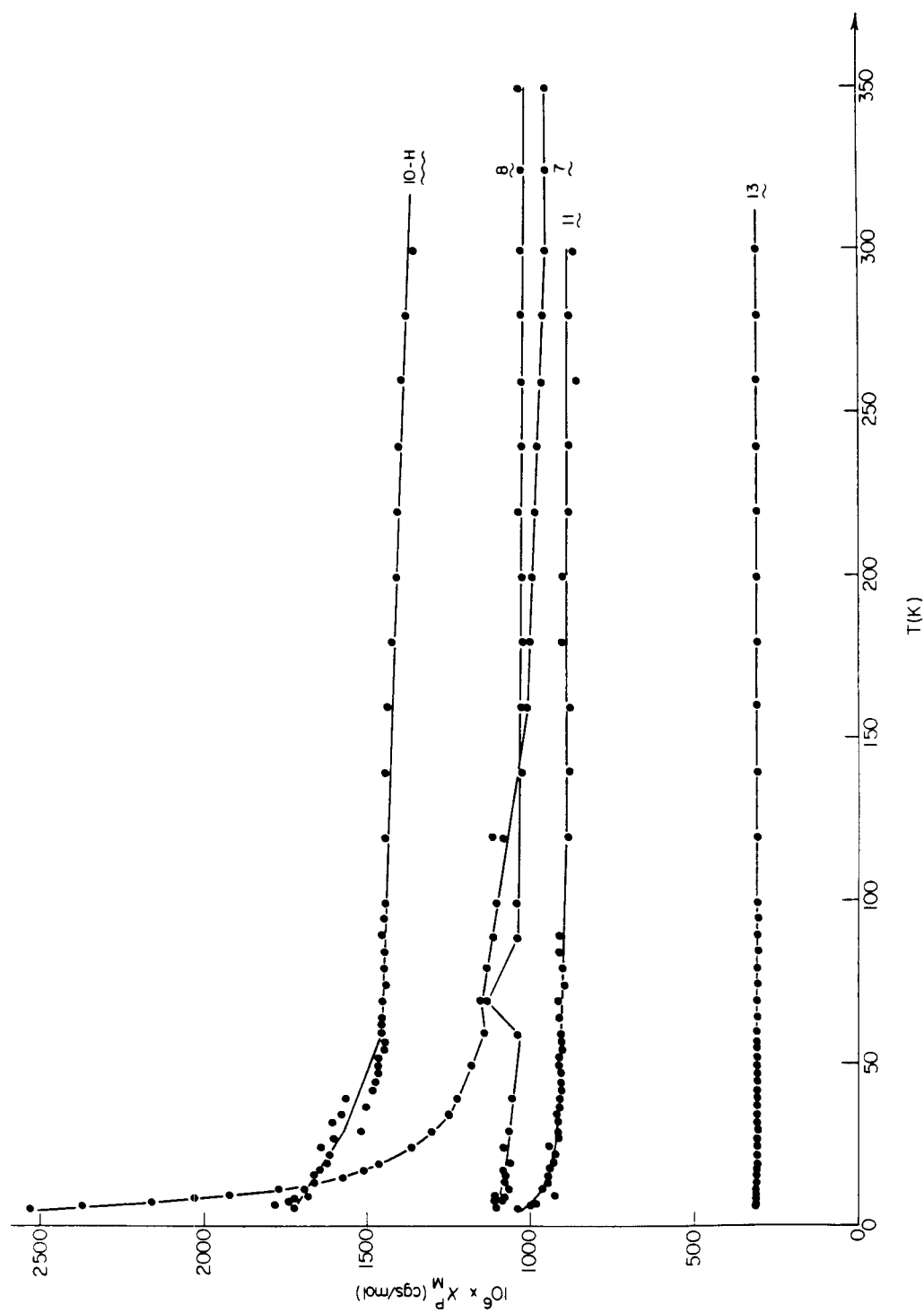


Figure 2.9. Plots of χ_m vs. temperature for Os(IV) complexes 7, 8, 10-H, 11, and 13.

Table 2.7. Magnetic Susceptibilities of the Compounds Studied (cgs/mole).^a

T (K)	7 χ_m	8 χ_m	10-H χ_m	11 χ_m	13 χ_m
6	2530	1100	1720	1040	303
7	2320	1100	1780	998	304
8	2160	1090	1740	984	303
9	2030	1080	1720	1110	303
10	1920	1110	1680	932	303
12	1770	1070	1690	955	303
14	1660	1090	1660	947	303
16	1570	1080	1660	948	303
18	1510	1090	1640	945	304
20	1460	1060	1620	926	303
22.5			1620	928	303
25	1360	1080	1640	945	303
27.5			1600	913	303
30	1300	1070	1510	929	303
32.5			1600	913	303
35	1250	1010	1580	921	303
37.5			1500	908	303
40	1220	1060	1560	905	303
42.5			1480	905	303
45			1470	909	303
47.5			1460	907	303
50	1180	1020	1460	913	303
52.5			1460	907	303
55			1450	898	303
57.5			1440	901	303
60	1140	1040	1450	906	303

^a χ_m values rounded to three significant digits. Blank entries indicate that no measurement was recorded at that temperature. Diamagnetic corrections for the PAC and auxiliary ligands can be found in the Experimental Section.

Table 2.7. (continued).

T (K)	7 χ_m	8 χ_m	10-H χ_m	11 χ_m	13 χ_m
65			1450	908	303
70	1150	1130	1450	913	303
75			1440	891	303
80	1130	1130	1450	902	303
85			1440	910	303
90	1110	1040	1450	909	303
95			1440	871	303
100	1100	1040	1440	872	303
120	1080	1110	1430	880	303
140	1020	1030	1420	878	303
160	1010	1020	1420	879	303
180	1000	1020	1410	898	303
200	994	1020	1390	894	303
220	983	1030	1400	878	303
240	971	1020	1390	874	303
260	964	1020	1380	853	303
280	959	1020	1370	876	303
300	953	1020	1350	862	303
325	949	1020			
350	947	1030			

^a χ_m values rounded to three significant digits. Blank entries indicate that no measurement was recorded at that temperature. Diamagnetic corrections for the PAC and auxiliary ligands can be found in the Experimental Section.

Conclusions

The new PAC ligand H₄CHBA-DCB is synthesized according to the procedure for producing H₄CHBA-Et. The ligand can be easily coordinated to osmium as *trans*-K₂[Os(η⁴-CHBA-DCB)(O)₂]. This *trans*-dioxo complex reacts cleanly with Brønstead acids and bromine to form K[Os(η⁴-CHBA-DCB)(O)(OX)] (X = H, Br), but reactions with chlorine or autoxidation produce an amorphous, intractable product.

Reduction of the *trans*-dioxo with triphenylphosphine generates a neutral Os(IV) complex, *trans*-Os(η⁴-CHBA-DCB)(PPh₃)₂. The phosphine groups of this complex can be oxidized with iodosobenzoic acid to produce *trans*-Os(η⁴-CHBA-DCB)(O=PPh₃)₂. The unexpected lability of the phosphine ligands makes substitution of them by other Lewis bases a convenient route to synthesize a series of Os(IV) compounds. Lewis bases that were reacted with the phosphine complex include 4-*tert*-butylpyridine, pyridine, 1,2-bis(diphenylphosphino)ethane, 2,2'-bipyridine, and *tert*-butylisocyanide. The phosphine lability is unprecedented in Os(IV) chemistry and is thought to proceed by either a dissociative, D, or a dissociative interchange mechanism, I_d, based on rate measurements of the first phosphine substitution by *t*-Bupy. The I_d mechanism seems more likely than the D, based on the feasibility of the seven-coordinate transition state in the I_d mechanism vs. a five-coordinate, unsaturated intermediate implied in the D mechanism.

These Os(IV) complexes exhibit clean electrochemistry in both CH₂Cl₂ at room temperature and SO₂ at -40 °C. The Os(III/II), Os(IV/III), and Os(V/IV) couples are fully reversible in CH₂Cl₂, and the formal potential associated with each couple shifts with varying auxiliary

ligands. This suggests that these couples are metal-centered. Stable solutions of monocationic Os(V) complexes can be generated by controlled-potential electrolysis of the neutral Os(IV) precursors. The Os(V) oxidation state is considered rare. In liquid SO₂, the Os(2+/+), Os(3+/2+), and Os(4+/3+) couples can be observed due to the high anodic limit of SO₂, *ca.* +3.5V vs. Fc⁺/Fc with TBABF₄ or TBAPF₆ supporting electrolyte. The formal potentials of Os(3+/2+) couples are measured at +1.7V vs. Fc⁺/Fc. The Os(2+/+) and Os(3+/2+) couples of *trans* complexes are fully reversible, but the Os(4+/3+) couple is irreversible. These couples, unlike those observed in CH₂Cl₂, are invariant with different auxiliary ligands, which indicates that they may be ligand-centered oxidation couples. Bulk electrolysis experiments reveal that of the di- and tricationic osmium species, only [*trans*-Os(η⁴-CHBA-DCB)(py)₂]²⁺ is stable at -40 °C over an extended period of time. Solutions of this complex warrant examination as potent oxidants of organic substrates (E^f(2+/+) = +1.29V vs. Fc⁺/Fc or *ca.* +2.0 vs. NHE).

The TIP exhibited by the Os(IV) centers induces large shifts in NMR spectra without broadening the peaks. Well-resolved spectra are always observed for these complexes, which aid the characterization of them. The lack of any Curie-Weiss component in the magnetic susceptibility renders magnetic measurements useless for deriving triplet-singlet or MO energy separations. This type of magnetism is common for osmium complexes because of large spin-orbit coupling associated with the element.

Experimental Section

Materials. All solvents were reagent grade (Aldrich, Baker, Mallinckrodt, M.C.B., or U.S.I.) and were used as received unless otherwise noted. Acetic anhydride (reagent, Mallinckrodt), acetyl chloride (reagent, Baker), 4-acetylpyridine (98%, Aldrich), 2,2'-bipyridine (99.5%, Aldrich), 1,2-bis(diphenylphosphine)ethane (Strem), bromine (reagent, Baker), butyl ether (98%, EM Science), *tert*-butylisocyanide (>98%, Fluka), 4-*tert*-butylpyridine (99%, Aldrich), 3,5-dichlorosalicylic acid (Pfaltz and Bauer), HCl (conc., Mallinckrodt), HClO₄ (60%, Mallinckrodt), H₂O₂ (30% Superoxol, Baker), *o*-iodosobenzoic acid (reagent, Sigma), KOH (reagent, Baker), OsO₄ (99.8%, Alfa), H₃PO₄ (85%, Baker), pyridine (reagent, Mallinckrodt), toluene (reagent, Aldrich), triethylamine (reagent, M.C.B.), trifluoroacetic acid (reagent, M.C.B.) and triphenylphosphine (99%, Aldrich) were used as received. Oxalyl chloride was freshly distilled under N₂. 4,5-dichloro-*o*-phenylenediamine was dissolved in THF containing excess PPh₃, gently heated for 15 min, passed through a silica gel plug with THF, and recrystallized from THF/hexane. 4-Acetylpyridine was vacuum distilled prior to use. Silica gel was 60-200 mesh (Davidson).

Physical Measurements. ¹H NMR spectra were recorded at 90 MHz on a Varian EM-390 at 89.83 MHz on a JEOL FX90-Q spectrometer, at 399.782 MHz on a JEOL GX-400 spectrometer or at 500.135 MHz on a Bruker WM-500 spectrometer. ¹H chemical shifts are reported in ppm (δ) vs. Me₄Si with the solvent (CDCl₃ δ 7.24, CD₂Cl₂ δ 5.32, Me₂SO-d₆ δ 2.49 or Me₂CO-d₆ δ 2.04) as internal standard. ¹³C NMR spectrum of **3** and the spectrum using the INEPTNON pulse sequence were recorded at 22.50

MHz on a JEOL FX90-Q spectrometer. ^{13}C chemical shifts are reported in ppm (δ) vs. Me_4Si with $\text{Me}_2\text{CO}-d_6$ δ 206.0 as internal standard. ^{31}P NMR spectra were recorded at 36.28 MHz on a JEOL FX90-Q spectrometer or at 109.352 MHz on an IBM/Bruker WP-270SY spectrometer. ^{31}P chemical shifts are reported in ppm (δ) vs. 85% H_3PO_4 external standard. Infrared spectra were recorded on a Beckman IR 4240 spectrophotometer or on a Mattson Series 100 FTIR spectrophotometer. Elemental analyses were obtained at the Caltech analytical facility. Solvents of crystallization were quantified by ^1H NMR spectroscopy of the authentic samples submitted for elemental analyses. All electrochemical experiments were performed by Dr. Stephen L. Gipson at Caltech. Details can be found in ref 4.

Synthesis. All reactions were carried out in air unless otherwise noted. $\text{K}_2[\text{Os}(\text{OH})_4(\text{O})_2]$ ³¹ and 3,5-dichlorosalicylic acid³² were prepared as described in the literature.

H₄CHBA-DCB, (1).¹ 3,5-Dichloroacetylsalicylic acid (12.55 g, 50.39 mmol) was converted to the acid chloride by gently warming in 10-15 mL of neat oxalyl chloride under N_2 for 12 h. After distilling off the excess oxalyl chloride *in vacuo*, the residue was thrice washed with 30 mL aliquots of CH_2Cl_2 and distilled to dryness *in vacuo*. 4,5-Dichloro-o-phenylenediamine (3.78 g, 21.3 mmol) was dissolved in 100 mL of CH_2Cl_2 and 15 mL of THF. The acid chloride was dissolved in 50 mL of CH_2Cl_2 and slowly added to the diamine solution at room temperature. After stirring for 1 h, 12 mL (>1 equiv) of triethylamine were added, and the solution was stirred for an additional 12 h at room temperature. This mixture was then treated with *ca.* 200 mL of 1 M NaOH and heated *in vacuo* to remove the organic volatiles. Ethanol was added to the resulting

mixture until it became homogeneous. The solution was then slowly neutralized with 1 M HClO₄. A beige precipitate was collected, washed with water, and recrystallized from THF/ethanol multiple times until clean ¹H NMR spectra were observed: yield 7.28 g (61%); ¹H NMR (Table 2.8); IR (Nujol) 1651 cm⁻¹ ν_{CO} (amide); Anal. calcd. for C₂₀H₁₀Cl₆N₂O₄: C, 43.28; H, 1.82; N, 5.05. Found: C, 43.34; H, 1.95; N, 5.00.

H₂CHP-DCBI, (2).¹ 3,5-Dichloroacetylsalicylic acid (15.02 g, 64.47 mmol, 2.4 equiv) and 4,5-dichloro-*o*-phenylenediamine (4.74 g, 26.7 mmol) were worked up as in the synthesis of 1. The CH₂Cl₂ solution of acid chloride, however, was added to a neat THF solution of the diamine already heated under reflux. The triethylamine was added 30 min later, and the reaction mixture remained heated under reflux (under N₂) for 16 h. The cooled reaction mixture was worked up (hydrolysis, recrystallization) as in the synthesis of 1 to yield a coarse white powder: yield 6.86 g (74%); ¹H NMR (Table 2.8); IR (Nujol) lacks the $\nu_{\text{C=O}}$ at 1651 cm⁻¹ present in 1; mass spectrum (m/e), 346 (M⁺, ³⁵Cl); small anomalous peaks were detected for masses greater than M⁺; Anal. calcd. for C₁₃H₆Cl₄N₂O: C, 44.87; H, 1.74; N, 8.05. Found: C, 45.18; H, 2.05; N, 7.77

trans-K₂[Os(η^4 -CHBA-DCB)(O)₂], (3). K₂[Os(OH)₄(O)₂] (1.345 g, 3.65 mmol) was dissolved in 150 mL of warm methanol, and the solution was flushed with N₂ for 0.5 h. H₄CHBA-DCB (2.00 g, 3.60 mmol) was dissolved in 100 mL of THF and also flushed with N₂ for 0.5 h. The blue osmate solution was added to the ligand solution at room temperature, producing a deep orange color indicative of product formation. The solution was stirred for 10 min under N₂, evaporated to dryness, and placed under vacuum for 2 h to completely remove solvents. Recrystallization from butyl ether/THF/MeOH afforded a brown

microcrystalline solid: yield 2.620 g (86%); ^1H NMR (Table 2.8); ^{13}C NMR δ ($\text{Me}_2\text{CO}-d_6$): 167.43 (Os-O-C), 164.57 (-NC(O)-), 150.21, 132.11 (aromatic C-H), 130.68 (aromatic C-H), 126.53, 126.39, 124.02, 121.88 (aromatic C-H), 118.56 ppm; IR (Nujol) 820 cm^{-1} $\nu_{\text{as}}\text{OsO}_2$ (vs), 1607 cm^{-1} ν_{CO} (amide); Anal. calcd. for $\text{C}_{20}\text{H}_6\text{Cl}_6\text{K}_2\text{N}_2\text{O}_6\text{Os} \cdot 1.5 (\text{H}_2\text{O})$; C, 27.40; H, 1.01; N, 3.20. Found: C, 27.60; H, 1.03; N, 3.19. Incorporation of ^{18}O was effected by dissolving the complex in dry THF, adding excess H_2^{18}O and placing the solution under N_2 for three days: IR (Nujol) 782 cm^{-1} , $\nu_{\text{as}}\text{Os}^{18}\text{O}_2$ (vs).

trans- $\text{K}[\text{Os}(\eta^4\text{-CHBA-DCB})(\text{O})(\text{OH})]$, (4). Three drops of conc. HCl were added to an acetone/ H_2O (1:5 v/v) solution of *trans*- $\text{K}_2[\text{Os}(\eta^4\text{-CHBA-DCB})(\text{O})_2]$ (100 mg, 0.114 mmol). A blue color was immediately produced. After 5 min, a fine dark blue precipitate of monoprotonated **3** was filtered away and washed twice with H_2O . The precipitate was recrystallized from acetone/ H_2O : yield 80 mg (86%); ^1H NMR (Table 2.8); IR (Nujol) 1619 cm^{-1} ν_{CO} (amide), the $\nu_{\text{as}}\text{OsO}_2$ stretch of **3** at 820 cm^{-1} was absent; Anal. calcd. for $\text{C}_{20}\text{H}_7\text{N}_2\text{O}_6\text{Cl}_6\text{OsK}$: C, 29.53; H, 0.87; N, 3.44. Found: C, 29.79; H, 1.87; N, 3.13.

$\text{Os}(\eta^4\text{-CHBA-DCB})(\text{O})$, (5). Eluting an acetone solution of **4** through a short column of MgSO_2 with excess acetone produced a red solution, presumably diprotonated and dehydrated **3**. Addition of excess hexane yielded a red microcrystalline solid, tentatively identified as the mono-oxo $\text{Os}(\eta^4\text{-CHBA-DCB})(\text{O})$, (5); ^1H NMR (Table 2.8); IR (Nujol) 1626 cm^{-1} ν_{CO} (amide), 939 cm^{-1} ν_{OsO} (vs), the $\nu_{\text{as}}\text{OsO}_2$ band of **3** was absent. Addition of three drops H_2O turned a red acetone solution of **5** to a blue solution of **4**. Addition of two drops of triethylamine changed the solution to orange. ^1H NMR and IR spectroscopies verified the final orange product as *trans*-(NEt_3H) $_2[\text{Os}(\eta^4\text{-CHBA-DCB})(\text{O})_2]$.

trans-K[Os(η^4 -CHBA-DCB)(O)(OBr)], (6). *trans*-K₂[Os(η^4 -CHBA-DCB)(O)₂] (103 mg, 0.117 mmol) was dissolved in 10 mL THF/CH₂Cl₂ (10:1 v/v), and K₂CO₃ (2.1 g, 15 mmol) was added but did not dissolve. After stirring for 5 min, excess bromine diluted with THF was added dropwise, and the solution was stirred for another 5 min. Dichloromethane was added (20 mL), and the solution was passed through a Celite pad, after which the product was recrystallized from THF/CH₂Cl₂/hexane: yield 75 mg (91%); ¹H NMR (Table 2.8); IR (Nujol) 1622 cm⁻¹ ν_{CO} (amide); Anal. calcd. for C₂₀H₆N₂BrCl₆OsO₆K·0.75 (C₄H₈O): C, 29.19; H, 1.28; N, 2.96. Found: C, 29.15; H, 1.14; N, 3.16.

trans-Os(η^4 -CHBA-DCB)(PPh₃)₂, (7). To a 50-mL Erlenmeyer Flask with stir bar were added *trans*-K₂[Os(η^4 -CHBA-DCB)(O)₂] (221 mg, 0.260 mmol), triphenylphosphine (450 mg), *ca.* 5 mL of trifluoroacetic acid, and 10 mL of THF. The orange solution was heated until the THF had evaporated, and a dark green molten triphenylphosphine mixture remained (*ca.* 10 min). After cooling, the mixture was dissolved in 10 mL of CH₂Cl₂ and placed on a short silica gel column. Elution with CH₂Cl₂ removed the product as a green band. Recrystallization from CH₂Cl₂/hexane yielded the product as a dark green crystalline solid: yield 236 mg (72%); ¹H and ³¹P NMR (Table 2.8); IR (Nujol) 1613 cm⁻¹ ν_{CO} (amide); Anal. calcd. for C₅₆H₃₆Cl₆N₂O₄OsP₂: C, 53.14; H, 2.87; N, 2.21. Found: C, 53.33; H, 2.94; N, 2.22.

trans-Os(η^4 -CHBA-DCB)(O=PPh₃)₂, (8). *trans*-Os(η^4 -CHBA-DCB)(PPh₃)₂, (75 mg, 59 μ mol) was dissolved in 10 mL of THF. Addition of *o*-iodosobenzoic acid (150 mg, 9.5 equiv (excess)) and heating gently for 10 min changed the solution color from green to red. The cooled solution was

placed on a short silica gel column and eluted with excess THF. The red band was collected, evaporated to dryness and recrystallized from CH₂Cl₂/MeOH to yield the product as a dark red crystalline product: yield 18 mg (24%); ¹H and ³¹P NMR (Table 2.8); IR (Nujol) 1608 cm⁻¹ ν_{CO} (amide); Anal. calcd. for C₅₆H₃₆Cl₆N₂O₆OsP₂: C, 51.83; H, 2.80; N, 2.16. Found: C, 51.86; H, 2.92; N, 2.18.

trans-Os(η⁴-CHBA-DCB)(PPh₃)(*t*-Bupy), (9-*t*Bu). *trans*-Os(η⁴-CHBA-DCB)(PPh₃)₂ (75 mg, 59 μmol) was dissolved in 50 mL of CH₂Cl₂. Addition of 4-*tert*-butylpyridine followed by gentle warming for 0.5 h produced a color change from dark green to turquoise. Removal of solvents *in vacuo* followed by recrystallization from CH₂Cl₂/hexane yielded the product as a dark blue crystalline solid: yield 58 mg (86%); ¹H NMR (Table 2.8); IR (Nujol) 1620 cm⁻¹ ν_{CO} (amide); Anal. calcd. for C₄₇H₃₄Cl₆N₃O₄OsP·0.5 (C₆H₁₄): C, 50.82; H, 3.50; N, 3.56. Found: C, 50.72; H, 3.51; N, 3.53.

trans-Os(η⁴-CHBA-DCB)(*t*-Bupy)₂, (10-*t*Bu). *trans*-Os(η⁴-CHBA-DCB)(PPh₃)₂ (200 mg, 0.158 mmol) was dissolved in 20 mL of neat *t*-Bupy. The solution was heated under reflux for 15 min, during which time the color changed from green to dark blue, almost black. The *t*-Bupy was removed *in vacuo*, and the crude product was recrystallized from CH₂Cl₂/hexane to yield a dark crystalline solid: yield 108 mg (68%); ¹H NMR (Table 2.8); IR (Nujol) 1620 cm⁻¹ ν_{CO} (amide); Anal. calcd. for C₃₈H₃₂Cl₆N₄O₄Os·0.25 (C₆H₁₄): C, 45.92; H, 3.46; N, 5.42. Found: C, 46.20; H, 3.52; N, 5.37.

trans-Os(η⁴-CHBA-DCB)(py)₂, (10-H), and *trans*-Os(η⁴-CHBA-DCB)(PPh₃)(py), (9-H). *trans*-Os(η⁴-CHBA-DCB)(PPh₃)₂ (400 mg, 0.316 mmol) was dissolved in 10 mL of neat pyridine under N₂ and heated under

reflux for 16 h, during which time the green color changed to tan. The py was removed *in vacuo*. The remaining residue was redissolved in THF/CH₂Cl₂ (1:3 v/v) and oxidized with a dilute Br₂/CH₂Cl₂ solution. During 10 min of stirring, the solution color turned dark blue. After vacuum removal of the excess Br₂, the solution was eluted through a short silica gel column with excess CH₂Cl₂. Partial recrystallization from CH₂Cl₂/hexane precipitated very dark crystalline 10-H: yield 219 mg (77.1%); ¹H NMR (Table 2.8); IR (Nujol) 1590 cm⁻¹ ν_{CO} (amide); Anal. calcd. for C₃₀H₁₆Cl₆N₄O₄Os·(H₂O): C, 39.28; H, 1.98; N, 6.11. Found: C, 39.26; H, 1.96; N, 6.14. Continued recrystallization of the mother liquor yielded dark blue crystalline 9-H: yield 60 mg (17.5%); ¹H NMR (Table 2.8).

cis-α-Os(η⁴-CHBA-DCB)(bipy), (12). *trans*-Os(η⁴-CHBA-DCB)(PPh₃)₂ (400 mg, 0.316 mmol) and 2,2'-bipyridine (800 mg, 5.12 mmol) were dissolved in toluene (25 mL) and heated under reflux (0.5 h) during which time the color darkened. The cooled solution was eluted through a silica gel column with excess CH₂Cl₂. Three bands separated: a front-running green band, a red band and finally a black band. The green material was isolated and recrystallized from CH₂Cl₂/hexane. It proved to be unreacted starting material (67 mg). Isolation of the red material followed by recrystallization from CH₂Cl₂/hexane afforded red microcrystalline product: yield 59 mg (25%; adjusted for recovered starting material); ¹H NMR (Table 2.8); IR (Nujol) 1631 cm⁻¹ ν_{CO} (amide); Anal. calcd. for C₃₀H₁₄Cl₆N₄O₄Os·0.33 (C₆H₁₄): C, 41.79; H, 2.03; N, 6.05. Found: C, 41.75; H, 2.07; N, 5.98.

cis-β-Os(η⁴-CHBA-DCB)(bipy), (11). The final black material off the column in the previous synthesis was isolated and recrystallized from

CH₂Cl₂/hexane to afford a black microcrystalline product: yield 12.5 mg (5.3%; adjusted for recovered starting material); ¹H NMR (Table 2.8); IR (Nujol) 1635 cm⁻¹ ν_{CO} (amide), 1622 cm⁻¹ ν_{CO} (amide); Anal. calcd. for C₃₀H₁₄Cl₆N₄O₄Os: C, 40.15; H, 1.57; N, 6.24. Found: C, 40.44; H, 1.74; N, 6.25.

cis-β-Os(η⁴-CHBA-DCB)(dppe), (13). *trans*-Os(η⁴-CHBA-DCB)(PPh₃)₂ (80 mg, 63 μmol) and 1,2-bis(diphenylphosphino)ethane (35 mg, 0.41 mmol) were dissolved in benzene (10 mL) and heated under reflux (15 min). The solution color remained green during heating. After cooling, the solvent was removed on a rotary evaporator. The resulting residue was eluted through a short silica gel column with excess CH₂Cl₂ and recrystallized from CH₂Cl₂/hexane to yield a green crystalline product: yield 67 mg (93%); ¹H and ³¹P NMR (Table 2.8); IR (Nujol) 1670 cm⁻¹ ν_{CO} (amide), 1608 cm⁻¹ ν_{CO} (amide); Anal. calcd. for C₄₆H₃₀Cl₆N₂O₄OsP₂·0.5(C₆H₁₄): C, 49.76; H, 3.15; N, 2.37. Found: C, 49.64; H, 3.10; N, 2.36.

cis-α-Os(η⁴-CHBA-DCB)(PPh₃)(*t*-BuNC), (14). *trans*-Os(η⁴-CHBA-DCB)(PPh₃)₂ (20 mg; 16 μmol) and excess *tert*-butylisocyanide were dissolved in benzene (10 mL) under nitrogen and heated under reflux (6 min) during which time the color changed from green to dark purple. The benzene was removed *in vacuo*, and the residue was recrystallized from CH₂Cl₂/hexane to give a dark crystalline product: yield 15 mg (85%); ¹H NMR (Table 2.8); IR (Nujol) 1650 cm⁻¹ ν_{CO} (amide), 2160 cm⁻¹ ν_{C≡N}; Anal. calcd. for C₄₃H₃₀Cl₆N₃O₄OsP: C, 47.53; H, 2.78; N, 3.87. Found: C, 47.79; H, 2.99; N, 3.81.

cis-α-Os(η⁴-CHBA-DCB)(*t*-BuNC), (15). *trans*-K₂[Os(η⁴-CHBA-DCB)(O)₂] (120 mg; 0.135 mmol), triphenylphosphine (81 mg, 2.2 equiv),

and *tert*-butylisocyanide (0.27 mL, 16 equiv) were dissolved in 10 mL of THF and gently heated for 0.5 h, during which time the color changed from orange to red-brown. The brown intermediate was precipitated with excess hexane, filtered, and twice recrystallized from THF/hexane. The precipitate, redissolved in THF and oxidized with Br₂, became deep blue. After removal of the solvent *in vacuo*, the blue product was eluted with excess CH₂Cl₂ through a short silica gel column and was recrystallized from CH₂Cl₂/hexane to yield a dark blue crystalline solid: yield 27 mg (23%); ¹H NMR (Table 2.8); IR (Nujol) 2209 cm⁻¹ $\nu_{\text{C}\equiv\text{N}}$ (vs), 2183 cm⁻¹ $\nu_{\text{C}\equiv\text{N}}$ (vs), 1653 cm⁻¹ $\nu_{\text{C=O}}$ (amide); Anal. calcd. for C₃₀H₂₄Cl₆N₄O₄Os: C, 39.71; H, 2.67; N, 6.17. Found: C, 39.75; H, 2.70; N, 6.19.

Exchange Reaction of 9-*t*-Bu and Acpy. 9-*t*-Bu (35 mg, 31 mmol) was dissolved in 4-acetylpyridine (4 mL) and heated to 75°C for 1.5 h while stirring. After cooling the solution, 30 mL of H₂O was rapidly added to precipitate the crude product, which was then filtered off and washed with more H₂O. The dark green product was dissolved in 10 mL CH₂Cl₂, dried over MgSO₄, and eluted down a short silica gel column with CH₂Cl₂/THF (2:1 v/v). The product was collected and recrystallized from CH₂Cl₂/hexane to yield dark green crystalline solid: yield 12 mg (35%); ¹H NMR (Table 2.8); IR (Nujol) 1710 cm⁻¹ $\nu_{\text{C=O}}$ (acetyl), 1611 cm⁻¹ $\nu_{\text{C=O}}$ (amide).

Kinetic Rate Measurements. Rates for the conversion of 7 into 10-*t*Bu were measured at different temperatures and concentrations of *t*-Bupy. These experiments were carried out by Sonny Lee using UV-vis spectroscopy. UV-vis spectra were recorded on a Hewlett-Packard HP8450A spectrophotometer equipped with an HP89100A temperature controller and an HP89101A temperature-control unit. A toluene solution

of **7** (2.5-3.0 mL) was added to a glass cuvette, which was sealed with a septum, flushed thoroughly with nitrogen, and heated to the desired temperature. *t*-Bupy was added by syringe and automatic data collection was started. Pseudo-first-order conditions were maintained, i.e., [*t*-Bupy] \gg [**7**] ($>400:1$). Data were collected for greater than three half-lives at wavelengths of 460, 550, 570, 640, and 800 nm and were analyzed by the Kedzy-Swinbourne method for first-order rate analysis.³³ Activation parameters were determined from rate measurements at temperatures of between 35 and 65 °C. Rate dependence on the concentration of *t*-Bupy was investigated by varying the *t*-Bupy concentration between 5.0 and 113 mM.

Magnetic Susceptibility Measurements. Magnetic susceptibility measurements were performed on an S.H.E. 905 SQUID susceptometer at the University of Southern California. Measurements were recorded between 6 and 300 K on sample sizes of 20-80 mg. Samples were analytically pure and were ground before being loaded into a titanium bucket for the magnetic measurement. The magnetization of the empty bucket was determined by a blank run without a sample and was subtracted out of the Os(IV) measurements. The following diamagnetic corrections were applied, χ_0 (cgs/mole): (η^4 -CHBA-DCB)⁴⁻, -168×10^{-6} ; PPh₃, -167×10^{-6} ; O=PPh₃, -168×10^{-6} ; dppe, -85×10^{-6} ; py, -49×10^{-6} ; bipy, -192×10^{-6} . All paramagnetic Os(IV) compounds exhibited temperature-independent paramagnetism, TIP, with negligible Curie-Weiss behavior. The χ_m values for **7** increased at low temperatures (6-50 K), suggesting that small amounts of paramagnetic impurities were present.

Table 2.8. ^1H and ^{31}P NMR Data (ppm).

Compound	Isomer	$(\eta^4\text{-CHBA-DCB})^{4-}$		Ancillary Ligand, L		
		DCB	CHBA ^a	H _o	H _m	H _p other L
1^b		8.12 s,2H	8.10 d,2H	7.87 d,2H		
2^c		(DCBI) 7.95 s,2H	(CHP) 8.26 d,1H	7.39 d,1H		
3^c	trans	9.47 s,2H	8.39 d,2H	7.40 d,2H		
4^c	trans	8.30 s,2H	7.82 d,2H	7.23 d,2H		
5^d		8.47 s,2H	8.07 d,2H	7.72 d,2H		
6^d	trans	8.19 s,2H	7.83 d,2H	7.11 d,2H		
7^d	trans	4.54 s,2H	9.33 d,2H	8.39 d,2H	8.05 m,12H $^3J_{o,m} = ^3J_{m,p} = 8\text{ Hz}$	7.42 t,6H $\delta(^{31}\text{P})^d\text{PPh}_3 = -899\text{ ppm}$ PPh ₃

Table 2.8. (Continued).

Compound	Isomer	$(\eta^4\text{-CHBA-DCB})^{4-}$			Ancillary Ligand, L		
		DCB	CHBA ^a	H _o	H _m	H _p	other L
8 ^c	trans	8.91	10.53	9.76	5.54	7.45	7.28 $\delta(^{31}\text{P})^d\text{O=PPh}_3$ O=PPh ₃
		s,2H	d,2H	d,2H	ddd,12H	ddd,12H	dt,6H = 143.9 ppm
9-H ^d	trans	5.36	11.77	9.24	9.18	7.34	7.70 PPh ₃
		s,2H	d,2H	d,2H	dd,6H	dd,6H	t,3H
9-tBu ^e	trans	5.60	11.64	9.31	9.13	7.29	7.68 PPh ₃
		s,2H	d,2H	d,2H	dd,6H	dd,6H	t,3H
10-H ^d	trans	7.31	10.57	9.61	-2.66	7.48	-C(CH ₃) ₃
		s,2H	d,2H	d,2H	$^3J_{o,p} = 13\text{ Hz}$	$^3J_{o,m} = 6\text{ Hz}$	0.30 t-Bupy
					d,2H	d,2H	s,9H
					$^3J_{o,m} = 6\text{ Hz}$		
					-7.15	8.30	-4.34 py
					d,4H	dd,4H	t,2H
					$^3J_{o,m} = 3J_{m,p} = 6\text{ Hz}$		

Table 2.8. (Continued).

Compound	Isomer	$(\eta^4\text{-CHBA-DCB})^{4-}$			Ancillary Ligand, L			L
		DCB	CHBA ^a	H _o	H _m	H _p	other	
10-<i>t</i>Bu^c	trans	7.50	11.10	-8.48	7.96	0.07	0.07	<i>t</i> -Bupy
		s,2H	d,2H	d,4H $^3J_{o,m} = 7\text{ Hz}$	d,4H		s,18H	
9-Ac^d	trans	5.50	11.44	9.24	7.35	7.73		PPh ₃
		s,2H	d,2H	dd,6H $^3J_{o,p} = 13\text{ Hz}$ $^3J_{o,m} = 7\text{ Hz}$	dd,6H	t,3H		
11^{d,f}	cis- β	7.80	7.63	-2.97	8.35	6.59		bipy
		s,1H	d,1H	d,1H	d,2H	dd,1H		
12^d	cis- α	3.19	10.33	-12.47	10.91	-2.28	8.83	
		s,1H	d,1H	d,1H	dd,1H	dd,1H	d,1H	
12^d	cis- α	8.28	8.20	7.96	7.56	7.81	8.58	bipy
		s,2H	d,2H	dd,2H $^3J_{o,m} = 5.6\text{ Hz}$ $^3J_{o,p} = 1.2\text{ Hz}$ $^4J_{m,m'} = 0.9\text{ Hz}$	ddd,2H	ddd,2H	dd,2H	

Table 2.8. (Continued).

Compound	Isomer	$(\eta^4\text{-CHBA-DCB})^{4-}$		Ancillary Ligand, L			L	
		DCB	CHBA ^a	H _o	H _m	H _p other		
13^{c,g}	cis- β	10.29	7.01	6.96	7.55	7.43	dppe	
		s,1H	d,1H	d,1H	d,2H	t,1H	-CH ₂ CH ₂ -	
		5.19	7.20	7.09	6.63	7.29	4.28	3.95
		s,1H	d,1H	d,1H	dd,2H	t,1H	br,1H	br,1H
14^e	cis- α	8.98	8.82	7.27	7.27	7.37	PPh ₃	
		s,1H	d,1H	d,1H	dd,6H	dd,6H	t,3H	
		7.34	7.87	7.06	$^3J_{o,P} = ^3J_{o,m} = 8.0\text{ Hz}$	$^3J_{m,p} = 7.0\text{ Hz}$	-C(CH ₃) ₃	t-BuNC
		s,1H	d,1H	d,1H			1.35 s,9H	
15^d	cis- α	8.39	8.42	7.43			t-BuNC	
		s,2H	d,2H	d,2H			1.44 s,18H	
$\delta(^{31}\text{P})^d$ dppe = -992.9, -1015.6 ppm								

^aEach CHBA doublet was not assigned relative to the other. The assignment is possible though of the DCB singlet by irradiation of the signal from the proximate CHBA proton (ref 36). ⁴J_{m,m'} = 2.7 – 3.0 Hz. ^b δ in Me₂SO-d₆. ^c δ in Me₂CO-d₆. ^d δ in CDCl₃. ^e δ in CD₂Cl₂. ^fResonance assignments of bipyr signals from a COSY 2-D experiment. ^gCoupled dppe protons established by decoupling experiments. NOE enhancement

References

1. PAC ligand abbreviations are as follows: 1,2-bis(3,5-dichloro-2-hydroxybenzamido)-ethane, H₄CHBA-Et; 1,2-bis(3,5-dichloro-2-hydroxybenzamido)-4,5-dichlorobenzene, H₄CHBA-DCB or "the Yogi ligand"; 1,2-bis(2-hydroxybenzamido)benzene, H₄HBA-B; 2-(3,5-dichloro-2-hydroxyphenyl)-5,6-dichlorobenzimidazole, H₂CHP-DCBI; 1,2-bis(2-hydroxy-2-methylpropanamido)-benzene, H₄HMPA-B; 1,2-bis(2-hydroxy-2-methylpropanamido), 2,4-dimethylpentan-3-one, H₄HMPA-DMP.
2. D°[H₃C-CH₃] = 88 kcal/mol; D°[aromatic C-C] ≈ 120 kcal/mol; D°[H-C₂H₅] = 98 kcal/mol; D°[H-C₆H₅] = 110 kcal/mol; from Benson, S. W. "Thermochemical Kinetics"; John Wiley and Sons: New York, 1976, p 309.
3. (a) Gaudiello, J. G.; Bradley, P. G.; Norton, K. A.; Woodruff, W. H.; Bard, A. J. *Inorg. Chem.* **1984**, *23*, 3-10. (b) Sharp, P. R.; Bard, A. J. *Inorg. Chem.* **1983**, *22*, 3462-3464. (c) *Ibid.*, 2689-2693. (d) Gaudiello, J. G.; Sharp, P. R.; Bard, A. J. *J. Am. Chem. Soc.* **1982**, *104*, 6373-6377. (e) Tinker, L. A.; Bard, A. J. *J. Electroanal. Chem.* **1982**, *133*, 275-285. (f) *Ibid.*, *J. Am. Chem. Soc.*, **1979**, *101*, 2316-2319.
4. Gipson, S. L., Ph.D. Thesis, California Institute of Technology, June 1985.
5. Spies, G. H., Ph.D. Thesis, California Institute of Technology, October 1984.

6. Krafft, T. E., Ph.D. Thesis, California Institute of Technology, February 1985.
7. For examples of Lewis acid-promoted reactions of amines with acetylating agents, see the following references: (a) Wilson, J. D.; Weingarten, H. *Can. J. Chem.* **1970**, *48*, 983-986. (b) Chan, T. H.; Wong, L. T. L. *J. Org. Chem.* **1969**, *34*, 2766-2767.
8. Stabb, H. A. *Angew. Chem., Int. Ed. Engl.* **1962**, *1*, 351-367.
9. Morgan, K. J.; Turner, A. M. *Tetrahedron* **1966**, *22*, 1175-1181.
10. Treco, B. G. R. T., California Institute of Technology, unpublished results.
11. "Handbook of Chemistry and Physics", 56th ed.; Weast, R. C., Ed.; CRC Press: Cleveland, 1975; pp F236-F254.
12. Christie, J. A., California Institute of Technology, unpublished results.
13. (a) Cotton, F. A.; Wilkenson, G. "Advanced Inorganic Chemistry", 4th ed.; John Wiley and Sons: New York, 1980, p 917. (b) *Ibid.*, p 156.
14. Sigel, H.; Martin, R. B. *Chem. Rev.* **1982**, *82*, 385-426.
15. Benn, R.; Günther, H. *Angew. Chem., Int. Ed. Engl.* **1983**, *22*, 350-380.
16. Nakamoto, K. "Infrared and Raman Spectra of Inorganic and Coordination Compounds", Wiley-Interscience: New York, 1978, p 230.
17. Collins, R. J.; Jones, J.; Griffith, W. P. *J. Chem. Soc., Dalton Trans.* **1974**, 1094-1097.
18. Schröder, M. *Chem. Rev.* **1980**, *80*, 187-213.

19. The frequency range for $\nu_{\text{Os}\equiv\text{O}}$ absorptions is between 1020 cm^{-1} for OsCl_4O and 978 cm^{-1} for $\text{Os}(\text{O}_2(\text{CMe}_2)_2)_2(\text{O})$. See ref 17.
 20. Bartlett, N.; Jha, N. K. *J. Chem. Soc. (A)* **1968**, 536-543.
 21. (a) Sargeson, A. M.; Searle, G. H. *Nature* **1963**, *200*, 356-357. (b) Sargeson, A. M.; Searle, G. H. *Inorg. Chem.* **1965**, *4*, 45-52.
 22. (a) Gullotti, M.; Pasini, A.; Zanderighi, G. M.; Ciani, G.; Sironi, A. *J. Chem. Soc., Dalton Trans.* **1981**, 902-908. (b) Van den Bergen, A.; Cozens, R. J.; Murray, K. S. *J. Chem. Soc. (A)*, **1970**, 3060-3064. (c) Calligaris, M.; Manzini, G.; Nardin, G.; Randaccio, L. *J. Chem. Soc., Dalton Trans.* **1972**, 543-547. (d) Calligaris, M.; Nardin, G.; Randaccio, L. *Ibid.*, 2003-2066. (e) Kawakami, K.; Miya-Uchi, M.; Tanaka, T. *J. Organomet. Chem.* **1974**, *70*, 67-77. (f) Yamanouchi, K.; Yamada, S. *Inorg. Chim. Acta* **1974**, *9*, 161-164. (g) Dey, K.; Rey, K. C. *Ibid.* **1974**, *10*, 139-143. (h) Cummins, D.; McKenzie, E.D.; Milburn, H. *Ibid.* **1975**, *12*, L17-L18. (i) Cummins, D.; McKenzie, E. D.; Milburn, H. *J. Chem. Soc., Dalton Trans.* **1976**, 130-135. (j) Gatehouse, B. M.; Reichert, B. E.; West, B. O. *Acta Crystallogr. Sect. B* **1976**, *32*, 30-34. (k) Armstrong, L. G.; Lindoy, L. F.; McPartlin, M.; Mockler, G. M.; Tasker, P. A. *Inorg. Chem.* **1977**, *16*, 1665-1669. (l) Thornback, J. R.; Wilkenson, G. *J. Chem. Soc., Dalton Trans.* **1978**, 110-115. (m) Hill, W. E.; Atabay, N.; McAuliffe, C. A.; McCullough, F. P.; Razzoki, S. M. *Inorg. Chim. Acta* **1979**, *35*, 35-41. (n) Brown, D. G.; Hemphill, W. D. *Inorg. Chem.* **1979**, *18*, 2039-2040. (o) Lauffer, R. B.; Heistand, R. H.; Que, L., Jr. *Ibid.* **1983**, *22*, 50-55. (p) Ebina, F.; Kyuno, E.; Uehara, A.; Tsuchiya, R. *Bull. Chem. Soc. Jpn.* **1975**, *48*, 3120-3123.
- Coordinated salen is normally planar. Three conditions can afford

cis complexes: (i) the use of bidentate auxiliary ligands (e.g., bipy, acac, or catachol),^{21c,h,i,n,o} (ii) increasing the length of the polymethylene salen bridge to generate steric strain that is relieved by isomerization to cis compounds,^{24p} and (iii) the incorporation of certain monodentate ligands, i.e., CO,^{24l} Cl-,^{24g} Me, ^{24b,d,e} (NCS)-, ^{24k} and *cis*-dioxo ligands.^{24a,f} The formation of cis complexes with two carbonyl ligands can be justified because cis carbonyls are inherently more stable than trans. Similarly, complexes with *cis*-dioxo ligands can be rationalized by the propensity for *cis*-dioxo formation. The driving force for producing cis compounds with either chloride or methyl ligands, however, has not been explained.

23. (a) Langford, C. H.; Gray, H. B. "Ligand Substitution Processes"; W. A. Benjamin: Don Mills, Ontario, 1974. For examples of studies distinguishing D and I_d mechanisms, see the following: (b) Darensbourg, D. J. In "Advances in Organometallic Chemistry"; Housecroft, C. E., Fehlner, T. P., Eds.; Academic: New York, 1982; Vol. 21, pp 113-150. (c) Darensbourg, D. J.; Ewen, J. A. *J. Am. Chem. Soc.* **1976**, *98*, 4317-4319. (d) Jensen, F. R.; Kiskis, R. C. *Ibid.* **1975**, *97*, 5820-5825.
24. Lee, S. C., California Institute of Technology, unpublished results.
25. Os(IV) seven-coordinate complexes are tetrahydride-tris-phosphine species. (a) Douglas, P. G.; Shaw, B. L. *J. Chem. Soc. (A)* **1970**, 334-338. (b) Bell, B.; Chatt, J.; Leigh G. J., *J. Chem. Soc. Dalton Trans.* **1973**, 997-1004 (c) Hart, D. W.; Bau, R.; Koetzle, T. F. *J. Am. Chem. Soc.* **1977**, *99*, 7557-7564. (d) Bruno, J. W .; Huffman, J. C.; Caulton, K. G. *Ibid.* **1984**, *106*, 1663-1669.

26. (a) Buckingham, D. A.; Dwyer, F. P.; Goodwin, H. A.; Sargeson, A. *M. Aust. J. Chem.* **1964**, *17*, 315-324. (b) Chatt, J.; Leigh, G. J.; Mingos, D. M. P.; Paske, R. J. *J. Chem. Soc. (A)* **1968**, 2636-2641. (c) Aslanov, L.; Wheeler, A. G.; Whimp, P. O. *J. Chem. Soc., Chem. Commun.* **1970**, 30-31. (d) Chatt, J.; Melville, D. P.; Richards, R. L. *J. Chem. Soc. (A)* **1971**, 895-899. (e) Gunz, H. P.; Leigh, G. J. *J. Chem. Soc. (A)* **1971**, 2229-2233. (f) Pawson, D.; Griffith, W. P. *J. Chem. Soc., Dalton Trans.* **1975**, 417-423. (g) Khan, M. M. T.; Ahamed, S. S.; Levenson, R. A. *J. Inorg. Nucl. Chem.* **1976**, *38*, 1135-1138.
27. (a) Many thanks are extended to J. Douglas Meinhardt for assisting in the collection and processing of the 2-D COSY spectrum of 11. (b) Many thanks are extended to Dr. Peter J. Desrosiers, who recorded the ³¹P NMR spectrum on an IBM/Bruker WP-270SY spectrometer at the University of Southern California.
28. For leading references of known Os(V) complexes, see the following: (a) Hargreaves, G. B.; Peacock, R. D. *J. Chem. Soc.* **1960**, 2618-2620. (b) Mitchell, S. J.; Hollaway, J. H. *J. Chem. Soc. (A)* **1971**, 2789-2794. (c) Hepworth, M. A.; Robinson, P. L.; Westland, G. J. *J. Chem. Soc.* **1954**, 4269-4275. (d) Hepworth, M. A.; Jack, K. H.; Westland, G. J. *J. Inorg. Nucl. Chem.* **1956**, *2*, 79-87. (e) Boston, J. L.; Sharp, D. W. A. *J. Chem. Soc.* **1960**, 907-908. (f) Burns, R. C.; O'Donnell, T. A. *Inorg. Chem.* **1979**, *18*, 3081-3086. (g) Magnuson, R. *Ibid.* **1984**, *23*, 387-392. (h) Kim, E. E.; Eriks, K.; Magnuson, R. *Ibid.*, 393-397. (i) Dehnicke, K.; Ulrich, M.; Rainer, W. *Ibid.*, 2563-2564.

29. The compound *trans*-OsCl₄(PPh₃)₂ was provided by Brian G. R. T. Treco, who had synthesized it by the procedure of Walton *et al.*: Armstrong, J. E.; Robinson, W. R.; Walton R. A. *Inorg. Chem.* **1983**, *22*, 1301-1306.
30. Elving, P. J.; Markowitz, J. M. *J. Chem. Ed.* **1960**, *37*, 75-81.
31. Malin, J. M. *Inorg. Synth.* **1980**, *20*, 61.
32. Durst, H. D.; Gokel, G. W. "Experimental Organic Chemistry"; McGraw Hill: New York, 1980, p 256.
33. Moore, J. W.; Pearson, R. G. "Kinetics and Mechanism", 3rd ed.; John Wiley and Sons: New York, 1981, p 72.
34. (a) Randall, E. W. ; Shaw, D. *J. Chem. Soc. (A)* **1969**, 2867-2872.
(b) Chatt, J.; Leigh, G. J.; Mingos, D. M. P.; Randall, E. W.; Shaw, D. *J. Chem. Soc., Chem. Commun.* **1968**, 419-420. See also refs 26b and 26f.
35. (a) Earnshaw, A.; Figgis, B. N.; Lewis, J.; Peacock, R. D. *J. Chem. Soc.* **1961**, 3132-3138. (b) Ref 13a, pp 642-652 and 412-417.
36. Peake, Geoffrey T., California Institute of Technology, unpublished results.

Chapter 3

Non-planar Amide Groups as Ligands

Introduction

In Chapter 2, the synthesis and reactivity of many Os(VI) and Os(IV) compounds are reported that incorporate the PAC ligand (η^4 -CHBA-DCB)⁴⁻ for stabilization.¹ This ligand frequently assumes planar coordination around the osmium, which together with two axial ligands forms the trans isomer. We presumed that only trans isomers would be produced because of the rigidity of the chelate framework. The stiff aromatic arms and bridge, together with N-amido linkages, which are typically planar, were thought to make the ligand resistant to deformation. Complexes of bidentate ligands (bipy or dppe) or electron-withdrawing *tert*-butylisocyanide, however, have non-planar PAC ligands and are characterized as *cis*- α or *cis*- β isomers, thus disproving our presumption. We were curious as to which deformations were responsible for the production of *cis* isomers. Two *cis* complexes have been structurally characterized by X-ray crystallography: *cis*- β -Os(η^4 -CHBA-DCB)(bipy), 11, and *cis*- α -Os(η^4 -CHBA-DCB)(PPh₃)(*t*-BuNC), 14.¹ TheORTEPs of these compounds reveal the presence of novel non-planar N-amido ligands.

The organic amide functional group, one of the most important building blocks in biological systems, is almost always found in its characteristic planar form. Rotational processes around the amide C-N bond disrupt amide delocalization and consequently are subject to substantial activation barriers (10-35 kcal/mol).² Non-planar amides have been recognized in formamide³ and in some constrained molecules such as certain lactams^{4,9} (including penicillin and cephalosporin antibiotics⁵), polycyclic spirodilactams⁶ and anti-Bredt bridgehead nitrogen compounds⁷ (Figure 3.1). With the growth of peptide conformation

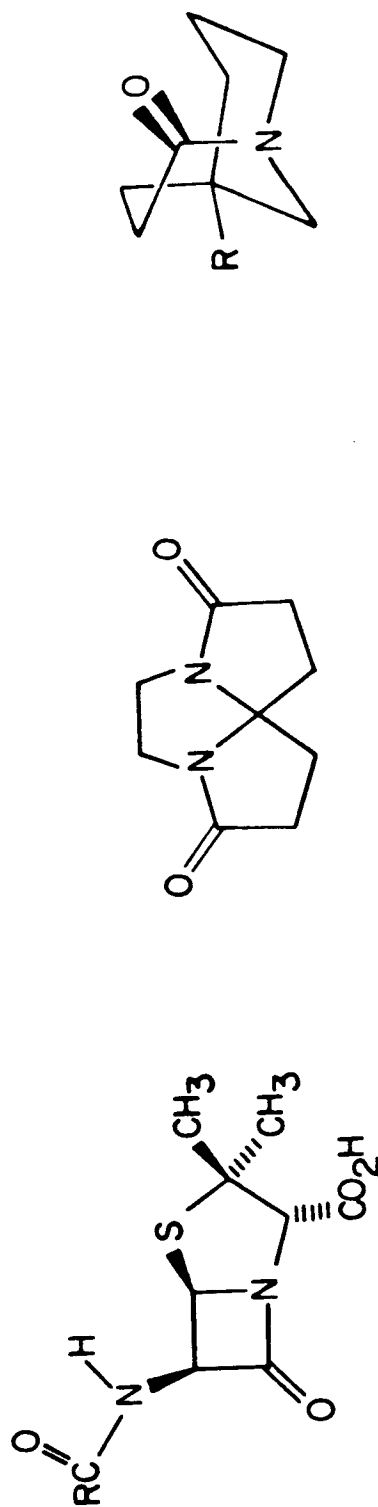


Figure 3.1. Organic complexes containing non-planar amide groups: penicillin, polycyclic spirodilactams, and anti-Bredt bridgehead nitrogen complexes.

analysis, many methods have been established for using structural data to quantify deviations from planarity in secondary amides.^{8,9} We have applied one such method⁹ to our systems by considering the osmium bound to the N-amido moiety ($\text{RC(O)NR}'\text{Os}$) in place of the secondary amide hydrogen atom ($\text{RC(O)NR}'\text{H}$).

Inorganic N-amido ligands are typically planar for the same reason that organic amides are planar—amide delocalization.¹⁰ To locate other examples of non-planar N-amido groups in the literature, we employed the Cambridge crystallographic database.¹⁹ We sought to identify all structurally characterized compounds containing N-amido ligands and subsequently calculate the non-planarity parameters of each N-amido unit. Based on this investigation, our complexes contain amide ligands that are substantially more non-planar than any other class of compounds containing N-amido groups.

Results and Discussion

Structural Data. As discussed in Chapter 2, the PAC ligand is sufficiently flexible to allow the production of *cis*- β and *cis*- α isomers. Crystals suitable for X-ray diffraction were grown of two of these *cis* complexes: the *cis*- β complex 11 and the *cis*- α complex 14. A crystallographic structure determination was completed for each compound. We wanted to learn which bond deformations occurred upon movement of a phenolate arm out of the equatorial plane to an axial site.

The ortep of 11 shown in Figure 3.2 shows an octahedral osmium coordination sphere. The PAC ligand of the *cis*- β complex occupies three equatorial and one axial site with the bipy ligand, filling the remaining two binding sites. All bond distances and bond angles are normal compared to structures of other Os(IV) PAC ligand complexes completed by the Collins group to date (Tables 3.1 and 3.2). The unexpected structural feature in this ortep is the non-planarity of one N-amido ligand, C3B-C2B (O2B)-N1B(Os)-C1B. The carbonyl group of this amide is in the plane of the attached phenolate arm rather than in the plane of the ligand bridge. The other amide is coplanar with both the other phenolate arm and the bridge of the chelate. Two non-planar amide ligands are seen in the structure of 14.

The ortep of 14 (Figure 3.3) again shows octahedral coordination around the osmium with both axial sites occupied by the phenolate arms of (η^4 -CHBA-DCB)⁴⁻. No unusual bond distance or bond angles are seen in the structure of 14 (Tables 3.3 and 3.4). As in the structure of 11, the significant feature in this structure is the non-planar N-amido ligands. Isomerization to form the *cis*- α isomer is achieved principally through

Figure 3.2. Ortep of *cis*- β -Os(η^4 -CHBA-DCB)(bipy), 11.

Table 3.1. Selected Bond Distances of 11.

Atom	Atom	Dist (Å)	Atom	Atom	Dist (Å)
Os	O1A	2.006(7)	C2A	C3A	1.51(2)
Os	O1B	1.987(8)	C2B	C3B	1.49(2)
Os	N1A	2.003(9)	C3A	C4A	1.41(2)
Os	N1B	1.977(9)	C3A	C8A	1.40(2)
Os	N2A	2.071(9)	C3B	C4B	1.43(2)
Os	N2B	2.112(9)	C3B	C8B	1.39(2)
Cl1A	C5A	1.75(1)	C4A	C5A	1.37(2)
Cl1B	C5B	1.75(1)	C4B	C5B	1.34(2)
Cl2A	C7A	1.73(1)	C5A	C6A	1.37(2)
Cl2B	C7B	1.74(1)	C5B	C6B	1.38(2)
Cl3A	C10A	1.73(1)	C6A	C7A	1.36(2)
Cl3B	C10B	1.73(1)	C6B	C7B	1.35(2)
O1A	C8A	1.31(1)	C7A	C8A	1.43(2)
O2A	C2A	1.22(1)	C7B	C8B	1.42(2)
O1B	C8B	1.36(1)	C9A	C10A	1.38(2)

Table 3.1. (continued).

Atom	Atom	Dist (Å)	Atom	Atom	Dist (Å)
O2B	C2B	1.24(1)	C9B	C10B	1.38(2)
N1A	C1A	1.42(1)	C10A	C10B	1.36(2)
N1A	C2A	1.39(1)	C11A	C11B	1.44(2)
N1B	C1B	1.40(1)	C11A	C12A	1.38(2)
N1B	C1B	1.37(1)	C11B	C12B	1.40(2)
N2A	C11A	1.35(1)	C12A	C13A	1.38(2)
N2A	C15A	1.38(1)	C12B	C13B	1.38(2)
N2B	C11B	1.38(1)	C13A	C14A	1.35(2)
N2B	C15B	1.32(2)	C13B	C14B	1.32(2)
C1A	C1B	1.41(2)	C14A	C15A	1.37(2)
C1A	C9A	1.39(2)	C14B	C15B	1.39(2)
C1B	C9B	1.42(2)			

Table 3.2. Selected Bond Angles of 11.

Atom	Atom	Atom	Angle (°)	Atom	Atom	Atom	Angle (°)
O1A	Os	O1B	88.6(3)	N1A	C2A	O2A	123(1)
O1A	Os	N1A	95.2(3)	C3A	C2A	O2A	117(1)
O1A	Os	N1B	171.9(3)	C3A	C2A	N1A	120(1)
O1A	Os	N2A	91.6(3)	N1B	C2B	O2B	123(1)
O1A	Os	N2B	84.1(3)	C3B	C2B	O2B	120(1)
O1B	Os	N1A	100.2(3)	C3B	C2B	N1B	117(1)
O1B	Os	N1B	85.7(3)	C4A	C3A	C2A	113(1)
O1B	Os	N2A	169.1(3)	C8A	C3A	C2A	127(1)
O1B	Os	N2B	91.9(3)	C8A	C3A	C4A	120(1)
N1A	Os	N1B	80.1(4)	C4B	C3B	C2B	116(1)
N1A	Os	N2A	90.6(3)	C8B	C3B	C2B	124(1)
N1A	Os	N2B	167.8(3)	C8B	C3B	C4B	119(1)
N1B	Os	N2A	95.1(3)	C5A	C4A	C3A	120(1)

Table 3.2. (continued).

Atom	Atom	Atom	Angle (°)	Atom	Atom	Atom	Angle (°)
N1B	Os	N2B	101.9(3)	C5B	C4B	C3B	120(1)
N2A	Os	N2B	77.2(3)	C4A	C5A	Cl1A	119(1)
C8A	O1A	Os	123.2(7)	C6A	C5A	Cl1A	120(1)
C8B	O1B	Os	118.8(7)	C6A	C5A	C4A	121(1)
C1A	N1A	Os	114.4(7)	C4B	C5B	Cl1B	119(1)
C2A	N1A	Os	125.4(7)	C6B	C5B	Cl1B	119(1)
C2A	N1A	C1A	120.1(9)	C6B	C5B	C4B	122(1)
C1B	N1B	Os	114.6(7)	C7A	C6A	C5A	120(1)
C2B	N1B	Os	122.6(7)	C7B	C6B	C5B	119(1)
C2B	N1B	C1B	121.4(9)	C6A	C7A	Cl2A	119(1)
C11A	N2A	Os	116.7(7)	C8A	O7A	Cl2A	118.8(9)
C15A	N2A	Os	125.9(7)	C8A	C7A	C6A	122(1)
C15A	N2A	C11A	117.4(9)	C6B	C7B	Cl2B	120(1)

Table 3.2. (continued).

Atom	Atom	Atom	Angle (°)	Atom	Atom	Atom	Angle (°)
C11B	N2B	Os	114.1(7)	C8B	C7B	C12B	118.2(9)
C15B	N2B	Os	126.3(8)	C8B	C7B	C6B	122(1)
C15B	N2B	C11B	120(1)	C3A	C8A	O1A	127(1)
C1B	C1A	N1A	112.8(9)	C7A	C8A	O1A	116(1)
C9A	C1A	N1A	128(1)	C7A	C8A	C3A	117(1)
C9A	C1A	C1B	119(1)	C3B	C8B	O1B	124(1)
C1A	C1B	N1B	115(1)	C7B	C8B	O1B	118(1)
C9B	C1B	N1B	125(1)	C7B	C8B	C3B	118(1)
C9B	C1B	C1A	120(1)	C10A	C9A	C1A	120(1)
C9A	C10A	C13A	118.9(9)	C12B	C11B	N2B	119(1)
C10B	C10A	C13A	120.4(9)	C12B	C11B	C11A	125(1)
C10B	C1A	C9A	121(1)	C13A	C12A	C11A	119(1)
C9B	C10B	C13B	117(1)	C13B	C12B	C11B	120(1)

Table 3.2. (continued).

Atom	Atom	Atom	Angle (°)	Atom	Atom	Atom	Angle (°)
C10A	C10B	C13B	122(1)	C14A	C13A	C12A	120(1)
C10A	C10B	C9B	121(1)	C14B	C13B	C12B	120(1)
C11B	C11A	N2A	115(1)	C15A	C14A	C13A	119(1)
C12A	C11A	N2A	122(1)	C15B	C14B	C13B	119(1)
C12A	C11A	C11B	123(1)	C14A	C15A	N2A	123(1)
C11A	C11B	N2B	116(1)	C14B	C15B	N2B	122(1)

14.

Table 3.3. Selected Bond Distances of 14.

Atom	Atom	Dist (Å)	Atom	Atom	Dist (Å)
Os	P	2.425(6)	C8	C13	1.44(3)
Os	O1	1.962(14)	C9	C10	1.40(3)
Os	O2	2.022(13)	C10	C11	1.36(3)
Os	N1	2.027(16)	C11	C12	1.36(3)
Os	N2	1.958(16)	C12	C13	1.37(3)
Os	C	1.96(2)	C14	C15	1.44(3)
P	P1	1.82(2)	C15	C16	1.43(3)
P	P7	1.82(2)	C15	C20	1.38(3)
P	P13	1.80(2)	C16	C17	1.33(3)
Cl1	C2	1.69(2)	C17	C18	1.41(3)
Cl2	C4	1.75(2)	C18	C19	1.39(3)
Cl3	C10	1.73(2)	C19	C20	1.39(3)
Cl4	C11	1.71(2)	C22	C23	1.46(5)
Cl5	C17	1.74(2)	C22	C24	1.43(5)
Cl6	C19	1.71(2)	C22	C25	1.44(5)

Table 3.3. (continued).

Atom	Atom	Dist (Å)	Atom	Atom	Dist (Å)
O1	C1	1.32(3)	P1	P2	1.36(3)
O2	C20	1.34(2)	P1	P6	1.36(3)
O3	C7	1.24(3)	P2	P3	1.37(4)
O4	C14	1.27(3)	P3	P4	1.35(4)
N	C	1.18(3)	P4	P5	1.39(3)
N	C22	1.54(4)	P5	P6	1.37(3)
N1	C7	1.43(3)	P7	P8	1.34(3)
N1	C8	1.38(3)	P7	P12	1.37(3)
N2	C13	1.38(3)	P8	P9	1.40(3)
N2	C14	1.44(3)	P9	P10	1.37(3)
C1	C2	1.40(3)	P10	P11	1.37(3)
C1	C6	1.41(3)	P11	P12	1.43(3)
C2	C3	1.34(3)	P13	P14	1.35(3)
C3	C4	1.40(3)	P13	P18	1.41(3)
C4	C5	1.36(3)	P14	P15	1.42(3)
C5	C6	1.42(3)	P15	P16	1.31(4)
C6	C7	1.45(3)	P16	P17	1.33(4)
C8	C9	1.45(3)	P17	P18	1.40(4)

Table 3.4. Selected Bond Angles of 14.

Atom	Atom	Atom	Angle (°)	Atom	Atom	Atom	Angle (°)
O1	Os	P	92.3(4)	C3	C2	Cl1	121(2)
O2	Os	P	77.7(4)	C3	C2	C1	121(2)
N1	Os	P	101.1(5)	C4	C3	C2	121(2)
N2	Os	P	158.1(5)	C3	C4	Cl2	120(2)
C	Os	P	93.2(6)	C5	C4	Cl2	119(2)
O2	Os	O1	167.1(5)	C5	C4	C3	121(2)
N2	Os	O1	108.8(6)	C5	C6	C1	121(2)
N1	Os	O1	84.8(6)	C6	C5	C4	118(2)
C	Os	O1	80.0(7)	C7	C6	C1	125(2)
N1	Os	O2	104.9(6)	C7	C6	C5	113(2)
N2	Os	O2	82.1(6)	N1	C7	O3	119(2)
C	Os	O2	92.5(7)	C6	C7	O3	125(2)
N2	Os	N1	76.1(7)	C6	C7	N1	115(2)

Table 3.4. (continued).

Atom	Atom	Atom	Angle (°)	Atom	Atom	Atom	Angle (°)
C	Os	N1	159.5(8)	C9	C8	N1	125(2)
C	Os	N2	95.9(8)	C13	C8	N1	115(2)
C1	O1	Os	128(3)	C13	C8	C9	121(2)
C20	O2	Os	121(1)	C10	C9	C8	115(2)
C22	N	C	175(2)	C9	C10	C13	114(2)
C7	N1	Os	122(1)	C11	C10	C13	121(2)
C8	N1	Os	117(1)	C11	C10	C9	125(2)
C8	N1	C7	121(2)	C10	C11	C14	121(2)
C13	N2	Os	122(1)	C12	C11	C14	120(2)
C14	N2	Os	119(1)	C12	C11	C10	119(2)
C14	N2	C13	114(2)	C13	C12	C11	123(2)
N2	C14	O4	119(2)	P7	P	Os	116.5(7)
C15	C14	O4	125(2)	P7	P	P1	106(1)

Table 3.4. (continued).

Atom	Atom	Atom	Angle (°)	Atom	Atom	Atom	Angle (°)
C15	C14	N2	116(2)	P8	P7	P	119(2)
C16	C15	C14	115(2)	P12	P7	P	119(2)
C20	C15	C14	123(2)	P12	P7	P8	122(2)
C20	C15	C16	120(2)	P9	P8	P7	119(2)
C17	C16	C15	120(2)	P10	P9	P8	120(2)
C16	C17	C15	118(2)	P11	P10	P9	122(2)
C18	C17	C15	119(2)	P12	P11	P10	117(2)
C18	C17	C16	122(2)	P11	P12	P7	120(2)
C19	C18	C17	117(2)	P13	P	Os	115.2(8)
C18	C19	C16	117(2)	P13	P	P7	103(1)
C20	C19	C16	119(2)	P14	P13	P	124(2)
C20	C19	C18	124(2)	P18	P13	P	122(2)
C15	C20	O2	123(2)	P18	P13	P14	114(2)

Table 3.4. (continued).

Atom	Atom	Atom	Angle (°)	Atom	Atom	Atom	Angle (°)
C19	C20	O2	119(2)	P15	P14	P13	124(2)
C19	C20	C15	117(2)	P16	P15	P14	119(2)
P1	P	Os	111.1(7)	P17	P16	P15	121(3)
P1	P	P13	104(1)	P18	P17	P16	120(3)
P2	P1	P	120(2)	P17	P18	P13	122(2)
P6	P1	P	120(2)	N	C	Os	169(2)
P6	P1	P2	119(2)	C23	C22	N	103(3)
P3	P2	P1	122(2)	C24	C22	N	103(3)
P4	P3	P2	119(2)	C25	C22	N	101(3)
P5	P4	P3	118(2)	C24	C22	C23	114(3)
P6	P5	P4	122(2)	C25	C22	C23	118(3)
P5	P6	P1	118(2)	C25	C22	C24	114(3)
C2	C1	O1	119(2)	C8	C13	N2	108(2)
C6	C1	O1	124(2)	C12	C13	N2	134(2)
C6	C1	C2	117(2)	C12	C13	C8	118(2)
C1	C2	C11	118(2)				

amide C-N bond rotation, which makes possible phenolate coordination to the axial site of the metal center. Viewing the ortep down the amide C-N bond better displays this point (Figure 3.4). In the center of the foreground of the ortep can be seen the "front" amide carbonyl C7-O3. The nitrogen atom of this amide, N1, can be partially seen behind C7. The carbonyl group of this amide is in the plane of the arm of the PAC ligand rather than in the plane of the bridge. The front amide obstructs the view of the rear amide carbon and nitrogen atoms. Only the carbonyl oxygen, O4, can be seen. If the positions of the hidden atoms are approximately behind those of the front amide, then the rear carbonyl is similarly in the plane of the rear PAC ligand arm.

The view of the PAC ligand in Figure 3.4 establishes three distinct planes comprised of each phenolate arm and the bridge. The dihedral angles between these elements have been calculated from the fitted least-squares planes (Table 3.5) and are shown unbracketed in Figure 3.4. The dihedral angles ($51(2)^\circ$ and $62(2)^\circ$) provide a measure of the PAC ligand distortions that are necessary to form the cis- α isomer. Certain amide C-N torsion angles, $\omega(\text{O3-C7-N1-C8})$ and $\omega(\text{O4-C14-N2-C13})$, describe the extent of C-N bond rotation that occurs upon isomerization. These values are shown in brackets in Figure 3.4 ($52(3)^\circ$ and $61(3)^\circ$). Within the standard deviations, the dihedral angle and amide torsion angle are equal for each side of the PAC ligand. Because the dihedral angles result from gross chelate deformations, the similarity of these angles with the amide torsion angles strongly suggests that amide-centered C-N bond rotations make possible the formation of cis isomers. Flexibility of the chelate primarily results from the changes in N-amido ligand bonding.

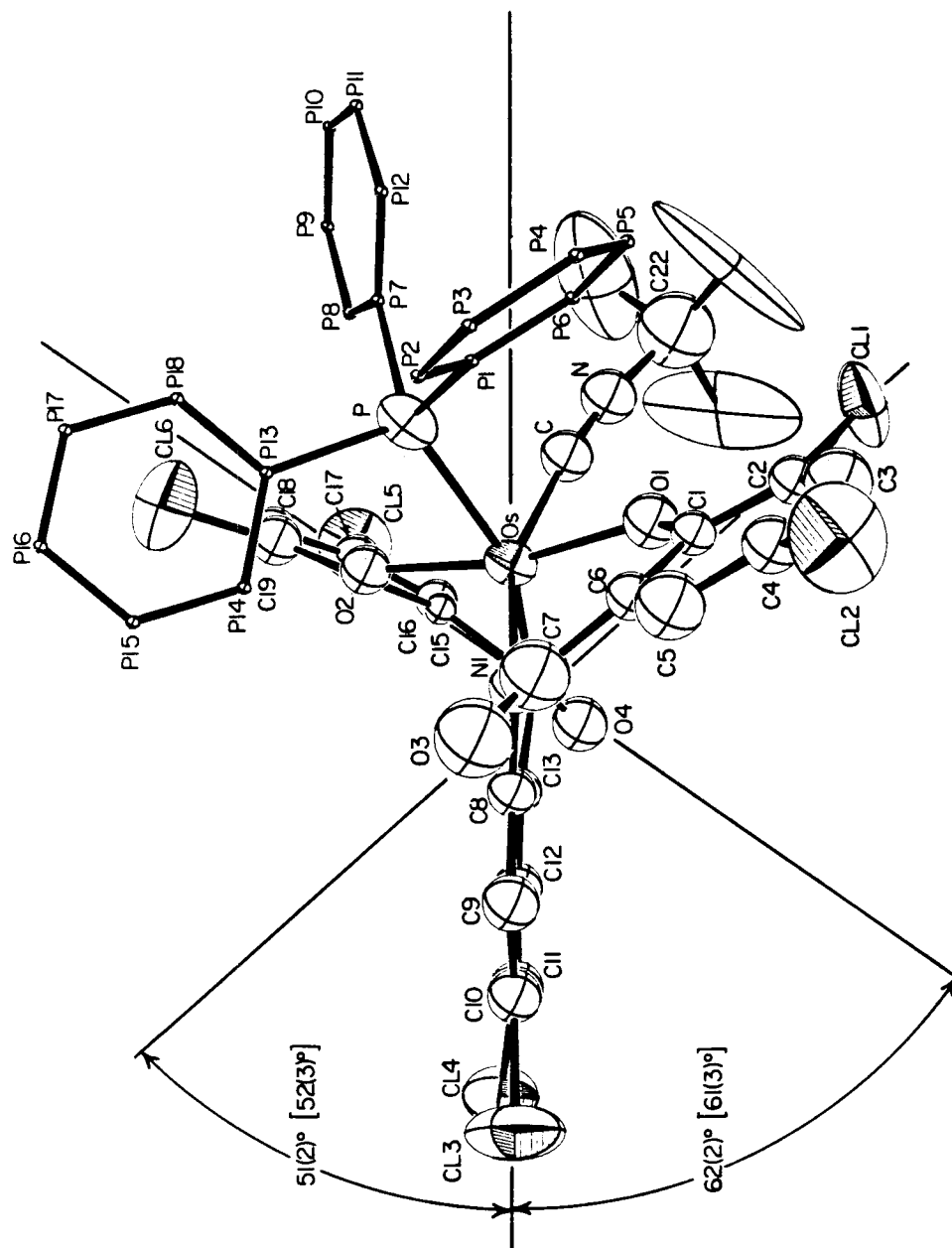


Figure 3.4. Ortep of 14 viewed down the amide C-N axis. The unbracketed angles are the dihedral angles between the calculated least-squares plane of the bridge atoms and the least-squares planes of the phenolate atoms. The bracketed angles are amide torsion angles, $\omega(\text{O-C-N-C})$.

Table 3.5. Best Least-squares Planes of the PAC Ligand Phenolate Arms and Bridge for 14.

CA Best Plane (PAC ligand arm)

Atoms: N1, C7, O3, C6, C5, C4, C3, C2, C1.

Direction cosines of plane normal: -0.4828, 0.0781, 0.8723.

Origin-to-plane distance : 2.740 Å

Deviations of atoms from plane CA:

<u>Atom</u>	<u>Dev. (Å)</u>	<u>Atom</u>	<u>Dev. (Å)</u>
N1	-0.0523	C4	-0.0601
C7	-0.0027	C3	0.1257
O3	0.2092	C2	0.1049
C6	-0.1476	C1	-0.0416
C5	-0.1356		

CB Best Plane (PAC ligand arm)

Atoms: N2, C14, O4, C15, C16, C17, C18, C19, C20.

Direction cosines of plane normal: 0.2397, 0.8891, -0.3899.

Origin-to-plane distance: 1.747 Å

Deviations of atoms from plane CB:

<u>Atom</u>	<u>Dev. (Å)</u>	<u>Atom</u>	<u>Dev. (Å)</u>
N2	-0.1804	C17	-0.0509
C14	0.0221	C18	-0.1028
O4	0.0361	C19	-0.0077
C15	0.1136	C20	0.1637
C16	0.0062		

Table 3.5. (continued).

D Best Plane (PAC ligand bridge)

Atoms: C7, N1, C8, C9, C10, C11, C12, C13, N2, C14.

Direction cosines of plane normal: -0.1095, 0.9097, 0.4006.

Origin-to-plane distance: 3.575 Å

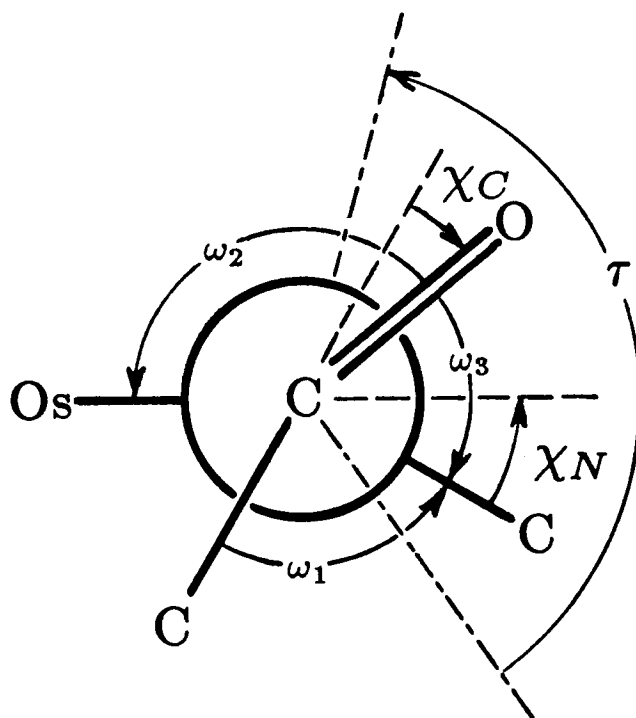
Deviations of atoms from plane D:

<u>Atom</u>	<u>Dev. (Å)</u>	<u>Atom</u>	<u>Dev. (Å)</u>
C7	0.0453	C11	-0.0291
N1	-0.1205	C12	0.0334
C8	0.0060	C13	0.0787
C9	-0.0087	N2	0.1223
C10	-0.0208	C14	-0.1067

Amide Non-planarity Parameters. We have used the analysis method of Dunitz and Winkler to quantify the non-planarity of the N-amido groups in 11 and 14. In their studies of amide group conformations, Dunitz and Winkler defined two out-of-plane bending parameters, χ_N and χ_C (which describe trigonal planar to pyramidal distortions at the amide nitrogen and carbonyl carbon atoms), and a twist parameter, τ (which approximates the angle between the nitrogen and carbonyl carbon $p\pi$ orbitals).⁹ These parameters measure the degree to which the three conditions contribute to amide non-planarity. The diagram in Figure 3.5 describes how τ , χ_N and χ_C are derived from amide C-N torsion angles ω_1 , ω_2 , and ω_3 calculated from structural data.¹¹ Linear combinations of the three meaningless torsion angles generate three quantities pertinent to understanding amide non-planarity. For a rigorously planar amide, both the nitrogen and carbonyl carbon atoms are sp^2 hybridized, so χ_N and χ_C are both equal to 0° . The limiting value of τ can be 0° if the parent organic chain has cisoid geometry or 180° if it has transoid geometry. Carbon-nitrogen $p\pi$ overlap is expected to be close to zero when τ is $\pm 90^\circ$. Here we define a modified version of τ , $\bar{\tau}$, such that

$$\bar{\tau} = (\tau) \bmod \pi.$$

In contrast to τ , this new term does not distinguish cisoid and transoid geometries. However, $\bar{\tau}$ provides an approximate measure of the smaller angle between the nitrogen and carbonyl carbon $p\pi$ orbitals and is easily visualized ($-90^\circ < \bar{\tau} \leq 90^\circ$). According to the measures, χ_C , χ_N , and $\bar{\tau}$, the N-amido ligands of 11 and 14 are decidedly non-planar (Table 3.6). The magnitudes of the $\bar{\tau}$ and χ_N values are frequently greater than those of χ_C .



$$\bar{\tau} = ((\omega_1 + \omega_2)/2) \bmod \pi$$

$$\chi_N = (\omega_2 - \omega_3 + \pi) \bmod 2\pi$$

$$\chi_C = (\omega_1 - \omega_3 + \pi) \bmod 2\pi$$

Figure 3.5. Parameters for describing non-planarity in N-amido groups.

Table 3.6. Selected Amide Torsion Angles and Calculated Non-planarity Parameters for 11 and 14.

Atoms	Torsion	Angle (°)	Parameter	Value (°)
Compound 11				
(planar amide)				
C3A-C2A-N1A-C1A	ω_{1a}	180(2)	χ_{Ca}	3(3)
O2A-C2A-N1A-Os	ω_{2a}	-178(2)	χ_{Na}	5(2)
O2A-C2A-N1A-C1A	ω_{3a}	-3(3)	$\bar{\tau}_a$	-1(3)
(non-planar amide)				
C3B-C2B-N1B-C1B	ω_{1b}	136(2)	χ_{Cb}	-4(3)
O2B-C2B-N1B-Os	ω_{2b}	155(2)	χ_{Nb}	15(2)
O2B-C2B-N1B-C1B	ω_{3b}	-40(3)	$\bar{\tau}_b$	-35(3)
Compound 14				
(amide trans to <i>t</i> -BuNC)				
C6-C7-N1-C8	ω_{1a}	124(2)	χ_{Ca}	4(3)
O3-C7-N1-Os	ω_{2a}	-138(2)	χ_{Na}	-10(2)
O3-C7-N1-C8	ω_{3a}	52(3)	$\bar{\tau}_a$	49(3)
(amide trans to PPh ₃)				
C15-C14-N2-C13	ω_{1b}	-117(2)	χ_{Cb}	2(3)
O4-C14-N2-Os	ω_{2b}	-143(2)	χ_{Nb}	-24(2)
O4-C14-N2-C13	ω_{3b}	61(3)	$\bar{\tau}_b$	50(2)

This trend is also observed in organic amide analyses. Amide deformations generally occur through C-N bond rotation and nitrogen atom pyramidalization with retention of planarity at the carbon atom. The $\bar{\tau}$ values in Table 3.6 for the non-planar amides are remarkably high compared to organic amide groups. No range of $\bar{\tau}$, χ_N , and χ_C values, however, has been defined as normal for N-amido ligands, so we undertook to determine them.

The Cambridge crystallographic database was used to locate all structurally characterized RC(O)NR'M and RC(OM')NR'M functionalities (R- and R'- are general groups, but do not include H). Bibliographic references, coordinate data and complete amide torsion angle analyses of these compounds were then compiled utilizing the Cambridge database programs.¹²⁻¹⁶ In Figures 3.6-3.9 the values of $\bar{\tau}$ and χ_N for 11 and 14 are compared with those of all other reported RC(O)NR'M and RC(OM')NR'M functionalities by plotting $\bar{\tau}$ vs. χ_N and $\bar{\tau}$ vs. χ_C . Besides the structures of 11 and 14 reported here, other complexes found to contain non-planar N-amido ligands are summarized in Table 3.7.

There are 457 data points in each of Figures 3.6 and 3.7. Of these points, 118 represent cases of monodentate N-amido ligands where the parent free-base ligand is a secondary organic amide functional group. The secondary amide data are plotted separately in Figures 3.8 and 3.9. The large values of $\bar{\tau}$ ($>25^\circ$) found for 14 and 16^{12a} (Table 3.7) are unprecedented for N-amido complexes that have the option to reduce $\bar{\tau}$ by isomerizing at the metal center. The primary cause of the non-planarity in these two complexes appears to be increased thermodynamic stabilization resulting from the trans to cis- α isomerization. The cis- β PAC ligand complexes 11 and 17^{12f} (Table 3.7) exhibit large $\bar{\tau}$ values apparently

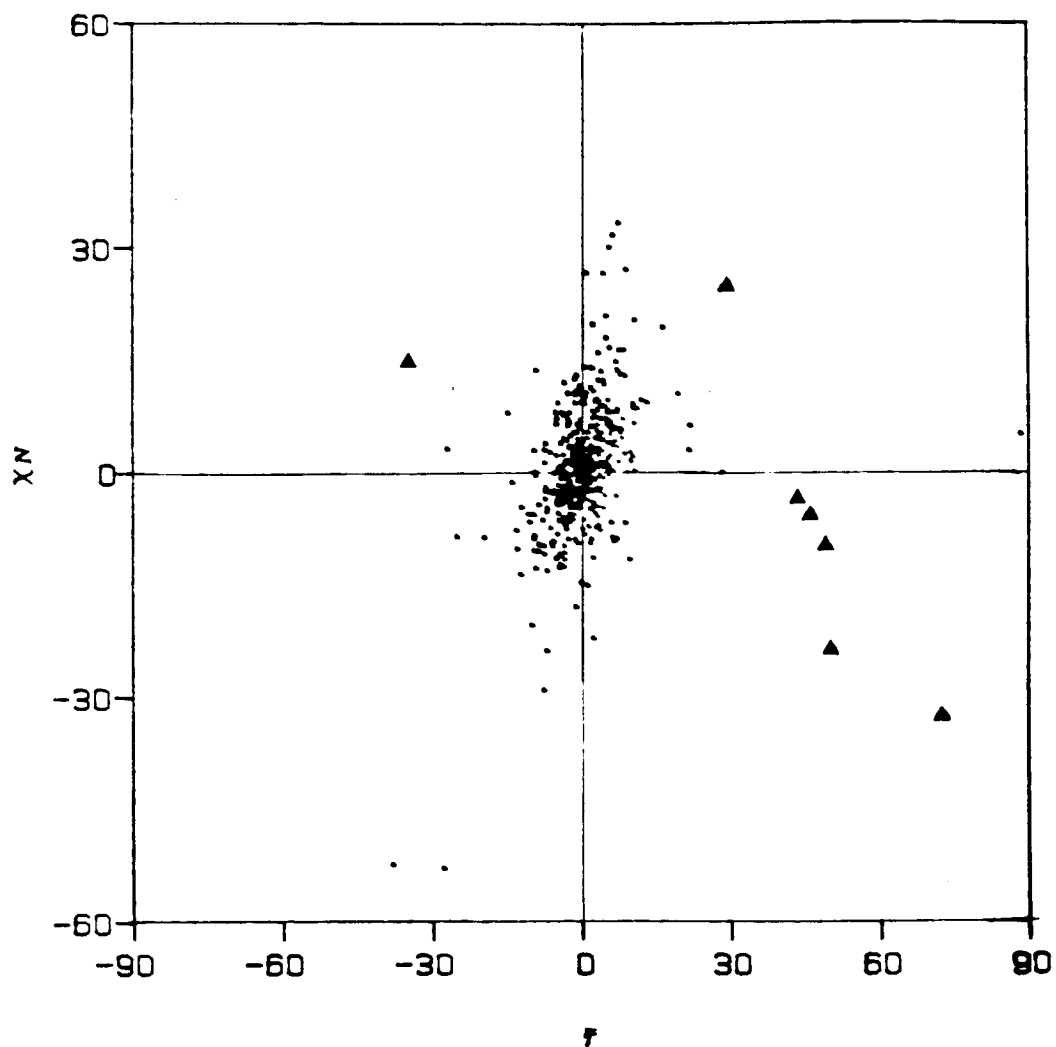


Figure 3.6. Plot of τ vs. χ_N for all $\text{RC}(\text{O})\text{NR}'\text{M}$ and $\text{RC}(\text{OM}')\text{NR}'\text{M}$ fragments. \bullet Literature points; \blacktriangle Points from this thesis and for osmium complexes of PAC ligands where large τ values ($> 25^\circ$) are found.

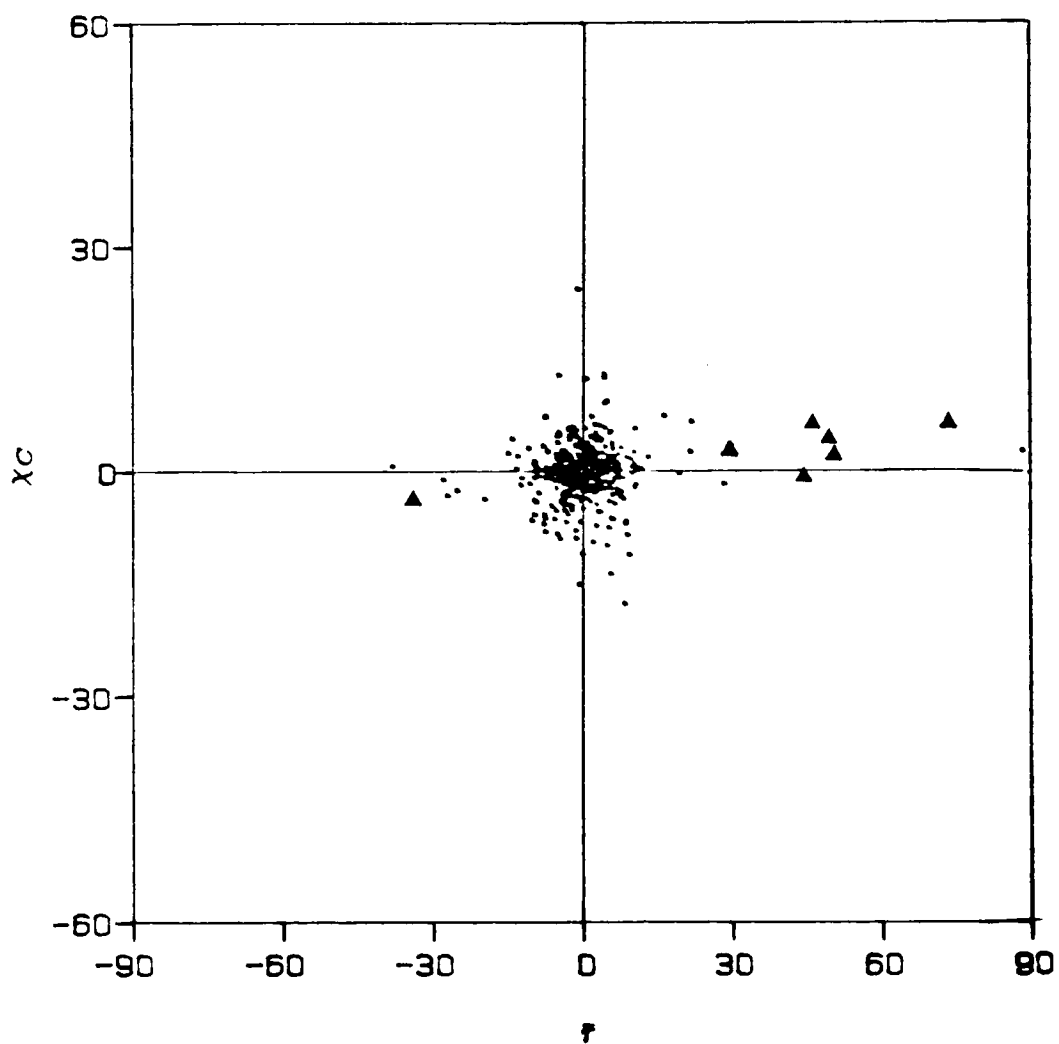


Figure 3.7. Plot of $\bar{\tau}$ vs. χ_C for all $\text{RC(O)NR}'\text{M}$ and $\text{RC(OM)NR}'\text{M}$ fragments. \bullet Literature points; \blacktriangle Points from this thesis and for osmium complexes of PAC ligands where large $\bar{\tau}$ values ($> 25^\circ$) are found.

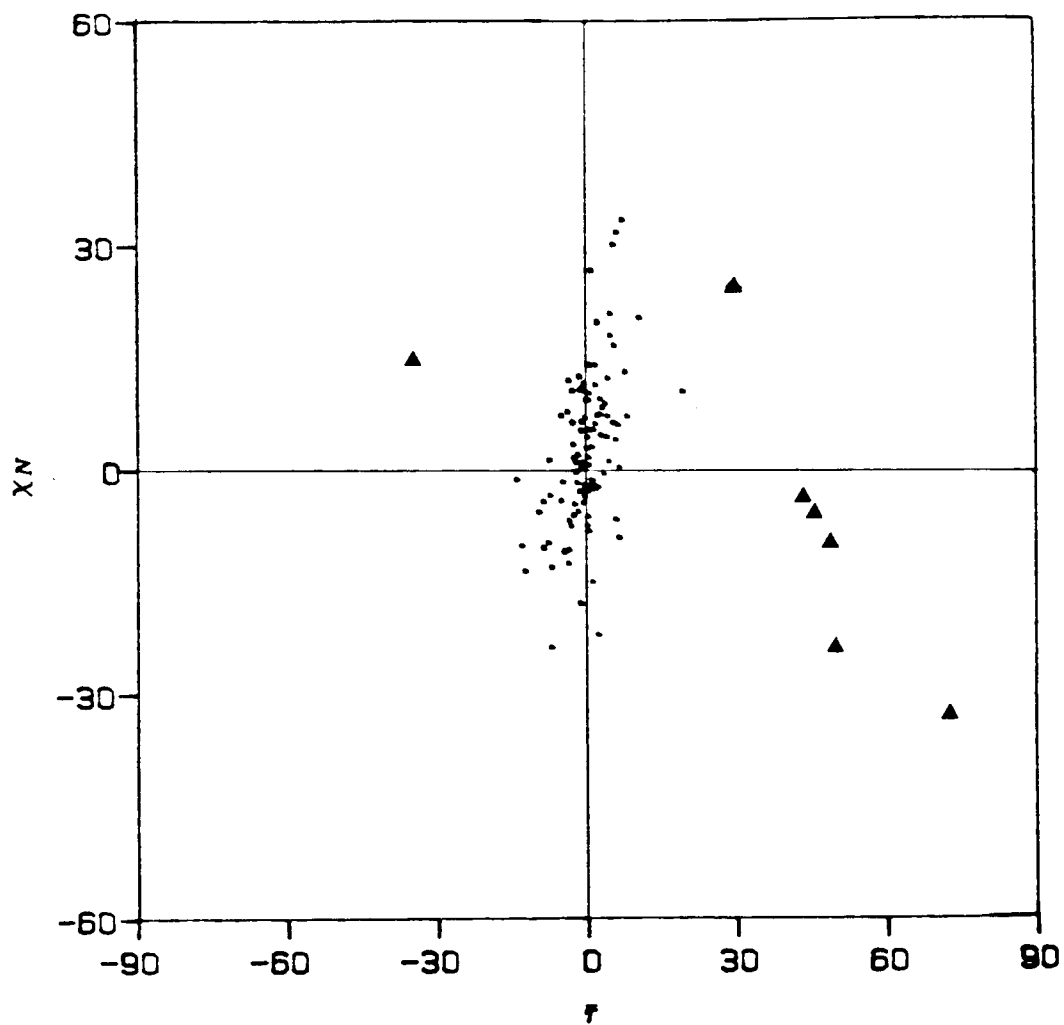


Figure 3.8. Plot of τ vs. χ_N for all $\text{RC(O)NR}'\text{M}$ fragments where the free base form, $\text{RC(O)NR}'\text{H}$, is a secondary amide. ● Literature points; ▲ Points from this thesis and for osmium complexes of PAC ligands where large τ values ($> 25^\circ$) are found.

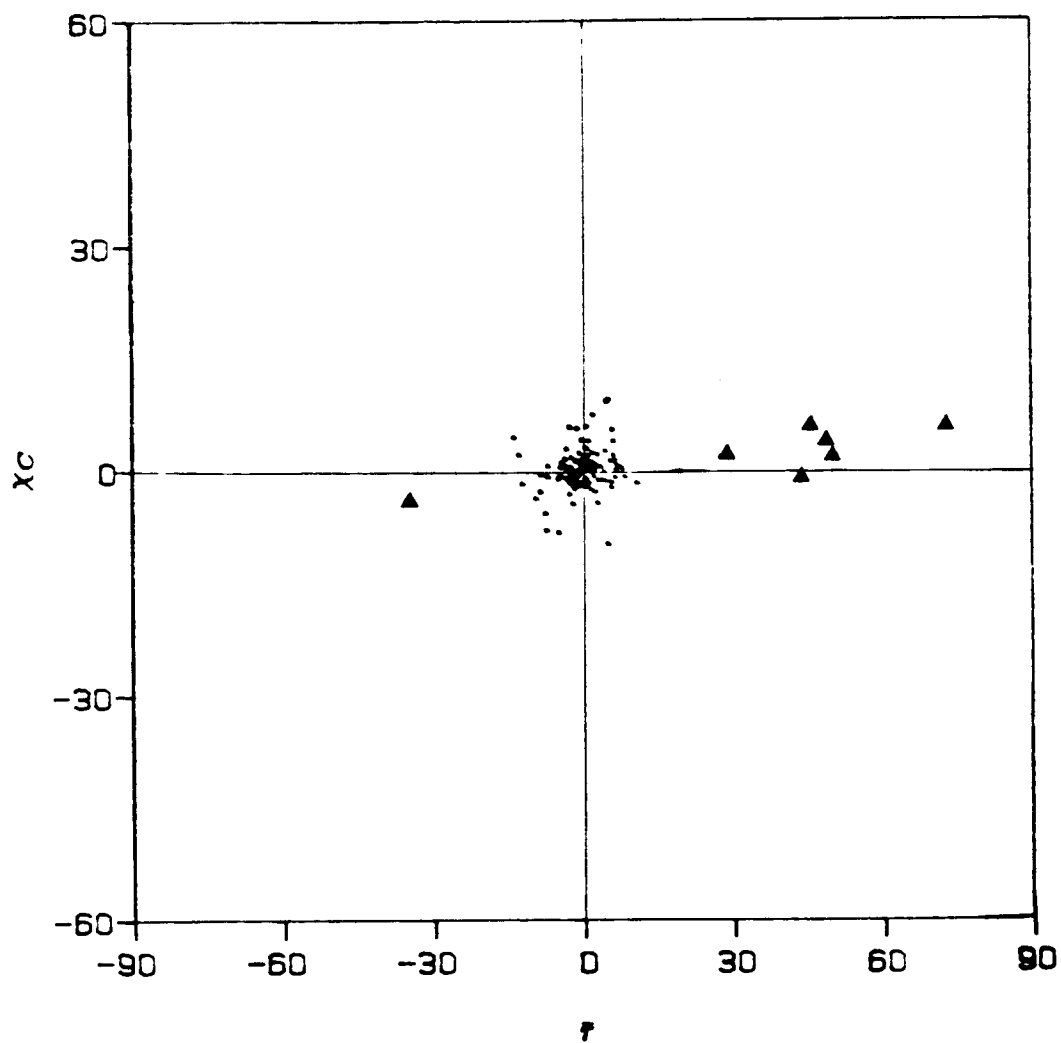


Figure 3.9. Plot of τ vs. χ_C for all $\text{RC(O)NR}'\text{M}$ fragments where the free base form, $\text{RC(O)NR}'\text{H}$, is a secondary amide. ● Literature points; ▲ Points from this thesis and for osmium complexes of PAC ligands where large τ values ($> 25^\circ$) are found.

Table 3.7. Amide Non-planarity Parameters for RC(O)NR'M and RC(OM')NR'M Fragments where $\tau > 25^\circ$.

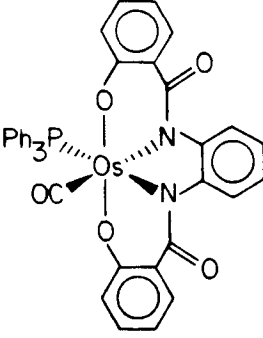
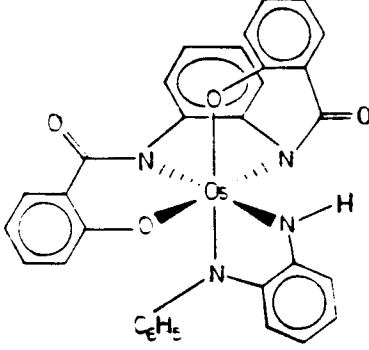
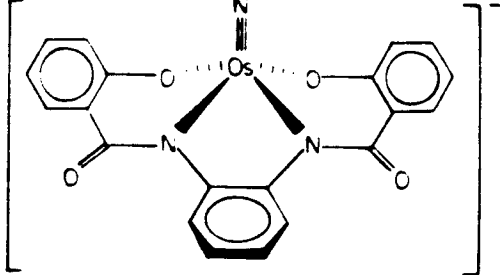
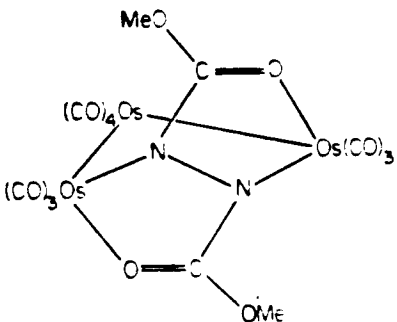
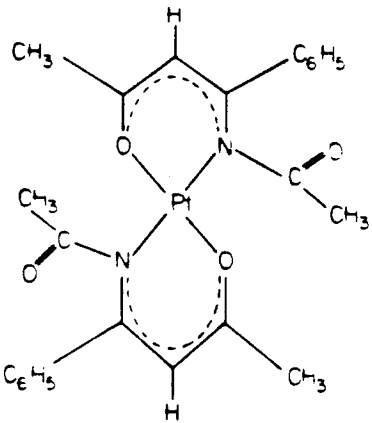
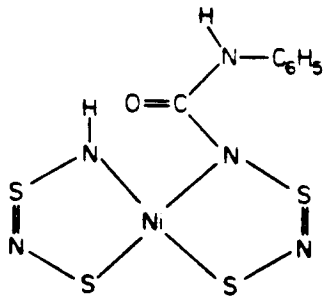
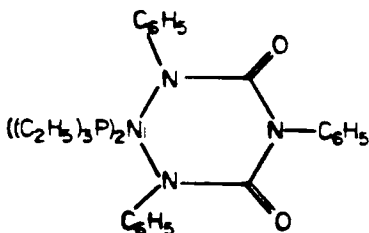
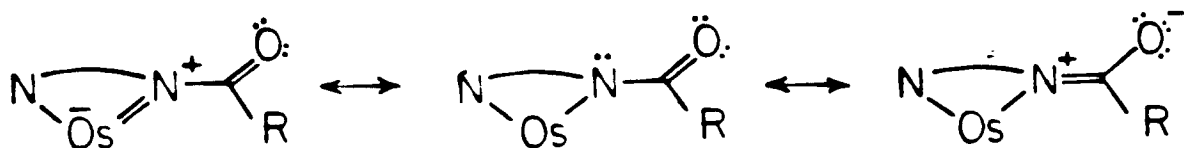
Compound	$\tau(^{\circ})$	$\chi_N(^{\circ})$	$\chi_C(^{\circ})$	Ref
 <p>16</p>	44	-6	6	12g
	73	-33	6	
 <p>17</p>	22	6	7	12f
	44	-4	-1	
 <p>18</p>	30	25	3	12f
	5	7	0	

Table 3.7. (continued).

Compound	$\tau(^{\circ})$	$\chi_N(^{\circ})$	$\chi_C(^{\circ})$	Ref.
	-28 -38	-53 -52	-1 1	14cx
	88	5	3	14xi
	29	0	-2	14xxxvi
	-27 -15	3 8	-3 3	14cvi

because of the structural constraints of the coordination sphere forcing the formation of non-planar N-amido ligands. Complex 18 also shows an unusually high $\bar{\tau}$ value.^{12f} It is likely that the non-planarity partially results from distortions caused by the osmium atom sitting 0.55 Å out of the plane of the coordinated nitrogen and oxygen atoms. In the other four cases where the $\bar{\tau}$ values of $\text{RC(O)NR}'\text{M}$ and $\text{RC(OM}')\text{NR}'\text{M}$ groups are greater than 25° (Table 3.7), the nitrogen atom has formal multiple bonds to its R' substituent, or the carbonyl group is involved in multiple bonding with its R substituent.¹⁴ None of the $\text{RC(O)NR}'$ -ligands in these four cases is derived from parent organic amide functional groups. Theoretical studies of amide group deformations^{8,9b} conclude that pyramidalization at the nitrogen atom is energetically less demanding than pyramidalization at carbon or rotation about the C-N bond. Consistent with these results, there is a wider distribution of χ_{N} values than either χ_{C} or $\bar{\tau}$ values in Figures 3.6-3.9. Amide non-planarity has been considered previously for N-amido groups that exhibit large χ_{N} values.^{13xxiv}

Amide Bonding Changes. The resulting amide geometries indicate an alteration of the amide bonding characteristics. The resonance structures for an N-amido ligand are shown below. Because of the C-N bond rotation that occurs in forming cis isomers, the overlap between the carbonyl π^* orbital and the nitrogen lone pair decreases; hence, the contribution from the dipolar resonance



form on the right is attenuated. The amide carbonyl groups of *cis* isomers should have correspondingly higher C=O bond order and IR stretching frequencies than those of *trans* isomers. The IR spectrum of **11** shows two bands in the carbonyl region: one at 1622 cm⁻¹ for the planar amide and the other at 1635 cm⁻¹ for the non-planar amide. The IR spectrum for *cis*-**14** shows one carbonyl band at 1650 cm⁻¹. Other *cis* complexes described in Chapter 2 also have high carbonyl stretching frequencies. The complex *cis*- α -Os(η^4 -CHBA-DCB)(*t*-BuNC)₂, **15**, has a carbonyl band at 1653 cm⁻¹ and *cis*- β -Os(η^4 -CHBA-DCB)(dppe), **13**, displays bands at 1607 cm⁻¹ (planar amide) and 1670 cm⁻¹ (non-planar amide). Unusually high amide carbonyl stretching frequencies also have been seen in organic compounds containing non-planar amide moieties.⁴⁻⁷

We wanted to correlate the structural non-planarity parameters of **11** and **14** to data reflecting amide bonding changes, specifically the IR carbonyl bands. Only negligible carbon atom pyramidalization occurs in forming non-planar amides. Of the two other deformations measured by $\bar{\tau}$ and χ_N , theoretical studies reveal C-N bond rotation to be energetically more demanding; therefore, we expected the best correlation to be that of ν_{CO} and some quantity derived from $\bar{\tau}$. Molecular orbital calculations show that as two adjacent π orbitals rotate about a common axis, the overlap integral changes as a function of $\cos(\theta)$, where θ is the torsion angle between the two orbitals.¹⁷ Aligned orbitals ($\theta = 0^\circ$) achieve optimal overlap, whereas orthogonal orbitals ($\theta = 90^\circ$) have no overlap. The contribution from the amide dipolar resonance form should be dependent upon the overlap of the π orbitals or, alternatively, $\cos(\bar{\tau})$. We chose to correlate $\cos(\bar{\tau})$ to ν_{CO} . The amide carbonyl IR bands of **11** and **14** vary linearly with $\cos(\bar{\tau})$ and a least-squares fit of the data reveals a correlation

coefficient (r) of 0.998 (Figure 3.10). Three of these N-amido groups are non-planar, and one is planar, yet all four correlate well to $\cos(\tau)$. If χ_N deformations had any effect on ν_{CO} , then with the large range of χ_N values for 11 and 14 ($5^\circ \leq \chi_N \leq 24^\circ$) we would expect a poorer correlation to $\cos(\tau)$ alone. Apparently, the different auxiliary ligands of 11 (bipy) and 14 (PPh_3 , $t\text{-BuNC}$) negligibly affect the carbonyl bands. For these Os(IV) complexes, N-amido C-N bond rotation primarily determines the ν_{CO} observed. At other osmium states, with a different PAC ligand, or for complexes of other metals, however, other effects may perturb ν_{CO} , such as nitrogen pyramidalization, different ligation, or the inherent Lewis acidity of the metal center. This correlation might be more appropriately carried out with force constants in place of the ν_{CO} values.

Complex 14 is a thermodynamically stable diastereomer, as upon heating isomerization is not observed. The amide nitrogen lone pair, which in the planar amide ligand can be delocalized onto both the metal and the amide carbonyl group, is more available for π -donation to the metal in the non-planar ligand. The amide nitrogen might also be expected to become a better σ -donor in the non-planar form. It is interesting that the geometry about the amide nitrogen atom remains very close to trigonal-planar for the amide trans to the π -acceptor $t\text{-BuNC}$ ligand, which suggests that π -donation is occurring through the metal center. The pyramidal distortions are larger for the N-amido ligands trans to the phosphine (Table 3.6). Metal-ligand bonding is probably greater with non-planar N-amido ligands relative to the planar ones. Conceivably, this increased bonding could compensate for the substantial destabilization resulting from the loss of amide delocalization. Evidence will be presented in Chapter 4 showing that there is a significant increase

in metal-ligand bonding for non-planar N-amido ligands relative to planar N-amido ligands in these systems.

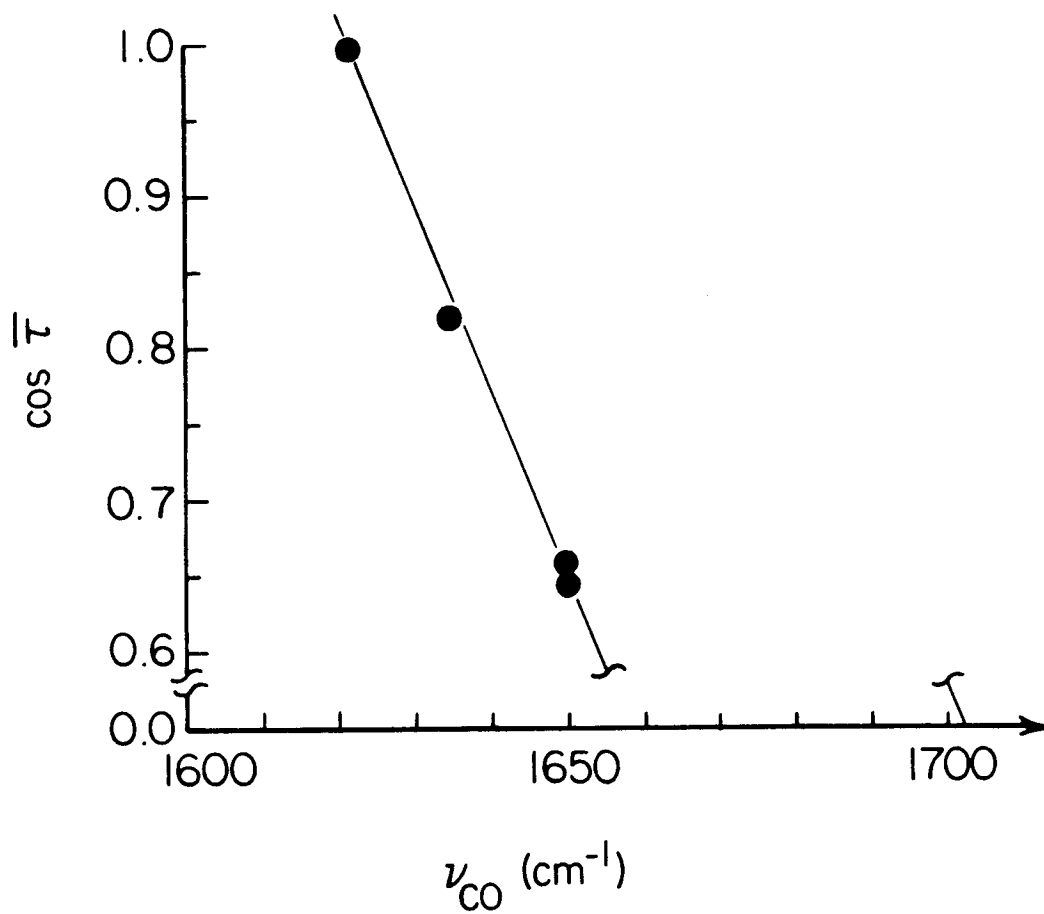


Figure 3.10. Plot of amide ν_{CO} vs. $\cos(\tau)$ for the N-amido groups of 11 and 14.

Conclusions

The crystallographic structural determinations of 11 and 14 show novel non-planar N-amido ligands. These N-amido linkages of the PAC ligand $(\eta^4\text{-CHBA-DCB})^{4-}$ provide sufficient flexibility to allow for the formation of cis- β and cis- α complexes. This is established by the similar magnitudes of PAC ligand distortions (measured by dihedral angles) and deformation in N-amido planarity (measured by the torsion angle $\omega(\text{O-C-N-C})$). N-Amido non-planarity can originate from three types of bonding changes: C-N bond rotation and pyramidalization at the nitrogen and carbon atoms. Using measures of these effects (τ , χ_N , and χ_C), we can assess the relative contributions from the bonding changes in a non-planar amide. Little non-planarity due to χ_C distortions is observed. Of the other two parameters, τ distortion is more destabilizing than that of χ_N . A survey of all characterized amide ligands shows ours to be the most non-planar examples known to date. Correlating these data, a wider range of χ_N values is observed than τ values, which would be expected because χ_N is the lower energy deformation.

The formation of non-planar amides changes the bonding characteristics of the N-amido ligand. Higher ν_{CO} bonds are observed in cis complexes because of the reduced contribution from the amide dipolar resonance form. The frequency of the carbonyl stretch linearly correlates with the amount of carbon and nitrogen p π orbital overlap estimated by $\cos(\tau)$. The successful correlation of two different isomers with different auxiliary ligands suggests that, for neutral Os(IV) complexes, τ deformations primarily determine the degree of amide delocalization present. By restricting delocalization, the nitrogen atom should be more

basic from the increased localization of the nitrogen lone pair, which can exert stronger ligand \rightarrow metal bonding. The stabilization from this increased bonding may be the factor that compensates for decreased amide delocalization stabilization. Chapter 4 discusses this point in detail and shows evidence for increased bonding from the non-planar N-amido group to the osmium metal center compared to the planar N-amido ligands.

Experimental Section

Syntheses. The syntheses of *cis*- β -Os(η^4 -CHBA-DCB)(bipy), **11**, and *cis*- α -Os(η^4 -CHBA-DCB)(PPh₃)(*t*-BuNC), **14**, are reported in Chapter 2. Dr. Robert J. Coots performed the crystallographic structure determination of **11**, and Tracy T. Furutani took the preliminary photographs and collected the X-ray data for **14**.

X-ray Data Collection and Structure Determination of 11. A crystal of **11** was obtained from a solution of CH₂Cl₂/EtOH. Oscillation and Weissenberg photographs indicated that the space group was triclinic. A hemisphere of intensity data was collected with unit cell parameters obtained by least-squares refinement of the orientation matrix using fifteen reflections in the range: $10.9 < 2\theta < 19.8^\circ$ (Table 3.8) with positive 2θ measurements only. The three check reflections, remeasured after every 100 reflections, indicated no significant decay over the 89 h of data collection. Absorption corrections were deemed unnecessary. The data were reduced to F_o^2 with anomalous dispersion corrections included for Os. The atomic position of the Os atom was derived from the Patterson map. Subsequent Fourier and difference maps revealed all non-hydrogen atoms.

Several cycles of full-matrix least-squares refinement on all non-hydrogen parameters yielded $R_F = 0.047$, $R_F' = 0.044$, and GOF = 3.44; final shift/errors < 0.10; data-to-parameter ratio = 11.0. All atomic coordinates as well as the scale factor, k , and Gaussian ellipsoids (anisotropic for all atoms except carbon and hydrogen) were in one block.

A difference map calculated after all non-hydrogen atoms had been located revealed the presence of additional electron density near a center of

symmetry. This was determined to be an ethanol molecule with the two carbon atoms related by the center of symmetry, and the oxygen atom disordered over two sites.

Hydrogen atoms were placed at a distance of 0.95 Å from their respective carbon or oxygen atoms by assuming ideal geometry and were not refined. The hydrogen atom temperature factors were set equal to the temperature factor of the atom to which they were attached.^{18a}

X-ray Data Collection and Structure Determination of 14. A suitable crystal was obtained by slow crystallization from CH₂Cl₂/hexane. A series of oscillation and Weissenberg photographs indicated orthorhombic symmetry. Intensity data to $2\theta = 30^\circ$ were collected on a locally-modified Syntex P2₁ diffractometer with graphite monochromator and MoK α radiation ($\lambda = 0.7107$ Å) using ω scans. Three check reflections, monitored after every 100 data measurements, indicated no decay for the first 3255 reflections ($\pm h, +k, +\ell$), but the intensity rapidly decreased thereafter; no further data were collected. The intensities were reduced to F_o 's, and multiple observations were averaged to yield 1706 reflections. No absorption correction was applied. Details of the data collection are summarized in Table 3.8.

The coordinates of the osmium atom were obtained from a three-dimensional Patterson function, and the remainder of the structure was determined from subsequent Fourier maps. Refinement was carried out by full-matrix least-squares, the quantity minimized was $\Sigma \omega(\Delta^2)$ with $\Delta = F_o^2 - F_c^2$ and weight $\omega = 1/\sigma^2(F_o^2)$. Form factors, with f' added for osmium, phosphorus, and chlorine, were obtained from *The International Tables for X-ray Crystallography, Vol. IV*, Table 2.2B. Calculations were carried out on a VAX 11/750 computer using the CRYM system.

Anisotropic Gaussian amplitudes were used for the osmium, phosphorus, chlorine, and methyl carbon atoms. The hydrogen atoms were fixed with $U = 0.20 \text{ \AA}^2$. Several cycles of least-squares refinements of the coordinates and thermal parameters of the non-hydrogen atoms yielded $\text{GOF} = \sqrt{\Sigma \omega \Delta^2 / (n - v)} = 1.35$, $n = 1706$ reflections, $v = 288$ parameters, with $R_F = \Sigma |F_o - |F_c || / \Sigma F_o = 0.063$ ($I > 0$, 1564 reflections), and $R_{3\sigma} = 0.035$ ($I \geq 3\sigma_I$, 1093 reflections).^{18b}

Cambridge Database Search. Programs used were (i) CONNSER for searching for entries of structures with N-amido connectivity (M-N-C=O), (ii) BIBSER for retrieving the bibliographic references of the entries, (iii) RETRIEVE for retrieving the crystallographic data of each structure, and (iv) GEOM 78 for calculating ω_1 , ω_2 , and ω_3 torsion angles of each N-amido group.^{19,20}

Table 3.8. Summary of Crystal Data and Intensity Collection Information for *cis*- β -Os(η^4 -CHBA-DCB)(bipy).0.5 EtOH, 11, and *cis*- α -Os(η^4 -CHBA-DCB)(PPh₃)(*t*-BuNC), 14.

Compound	11	14
Formula	OsC ₃₀ H ₁₄ N ₄ O ₄ Cl ₆ ·O.5C ₂ H ₆ O	OsC ₄₃ H ₃₀ N ₃ Cl ₆ O ₄ P
Formula weight	920.42	1086.63
Space group	$P\bar{1}$	P_{bca}
a	10.860(3) Å	22.09(2) Å
b	12.633(3) Å	19.92(2) Å
c	12.844(4) Å	19.40(2) Å
α	117.47(2) °	90°
β	90.42(3) °	90°
γ	95.90(3) °	90°
V	1552.2(7) Å ³	8537(4) Å ³
Z	2	8
λ	0.7107 Å	0.7107 Å
μ	4.68 mm ⁻¹	3.45 mm ⁻¹
D _{calc}	1.97 g/cm ³	1.69 g/ml
Scans	θ -2 θ	ω ; 1.0°

* The number of reflections contributing to sums in parentheses.

Table 3.8. (continued).

Compound	11	14
Reflections	$4 < 2\theta < 40^\circ$	$4^\circ < 2\theta < 30^\circ, \pm h, +k, +\ell$
Background time/ scan time		1.0
Collected	3283 reflections	3255 reflections
Averaged	2915 reflections	1706 reflections
Final no. of parameters	264	288
Final cycle: R R _{3σ} S	0.047(2888*) 0.044(2710) 3.44(2915)	0.063(1564*) 0.035(1093) 1.35(1706)

* The number of reflections contributing to sums in parentheses.

Table 3.9. Atomic Coordinates and Gaussian Amplitudes for 11.

	X	Y	Z	U11	U22	U33	U12	U13	U23	UEQ
OS	29377 (4)	33256 (4)	14412 (4)	323 (3)	261 (3)	342 (3)	102 (2)	109 (2)	122 (9)	310 (1)
CL1A	69339 (35)	88265 (30)	42681 (40)	661 (26)	375 (21)	1343 (36)	-63 (19)	86 (25)	36 (22)	946 (15)
CL1B	-8084 (41)	-6724 (34)	33332 (35)	1183 (34)	682 (25)	927 (28)	-173 (24)	336 (26)	440 (22)	925 (12)
CL2A	18041 (31)	72295 (29)	45685 (28)	601 (22)	601 (21)	533 (20)	193 (18)	150 (17)	29 (17)	660 (9)
CL2B	21152 (39)	35378 (34)	52411 (29)	1064 (31)	768 (26)	478 (21)	-104 (23)	50 (21)	176 (19)	829 (12)
CL3A	66612 (36)	10048 (28)	-22810 (28)	541 (21)	598 (21)	625 (21)	154 (17)	307 (18)	126 (17)	634 (9)
CL3B	49104 (40)	-12967 (30)	-20060 (37)	1057 (32)	393 (20)	1095 (31)	191 (21)	631 (27)	27 (20)	962 (14)
O1A	26547 (64)	56832 (56)	26460 (60)	408 (46)	215 (41)	471 (46)	65 (36)	119 (38)	44 (36)	407 (22)
O2A	50023 (77)	45788 (71)	10227 (80)	497 (57)	462 (53)	913 (69)	-71 (44)	337 (52)	-69 (48)	781 (32)
O1B	23860 (67)	31712 (63)	28252 (62)	450 (48)	395 (46)	460 (47)	45 (39)	14 (39)	127 (38)	459 (20)
O2B	13777 (79)	-3378 (67)	-971 (69)	750 (62)	391 (53)	548 (52)	-62 (45)	195 (47)	60 (45)	626 (26)
N1A	37631 (78)	34735 (69)	9430 (69)	451 (58)	215 (49)	334 (51)	114 (44)	36 (45)	62 (41)	355 (24)
N1B	22372 (79)	16072 (64)	4876 (70)	472 (57)	95 (44)	422 (54)	18 (41)	216 (47)	81 (41)	345 (33)
N2A	13252 (77)	35293 (70)	529 (74)	316 (55)	224 (49)	442 (56)	35 (42)	-39 (46)	-24 (43)	397 (28)
N2B	1141 (77)	32537 (70)	16771 (72)	403 (56)	294 (51)	373 (54)	65 (44)	158 (47)	166 (43)	349 (21)
			Z	B		X	Y	Z		B
C1A	4095 (9)	2405 (6)	6 (9)	2.45 (0.21)		5974 (0)	6488 (0)	2465 (0)		3.52 (0.00)
C1B	3259 (10)	1387 (10)	-215 (9)	3.13 (0.23)		151 (0)	-550 (0)	1406 (0)		3.57 (0.00)
C2A	4673 (11)	4627 (10)	1376 (10)	3.36 (0.23)		3860 (0)	8620 (0)	4948 (0)		4.42 (0.00)
C2B	1608 (11)	720 (11)	692 (10)	3.49 (0.24)		685 (0)	1431 (0)	4902 (0)		4.06 (0.00)
C3A	4215 (10)	5667 (10)	2370 (9)	3.08 (0.22)		5834 (0)	2958 (0)	-588 (0)		3.10 (0.00)
C3B	1274 (10)	1059 (9)	1907 (9)	2.97 (0.22)		2969 (0)	483 (0)	-1203 (0)		3.94 (0.00)
C4A	5199 (11)	6606 (10)	2815 (10)	3.52 (0.24)		-1377 (0)	3252 (0)	-1194 (0)		3.96 (0.00)
C4B	496 (10)	171 (10)	2068 (10)	3.57 (0.24)		H12A	3063 (0)	4.52 (0.00)		4.44 (0.00)
C5A	5045 (11)	7689 (11)	3750 (10)	4.17 (0.26)		H13A	3767 (0)	4.91 (0.00)		4.51 (0.00)
C5B	253 (11)	360 (11)	3158 (10)	4.02 (0.26)		H13B	3024 (0)	4.91 (0.00)		4.51 (0.00)
C6A	3947 (12)	7874 (11)	4284 (11)	4.42 (0.27)		H14A	4083 (0)	3.71 (0.00)		4.17 (0.00)
C6B	810 (11)	1353 (11)	4139 (10)	4.06 (0.26)		H14B	3267 (0)	3.71 (0.00)		4.17 (0.00)
C7A	2980 (10)	6987 (10)	3863 (9)	3.38 (0.23)		H15A	3935 (0)	3.38 (0.00)		3.38 (0.00)
C7B	1534 (10)	2213 (10)	4008 (10)	3.59 (0.24)		H15B	3417 (0)	3.95 (0.00)		3.95 (0.00)
C8A	3066 (10)	5649 (10)	2870 (9)	3.01 (0.22)		H16A	4844 (0)	7.32 (0.00)		7.32 (0.00)
C8B	1762 (10)	2112 (10)	2863 (9)	3.75 (0.23)		H16B	4854 (0)	8.00 (0.00)		8.00 (0.00)
C9A	5110 (10)	2270 (9)	-873 (9)	3.09 (0.22)		H16C	4141 (0)	8.00 (0.00)		8.00 (0.00)
C9B	3520 (11)	233 (10)	-1052 (10)	3.93 (0.26)		H03	3619 (0)	3341 (0)		3341 (0)
C10A	5364 (10)	1136 (10)	-1474 (9)	3.36 (0.23)						
C10B	4594 (11)	138 (11)	-1648 (10)	4.24 (0.28)						
C11A	77 (10)	3358 (9)	-128 (9)	2.88 (0.22)						
C11B	-693 (10)	3201 (9)	766 (9)	3.00 (0.22)						
C12A	-500 (11)	3410 (10)	-1061 (10)	3.96 (0.25)						
C12B	-1882 (12)	3118 (11)	821 (11)	4.44 (0.27)						
C13A	219 (12)	3698 (11)	-1802 (11)	4.51 (0.27)						
C13B	2413 (12)	3114 (11)	1796 (11)	4.81 (0.28)						
C14A	1468 (11)	3890 (10)	-1630 (10)	4.17 (0.26)						
C14B	-1709 (11)	3235 (11)	2692 (11)	4.37 (0.23)						
C15A	2006 (10)	3602 (10)	706 (10)	3.37 (0.26)						
C15B	-426 (11)	3316 (11)	2622 (11)	3.96 (0.25)						
C16	5262 (16)	4431 (14)	4657 (15)	7.32 (0.39)						
O3	5090 (15)	4082 (17)	3583 (18)	6.79 (0.47)						

Table 3.10. Atomic Coordinates and Gaussian Amplitudes for 14.

	X	Y	Z	U11	U22	U33	U12	U13	U23	UEQ
OS	2658(4)	17688(5)	8408(5)	226(7)	475(7)	350(7)	-17(8)	-22(7)	-16(9)	356(3)
P	1173(27)	27574(31)	1314(31)	204(49)	620(54)	453(53)	33(46)	-9(43)	-23(44)	426(26)
CL1	4349(26)	3036(31)	-11563(31)	552(54)	815(54)	918(59)	127(45)	52(42)	-447(47)	762(24)
CL2	-19184(28)	7398(36)	-17578(36)	668(56)	1364(76)	957(62)	-211(53)	-439(51)	-266(56)	996(28)
CL3	-20091(28)	4279(36)	26399(35)	675(60)	1248(68)	1170(67)	-192(53)	359(50)	322(60)	1031(28)
CL4	-8548(30)	37861(31)	37861(31)	1271(84)	638(81)	494(55)	-60(53)	204(45)	216(47)	884(28)
CL5	27115(25)	24236(37)	30691(33)	466(46)	1260(67)	973(64)	-138(52)	-324(44)	-63(56)	906(27)
CL6	8549(32)	38117(34)	20367(41)	1097(88)	599(61)	1393(76)	71(53)	382(60)	-80(58)	1036(30)
	X	Y	Z	B			X	Y	Z	B
O1	179(7)	1165(6)	48(7)	3.67(0.38)			-686(7)	324(0)	-1756(0)	4.00(0.00)
O2	453(5)	2523(7)	1505(7)	3.16(0.38)			-1794(0)	1315(0)	-453(0)	4.00(0.00)
O3	-1589(7)	1769(8)	688(8)	6.38(0.42)			-1656(0)	1067(0)	1656(0)	4.00(0.00)
O4	1059(6)	691(8)	2347(7)	4.37(0.43)			99(0)	701(0)	2984(0)	4.00(0.00)
N	1586(7)	1537(9)	345(9)	4.24(0.51)			1938(0)	1447(0)	2601(0)	4.00(0.00)
N1	-539(7)	1511(7)	1048(8)	3.03(0.48)			1927(0)	3472(0)	2667(0)	4.00(0.00)
N2	327(9)	1229(7)	1681(8)	2.29(0.41)			-9(0)	4166(0)	41(0)	4.00(0.00)
C1	-314(12)	1038(9)	-316(11)	2.21(0.52)			-539(0)	4992(0)	557(0)	4.00(0.00)
C2	-206(11)	684(9)	-925(12)	2.60(0.56)			-1215(0)	4708(0)	1473(0)	4.00(0.00)
C3	-736(12)	575(11)	-1343(12)	4.59(0.66)			-1361(0)	3562(0)	1261(0)	4.00(0.00)
C4	-1395(11)	842(11)	-1184(12)	3.23(0.63)			407(0)	2764(0)	-1096(0)	4.00(0.00)
C5	-1492(10)	1162(12)	-677(13)	4.69(0.67)			-1361(0)	2071(0)	-2182(0)	4.00(0.00)
C6	-900(10)	1262(10)	-133(11)	2.51(0.56)			-998(0)	1947(0)	-2387(0)	4.00(0.00)
C7	-1063(12)	1544(12)	633(13)	5.29(0.73)			-1512(0)	2415(0)	-1528(0)	4.00(0.00)
C8	-787(10)	1205(10)	1672(11)	2.72(0.58)			-992(0)	3185(0)	-458(0)	4.00(0.00)
C9	-1237(10)	997(11)	1916(12)	3.35(0.63)			598(0)	3427(0)	-1067(0)	4.00(0.00)
C10	-1299(11)	684(11)	2564(12)	3.65(0.62)			1482(0)	4020(0)	-1361(0)	4.00(0.00)
C11	-798(12)	586(11)	2960(13)	3.53(0.63)			2218(0)	4152(0)	-554(0)	4.00(0.00)
C12	-249(10)	774(10)	2707(11)	3.03(0.57)			2116(0)	3707(0)	519(0)	4.00(0.00)
C13	-112(11)	1665(9)	2672(12)	3.80(0.64)			1233(0)	3140(0)	832(0)	4.00(0.00)
C14	886(11)	1232(13)	2062(12)	3.41(0.47)						
C15	1152(9)	1870(12)	2111(9)	1.41(0.47)						
C16	1757(9)	1862(12)	2476(10)	2.61(0.50)						
C17	2027(9)	2439(13)	2637(10)	3.35(0.59)						
C18	1750(10)	3054(11)	2514(10)	3.27(0.55)						
C19	1204(10)	3056(12)	2159(11)	3.56(0.60)						
C20	918(9)	2474(13)	1945(10)	1.96(0.54)						
P1	-327(9)	3387(10)	581(9)	2.03(0.51)						
P2	-292(11)	4045(14)	398(11)	5.70(0.67)						
P3	-618(11)	4540(13)	709(15)	6.98(0.74)						
P4	-989(10)	4374(13)	1237(13)	5.23(0.69)						
P5	-1032(9)	3703(13)	1425(11)	3.53(0.60)						
P6	-701(10)	3209(12)	1167(11)	4.03(0.57)						
P7	-257(10)	2630(10)	-694(11)	2.71(0.50)						
P8	24(8)	2270(10)	-1184(12)	4.11(0.63)						
P9	-258(10)	2193(9)	-1828(10)	3.50(0.56)						
P10	-815(11)	2470(12)	-1947(11)	4.83(0.66)						
P11	-1118(9)	2626(11)	-1449(12)	3.12(0.53)						
P12	800(10)	2920(9)	-807(11)	3.12(0.53)						
P13	800(10)	3198(11)	-102(12)	3.70(0.55)						
P14	902(9)	3475(10)	-724(13)	3.85(0.60)						
P15	1435(12)	3836(11)	-224(13)	5.49(0.82)						
P16	1891(11)	3911(13)	-902(13)	6.59(0.78)						
P17	1800(14)	3654(15)	-440(16)	9.65(0.93)						
P18	1273(12)	3307(13)	192(17)	6.45(0.63)						
C	1118(10)	1676(11)	571(10)	3.55(0.65)						
C22	2183(17)	1306(19)	17(19)	8.47(0.92)						
	X	Y	Z	U11	U22	U33	U12	U13	U23	UEQ
C23	25817(126)	18812(200)	1108(195)	1006(254)	2637(516)	3256(530)	-651(330)	876(231)	-1864(487)	2310(191)
C24	20114(121)	11887(235)	-6867(153)	682(228)	6354(789)	635(268)	575(321)	112(227)	-1386(390)	2557(301)
C25	23070(150)	7064(219)	4657(203)	1821(370)	3446(564)	3225(539)	2437(421)	1832(362)	2225(490)	2831(206)

References

1. PAC ligand is abbreviated as follows: 1,2-bis(3,5-dichloro-2-hydroxybenzamido)-4,5-dichlorobenzene, H₄CHBA-DCB or "the Yogi ligand". Number references of compounds are those assigned in Chapter 2.
2. Stewart, W. E.; Siddall, T. H., III *Chem. Rev.* **1970**, *70*, 517-551.
3. Costain, C. C.; Dowling, J. M. *J. Chem. Phys.* **1960**, *32*, 158-165.
4. (a) Winkler, F. K.; Dunitz, J. D. *Acta Crystallogr., Sect. B* **1975**, *B31*, 270-272. (b) *Ibid.*, 276-278. (c) *Ibid.*, 281-283. (d) *Ibid.*, 283-286. (e) Smolíková, J.; Tichy, M.; Bláha, K. *Collect. Czech. Chem. Commun.* **1978**, *41*, 413-429. (f) Kálal, P.; Bláha, K.; Langer, V. *Acta Crystallogr., Sect. C* **1984**, *C40*, 1242-1245. (g) Hossain, M. B.; Baker, J. R.; van der Helm, D. *Ibid., Sect. B* **1981**, *B37*, 575-579. (h) Barnes, C. L.; McGuffey, F. A.; van der Helm, D. *Ibid., Sect. C* **1985**, *C41*, 92-95. (i) Paquette, L. A.; Kakihana, T.; Hansen, J. F.; Philips, J. C. *J. Am. Chem. Soc.* **1971**, *93*, 152-161. (j) Blackburn, G. M.; Plackett, J. D. *J. Chem. Soc., Perkin Trans. 2* **1972**, 1366-1371.
5. (a) Sweet, R. M.; Dahl, L. F. *J. Am. Chem. Soc.* **1970**, *92*, 5489-5507. (b) Woodward, R. B. "Recent Advances in the Chemistry of β -Lactam Antibiotics", Elks, J., Ed.; Chemical Society: London, 1977, pp 167-180. (c) Butler, A. R.; Freeman, K. A.; Wright, D. E. *Ibid.*, pp 299-303. (d) Proctor, P.; Gensmantel, N. P.; Page, M. I. *J. Chem. Soc., Perkin Trans. 2* **1982**, 1185-1192. (e) Page, M. I. *Acc. Chem. Res.* **1984**, *17*, 144-151.

6. (a) Smolíková, J.; Koblicová, Z.; Bláha, K. *Collect. Czech. Chem. Commun.* **1973**, *38*, 532-547. (b) Bláha, K.; Budesínský, M.; Koblicová, Z.; Malon, P.; Tichý, M.; Baker, J. R.; Hossain, M. B.; van der Helm, D. *Ibid.* **1982**, *47*, 1000-1019. (c) Ealick, S. E.; van der Helm, D. *Acta Crystallogr., Sect B* **1975**, *B31*, 2676-2680. (d) Ealick, S. E.; Washecheck, D. M.; van der Helm, D. *Ibid.* **1976**, *B32*, 895-900. (e) Ealick, S. E.; van der Helm, D. *Ibid.* **1977**, *B33*, 76-80.
7. (a) Pracejus, H. *Chem. Ber.* **1959**, *92*, 988-998. (b) *Ibid.* **1965**, *98*, 2897-2905. (c) Pracejus, H.; Kehlen, M.; Kehlen, H.; Matschiner, H. *Tetrahedron* **1965**, *21*, 2257-2270. (d) Hall, H. K., Jr.; Shaw, R. G., Jr.; Deutschmann, A. *J. Org. Chem.* **1980**, *45*, 3722-3724. (e) Hall, H. K., Jr.; El-Shekeil, A. *Ibid.*, 5325-5328. (f) Hall, H. K., Jr.; El-Shekeil, A. *Chem. Rev.* **1983**, *83*, 549-555. (g) Buchanan, G. L. *J. Chem. Soc., Perkin Trans. 1* **1984**, 2669-2670. (h) Coqueret, X.; Bourelle-Wagnier, F.; Chuche, J. *J. Org. Chem.* **1985**, *50*, 910-912.
8. (a) Ramachandran, G. N.; Lakshminarayanan, A. V.; Kolaskar, A. S. *Biochim. Biophys. Acta* **1973**, *303*, 8-13 (b) Kolaskar, A. S.; Lakshminarayanan, A. V.; Sarathy, K. P.; Sasisekharan, V. *Biopolymers* **1975**, *14*, 1081-1094.
9. (a) Dunitz, J. D.; Winkler, F. K. *J. Mol. Biol.* **1971**, *59*, 169-182, and references contained therein. (b) Dunitz, J. D.; Winkler, F. K. *Acta Crystallogr., Sect. B* **1975**, *B31*, 251-263. (c) Warshel, A.; Leviny, M.; Lifson, S. *J. Mol. Spectrosc.* **1970**, *33*, 84-99.
10. Sigel, H.; Martin, R. B. *Chem. Rev.* **1982**, *82*, 385-426.
11. Definitions of amide non-planarity parameters (ref 9) are as follows: $\tau = (\omega_1 + \omega_2)/2$, with the necessary condition $|\omega_1 - \omega_2| < \pi$. When this condition is not obeyed, $\tau = ((\omega_1 + \omega_2)/2) \bmod 2\pi$. For

$-90^\circ < \tau < 90^\circ$ the amide is cisoid along the principal chain, and for $-180^\circ < \tau < -90^\circ$ or $90^\circ < \tau < 180^\circ$ the amide is transoid along the principal chain; $\chi_N = (\omega_2 - \omega_3 + \pi) \bmod 2\pi$; $\chi_C = (\omega_1 - \omega_3 + \pi) \bmod 2\pi$. Amide torsion angles are: $\omega_1 = \text{C-C-N-C}$; $\omega_2 = \text{O-C-N-Os}$; $\omega_3 = \text{O-C-N-C}$. Torsion angles have been numbered to coincide with those used previously for organic secondary amides with Os replacing H in ω_2 and are consistent with the recommendations of the IUPAC-IUB Commission on Biochemical Nomenclature; *J. Mol. Biol.* **1970**, *52*, 1-17.

12. (a) Anson, F. C.; Christie, J. A.; Collins, T. J.; Coots, R. J.; Furutani, T. T.; Gipson, S. L.; Keech, J. T.; Krafft, T. E.; Santarsiero, B. D.; Spies, G. H. *J. Am. Chem. Soc.* **1984**, *106*, 4460-4472. (b) Christie, J. A.; Collins, T. J.; Krafft, T. E.; Santarsiero, B. D.; Spies, G. H. *J. Chem. Soc., Chem. Commun.* **1984**, 198-199. (c) Collins, T. J.; Santarsiero, B. D.; Spies, G. H. *J. Chem. Soc., Chem. Commun.* **1983**, 681-682. (d) Anson, F. C.; Collins, T. J.; Coots, R. J.; Gipson, S. L.; Richmond, T. G. *J. Am. Chem. Soc.* **1984**, *106*, 5037-5038. (e) Collins, T. J.; Richmond, T. G.; Santarsiero, B. D.; Treco, B. G. R. *J. Am. Chem. Soc.*, in press. (f) Barner, C. J.; Collins, T. J.; Mapes, B. E.; Santarsiero, B. D. *Inorg. Chem.*, in press. (g) Collins, T. J.; Coots, R. J.; Keech, J. T.; Peake, G. T.; Furutani, T. T.; Santarsiero, B. D. *J. Am. Chem. Soc.*, in press.
13. The following are cases where the RC(O)NHR' parent free base is an organic secondary amide: (i) Battaglia, L. P.; Corradi, A. B.; Nardelli, M.; Pelizzi, C.; Tani, M. E. V. *J. Chem. Soc., Dalton Trans.* **1976**, 1076-1080. (ii) Matsumoto, K.; Ooi, S.; Nakao, Y.; Mori, W.; Nakahara, A. *J. Chem. Soc., Dalton Trans.* **1981**, 2045-

2048. (iii) Kojima, Y.; Hirotsu, K.; Matsumoto, K. *Bull. Chem. Soc. Jpn.* **1977**, *50*, 3222-3231. (iv) Freeman, H. C.; Guss, J. M.; *Acta Crystallogr., Sect. B* **1978**, *34*, 2451-2458. (v) Freeman, H. C.; Guss, J. M.; Sinclair, R. L. *Ibid.* **1978**, *34*, 2459-2466. (vi) Freeman, H. C.; Guss, J. M. *Ibid.* **1978**, *34*, 2451-2458. (vii) Bear, C. A.; Freeman, H. C. *Ibid.* **1976**, *32*, 2534-2536. (viii) Freeman, H. C.; Taylor, M. R. *Acta Crystallogr.* **1965**, *18*, 939-952. (ix) Blount, J. F.; Fraser, K. A.; Freeman, H. C.; Szymanski, J. T.; Wang, C.-H. *Ibid.* **1967**, *22*, 396-405. (x) Freeman, H. C.; Shoone, J. C.; Sime, J. G. *Ibid.* **1965**, *18*, 381-392. (xi) Freeman, H. C.; Healy, M. J.; Scudder, M. L. *J. Biol. Chem.* **1977**, *252*, 8840-8847. (xii) Blount, J. F.; Freeman, H. C.; Holland, R. V.; Milburn, G. H. W. *Ibid.* **1970**, *245*, 5177-5185. (xiii) van der Helm, D.; Ealick, S. E.; Burks, J. E. *Acta Crystallogr., Sect. B* **1975**, *31*, 1013-1018. (xiv) Franks, W. A.; van der Helm, D. *Ibid.* **1970**, *27*, 1299-1310. (xv) Stephens, F. S.; Vagg, R. S. *Inorg. Chim. Acta* **1984**, *90*, 17-24. (xvi) *Ibid.* **1984**, *88*, 7-14. (xvii) *Ibid.* **1982**, *57*, 9-13. (xviii) *Ibid.* **1982**, *57*, 43-49. (xix) *Ibid.* **1981**, *51*, 149-154. (xx) Mulqi, M.; Stephens, F. S.; Vagg, R. S. *Ibid.* **1982**, *62*, 221-229. (xxi) *Ibid.* **1981**, *52*, 177-182. (xxii) *Ibid.* **1981**, *52*, 73-77. (xxiii) *Ibid.* **1981**, *51*, 9-14. (xxiv) Chapman, R. L.; Stephens, F. S.; Vagg, R. S. *Ibid.* **1981**, *52*, 169-176. (xxv) *Ibid.* **1980**, *43*, 29-33. (xxvi) Chapman, R. L.; Stephens, F. S.; Vagg, R. S. *Acta Crystallogr., Sect. B* **1981**, *37*, 75-79. (xxvii) Dehand, J.; Jordanov, J.; Keck, F.; Mosset, A.; Bonnet, J.-J.; Galy, J. *Inorg. Chem.* **1979**, *18*, 1543-1549. (xxviii) Mosset, A.; Bonnet, J. J. *Ibid.* **1977**, *33*, 2807-2812. (xxix) Van Riel, W.; Dessyn, H. O.; Van de Mierop, W.; Lenstra, A. T. H. *Transition Met. Chem.* **1980**, *5*, 330-

332. (xxx) Toscano, P. J.; Marzilli, L. G. *Inorg. Chem.* **1983**, *22*, 3342-3350. (xxxi) Marzilli, L. G.; Wilkowski, K.; Chiang, C. C.; Kistenmacher, T. J. *J. Am. Chem. Soc.* **1979**, *101*, 7504-7510. (xxxii) Kistenmacher, T. J.; Szalda, D. J.; Marzilli, L. G. *Acta Crystallogr., Sect. B* **1977**, *31*, 2416-2422. (xxxiii) Szalda, D. J.; Kistenmacher, T. J. *Ibid.* **1977**, *33*, 865-869. (xxxiv) Kistenmacher, T. J.; Marzilli, L. G.; Szalda, D. J. *Ibid.* **1976**, *32*, 186-193. (xxxv) Kistenmacher, T. J.; Szalda, D. J. *Ibid.* **1975**, *31*, 1659-1662. (xxxvi) Brown, D. A.; Roche, A. L.; Pakkanen, T. A.; Pakkanen, T. T.; Smolander, K. *J. Chem. Soc., Chem. Commun.* **1982**, 676-677. (xxxvii) Amirthalingam, V.; Muralidharan, K. V. *Pramana* **1982**, *19*, 51-57. (xxxviii) Amirthalingam, V.; Muralidharan, K. V. *Acta Crystallogr., Sect. B* **1976**, *32*, 3153-3156. (xxxix) Herak, R.; Solujic, L.; Krstanovic, I.; Prelesnik, B.; Celap, M. B. *Rev. Chim. Miner.* **1982**, *19*, 282-290. (xl) Evans, E. J.; Hawkisn, C. J.; Rodgers, J.; Snow, M. R. *Inorg. Chem.* **1983**, *22*, 34-38. (xli) Sabat, M.; Satyshur, K. A.; Sundaralingam, M. *J. Am. Chem. Soc.* **1983**, *105*, 976-980. (xlii) Diaddario, L. L.; Robinson, W. R.; Margerum, D. W. *Inorg. Chem.* **1983**, *22*, 1021-1025. (xliii) Strandberg, B.; Lindqvist, I.; Rosenstein, R. Z. *Kristallogr.* **1961**, *116*, 266-289. (xliv) Udupa, M. R.; Krebs, B. *Inorg. Chim. Acta* **1981**, *55*, 153-156. (xlv) Canty, A. J.; Chaichit, N.; Gatehouse, B. M. *Acta Crystallogr., Sect. B* **1979**, *35*, 592-596. (xlvi) Canty, A. J.; Fyfe, M.; Gatehouse, B. M. *Inorg. Chem.* **1978**, *17*, 1467-1471. (xlvii) Camerman, N.; Camerman, A.; Sarkar, B. *Can. J. Chem.* **1976**, *54*, 1309-1316. (xlviii) Sugihara, A.; Ashida, T.; Sasada, Y.; Kakudo, M. *Acta Crystallogr., Sect. B* **1968**, *24*, 203-211. (xlix)

- Lim, M. C.; Sinn, E.; Martin, R. B. *Inorg. Chem.* **1976**, *15*, 807-811.
- (l) de Meester, P.; Hodgson, D. J. *Ibid.* **1978**, *17*, 440-444. (li) de Meester, P.; Hodgson, D. J. *Acta Crystallogr., Sect. B* **1977**, *33*, 3505-3510. (lii) Hursthouse, M. B.; Jaraweera, S. A. A.; Milburn, H.; Quick, A. *J. Chem. Soc., Dalton* **1975**, 2569-2572. (liii) Simmons, C. J.; Lundeen, M.; Seff, K. *Inorg. Chem.* **1978**, *17*, 1429-1435. (liv) Tsuboyama, S.; Sakurai, T.; Kobayashi, K.; Azuma, N.; Kajikawa, Y.; Ishizu, K. *Ibid.* **1984**, *40*, 466-473. (lv) Mikuriya, N.; Harada, T.; Okawa, H.; Kida, S. *Inorg. Chim. Acta* **1983**, *75*, 1-7. (lvi) Mauguen, Y.; Vilkas, E.; Amar, C. *Acta Crystallogr., Sect. C* **1984**, *40*, 82-85. (lvii) Antolovich, M.; Phillips, D. J.; Rae, A. D. *J. Chem. Soc., Chem. Commun.* **1984**, 582-583. (lviii) Khodashova, T. S.; Porai-Koshits, M. A.; Davidenko, N. K.; Vlasova, N. M. *Koord. Khim.* **1984**, *10*, 262-268. (lix) Perkins, C. M.; Rose, N. J.; Weinstein, P.; Stenkamp, R. E.; Jensen, L. H.; Pickart, L. *Inorg. Chim. Acta* **1984**, *82*, 93-99. (lx) Hedden, D.; Roundhill, D. M.; Fultz, W. C.; Rheingold, A. L. *J. Am. Chem. Soc.* **1984**, *106*, 5014-5016. (lxi) Fleischer, E. B.; Jeter, D.; Florian, R. *Ibid.* **1974**, *13*, 1042-1047.
14. (i) Fazakerley, G. V.; Linder, P. W.; Nassimbeni, L. R.; Rodgers, A. L. *Cryst. Struct. Commun.* **1974**, *3*, 463-468. (ii) Fazakerley, G. V.; Linder, P. W.; Nassimbeni, L. R.; Rodgers, A. L. *Inorg. Chim. Acta* **1974**, *9*, 193-201. (iii) Caira, M. R.; Fazakerley, G. V.; Linder, P. W.; Nassimbeni, L. R. *Acta Crystallogr., Sect. B* **1973**, *29*, 2898-2904. (iv) Nassimbeni, L. R.; Rodgers, A. *Ibid.* **1974**, *30*, 1953-1961. (v) Nassimbeni, L. R.; Rodgers, A. *Ibid.* **1973**, *30*, 2593-2602. (vi) Mason, R.; Thomas, K. M.; Galbraith, A. R.; Shaw, B. L.; Elson, C.

M. *J. Chem. Soc., Chem. Commun.* **1973**, 297-299. (vii) Cavalca, L.; Nardelli, M.; Coghi, L. *Nouovu Cimento* **1957**, 6, 278. (viii) Bonamartini, A. C.; Montenero, A.; Nardelli, M.; Palmieri, C.; Pelizzi, C. *J. Cryst. Mol. Struct.* **1971**, 1, 389-396. (ix) Solin, T.; Matsumoto, K.; Fuwa, K. *Bull. Chem. Soc. Jpn* **1981**, 54, 3731-3734. (x) Uchiyama, T.; Takagi, K.; Matsumoto, K.; Ooi, S.; Nakamura, Y.; Kawaguchi, S. *Bull. Chem. Soc. Jpn* **1981**, 54, 1077-1084. (xi) Uchiyama, T.; Takagi, K.; Matsumoto, K.; Ooi, S.; Nakamura, Y.; Kawaguchi, S. *Chem. Lett.* **1979**, 1197-1200. (xii) Cotton, F. A.; Lewis, G. E.; Murillo, C. A.; Schwotzer, W.; Valle, G. *Inorg. Chem.* **1984**, 23, 4038-4041. (xiii) Baral, S.; Cotton, F. A.; Ilsley, W. H.; Kaim, W. *Inorg. Chem.* **1982**, 21, 1644-1650. (xiv) Baral, S.; Cotton, F. A.; Ilsley, W. H.; Kaim, W. *Ibid.* **1981**, 20, 2696-2703. (xv) Cotton, F. A.; Ilsley, W. H.; Kaim, W. *Ibid.* **1980**, 19, 3586-3589. (xvi) Cotton, F. A.; Ilsley, W. H.; Kaim, W. *Ibid.* **1979**, 18, 2717-2719. (xvii) Cotton, F. A.; Ilsley, W. H.; Kaim, W. *J. Am. Chem. Soc.* **1980**, 102, 3475-3479. (xviii) Cotton, F. A.; Ilsley, W. H.; Kaim, W. *J. Am. Chem. Soc.* **1980**, 102, 3464-3473. (xix) Lewis, R. M.; Nancollas, G. H.; Coppens, P. *Inorg. Chem.* **1972**, 11, 1371-1375. (xx) Gillard, R. D.; McKenzie, E. D.; Mason, R.; Robertson, G. B. *Nature* **1966**, 209, 1347-1348. (xxi) Oliver, K. J.; Waters, T. N. *J. Chem. Soc., Chem. Commun.* **1982**, 1111-1112. (xxii) Clark, G. R.; Skelton, B. W.; Waters, T. N. *J. Chem. Soc., Dalton* **1976**, 1528-1536. (xxiii) Schneider, M. L.; Ferguson, G.; Balahura, R. J. *Can. J. Chem.* **1973**, 51, 2180-2185. (xxiv) Schollhorn, H.; Thewalt, U.; Lippert, B. *Inorg. Chim. Acta* **1984**, 93, 19-26. (xxv) Lippert, B.; Neugebauer, D.; Raudaschl, G. *Ibid.* **1983**,

- 78, 161-170. (xxvi) Neugebauer, D.; Lippert, B. *Ibid.* **1982**, *67*, 151-158. (xxvii) Lippert, B.; Schubert, U. *Ibid.* **1981**, *56*, 15-20. (xxviii) Lippert, B.; Neugebauer, D. *Ibid.* **1980**, *46*, 171-179. (xxix) Schollhorn, H.; Thewalt, U.; Lippert B. *J. Chem. Soc., Chem. Commun.* **1984**, 769-770. (xxx) Lippert, B.; Thewalt, U.; Schollhorn, H.; Goodgame, D. M. L.; Rollins, R. W. *Inorg. Chem.* **1984**, *23*, 2807-2813. (xxxi) Lippert, B.; Neugebauer, D. *Ibid.* **1982**, *21*, 451-452. (xxxii) Faggiani, R.; Lippert, B.; Lock C. J. L.; Pfab, R. *Ibid.* **1981**, *20*, 2381-2386. (xxxiii) Faggiani, R.; Lippert, B.; Lock C. J. L. *Ibid.* **1980**, *19*, 295-300. (xxxiv) Lippert, B.; Schollhorn, H.; Thewalt, U. *Z. Naturforsch., Teil B* **1983**, *38*, 1441-1445. (xxxv) Neugebauer, D.; Lippert, B. *J. Am. Chem. Soc.* **1982**, *104*, 6596-6601. (xxxvi) Weiss, J.; Thewalt, U. *Z. Anorg. Allg. Chem.* **1966**, *343*, 274-285. (xxxvii) Mangia, A.; Pelizzi, C.; Pelizzi, G. *Acta Crystallogr., Sect. B* **1974**, *30*, 2146-2150. (xxxviii) Latavalya, N.; Taylor, M. R. *Cryst. Struct. Comm.* **1975**, *4*, 163-166. (xxxix) Cumming, H. J.; Hall, D. *Acta Crystallogr., Sect. B* **1976**, *32*, 1281-1283. (xl) Mosset, A.; Bonnet, J.-J.; Galy, J. *Acta Crystallogr., Sect. B.* **1977**, *33*, 2639-2644. (xli) Orbell, J. D.; Wilkowski, K.; Marzilli, L. G.; Kistenmacher, T. J. *Ibid.* **1982**, *21*, 3478-3483. (xlii) de Castro, B.; Chiang, C. C.; Wilkowski, K.; Marzilli, L. G.; Kistenmacher, T. J. *Inorg. Chem.* **1981**, *20*, 1835-1844. (xliii) Kistenmacher, T. J.; Sorell, T.; Marzilli, L. G. *Ibid.* **1975**, *14*, 2479-2485. (xliv) Kistenmacher, T. J.; de Castro, B.; Wilkowski, K.; Marzilli, L. G. *J. Inorg. Biochem.* **1982**, *16*, 33-46. (xlv) Szalda, D. J.; Marzilli, L. G.; Kistenmacher, T. J. *Biochem. Biophys. Res. Commun.* **1975**, *63*, 601-605. (xlv) Mascharak, P.

K.; Williams, I. D.; Lippard, S. J. *Ibid.* **1984**, *106*, 6428-6430. (xlvii) O'Halloran, T. V.; Roberts, M. M.; Lippard, S. J. *Ibid.* **1984**, *106*, 6427-6428. (xlviii) Hollis, L. S.; Lippard, S. J. *J. Am. Chem. Soc.* **1983**, *105*, 3494-3503. (xlix) *Ibid.* **1981**, *103*, 6761-6763. (l) *Ibid.* **1981**, *103*, 1239-1232. (li) Barton, J. K.; Szalda, D. J.; Rabinowitz, H. N.; Waszcak, J. V.; Lippard, S. J. *Ibid.* **1979**, *101*, 1434-1441. (lii) Hollis, L. S.; Roberts, M. M.; Lippard, S. J. *Inorg. Chem.* **1983**, *22*, 3637-3644. (liii) Hollis, L. S.; Lippard, S. J. *Ibid.* **1983**, *22*, 2708-2713. (liv) *Ibid.* **1983**, *22*, 2605-2614. (lv) *Ibid.*, 2600-2604. (lvi) Lerner, E. I.; Lippard, S. J. *Ibid.* **1977**, *16*, 1546-1551. (lvii) Marabella, C. P.; Enemark, J. H.; Newton, W. E.; McDonald, J. W. *Ibid.* **1982**, *21*, 623-627. (lviii) Allaire, F.; Beauchamp, A. L. *Can. J. Chem.* **1984**, *62*, 2249-2259. (lix) Perron, J.; Beauchamp, A. L. *Ibid.* **1984**, *62*, 1287-1291. (lx) Bélanger-Gariépy, F.; Beauchamp, A. L. *Cryst. Struct. Commun.* **1982**, *11*, 991-998. (lxi) Guay, F.; Beauchamp, A. *Inorg. Chim. Acta* **1982**, *66*, 57-63. (lxii) Sletten, J. *Acta Chem. Scand. Ser. A* **1982**, *36*, 345-351. (lxiii) Sakaguchi, H.; Anzai, H.; Furuhata, K.; Ogura, H.; Iitaka, Y. *Chem. Pharm. Bull.* **1977**, *25*, 2267-2272. (lxiv) Mitschler, A.; Rees, B.; Weist, R.; Benard, M. *J. Am. Chem. Soc.* **1982**, *104*, 7501-7509. (lxv) Arrizabalaga, P.; Castan, P.; Dahan, F. *Inorg. Chem.* **1983**, *22*, 2245-2252. (lxvi) Laurent, J. P.; Lepage, P.; Dahan, F. *J. Am. Chem. Soc.* **1982**, *104*, 7335-7336. (lxvii) Ittel, S. D.; Ibers, J. A. *Ibid.* **1973**, *12*, 2290-2295. (lxviii) Halfpenny, J.; Small, R. W. H. *Acta Crystallogr., Sect. B* **1980**, *36*, 1194-1196. (lxix) Doedens, R. J. *Inorg. Chem.* **1978**, *17*, 1315-1318. (lxx) Dippenaar, A.; Holzapfel, C. W.; Boeyens, J. C. A. *J. S. Afr. Chem. Inst.* **1977**, *30*,

161-168. (lxxi) Gozen, S.; Peters, R.; Owston, P. G.; Tasker, P. A. *J. Chem. Soc., Chem. Commun.* **1980**, 1199-1201. (lxxii) Fuhrhop, J.-H.; Krüger, P.; Sheldrick, W. S. *Justus Liebigs Ann. Chem.* **1977**, 339-359. (lxxiii) Sinn, E.; Flynn, C. M., Jr.; Martin, R. B. *J. Am. Chem. Soc.* **1978**, *100*, 489-492. (lxxiv) Haider, S. Z.; Malik, K. M. A.; Das, S.; Hursthouse, M. B. *Acta Crystallogr., Sect. C* **1984**, *40*, 1147-1150. (lxxv) Bradley, D. C.; Hursthouse, M. B.; de M. Jelfs, A. N.; Short, R. L. *Polyhedron* **1983**, *2*, 849-852. (lxxvi) Bonfiglio, J. V.; Bonnett, R.; Buckley, D. G.; Hamzesh, D.; Hursthouse, M. B.; Malik, K. M. A.; McDonagh, A. F.; Trotter, J. *Tetrahedron* **1983**, *39*, 1865-1874. (lxxvii) Haider, S. Z.; Malik, K. M. A.; Ahmed, K. J.; Hess, H.; Riffel, H.; Hursthouse, M. B. *Inorg. Chim. Acta* **1983**, *72*, 21-27. (lxxviii) Bonfiglio, J. V.; Bonnett, R.; Hursthouse, M. B.; Malik, K. M. A. *J. Chem. Soc., Chem. Commun.* **1977**, 83-86. (lxxix) Malik, N. A.; Sadler, P. J.; Neidle, S.; Taylor, G. L. *J. Chem. Soc., Chem. Commun.* **1978**, 711-712. (lxxx) Kamenar, B.; Jovanovski, G.; Grdenic, D. *Cryst. Struct. Commun.* **1982**, *11*, 263-268. (lxxxii) Kamenar, B.; Jovanovski, G. *Ibid.*, 257-261. (lxxxiii) Kamenar, B.; Grdenic, D. *Inorg. Chim. Acta* **1969**, *3*, 25-28. (lxxxiiii) Neverov, V. A.; Buyshkin, V. N.; Nezhel'skaya, L. A.; Belichuk, N. I. *Kristallogr.* **1984**, *29*, 731-735. (lxxxv) Neverov, V. A.; Buyshkin, V. N.; Belichuk, N. I.; Nezhel'skaya, L. A. *Kristallogr.* **1981**, *26*, 717-721. (lxxxvi) Murthy, R. V. A.; Murthy, B. V. R. *Z. Kristallogr.* **1976**, *144*, 259-273. (lxxxvii) Tsukihara, T.; Katsube, T.; Fujimori, K.; Kawashima, K.; Kan-nan, Y. *Bull. Chem. Soc. Jpn.* **1974**, *47*, 1582-1585. (lxxxviii) Tsukihara, T.; Katsube, Y.; Fujimori, K.; Ishimura, Y. *Ibid.* **1972**, *45*, 1367-1371.

(lxxxvii) Tsukihara, T.; Katsube, Y.; Fujimori, K.; Ito, T. *Ibid.* **1972**, *45*, 2959-2963. (lxxxix) Kuno, N.; Miyamoto, K.; Fujimori, K.; Tsukihara, T.; Katsube, Y. *Rep. Fac. Eng., Tottori Univ.* **1973**, *4*, 64-68. (xc) Senoh, Y.; Fujimori, K.; Tsukihara, T.; Katsube, Y. *Ibid.* **1973**, *4*, 69-73. (xci) Struchkov, Yu. T.; Belokon', Yu. N.; Belikov, V. M.; Zal'tser, I. E.; Aleksandrov, G. G. *J. Organomet. Chem.* **1981**, *210*, 411-421. (xcii) Faggiani, R.; Lock, C. J. L.; Pollock, R. J.; Rosenberg, B.; Turner, G. *Inorg. Chem.* **1981**, *20*, 804-807. (xciii) Lock, C. J. L.; Peresie, H. J.; Rosenberg, B.; Turner, J. *J. Am. Chem. Soc.* **1978**, *100*, 3371-3374. (xciv) Kosturko, L. D.; Folzer, C.; Stewart, R. F. *Biochemistry* **1974**, *13*, 3949-3952. (xcv) Nawata, Y.; Iwasaki, H.; Saito, Y. *Bull. Chem. Soc. Jpn.* **1967**, *40*, 515-521. (xcvi) Chang, S. C.; Parkin, D. Y.; Li, N. C. *Inorg. Chem.* **1968**, *7*, 2144-2150. (xcvii) Shimizu, N.; Uno, T. *Cryst. Struct. Commun.* **1980**, *9*, 389-392. (xcviii) Shimizu, N.; Uno, T. *Ibid.* **1980**, *9*, 223-226. (xcix) Bertrand, J. A.; Fujita, E.; Eller, P. G. *Inorg. Chem.* **1974**, *13*, 2067-2071. (c) Klein, C. L.; Stevens, E. D.; O'Connor, C. J.; Majeste, R. J.; Trefonas, L. M. *Inorg. Chim. Acta* **1983**, *70*, 151-158. (ci) Dennis, A. M.; Korp, J. D.; Bernal, I.; Howard, R. A.; Bear, J. L. *Inorg. Chem.* **1983**, *22*, 1522-1529. (cii) Shaver, A.; Hartgerink, J.; Lai, R. D.; Bird, P.; Ansari, N. *Organometallics*, **1983**, *32*, 939-940. (ciii) Lumme, P.; Mutikainen, I. *Acta Crystallogr., Sect. B* **1980**, *36*, 2251-2254. (civ) Mutikainen, I.; Lumme, P. *Ibid.* **1980**, *36*, 2237-2240. (cv) Mutikainen, I.; Lumme, P. *Ibid.* **1980**, *36*, 2233-2237. (cvi) Hoberg, H.; Oster, B. W.; Kruger, C.; Tsay, Y. H. *J. Organomet. Chem.* **1983**, *252*, 365-373. (cvii) Khayata, W.; Baylocq, D.; Pellerin, N.;

Rodier, N. *Acta Crystallogr., Sect. C* **1984**, *40*, 765-767. (cviii)
 Aoki, K.; Saenger, W. *Ibid.* **1984**, *40*, 775-778. (cix) Aoki, K.;
 Saenger, W. *J. Inorg. Biochem.* **1984**, *20*, 225-245. (cx) Einstein, F.
 W. B.; Nussbaum, S.; Sutton, D.; Willis, A. C. *Organometallics*
1984, *3*, 568-574. (cxii) Bencini, A.;
 Di Vaira, M.; Fabretti, A. C.; Gatteschi, D.; Zanchini, C. *Inorg.*
Chem. **1984**, *23*, 1620-1623. (cxiii) Lanfredi, A. M. M.; Tiripicchio,
 A.; Uson, R.; Oro, L. A.; Ciriano, M. A.; Villaroya, B. E. *Inorg.*
Chim. Acta **1984**, *88*, L9-L10. (cxiv) Bolinger, C. M.; Rauchfuss, T.
 B.; Wilson, S. R. *J. Am. Chem. Soc.* **1984**, *106*, 7800-7807. (cxv)
 Korswagen, R.; Weidenhammer, K.; Ziegler, M. L. *Acta*
Crystallogr., Sect. B. **1979**, *35*, 2554-2558. (cxvi) Slade, P. G.;
 Raupach, M.; Radoslovich, E. W. *Ibid.* **1973**, *29*, 279-286. (cxvii)
 Birker, P. J. M. W. L. *J. Chem. Soc., Chem. Commun.* **1977**, 444-
 445. (cxviii) Birker, P. J. M. W. L. *Inorg. Chem.* **1977**, *16*, 2478-
 2482. (cxix) van Santvoort, F. A. J. J.; Krabbendam, H.; Spek, A.
 L.; Boersma, J. *Inorg. Chem.* **1978**, *17*, 388-394. (cxx) Mazus, M.
 D.; Byushkin, V. N.; Ablov, A. V.; Malinovskii, T. I.; Ablova, M. A.;
 Savushkina, T. I. *Dokl. Akad. Nauk SSSR* **1975**, *225*, 574-576.

15. The *cis*-diammineplatinum α -pyrrolidonato complex
 $[\text{Pt}_4(\text{NH}_3)_8(\text{C}_4\text{H}_6\text{NO})_4](\text{NO}_3)_{5.48} \cdot 3\text{H}_2\text{O}$, which is an apparent
 mixture of two tetranuclear species at different oxidation states,
 shows several abnormally large χ_{C} (21° , 25° , 26° , 30° , 36° , 45° , -45° ;
 there are two distinct molecules per unit cell) and χ_{N} (35° , -39° ,
 -48°) parameters that are difficult to rationalize. This structure
 also contains abnormal bond distances. For instance, C-C single
 bond distances vary from 1.36-1.90 Å. The points derived from this

work are not included in Figures 3.6-3.9. Matsumoto, K.; Takahashi, H.; Fuwa, K. *J. Am. Chem. Soc.* **1984**, *106*, 2049-2054. The related pyrrolidinato, mixed-valence, tetranuclear species $[\text{Pt}_4(\text{NH}_3)_8(\text{C}_6\text{H}_6\text{NO})_4](\text{NO}_3)_6 \cdot \text{H}_2\text{O}$ has been the subject of two reports: Matsumoto, K.; Fuwa, K. *J. Am. Chem. Soc.* **1982**, *104*, 897-898.; Matsumoto, K.; Takahashi, H.; Fuwa, K. *Inorg. Chem.* **1983**, *22*, 4086-4090. In the former report, a trihydrate is claimed for which several χ_C values are extremely large (-24° , 39°). In the latter a dihydrate is claimed where one χ_C value is unreasonable (-74°) and another is at least inexplicably large (-28°). Presumably, some atomic coordinates are inaccurate. The authors noted difficulties with this determination. The points for these structures are also excluded from Figures 3.6-3.9.

16. Complete bibliographic references can be found in refs 13-15. Calculated torsion angles for all of the compounds can be found in the supplementary material to ref 12g.
17. Streitweiser, A., Jr. "Molecular Orbital Theory for Organic Chemists"; John Wiley and Sons: New York, 1961; pp 14-16.
18. (a) Structure factor amplitudes of 11 can be found in the supplementary material of ref 12a. (b) Structure factor amplitudes of 14 can be found in the supplementary material of ref 12g.
19. Allen, F. H.; Bellard, S.; Brice, M. D.; Cartwright, B. A.; Doubleday, A.; Higgs, H.; Hummelink-Peters, B. G.; Kennard, O.; Motherwell, W. D. S.; Rodgers, J. R.; Watson, D. G. *Acta Crystallogr., Sect. B* **1979**, *35*, 2331-2339.
20. This project was done with Geoffrey T. Peake. Many thanks are extended to Professor Richard E. Marsh for helpful discussions and

Dr. B. Jean Westphal for assistance with the operation of the Cambridge crystallographic database programs.

Chapter 4

Thermodynamic and Bonding Differences Between Planar and Non-planar N-amido Ligands

Introduction

Evidence for the formation of novel non-planar N-amido ligands is discussed in Chapter 3. Although some precedent for non-planar organic amide groups can be found in the literature, no comparable inorganic examples of non-planar N-amido ligands exist. This has been verified by an extensive search for all structurally characterized N-amido groups, followed by a complete torsion angle analysis of each ligand. The increased amide carbonyl IR stretching frequencies observed for non-planar N-amido groups signal that less amide delocalization resonance and a distinctly different bonding occur in a non-planar amide compared to its planar analog. We wanted to elucidate these changes and understand what factors were responsible for the formation of cis complexes. In Chapter 3, it is suggested that restricted amide resonance leads to greater localization of the lone pair on nitrogen, making the nitrogen atom more basic in a non-planar N-amido moiety than in a planar one. Presumably, strong σ - and π -bonding between the metal and N-amido ligand compensates for the destabilization resulting from reduced amide delocalization. An original objective in designing PAC ligands was to produce a strongly donating chelate for stabilizing a high valent metal center. The unexpected isomerization phenomenon apparently increases this capacity for electron-donation. We wanted to verify this effect and quantify the thermodynamic consequences of it.

A system in which like cis and trans isomers interconverted was needed to study equilibria conditions and thereby obtain thermodynamic information. All of the compounds reported in Chapter 2 and those structurally characterized in Chapter 3 are isomerically static. In

controlled-potential electrolysis experiments, we discovered an isomerizing system. The oxidation of *trans*-Os(η^4 -CHBA-DCB)(*t*-Bupy)₂, **10-*t*Bu**, in a bulk electrolysis experiment produces two compounds proven to be in equilibrium with one another: [**10-*t*Bu**]⁺ and [*cis*- α -Os(η^4 -CHBA-DCB)(*t*-Bupy)₂]⁺, [**19-*t*Bu**]⁺. The equilibrium constant between the two isomers can be measured by normal pulse voltammetry. The trend in this equilibrium constant over different osmium oxidation states is consistent with the *cis*- α isomer being a stronger donor than the *trans*. Syntheses of compounds with various substituents in place of the *tert*-butyl group in **10-*t*Bu** made it possible to establish linear free energy relationships (LFER) between isomerization equilibrium constants and the basicities of the free pyridines. This demonstrates that demand for electron density at the metal center can induce isomerization from the *trans* to *cis*- α isomer, which contains the more donating non-planar N-amido ligands. Finally, by comparing these results to those of osmium complexes containing two bidentate salicylamide ligands and no chelate bridge, the strong electron-donation of the *cis*- α isomers can be shown to be amide-centered. The effect does not emanate from the different ligand positions in *cis*- α and *trans* coordination spheres.

Results and Discussion

Thermodynamic Studies of $\text{trans} \rightleftharpoons \text{cis-}\alpha$ Equilibrium Processes. The cyclic voltammogram (CV) of *trans*-Os(η^4 -CHBA-DCB)(*t*-Bupy)₂, **10-*t*Bu**, is shown in Figure 4.1a. The CV shown in Figure 4.1b is obtained following room temperature, controlled-potential electro-oxidation of **3** by one Faraday per mole of osmium.¹ The oxidation produces a mixture of [**10-*t*Bu**]⁺ and a new compound, [**19-*t*Bu**]⁺, as indicated by the appearance of a new set of waves. The peak currents for the couples associated with **10-*t*Bu** in Figure 4.1a equal the sum of the peak currents associated with [**10-*t*Bu**]⁺ and [**19-*t*Bu**]⁺ in Figure 4.1b; hence, material balance is maintained. When the oxidized solution is reduced at +0.60 V, between the **10-*t*Bu** Os(V/IV) couple at +0.70 V and the new couple at +0.50 V, the couples of **10-*t*Bu** steadily increase while those of the new compound conversely decrease until the original CV in Figure 4.1a is restored. If, on the other hand, the mixture of [**10-*t*Bu**]⁺ and [**19-*t*Bu**]⁺ is rapidly reduced by the addition of excess ferrocene at -78 °C, a stable solution of neutral **10-*t*Bu** and **19-*t*Bu** is produced, which can be separated by column chromatography on silica gel, using chlorobenzene/bromoethane (1:1 v/v) eluent. Recrystallization of the new red complex from CH₂Cl₂/hexane affords analytically pure **19-*t*Bu**. This compound is stable at room temperature. ¹H NMR and IR spectroscopies establish **19-*t*Bu** to be the *cis-α* isomer of Os(η^4 -CHBA-DCB)(*t*-Bupy)₂. The couples of isolated **19-*t*Bu** match the new couples in Figure 4.1b. Evidently, oxidation of the *trans* isomer produces a mixture of both cationic *trans* and *cis-α* isomers.² Electro-oxidation of **10-*t*Bu** or **19-*t*Bu** by one Faraday per mole of osmium at -78 °C affords pure solutions of [**10-**

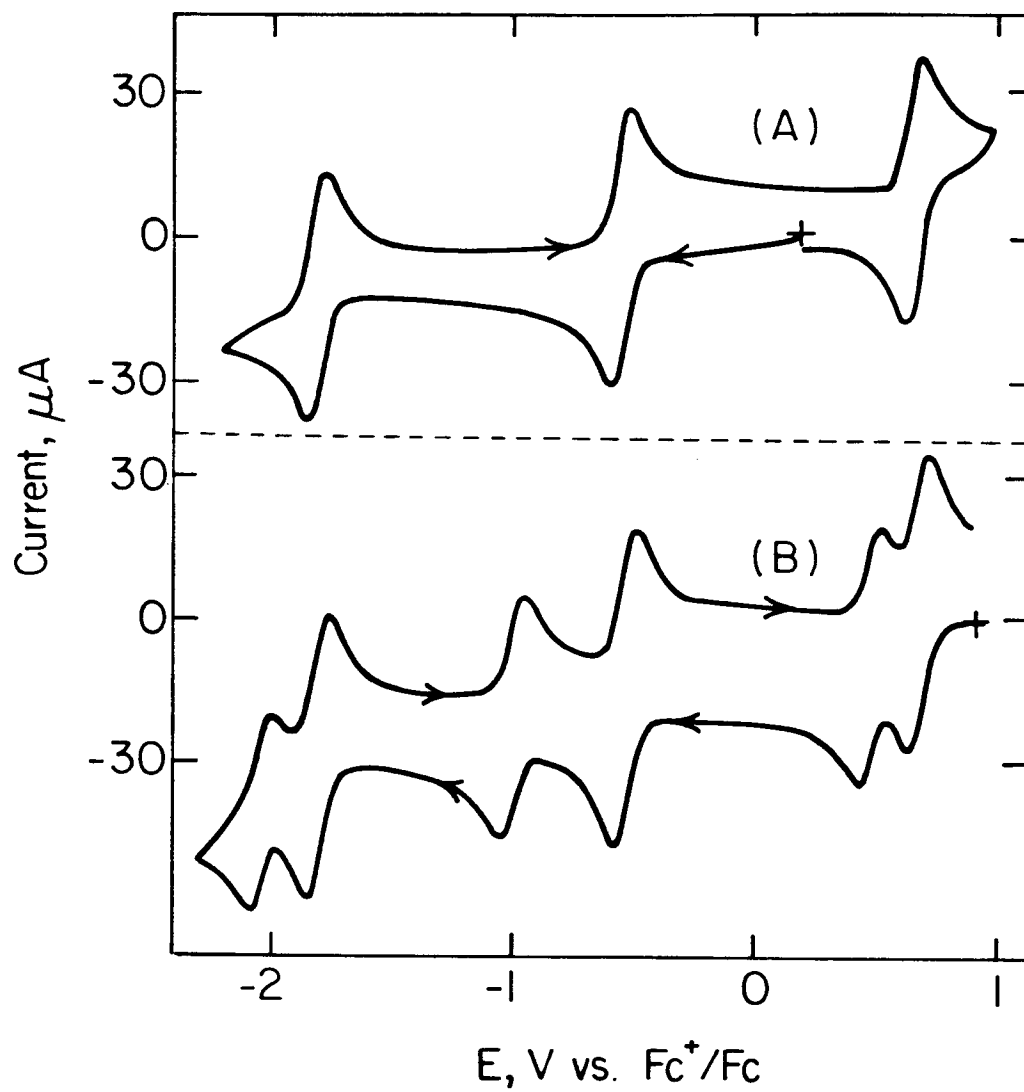
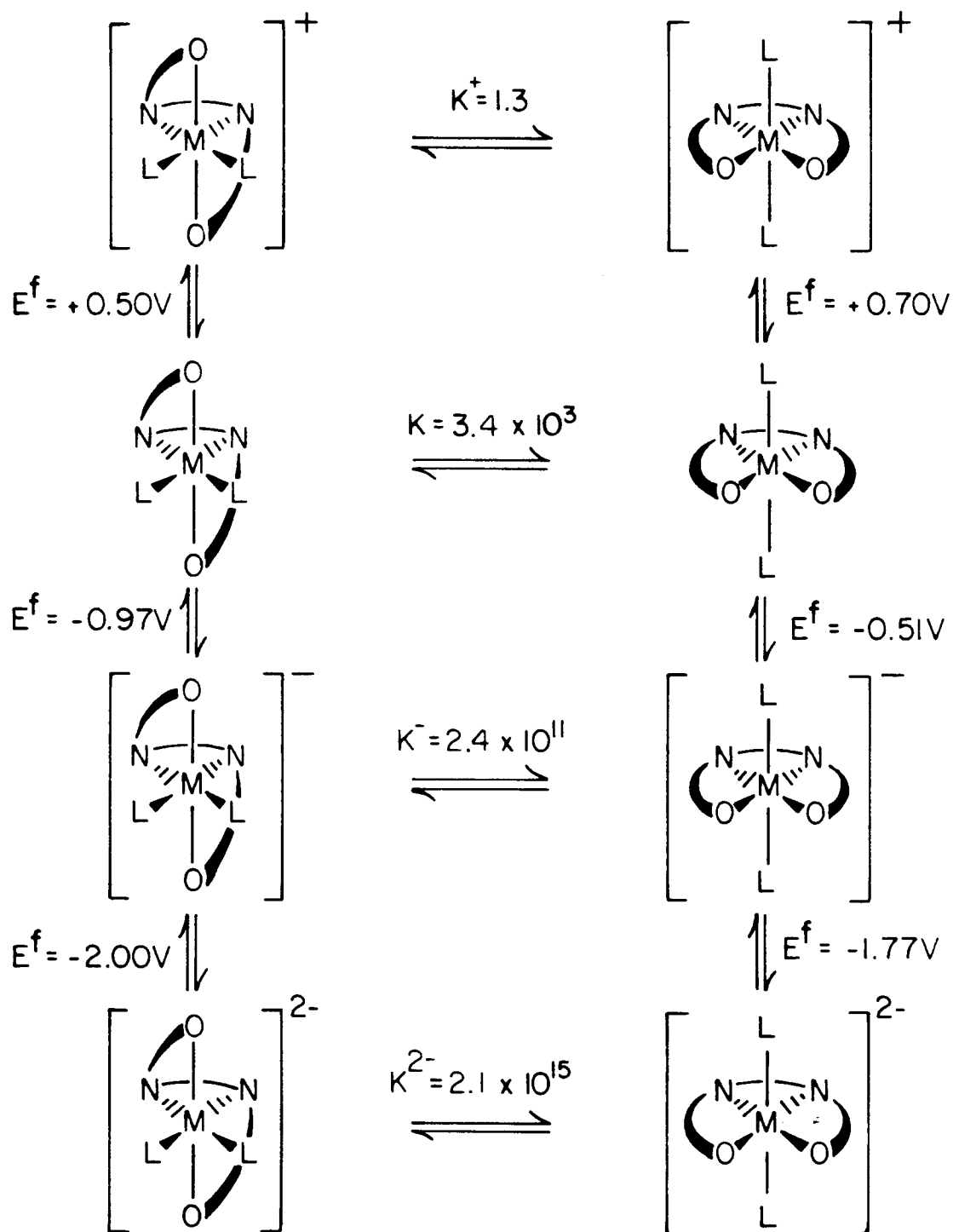


Figure 4.1. Cyclic voltammograms of 4.1 mM 10-*t*Bu in $\text{CH}_2\text{Cl}_2/0.1 \text{ M TBAP}$ at 0.03 cm^2 Pt electrode. Scan rate = 200 mV/sec. (A) Os(IV). (B) Os(V).

$t\text{Bu}]^+$ or $[19\text{-}t\text{Bu}]^+$ as determined by CVs. Isomerization occurs upon warming each solution to room temperature, and identical distributions of $[10\text{-}t\text{Bu}]^+$ and $[19\text{-}t\text{Bu}]^+$ are produced, each displaying a CV identical to that shown in Figure 4.1b. Hence, the cationic Os(V) isomers are at equilibrium at room temperature. Assuming that $[10\text{-}t\text{Bu}]^+$ and $[19\text{-}t\text{Bu}]^+$ have similar diffusion coefficients, the limiting current from the normal pulse voltammogram (NPV) of each isomer can be used to measure the equilibrium concentration ratio.³ The ratio of these limiting currents is equal to the equilibrium constant for $[19\text{-}t\text{Bu}]^+ \rightleftharpoons [10\text{-}t\text{Bu}]^+$, K^+ , which at 22 °C is 1.3 in favor of the trans isomer.

The formal potentials of each diastereomer, together with K^+ , form three sides of a thermodynamic cycle whereby the fourth side, K° (the equilibrium constant for the neutral species), can be derived (Scheme 4.1). Similarly, the equilibrium constants at the Os(III) and Os(II) oxidation states, K^- and K^{2-} , can be calculated. The value of K° , 3.4×10^3 in favor of the trans isomer, is sensible in light of the synthesis of **10-*t*Bu** where **19-*t*Bu** is never observed. This equilibrium constant indicates that **19-*t*Bu** isolated from the ferrocene reduction of the cationic isomer mixture is thermodynamically unstable. Compound **19-*t*Bu** does, indeed, revert to **10-*t*Bu** upon warming ($t_{\frac{1}{2}} = 2.7 \times 10^4$ s in 1,2-dichloroethane at 60 °C).⁴ The derived values for K^- and K^{2-} at 22 °C are 2.4×10^{11} and 2.1×10^{15} in favor of the trans isomer. The equilibrium constants in Scheme 4.1 show an informative trend. The equilibrium constants shift increasingly toward the cis- α isomer as the oxidation state of the osmium increases until at Os(V) the equilibrium constant is ~ 1 and the isomers are approximately isoenergetic. This suggests that the cis- α isomer better stabilizes the metal than the trans isomer as the metal becomes progressively more electron-

Scheme 4.1. Thermodynamic Ladder for the $\text{cis-a} \rightleftharpoons \text{trans}$ Equilibrium of $\text{Os}(\eta^4\text{-CHBA-DCB})(t\text{-Bupy})_2$ at Os(V), Os(IV), Os(III), and Os(II) Oxidation States.



deficient. This *cis-α* ligand set is apparently more electron-donating than the *trans* set. When the metal is electron-rich in the Os(II) state, *cis-α* stabilization is not needed, so the equilibrium lies far to the right. This hypothesis about the relative donating strengths of the two isomers can also be deduced from the CV in Figure 4.1b. The formal potentials of the *cis-α* couples are consistently lower than those of the *trans* couples by as much as 460 mV. This is consistent with the *cis-α* ligand set being more electron-releasing than the *trans* set, which could conceivably arise from the greater basicity of the nitrogen atoms in non-planar N-amido groups as hypothesized in Chapter 3. Electronic demands at the metal center seem to control the isomer equilibria.

The isomerization processes are also affected by the steric influence of the monodentate ancillary ligands. CV and controlled-potential electrolysis studies reveal that *trans*-[Os(η^4 -CHBA-DCB)(PPh₃)₂]⁺ is the only isomer formed upon oxidation of the Os(IV) precursor at room temperature. Presumably steric factors prohibit the formation of *cis* phosphine ligands. We wanted to verify the influence of electronic factors in the absence of these types of steric effects. One approach for confirming the role of electronic factors in equilibrium processes is to establish linear free energy relationships (LFER).^{5a,b} In such a study, experimental rate constants (*k*) or equilibrium constants (*K*) are correlated, as some chosen substituent is varied, with substituent constants (σ) that have been predetermined by employing the Hammett equation for a related parent system (eq 4.1).

$$\log (k/k_0)=\rho\sigma \text{ or } \log (K/K_0)=\rho\sigma \quad (4.1)$$

A good correlation shows that the system being studied responds to the electronic properties of the substituents as a linear function of the response of the parent system. This implies that perturbations induced by other effects are minimal. The LFER also provides information about the sensitivity of the response relative to the parent system. The sensitivities are reflected in the ρ values, i.e., the slopes of the linear relationships. Because the Hammett equation is a single equation in two variables, all LFERs are related to the parent system from which the original σ values are derived by arbitrarily setting ρ at 1. For the original Hammett substituent parameters, σ , the parent system is based on substituted benzoic acid pK_a values.^{5c} Another set of substituent parameters pertinent to our study is Fischer $\bar{\sigma}$ constants, which are based on substituted pyridinium pK_a values or, conversely, substituted pyridine basicities.⁶

If the isomerization process was under electronic control, then in the absence of steric effects we would expect variations in the donating ability of the pyridine ligands to predictably alter the equilibrium constants. With electron-donating substituents, the equilibrium should shift toward the less donating trans isomer, whereas with electron-withdrawing substituents the cis- α isomer should be favored. This hypothesis was tested by synthesizing the series of complexes *trans*-Os(η^4 -CHBA-DCB)(*p*-X-py)₂, 10-X (X = MeO, Et, Me, H, Cl, Br, and CH₃CO),

measuring the formal potentials and K^+ of each compound, and deriving the complete equilibrium data for comparisons with the *p*-*tert*-butylpyridine system. All of the substituted complexes were synthesized by reducing the *trans*-dioxo Os(VI) complex, **3**, with triphenylphosphine in the presence of *p*-X-py and oxidizing the resulting Os(III) residue with bromine. This affords good to moderate yields of products. Only para substituted pyridine complexes were studied because it was anticipated that undesirable steric interaction of meta substituents in the *cis*- α isomer would affect the equilibrium constants. One compound was synthesized with meta substituents, *trans*-Os(η^4 -CHBA-DCB)(3,4-Me₂py)₂ (**10-Me₂**). This compound does not correlate with the **10-X** series of complexes, as was anticipated. Even in the absence of meta substituents, there is sufficient steric "friction" of the *t*-Bupy ligands in *cis*- α **19-*t*Bu** to hinder pyridine rotation about the Os-N axes (Figure 4.2). At 30 °C, two broad peaks are seen for the aromatic pyridine protons in the 400 MHz ¹H NMR spectrum. As the temperature is lowered to 0 °C, the peaks broaden and disappear into the baseline. At -50 °C, four doublets are observed for the pyridine protons. Although at room temperature the pyridine rotation averages the ortho signals and averages the meta signals, at -50 °C the rotation is sufficiently slow to distinguish each of the four protons. The activation energy for pyridine rotation is calculated at 13 ± 1 kcal/mol at 0 °C from coalescence experiments.⁷ As the temperature is lowered, neither the PAC ligand nor the *tert*-butyl protons signals change except for slight variations in chemical shift. Thus, even without meta substituents, steric interaction of the two pyridine ligands can be detected.

For a strong LFER between the equilibrium constants and the pyridine basicities, the metal center must be influenced by the different

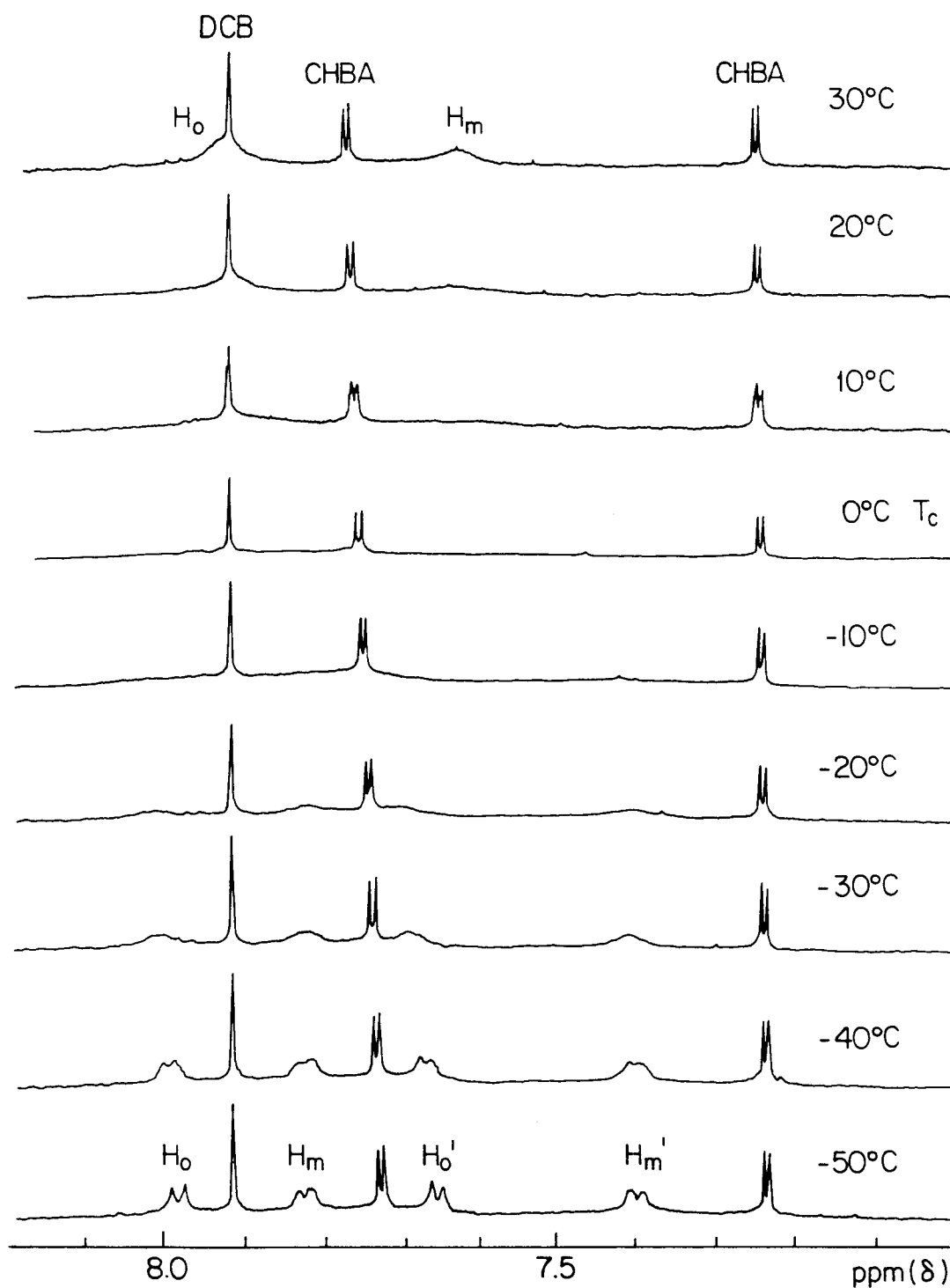
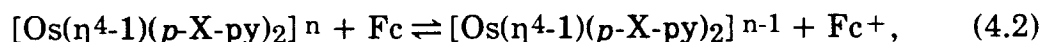


Figure 4.2. Low temperature 400 MHz ^1H NMR spectra of 19-*t*Bu showing coalescence of aromatic *t*-Bupy signals. Temperature range = -50 to 30 °C. Solvent = CD_2Cl_2 .

pyridine ligands. The formal potentials of the compounds would be expected to change if the metal was affected by the different pyridine substituents (Table 4.1). Correlation of the formal potentials and the pyridine basicities confirms this condition. In Figure 4.3, the formal potentials for the couples of all of the compounds are plotted against the $\bar{\sigma}$ substituent constants. As observed in the electrochemistry of **10-*t*Bu** and **19-*t*Bu**, the *cis-α* complexes consistently have formal potentials negative of the *trans* potentials. For a given couple, the expected trend is observed. That is, compounds with electron-donating substituents have formal potentials lower than those of compounds with electron-withdrawing substituents. The data correlate well with the exception of the formal potentials for the Os(IV/III) and Os(III/II) couples of **10-Ac** and **19-Ac**. When the formal potential data are converted to log K values for the equilibria



the derived $\rho/2$ values ($\rho/2$ being the sensitivity per pyridine) are in the range of 1.19 to 4.58, signaling a moderate to substantial sensitivity of the couples to the electronic effects of the pyridine substituents (Table 4.2). The slopes of the plots increase as the osmium becomes more reduced. Whereas we expected the greatest sensitivity of the formal potential with the substituted pyridines to be at the electron-deficient Os(IV) oxidation

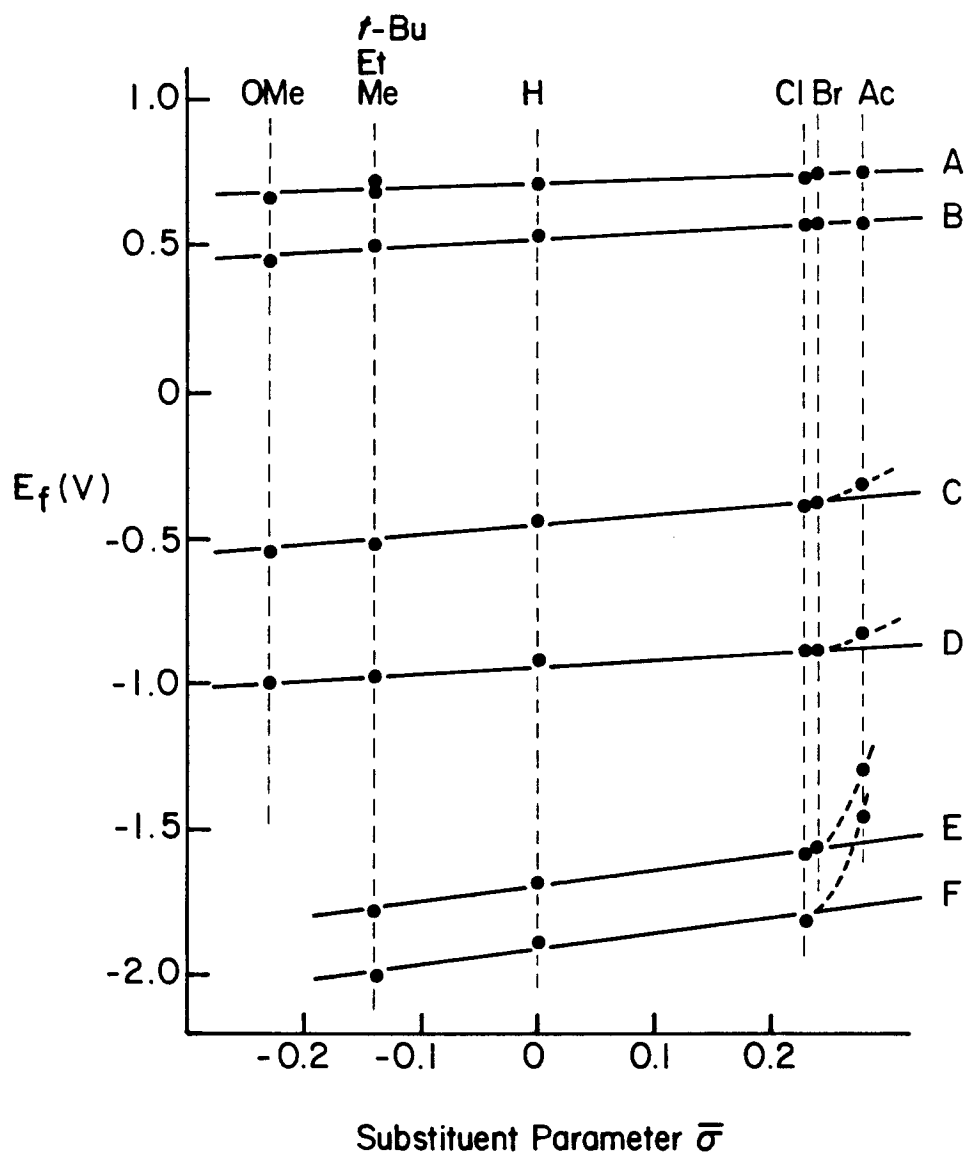


Figure 4.3. Plot of formal potentials versus Fischer $\bar{\sigma}$ substituent parameters⁶ for $\text{Os}(\eta^4\text{-CHBA-DCB})(p\text{-X-py})_2$. Data measured in CH_2Cl_2 at $22 \pm 1^\circ\text{C}$. (A) *trans*-Os(V/IV) couples; slope = 0.140. (B) *cis*- α -Os(V/IV) couples; slope = 0.239. (C) *trans*-Os(IV/III) couples; slope = 0.347.^a (D) *cis*- α -Os(IV/III) couples; slope = 0.231.^a (E) *trans*-Os(III/II) couples; slope = 0.537.^a (F) *cis*- α -Os(III/II) couples; slope = 0.518.^a

^aDatum for *p*-Acpy systems not included in correlation.

state, the slopes of the correlations show that the saturated Os(II) center is most influenced by the pyridine substituent effects.

Table 4.2. Values for Correlation of Formal Potentials with $\bar{\sigma}$ Constants.

Couple	ρ^a	r
<i>trans</i> -Os(V/IV)	2.39	0.975
<i>cis</i> - α -Os(IV/IV)	4.08	0.977
<i>trans</i> -Os(IV/III)	5.91	0.985
<i>cis</i> - α -Os(IV/III)	3.94	0.977
<i>trans</i> -Os(III/II)	9.17	0.992
<i>cis</i> - α -Os(III/II)	8.85	0.981

^a Ref 10.

Note that the formal potentials for the *p*-acetylpyridine system lie on the line for the Os(V/IV) couples, but deviate with increasing magnitude from the line as the oxidation states are lowered. The deviations imply that the acetyl substituents exert a much larger electron-withdrawing effect in these redox processes than expected from the correlation. N-aromatic heterocycles have been described as being a general class of moderately strong π -acids^{8a} and persuasive arguments for the existence of π -backbonding in ruthenium and osmium systems are based upon a considerable amount of experimental data.⁸ It is tempting to speculate that the increase in the deviation with increasing metal basicity signals the presence of unusual π -acceptor properties for *p*-acetylpyridine relative to the other pyridine ligands.

The plots of formal potentials vs. $\bar{\sigma}$ in Figure 4.3 show positive slopes and good correlations (r) for all couples. Assuming that all of the couples are metal-centered, then the different pyridine ligands perturb the osmium in a predictable manner. With K^+ measured for each compound, the other equilibrium constants were derived (Table 4.1) and examined for LFERs.

The $\log K^\circ$ values for the equilibrium $19\text{-X} \rightleftharpoons 10\text{-X}$ were plotted against a variety of substituent parameters.^{5c} The best fits at the Os(IV) oxidation state were found for the substituent parameters σ_p ($\rho = -1.60$, $r = 0.949$, Figure 4.4) and Fischer $\bar{\sigma}$ (the substituent parameter for pyridinium acid dissociation, $\rho = -2.10$, $r = 0.948$, Figure 4.4).^{6a,b} The existence of these LFERs supports the suggestion that K° responds to electronic effects. As the ancillary pyridine ligands become less donating, the equilibrium favors the more donating *cis-a* ligand geometry. Since two pyridine ligands affect the isomerization reactions, $\rho/2$ is a more appropriate measure of the relative sensitivities for pyridine. The $\rho/2$ value of -1.05 found for the correlation with $\bar{\sigma}$ is smaller than the ρ value found for the correlation of pyridinium pK_a constants to $\bar{\sigma}$, 6.01 .^{6a} The smaller ρ value for the isomerization process may result from the electro-neutrality of both species involved. Although the degree of fit for both plots (~ 0.95) is poor by the standards of physical organic chemistry, the correlations are thought to be meaningful considering the differences between this isomerization process and pyridinium and benzoic acid deprotonation reactions to which it is compared.

No LFER was found between K^+ and any substituent parameters. We anticipated that one might be made with σ^+ parameters, because resonance forms can be drawn that delocalize the cationic charge of the

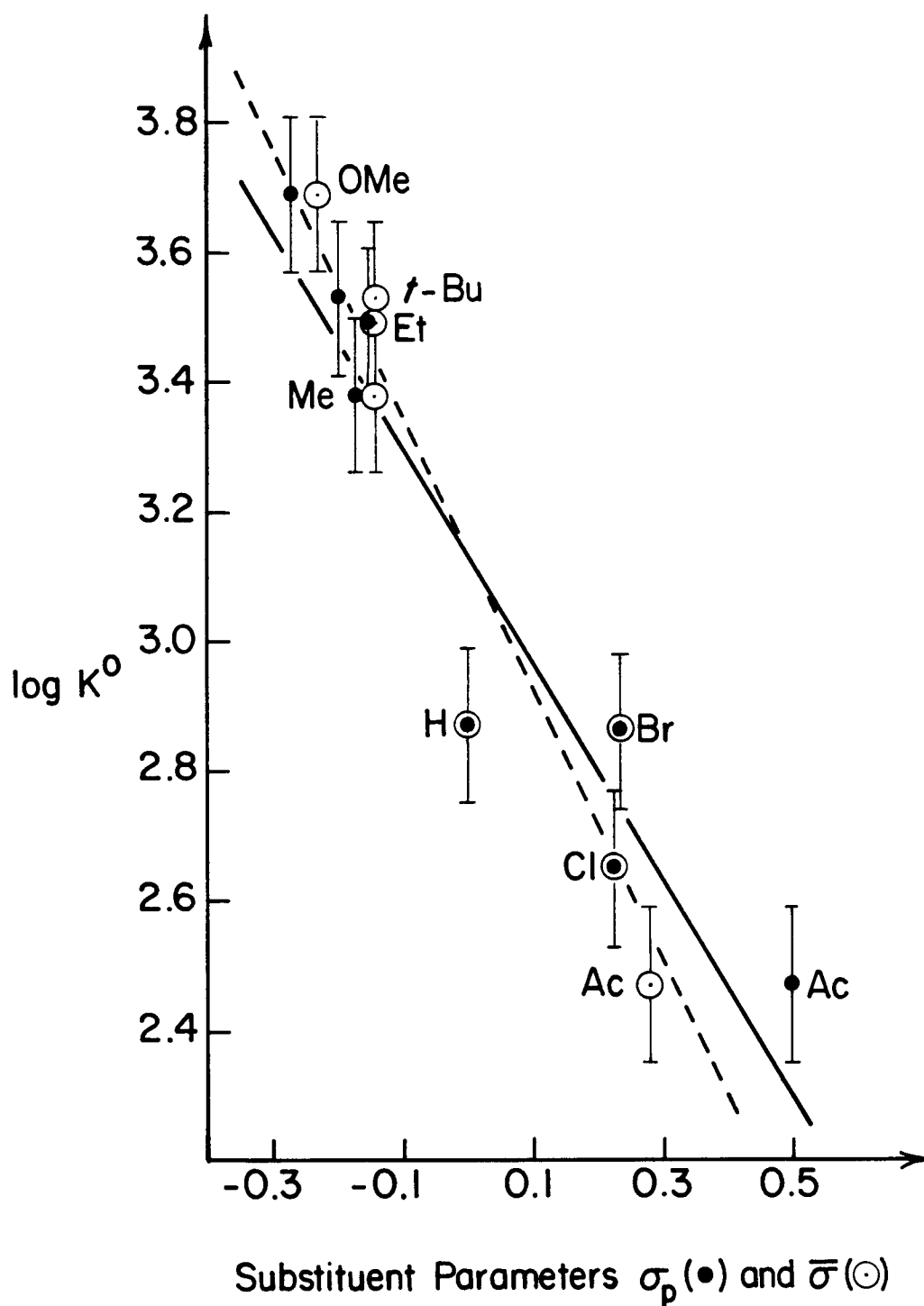


Figure 4.4. Linear free energy correlations of $\log K^\circ$ for $\text{cis-a} \rightleftharpoons \text{trans}$ equilibrium of $\text{Os}(\eta^4\text{-CHBA-DCB})(p\text{-X-py})_2$ and both Hammett σ_p and Fischer $\bar{\sigma}$ constants. Data measured in CH_2Cl_2 at $22 \pm 1^\circ\text{C}$.

Os(V) center onto the pyridine ring and adjacent to the substituent.^{5b,d} This, however, was not observed. LFERs were not sought with K^- or K^2 -equilibrium constants because the propagated errors associated with these data were considered too large for meaningful correlations to be made.⁹

LFERs have been established for other inorganic equilibrium processes involving pyridine ligands. For instance, a ρ value of -1.64 was found for $\bar{\sigma}$ correlation with the equilibrium constants for the replacement of piperidine by *p*-substituted pyridines in an alkyl(piperidine)cobaloxime complex in chloroform at 25 °C.^{11a} The ρ values of -1.50,^{11b} -2.21^{11c}, and -3.11^{11c} were found for the σ_p correlations with the stability constants for formation of pyridine adducts of zinc, cadmium and mercury tetraphenylporphyrin complexes, respectively. When the correlation of pyridine basicities with the binding constants of *p*-substituted pyridine ligands to meso-tetrakis[α^4 -2-(neopentylcarbonylamino)phenyl]-porphyrinato-cobalt(II) at 25 °C in toluene is converted to a correlation with $\bar{\sigma}$, a ρ value of -1.38 ($r = 0.99$) is found.^{11d} Similarly, ρ values of -2.25 ($r = 0.99$) and -4.62 ($r = 0.98$) have been derived from Jones' and Twiggs' data for the correlation of $\bar{\sigma}$ with the first and second binding constants, respectively, of *p*-substituted pyridine ligands to iron(II) phthalocyanine in DMSO at 25 °C.^{11e} While the ρ value of -2.10 for the isomerization equilibria studied in this work lies in the general range of the values for ligand-binding equilibria, any comparison is limited by the differences of the processes involved. Also, two pyridine ligands influence our isomerization systems, whereas only one is involved in each of the other studies mentioned.

Role of Non-planar N-Amido Ligands. The reduction in amide resonance that accompanies distortions from planarity should increase the σ - and π -basicity of the amide nitrogen. Evidence is now presented that suggests that non-planar N-amido ligands play an important role in the reduction of formal potentials found for the cis- α complexes and in the related increased donor capacities of the cis- α ligand set.

In Chapter 3, structural characterization of complexes 11 and 14 revealed remarkable non-planar N-amido groups. While none of the 19-X series of compounds has been structurally characterized, certain properties are common to both cis- α complexes [19-X]⁺ and 14. Each compound has an electron-deficient metal center that apparently causes the isomerization. Compounds [19-X]⁺ are depleted of electron density through electro-oxidation, whereas 14 has a π -acidic *t*-BuNC ancillary ligand. Unusually high amide carbonyl IR bands are seen for both types of complexes. The shift is presumably due to the loss of amide resonance expected in the non-planar form, which enhances the electron-donation from the amide nitrogen. In Chapter 3, the increase in ν_{CO} bands is correlated to the cosine of a structural parameter, $\bar{\tau}$, which is a measure of the torsion angle between the carbon and nitrogen π orbitals. The value $\cos(\bar{\tau})$ approximates the change in overlap between the π orbitals as a function of $\bar{\tau}$ and thus, roughly determines the degree of amide delocalization possible. The $\nu_{C=O}$ band can be considered a crude measure of the N-amido donation to the metal center. An interesting progression of ν_{CO} bands is seen for 10-*t*Bu, 19-*t*Bu, [10-*t*Bu]⁺, and [19-*t*Bu]⁺ (Figure 4.5, top).¹⁸ At the neutral Os(IV) oxidation state, the $\nu_{C=O}$ only mildly increases in isomerizing from trans 10-*t*Bu to cis- α 19-*t*Bu ($\Delta\nu_{CO} = +20$ cm⁻¹). At the cationic Os(V) state, where more stabilization should be

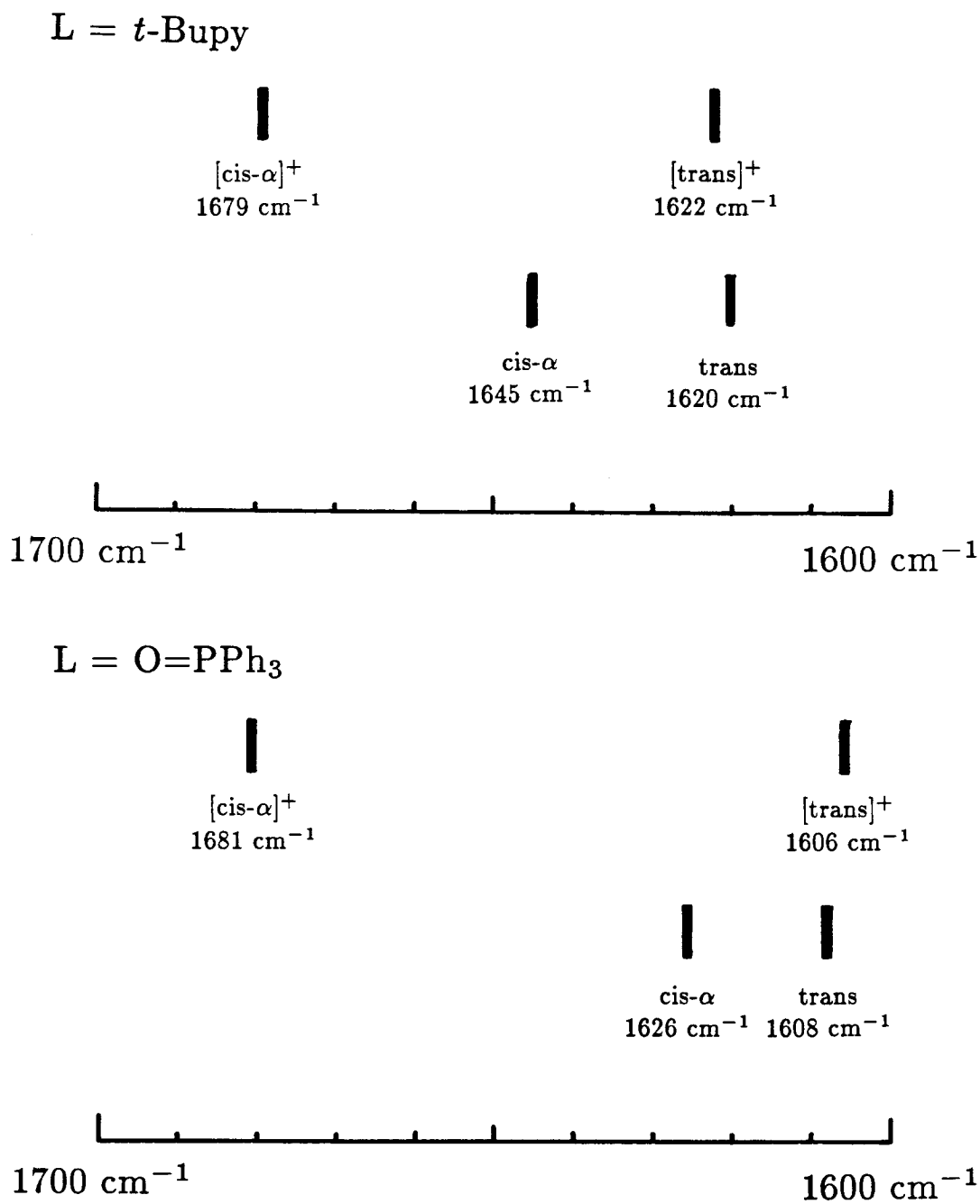


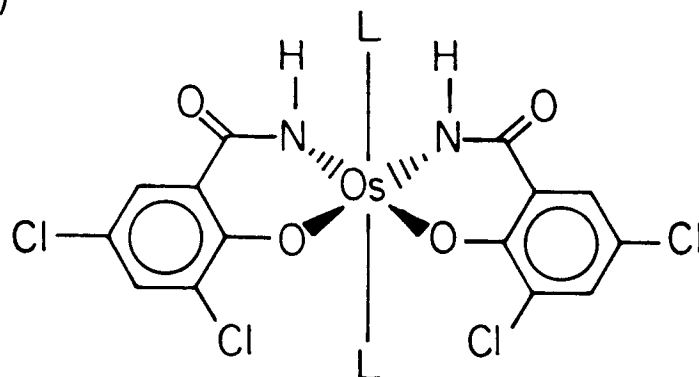
Figure 4.5. Amide carbonyl IR bands for neutral and cationic forms of both *cis-α*- and *trans*-Os(η^4 -CHBA-DCB)L₂, where L = *t*-Bupy (top) and O=PPh₃ (bottom).

needed by the osmium, a greater change is recorded in going from [10-*t*Bu]⁺ to [19-*t*Bu]⁺ ($\Delta\nu_{\text{CO}}^+ = +57 \text{ cm}^{-1}$). Besides structural deformations of the N-amido group causing increased ν_{CO} , enhanced Lewis acidity of the metal center may be thought to increase ν_{CO} without structural changes taking place. In this osmium system, however, no evidence for this phenomenon is observed. In oxidizing 10-*t*Bu to [10-*t*Bu]⁺, only planar N-amido ligands should be present and $\Delta\nu_{\text{CO}}$ equals only +2 cm⁻¹.

A system analogous to the *t*-Bupy complexes, except with O=PPh₃ auxiliary ligands in place of *t*-Bupy, has been synthesized. These complexes are more convenient for studying the cationic isomers because the lower oxidation potentials of the compounds make chemical oxidation possible with solid nitrosonium salts in lieu of electrochemical oxidation.¹⁹ The synthesis of the neutral trans isomer, **8**, is described in Chapter 2. As with 10-*t*Bu, oxidation of **8** generates a mixture of trans and cis- α isomers, [8]⁺ and [20]⁺. Addition of excess ferrocene at -78 °C reduces the mixture to the neutral isomers. Neutral cis- α -Os(η^4 -CHBA-DCB)(O=PPh₃)₂, **20**, rapidly isomerizes back to trans **8**, so the resulting mixture from the ferrocene reduction must be quickly separated by flash chromatography¹² at 5 °C and crystallized out of solution. The phosphine oxide system shows the same ν_{CO} pattern that the *t*-Bupy compounds show for cis- α and trans isomers at both neutral and cationic states (Figure 4.5, bottom). The increase found for cis- α complexes is consistent with the presence of non-planar N-amido ligands and suggests that cationic compounds distort further from planarity than do neutral compounds. Apparently, as the metal needs more stabilization, the PAC ligand incurs greater C-N bond rotation to deliver more electron density to the osmium.

Consider the process of moving the in-plane phenolate donors of **10-*t*Bu** to the axial position of **19-*t*Bu**. In structurally characterized Os(IV) complexes (Chapter 3), C-N bond rotation principally enables this movement. Removal of the dichlorophenylene bridge, as in *trans*-Os(η^2 -salicylamido)₂(*t*-Bupy)₂ (Figure 4.6), should free the N-amido ligand permitting Os-N bond rotation during isomerization, a process that preserves N-amido planarity in *cis-α*-Os(η^2 -salicylamido)₂(*t*-Bupy)₂ (Figure 4.6). The ν_{CO} bands of these salicylamide complexes are found at 1618 cm⁻¹ for the *trans* isomer and 1620 cm⁻¹ for the *cis-α* isomer. These complexes were synthesized in a related PAC ligand project.¹³ If the added stabilization of the *cis-α* ligand set actually results from the different relative positions of the ligands about the osmium coordination sphere, and the N-amido deformations are inconsequential, then the same effect should occur in the salicylamide compounds upon *trans* → *cis-α* isomerization. Unlike the large formal potential differences for **10-*t*Bu** and **19-*t*Bu**, the *trans* and *cis-α* salicylamide complexes exhibit similar Os(IV/III) and Os(III/II) formal potentials (-0.70 V and -1.99 V for *trans*; -0.70 V and -1.97 V for *cis-α*).¹⁴ The Os(V/IV) couples are irreversible for both isomers. Even at elevated temperatures, the *trans* and *cis-α* isomers unfortunately do not equilibrate, so equilibrium constants cannot be determined. This is not important because the trend in equilibrium constants observed with different oxidation states is more informative than the actual constants themselves (as in the discussion of Scheme 4.1). If K° is arbitrarily assigned a value of 1.0 for the neutral Os(IV) equilibrium, then a ladder-type derivation predicts that K^- also equals 1.0 and K^{2-} equals *ca.* 2.2 in favor of the *cis-α* isomer. The values of K^{2-} and K° differ by a factor of two for the bridgeless compounds, whereas for the **10-**

(A)



(B)

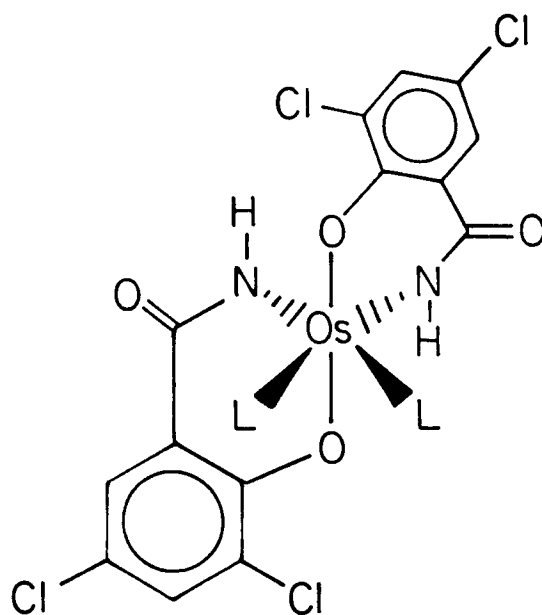


Figure 4.6. Bridgeless complexes of salicylamide ligands.

(A) *trans*-Os(η^2 -salicylamido)(*t*-Bupy)₂.

(B) *cis-α*-Os(η^2 -salicylamido)(*t*-Bupy)₂.

$t\text{Bu} \rightleftharpoons 19\text{-}t\text{Bu}$ equilibrium, they are separated by twelve orders of magnitude. These thermodynamic results are not particular to this pair of bridgeless compounds. Others have been synthesized and show similar formal potentials for the trans and cis- α isomers.¹³ These comparisons demonstrate that the non-planar N-amido ligands are primarily responsible for the reduction in formal potentials and the greater donation by the chelate in the cis- α 19-X series relative to the PAC ligand in the trans 10-X series of complexes.

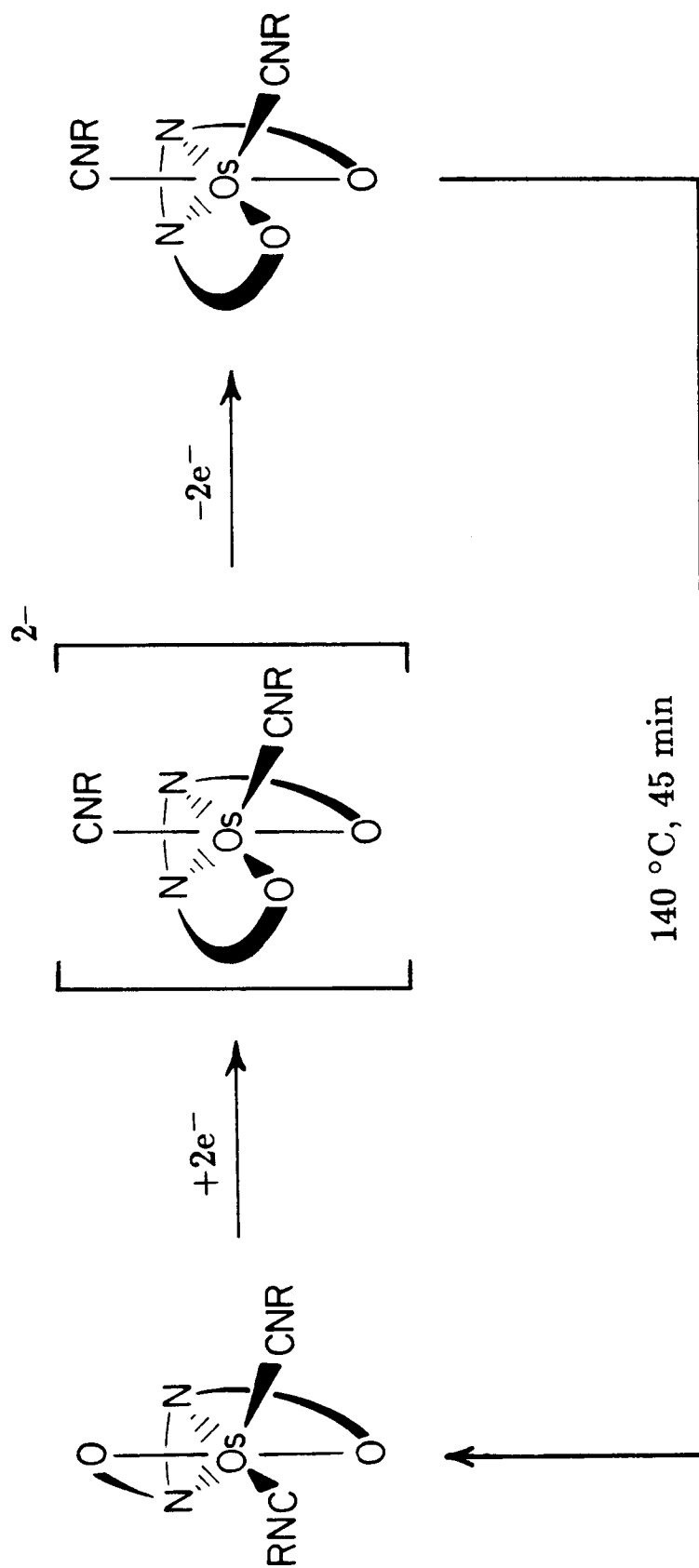
To date, cis- α Os(II) and Os(III) complexes have neither been studied by IR spectroscopy nor isolated. While lower formal potentials for the Os(IV/III) and Os(III/II) couples are found for the cis- α isomers relative to the trans isomers, there is as yet no physical evidence for non-planar amides in the cis compounds at these oxidation states.

From the evidence provided, it seems likely that the balance of two opposing effects determines which isomer is thermodynamically most stable for a given complex. One of these factors, which has been focused upon in this chapter, is the increased electron-donating capacity of the cis- α ligand set due to non-planar N-amido groups. Enhanced ligand-metal bonding can stabilize an electron-deficient metal center. However, there is a cost for this electron-donation. Amide delocalization resonance, which is the driving force for planarity in amides, provides from 10 to 35 kcal/mol of stabilization as determined from dynamic ^1H NMR studies of amide rotational processes. For an electron-rich complex that requires little donation from the PAC ligand, amide delocalization should favor the formation of trans isomers with planar N-amido groups. If these two effects balance one another, then both isomers should equilibrate. This

may be the case for the complexes $[10-X]^+$ and $[19-X]^+$, where K^+ is approximately equal to one.

If this scenario is valid, then reduction of a cis isomer should initiate isomerization to a more planar, less electron-donating isomer. For example, the cis- α complexes of π acids should isomerize to trans or cis- β isomers upon reduction; this does indeed occur (Scheme 4.2). The purple compound *cis*- α -Os(η^4 -CHBA-DCB)(*t*-BuNC)₂, **15**, is easily synthesized (Chapter 2). IR and ¹H NMR spectroscopies establish its *cis*- α formulation. The CV of a pure solution of **15** in dichloromethane is shown in Figure 4.7a. No change is observed upon reduction to Os(III), but a new species is produced upon reduction to Os(II) (Figure 4.7b). The new couples are found at the same potentials as small waves that appear in the CV of the *cis*- α compound on cycling to Os(II). Thus, the process that occurs upon formation of Os(II) is rapid on the CV time scale. The CV of Figure 4.7b is retained upon re-oxidation of the Os(II) solution of Os(IV). A new green Os(IV) compound, **21**, was isolated and shown by ¹H NMR and IR spectroscopies to be the *cis*- β isomer of **15**.²⁰ Upon heating under reflux in xylene, *cis*- β **21** is converted completely to *cis*- α **15**, with some decomposition. It is interesting that reduction to Os(II) produces the *cis*- β ligand set, not the less-donating trans ligand set. The π -acid isocyanide ligands might be sufficiently electron-withdrawing to require that a more donating isomer than the trans be adopted. Alternatively, the mutual trans disposition of the π -acid isocyanide ligands in the trans diastereomer might be unfavorable. We favor the former explanations because controlled-potential electro-reduction of *cis*- α -Os(η^4 -CHBA-DCB)(PPh₃)(*t*-BuNC) by two Faradays per mole also produces the *cis*- β isomer.¹ This experiment does not verify that the two effects (strong Os-N bonding and

Scheme 4.2. Reduction of *cis*- α -Os(η^4 -CHBA-DCB)(*t*-BuNC)₂, 15.



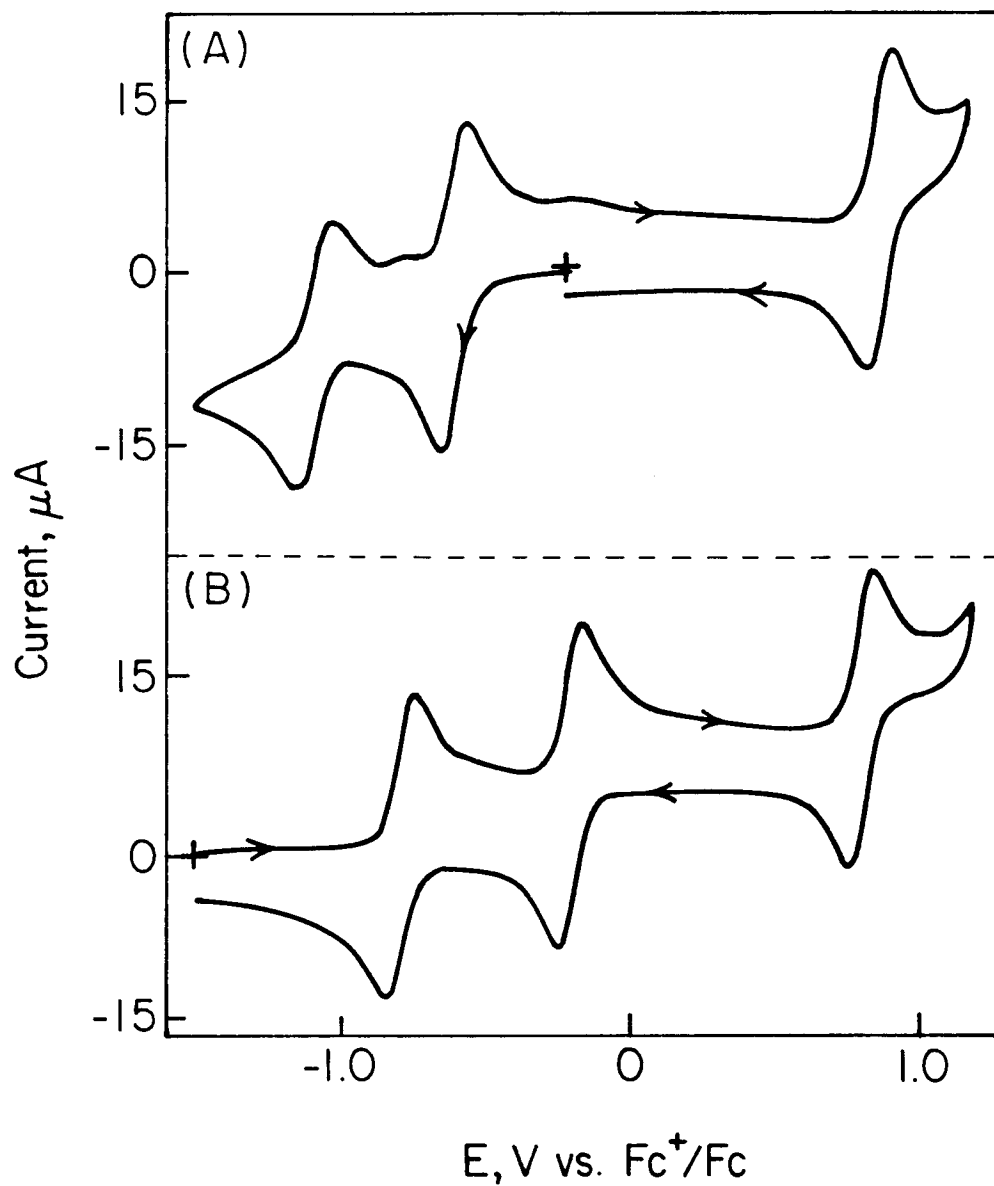


Figure 4.7. Cyclic voltammograms of 1.2 mM *cis*- α -Os(η^4 -CHBA-DCB)(*t*-BuNC) $_2$ in CH $_2$ Cl $_2$ /0.1 M TBAP at 0.03 cm 2 Pt electrode. Scan rate = 200 mV/sec. (A) Os(IV). (B) Os(II).

amide delocalization) control the isomerization reactions, but it is consistent with such a description.

Cis- β Complexes. Thus far, this discussion has focused on trans and cis- α isomers when a third isomer, intermediate to these isomers in the degree of PAC ligand deformation, exists—the cis- β isomer. Fewer cis- β complexes have been synthesized and studied than either trans or cis- α complexes. It is interesting that in the trans \rightleftharpoons cis- α equilibrium experiments, cis- β intermediates are not observed. This will be shown in Chapter 5 to be a consequence of the particular mechanism of isomerization. Three cis- β compounds have been discussed, which incorporate bipy (11), dppe (13), and two *t*-BuNC ligands (21). The IR spectra of all of the complexes show two $\nu_{C=O}$ bands: a high band due to the non-planar N-amido group and a normal frequency band due to the planar group (Table 4.3).

Only one compound has been synthesized in all three isomers, Os(η^4 -CHBA-DCB)(*p*-Cl-py)₂. The trans (10-Cl) and cis- α (19-Cl) isomers were synthesized in the course of the LFER study. A small amount of the cis- β isomer, 22, was isolated from a bad synthesis of 10-Cl. The formal potentials for the three isomers are shown in Table 4.4. Consistent with the progression of from zero to two non-planar N-amido groups in going from trans to cis- β to cis- α isomers, the formal potentials of the cis- β isomer lie between those of the trans and cis- α isomers. The formal potentials of the Os(V/IV) couple for the cis- α and cis- β isomers, however, are similar. This electrochemical evidence, as well as the IR ν_{CO} pattern for cis- β isomers, suggests that the isomeric order of donation from the PAC ligands is cis- α > cis- β > trans.

Table 4.3. Amide Carbonyl IR Bands for Three *cis*- β -Os(η^4 -CHBA-DCB)L₂ Complexes.

Compound	L	Non-planar Amide $\nu_{C=O}$ (cm ⁻¹) ^a	Planar Amide $\nu_{C=O}$ (cm ⁻¹) ^a
11	(bipy)	1635	1620
13	(dppe)	1670	1608
21	(<i>t</i> -BuNC) ₂	1694	1622

^aNujol mull samples

Table 4.4. Formal Potentials of the Three Isomers of Os(η^4 -CHBA-DCB)(*p*-Cl-py)₂.

Isomer	Formal Potential (V) ^a		
	Os(III/II)	Os(IV/III)	Os(V/IV)
trans	-1.59	-0.39	+0.74
<i>cis</i> - β	b	-0.48	+0.60
<i>cis</i> - α	-1.81	-0.89	+0.58

^a Measured in CH₂Cl₂/0.1 M TBAP and referenced to Fc⁺/Fc internal standard. ^b Not observed.

Conclusions

It has been shown that the *trans*-[Os(η^4 -CHBA-DCB)(*p*-X-py)₂]ⁿ complexes become increasingly favored upon stepwise reduction of the cationic compounds to the dianionic oxidation state. The *cis-α* ligand set is the thermodynamically stable diastereomer at the neutral Os(IV) oxidation state when electron-withdrawing π -acid ligands are present. These results suggest that the complexes undergo *trans* to *cis-α* isomerization when increased donation is required by the metal center. It has been demonstrated that the *cis-α* complexes contain non-planar N-amido ligands for the Os(IV) and Os(V) complexes, whereas the *trans* complexes contain planar N-amido ligands at these oxidation states. Because all the ligands in the *cis-α* and *trans* complexes have different positions in the osmium coordination sphere, one might expect the different donor capacities of the two ligand sets to be the sum of many small changes in σ -donor, π -donor and π -acceptor properties for all of the coordinated groups. However, the reduction in formal potentials observed for the *cis-α* complexes appears to be due to the presence of the non-planar N-amido ligands. Thus, the increased donor capacity of the *cis-α* ligand set is also derived from this source. The equilibrium processes likely reflect a balance between the influence of amide resonance, which stabilizes the *trans* isomer, and increased donation from the *cis-α* ligand set, which stabilizes the *cis-α* isomer in the oxidized complexes. The increased donation may also destabilize the *cis-α* isomer in the reduced species. The increase in ligand-to-metal bonding in the stable *cis-α* complexes must be substantial, since rotational processes around the C-N bond of organic

amides are typically subject to large activation barriers.¹⁵ These results imply that the trans \rightarrow cis- α isomerizations occur specifically to produce non-planar amido ligands. The cis- β compounds appear to have donating characteristics intermediate to those of the trans and cis- α complexes. From this, the isomeric order of PAC ligand donation is cis- α > cis- β > trans.

An unexpected PAC ligand design principle is implicit in this work. If N-amido PAC ligands are being designed to produce highly oxidizing metal complexes, then it might be important to design the PAC ligands where spontaneous formation of non-planar N-amido ligands is blocked. Incorporation of the N-amido ligand in an inflexible macrocyclic ligand might be a sufficient constraint. If, on the other hand, stabilized complexes are desirable, then PAC ligands capable of isomerization can deliver added electron density to a metal center as needed.²¹

Experimental Section

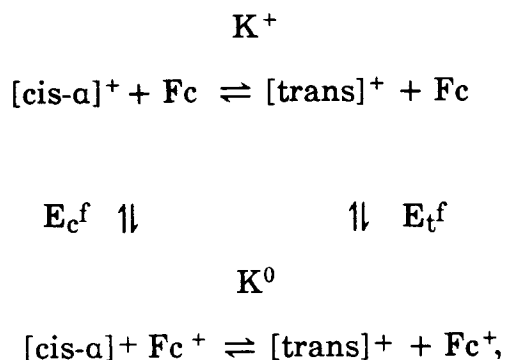
Materials. Diethylether (Baker), hexanes (Aldrich), and toluene (Baker) were reagent grade and were used as received, unless otherwise noted. Dichloromethane (Baker) and tetrahydrofuran (Baker) were distilled from calcium hydride prior to use. 1,2-Dichloroethane was distilled from P_2O_5 prior to use. *p*-Acetylpyridine (98%, Aldrich), bromine (reagent, Baker), bromoethane (98%, Aldrich), chlorobenzene (99%, Aldrich), *p*-ethylpyridine (98%, Aldrich), ferrocene (98%, Aldrich), 3,4-lutidine (98%, Aldrich), nitrosonium hexafluorophosphate (Pfaltz and Bauer), *p*-picoline (M.C.B.), potassium hydroxide (Baker), and triphenylphosphine (99%, Aldrich) were all used as received. A 9.2 M solution of *p*-chloropyridine in diethylether was prepared from *p*-chloropyridine hydrochloride (97%, Lancaster Synthesis) by dissolving it in aqueous 1 M KOH and extracting it into diethylether. Molarity was estimated by 1H NMR spectroscopy. An 8.8 M solution of *p*-bromopyridine in diethylether was prepared similarly from *p*-bromopyridine hydrochloride (95%, Aldrich). *p*-Methoxypyridine was prepared from its N-oxide (Lancaster Synthesis) using PCl_3 by the method of Ochaia.¹⁶ Silica gel used in column chromatography was 60-200 mesh (Davidson). Preparatory TLC plates were silica gel (GF2000, Analtech).

Physical Measurements. 1H NMR spectra were recorded at 90 MHz on a Varian EM-390, at 89.83 MHz on a JEOL FX90-Q spectrometer, at 399.782 MHz on a JEOL GX-400 spectrometer or at 500.135 MHz on a Bruker WM-500 spectrometer. 1H chemical shifts are reported in ppm (δ) vs. Me_4Si with the solvent ($CDCl_3$ δ 7.24, CD_2Cl_2 δ 5.32, Me_2SO-d_6 δ 2.49 or Me_2CO-d_6 δ 2.04) as internal standard. ^{31}P NMR spectra were recorded

at 36.28 MHz on a JEOL FX-90Q spectrometer. ^{31}P chemical shifts are reported in ppm (δ) *vs.* 85% H_3PO_4 external standard. Infrared spectra were recorded on a Beckman IR 4240 spectrophotometer or on a Mattson Series 100 FTIR spectrophotometer. Elemental analyses were obtained at the Caltech analytical facility. Solvents of crystallization were quantified by ^1H NMR spectroscopy of the authentic samples submitted for elemental analyses.

Electrochemical Procedures. Dr. Stephen L. Gipson performed all cyclic voltammetry, controlled-potential electrolyses, and normal pulse voltammetry reported in this chapter. Details of these procedures can be found in ref 1.

Deviation of Successive Equilibrium Constants. Given the following Scheme:



where K^+ is determined by normal pulse voltammetry and E_t^f and E_c^f are determined by cyclic voltammetry, K^0 can be calculated as follows:

Since

$$\Delta G^+ = -RT \ln K^+ = G([trans]^+) - G([cis-a]^+)$$

and

$$\Delta G([trans]^+/[trans]) = -FE_t^f = G([trans]) + G(Fc^+) - G([trans]^+) - G(Fc)$$

$$\Delta G([cis-a]^+[cis-a]) = -FE_t^f = G([cis-a]) + G(Fc^+) - G([cis-a]^+) - G(Fc),$$

then

$$\Delta G^+ + \Delta G([trans]^+[trans]) - \Delta G([cis-a]^+[cis-a]) = G([trans]) - G(cis-a) = \Delta G.$$

Alternatively,

$$K^0 = K^+ \exp \left[\frac{F}{RT} (E_t^f - E_c^f) \right],$$

which at 22 °C can be expressed in the general form

$$K^n = K^{n+1} \exp \left[39.32 (E_t^{f(n+1/n)} - E_c^{f(n+1/n)}) \right].$$

Errors were propagated according to the equation

$$\sigma_F^2 = \left[\sum_i \left(\frac{\delta F}{\delta x_i} \right)^2 \sigma_{x_i}^2 \right]^{1/2},$$

where $F = F(x_1, x_2, \dots, x_n)$. Uncertainties were calculated at the 95% confidence level.¹⁷ Errors of ± 5 mV for E_f and ± 2 K for temperature were assumed. Error in K^+ measurements can be found in Table 4.1.

Syntheses. All reactions were carried out in air unless otherwise noted. The syntheses of the following compounds are reported in Chapter

2: $K_2[trans-Os(\eta^4-CHBA-DCB)(O)_2]$, **3**; $trans-Os(\eta^4-CHBA-DCB)(PPh_3)_2$, **7**; $trans-Os(\eta^4-CHBA-DCB)(py)_2$, **10-H**; $trans-Os(\eta^4-CHBA-DCB)(t-Bupy)_2$, **10-tBu**; $cis-\alpha-Os(\eta^4-CHBA-DCB)(PPh_3)(t-BuNC)$, **14**; $cis-\alpha-Os(\eta^4-CHBA-DCB)(t-BuNC)_2$, **15**; $trans-Os(\eta^4-CHBA-DCB)(O=PPh_3)_2$, **8**.

$cis-\alpha-Os(\eta^4-CHBA-DCB)(t-Bupy)_2$, (**19-tBu**). $trans-Os(\eta^4-CHBA-DCB)(t-Bupy)_2$ (200 mg; 0.198 mmol) was electro-oxidized by one Faraday per mole (1.42 V vs. Fc^+/Fc , $CH_2Cl_2/0.1$ M TBAP). At room temperature, isomerization to the equilibrium mixture of isomers had occurred when the electrolysis was complete. The solution was cooled ($-78^\circ C$) and reduced with excess ferrocene dissolved in dichloromethane. The solvent volume was reduced on a rotary evaporator at room temperature, and the supporting electrolyte was precipitated with diethylether and collected by filtration. The procedure was repeated to ensure complete TBAP removal. Separation of the $cis-\alpha$ and $trans$ isomers was achieved by column chromatography using silica gel (32-63 micron, Woelm, 150 g) and chlorobenzene/bromoethane (1:1 v/v) eluent. The front-running ferrocene band was collected and discarded. The next red band and the final dark band were separately collected, and the solvents were removed on a rotary evaporator. Both residues were recrystallized from CH_2Cl_2 /hexane. The red compound was the pure $cis-\alpha$ isomer: yield 64 mg (74% based on $K^+ = 1.3$; 32% based on recovered osmium); 1H NMR (Table 4.5); IR (Nujol) 1645 cm^{-1} ν_{CO} (non-planar amide, br); Anal. calcd. for $C_{38}H_{32}N_4O_4OsCl_6 \cdot 0.25 (C_6H_{14})$: C, 45.92; H, 3.46; N, 5.42. Found: C, 45.90; H, 3.46; N, 5.42. The dark band proved to be a mixture of $cis-\alpha$ and $trans$ isomers (1:2.6 by 1H NMR: yield 75 mg (48% of **10-tBu** and 34% of **19-tBu** based on $K^+ = 1.3$; 38% based on recovered osmium).

trans-Os(η^4 -CHBA-DCB)(*p*-MeOpy)₂, (10-MeO). K₂[*trans*-Os(η^4 -CHBA-DCB)(O)₂].4H₂O (300 mg; 0.350 mmol), triphenylphosphine (210 mg; 0.801 mmol), and *p*-methoxypyridine (4 mL; *ca.* 40 mmol) were dissolved in water (3 mL) and gently heated (20 min). After cooling, all volatiles were removed *in vacuo*. The residue was purified by twice precipitating it from THF with hexane. The precipitate was dissolved in THF (10 mL) and oxidized with excess bromine. After removal of the solvent on a rotary evaporator, the product was eluted through a short silica gel column with CH₂Cl₂ and recrystallized from CH₂Cl₂/hexane to yield a blue microcrystalline powder: yield 211 mg (63%); ¹H NMR (Table 4.5); Anal. calcd. for C₃₂H₂₀N₄Cl₆OsO₆·0.15 (C₆H₁₄): C, 40.64; H, 2.29; N, 5.76. Found: C, 40.61; H, 2.24; N, 5.74.

trans-Os(η^4 -CHBA-DCB)(*p*-Etpy)₂, (10-Et). K₂[*trans*-Os(η^4 -CHBA-DCB)(O)₂].4H₂O (120 mg; 0.130 mmol), triphenylphosphine (85 mg; 0.324 mmol), and *p*-ethylpyridine (3.7 g; *ca.* 35 mmol) were dissolved in water (3 mL) and gently heated (45 min). After cooling, all volatiles were removed *in vacuo*. The residue was purified by twice precipitating it from THF with hexane. The precipitate was dissolved in THF (10 mL) and oxidized with bromine. After removal of the solvent on a rotary evaporator, the product was eluted through a short silica gel column with CH₂Cl₂ and recrystallized from CH₂Cl₂/hexane to yield a blue crystalline product: yield 60 mg (48%); ¹H NMR (Table 4.5); Anal. calcd. for C₃₄H₂₄N₄Cl₆OsO₄·0.2 (C₆H₁₄): C, 43.46; H, 2.78; N, 5.76. Found: C, 43.12; H, 2.84; N, 5.70.

trans-Os(η^4 -CHBA-DCB)(*p*-Mepy)₂, (10-Me). K₂[*trans*-Os(η^4 -CHBA-DCB)(O)₂].4H₂O (120 mg; 0.130 mmol), triphenylphosphine (85 mg; 0.324 mmol), and *p*-picoline (3.8 g; *ca.* 41 mmol) were dissolved in

water (3 mL) and gently heated (45 min). After cooling, all volatiles were removed *in vacuo*. The residue was purified by twice precipitating it from THF with hexane. The precipitate was dissolved in THF (25 mL) and oxidized with bromine. After removal of the solvent on a rotary evaporator, the product was eluted through a short silica gel column with CH₂Cl₂ and recrystallized from CH₂Cl₂/hexane to yield a dark blue crystalline solid. An analytical sample was obtained by purification on a preparatory TLC plate using toluene eluent followed by recrystallization from CH₂Cl₂/hexane: yield 74 mg (65%); ¹H NMR (Table 4.5); Anal. calcd. for C₃₂H₂₀N₄Cl₆OsO₄·0.3(C₆H₁₄): C, 42.58; H, 2.56; N, 5.88. Found: C, 42.90; H, 2.44; N, 6.18.

trans-Os(η⁴-CHBA-DCB)(*p*-Clpy)₂, (10-Cl). K₂[*trans*-Os(η⁴-CHBA-DCB)(O)₂].4H₂O (200 mg; 0.217 mmol), triphenylphosphine (140 mg; 0.534 mmol), and 4 mL of *ca.* 9.2 M *p*-chloropyridine solution in diethylether (*ca.* 37 mmol) were dissolved in water (2.5 mL) and gently heated (0.5 h). After cooling, all volatiles were removed *in vacuo*. The residue was purified by twice precipitating it from THF with hexane. The precipitate was dissolved in THF (25 mL) and oxidized with bromine. After removal of the solvent on a rotary evaporator, the product was eluted through a short silica gel column with CH₂Cl₂ and recrystallized from CH₂Cl₂/hexane to yield a dark blue microcrystalline powder: yield 143 mg (68%); ¹H NMR (Table 4.5); Anal. calcd. for C₃₀H₁₄N₄Cl₈OsO₄: C, 37.21; H, 1.46; N, 5.79. Found: C, 37.28; H, 1.61; N, 5.71.

trans-Os(η⁴-CHBA-DCB)(*p*-Brpy)₂, (10-Br). K₂[*trans*-Os(η⁴-CHBA-DCB)(O)₂].4H₂O (120 mg; 0.130 mmol), triphenylphosphine (85 mg; 0.324 mmol), and 2.7 mL of *ca.* 8.8 M *p*-bromopyridine solution in diethylether (*ca.* 24 mmol) were dissolved in water (1.8 mL) and gently

heated (0.5 h). After cooling, all volatiles were removed *in vacuo*. The residue was purified by twice precipitating it from THF with hexane. The precipitate was dissolved in THF (25 mL) and oxidized with bromine. After removal of the solvent on a rotary evaporator, the product was eluted through a short silica gel column with CH₂Cl₂/THF (10:1 v/v) and recrystallized from CH₂Cl₂/hexane to yield a dark blue crystalline product: yield 65mg (47%); ¹H NMR (Table 4.5); Anal. calcd. for C₃₀H₁₄N₄Br₂Cl₆OsO₄: C, 34.08; H, 1.33; N, 5.30. Found: C, 34.34; H, 1.58; N, 5.10.

trans-Os(η⁴-CHBA-DCB)(*p*-Acpy)₂, (10-Ac). K₂[*trans*-Os(η⁴-CHBA-DCB)(O)₂].4H₂O (120 mg; 0.130 mmol), triphenylphosphine (85 mg; 0.324 mmol), and *p*-acetylpyridine (4.4 g; 36 mmol) were dissolved in water (3 mL) and gently heated (1 h). After cooling, all volatiles were removed *in vacuo*. The residue was purified by twice precipitating it from THF with hexane. The precipitate was dissolved in THF (25 mL) and oxidized with bromine. After removal of the solvent on a rotary evaporator, the product was eluted through a short silica gel column with excess CH₂Cl₂ and recrystallized from CH₂Cl₂/hexane to yield a dark blue-green crystalline solid: yield 73 mg (57%); ¹H NMR (Table 4.5); Anal. calcd. for C₃₄H₂₀N₄Cl₆OsO₆·0.1(C₆H₁₄): C, 41.89; H, 2.17; N, 5.65. Found: C, 42.00; H, 2.21; N, 5.67.

trans-Os(η⁴-CHBA-DCB)(3,4-Me₂py)₂, (10-Me₂). K₂[*trans*-Os(η⁴-CHBA-DCB)(O)₂].4H₂O (120 mg; 0.130 mmol), triphenylphosphine (84 mg; 0.324 mmol), and 3,4-lutidine (1.9 g; 18 mmol) were dissolved in water (3 mL) and gently heated (25 min). After cooling, all volatiles were removed *in vacuo*. The residue was purified by twice precipitating it from CH₂Cl₂/hexane. The precipitate was dissolved in THF (10 mL) and

oxidized with bromine. After removal of the solvent on a rotary evaporator, the product was eluted through a short silica gel column with excess chloroform and recrystallized from CHCl_3 /hexane to yield a dark blue microcrystalline product: yield 95 mg (77%); ^1H NMR (Table 4.5); Anal. calcd. for $\text{C}_{34}\text{H}_{24}\text{N}_4\text{Cl}_6\text{OsO}_4$: C, 42.74; H, 2.53; N, 5.86. Found: C, 42.93; H, 2.63; N, 5.80.

Mixture of *trans*- and *cis*- α -[Os(η^4 -CHBA-DCB)(O=PPh₃)₂]-[PF₆], (8⁺) and (20⁺). *trans*-Os(η^4 -CHBA-DCB)(O=PPh₃)₂ (30 mg; 0.023 mmol) was dissolved in dichloromethane (5 mL), and excess solid nitrosonium hexafluorophosphate was added, but did not dissolve. The solution was sealed with a septum and stirred at room temperature (0.5 h), during which the solution turned from red to purple, indicative of product formation. The purple solution was filtered away from unreacted NO[PF₆], and the solvent was removed *in vacuo* to afford deep purple crystalline product: yield 30 mg (96%); IR (KBr) 1680 cm^{-1} ν_{CO} (non-planar amide, *cis*- α isomer); 1605 cm^{-1} ν_{CO} (planar amide, *trans* isomer); Anal. calcd. for $\text{C}_{56}\text{H}_{36}\text{Cl}_6\text{F}_6\text{N}_2\text{O}_6\text{OsP}_3\cdot\text{H}_2\text{O}$ (solvate was not quantified); C, 46.05; H, 2.62; N, 1.92. Found: C, 46.08; H, 2.57; N, 1.95.

Mixture of *trans*- and *cis*- α -Os(η^4 -CHBA-DCB)(O=PPh₃)₂, (8) and (20). *trans*-Os(η^4 -CHBA-DCB)(O=PPh₃)₂ (150 mg; 0.116 mmol) was dissolved in dichloromethane (15 mL), and excess solid nitrosonium hexafluorophosphate was added but did not dissolve. After stirring the solution at room temperature (15 min), the resulting purple solution was filtered away from unreacted NO[PF₆], cooled (-78 °C) and reduced with ferrocene (1.5 equiv). In a walk-in cold room (5 °C) the material was flash chromatographed¹² through silica gel (250 g) with pre-cooled dichloromethane. The front-running ferrocene band was collected and

discarded. The subsequent red band was collected and crystallized from CH₂Cl₂/hexane at -20 °C to yield a red powder. The ¹H NMR of this material revealed it to be a 3:1 mixture of cis-α and trans isomers: yield 90.2 mg (60% based on recovered osmium); ³¹P and ¹H NMR (Table 4.5); IR (Nujol) 1626 cm⁻¹ ν_{CO} (non-planar amide, br).

cis-β-Os(η⁴-CHBA-DCB)(*t*-BuNC)₂ (21). cis-α-Os(η⁴-CHBA-DCB)(*t*-BuNC)₂ (15 mg; 15 μmol) was electro-reduced by two Faradays per mole at -1.20 V *vs.* Fc⁺/Fc. The solution turned green. The solution was reoxidized by two Faradays per mole and diethylether was added (*ca.* 300 mL) to precipitate the supporting electrolyte. After filtration, the solvent was removed on a rotary evaporator, and the product was eluted through a silica gel column with excess CH₂Cl₂/THF (100:1 v/v). Recrystallization from CH₂Cl₂/hexane afforded a green microcrystalline product: yield 12 mg (80%); ¹H NMR (Table 4.5); IR(Nujol) 1694 cm⁻¹ ν_{CO} (non-planar amide), 1622 cm⁻¹ ν_{CO} (planar amide), 2154 cm⁻¹ ν_{C≡N}, 2002 cm⁻¹ ν_{C≡N}.

cis-β-Os(η⁴-CHBA-DCB)(*p*-Clpy)₂, (22). K₂[*trans*-Os(η⁴-CHBA-DCB)(O)₂].4H₂O (200 mg; 0.217 mmol), triphenylphosphine (140 mg; 0.534 mmol), and 3 mL of *ca.* 9.2 M *p*-chloropyridine solution in diethylether (*ca.* 28 mmol) were dissolved in water (2.0 mL) and gently heated (0.5 h). After cooling, all volatiles were removed and the residues dried *in vacuo* for 24 h. After dissolving the residues in 10 mL dry THF, excess bromine was added and the solution kept at 10 °C for *ca.* 4 weeks, after which all volatiles were removed on a rotary evaporator and the remaining material separated using flash chromatography¹² with silica gel and toluene eluent. A green band was isolated and the solvent removed to yield a green microcrystalline product: yield 6 mg (3%); ¹H NMR (Table 4.5); Anal.

Calcd. for $\text{C}_{30}\text{H}_{14}\text{N}_4\text{Cl}_8\text{OsO}_4$: C, 37.21; H, 1.46; N, 5.79. Found: C, 37.10; H, 1.67; N, 5.55.

Table 4.5. (Continued).

Compound	Isomer	$(\eta^4\text{-CHBA-DCB})^{4-}$		Ancillary Ligand, L		
		DCB	CHBA ^a	H _o	H _m	H _p other L
21^b	cis- β	9.79	7.82			-C(CH ₃) ₃
		br,1H	br,2H			1.22 t-BuNC
		5.77	7.44			s,9H
22^{b,e,h}	cis- β	br,1H				1.44
		9.78	7.74	5.95	9.37	s,9H
		s,1H	d,1H	d,2H	d,2H	
22^{b,e,h}	cis- β	3.74	7.64	2.57	8.47	
		s,1H	d,1H	d,2H	d,2H	
				³ J _{o,m} = 7 Hz		

^aEach CHBA doublet was not assigned relative to the other. ⁴J_{m,m'} = 2.7 – 3.0 Hz. ^b δ in CDCl₃. ^c δ in CD₂Cl₂. ^dSpectrum measured at -50 °C. ^eCoupled protons established by decoupling experiments. ^fSpectrum measured at -20 °C. ^g3,4-Me₂py protons were assigned by selective NOE enhancement experiments. ^hHindered pyridine rotation at room temperature.

References

1. Details of the electrochemical experiments and procedures can be found in the following: Gipson, S. L., Ph.D. Thesis, California Institute of Technology, June 1985.
2. For examples of studies of interconversions of diastereomeric complexes induced by redox processes, see: (a) Gaudiello, J. G.; Wright, T. C.; Jones, R. A.; Bard, A. J. *J. Am. Chem. Soc.* **1985**, *107*, 888. (b) Datta, S.; Dezube, B.; Kouba, J. K.; Wreford, S. S. *J. Am. Chem. Soc.* **1978**, *100*, 4404-4412. (c) Lewis, J.; Whyman, R. *J. Chem. Soc.* **1965**, 5486-5491. (d) Crossing, P. F.; Snow, M. R. *J. Chem. Soc. A* **1971**, 610-612. (e) Reiman, R. H.; Singleton, E. J. *Organomet. Chem.* **1971**, *32*, C44-C46. (f) Johnson, B. F. G.; Bhaduri, S.; Connelly, N. G. *J. Organomet. Chem.* **1972**, *40*, C36-C38. (g) George, T. A.; Siebold, C. D. *Inorg. Chem.* **1973**, *12*, 2458-2552. (h) Wimmer, F. I.; Snow, M. R.; Bond A. M. *Inorg. Chem.* **1974**, *13*, 1617-1623. (i) Bond, A. M.; Colton, R.; Jackowski, J. J. *Ibid.* **1975**, *14*, 274-278. (j) *Ibid.* **1975**, *14*, 2526-2530. (k) Bond, A. M.; Colton, R.; McCormick, M. J. *Ibid.* **1977**, *16*, 155-159. (l) Bond, A. M.; Grabaric, B. S.; Grabaric, Z. *Ibid.* **1978**, *17*, 1013-1018. (m) Bond, A. M.; Colton, R.; Jackowski, J. J. *Ibid.* **1978**, *17*, 2153-2160. (n) Bond, A. M.; Colton, R.; McDonald, M. E. *Ibid.* **1978**, *17*, 2842-2847. (o) Bond, A. M.; Keene, F. R.; Rumble, N. W.; Searle, G. H.; Snow, M. R. *Ibid.* **1978**, *17*, 2847-2853. (p) Connor, J. A.; Riley, P. I.; Rix, C. J. *J. Chem. Soc., Dalton Trans.* **1977**, 1317-1323. (q) Connor, J. A.; Riley, P. I. *J. Chem. Soc., Dalton Trans.* **1979**, 1231-1237. (r) *Ibid.* **1979**, 1318.

3. Bard, A. J.; Faulkner, L. F. "Electrochemical Methods: Fundamentals and Application"; John Wiley and Sons: New York, 1980; pp 186-199.
4. Alternatively, **19-*t*Bu** can be rapidly converted to **10-*t*Bu** at room temperature by addition of a trace of [**19-*t*Bu**]⁺ or [**10-*t*Bu**]⁺. These cations catalyze the isomerization processes by cycling the neutral compounds through the cationic state where the isomerization is fast.
5. (a) Johnson, C. D. "The Hammett Equation"; Cambridge University Press: Cambridge, 1973. (b) Lowry, T. H.; Richardson, K. S. "Mechanism and Theory in Organic Chemistry", 2nd ed.; Harper & Row Publishers: New York, 1981; pp 130-145. (c) Substituent parameters taken from Gordon, A. J.; Ford, R. A. "The Chemists Companion"; John Wiley and Sons: New York, 1972; pp 144-155. (d) Ritchie, C. D.; Sager, W. F. "Progress in Physical Organic Chemistry", Cohen, S. G.; Streitwieser, A., Jr.; Taft, R. W.; John Wiley and Sons: New York, 1964; Vol. 2, pp 323-400.
6. (a) Fischer, A.; Galloway, W. J.; Vaughan, J. J. *Chem. Soc.* **1964**, 3591-3596. The σ values are as follows: 4-MeO, -0.23; 4-Et, -0.14; 4-Me, -0.14; H, 0.00; 4-Cl, 0.23; 4-Br, 0.24; 4-Ac, 0.28. (b) For a recent treatment of the relative field/inductive and resonance contributions to pyridine basicity, see Taagepera, M.; Summerhays, K. D.; Hehre, W. J.; Topsom, R. D.; Pross, A.; Radom, L.; Taft, R. W. *J. Org. Chem.* **1981**, *46*, 891-903. (c) The σ value for *p-t*-Bupy, -0.14, was calculated from its pK_a found in Sawada, M.; Ichihara, M.; Yukawa, Y.; Nakachi, T.; Tsuno, Y. *Bull. Chem. Soc. Jpn.* **1980**, *53*, 2055-2060.

7. ΔG^\ddagger was determined by variable temperature coalescence experiment as described in: Sandstrom, J. "Dynamic NMR Spectroscopy"; Academic Press: New York, 1982; p 79. Coalescence of the H_m peaks occurred at 0 °C at 400 MHz. The frozen spectrum was recorded at -50 °C; $\delta\nu(H_m) = 174$ Hz.
8. (a) Creutz, C. *Prog. Inorg. Chem.* **1983**, 30, 1-73. (b) Bino, A.; Lay, P. A.; Taube, H.; Wishart, J. F. *J. Am. Chem. Soc.* **1985**, 24, 3969-3971, and references therein.
9. The major error component in the equilibrium data propagates from the error in measuring the formal potentials (± 5 mV). Over the range of pyridine complexes investigated, for K° the error depends on σ_{K^+} by 0.6-3.5%, on σ_{E_f} by 94-97%, and on σ_τ by 2.3-4.2%; for K^- the error depends on σ_{K^+} by 0.3-1.6%, on σ_{E_f} 87-89%, and on σ_τ by 10.2-11.8%; and for K^{2-} the error depends on σ_{K^+} by 0.2-1.1%, on σ_{E_f} by 90-91%, and on σ_τ by 8.3-9.0%.
10. Slopes are converted into ρ by multiplication with the factor converting E_f into $\log K$ for the equilibrium in eq 4.2. The factor equals $F/(2.303 RT)$, which at 22 °C equals 17.08.
11. (a) Jensen, F. R.; Kiskis, R. C. *J. Am. Chem. Soc.* **1975** 97, 5820-5825. (b) Kirksey, C. H.; Hambright, P.; Storm, C. B. *Inorg. Chem.* **1969**, 8, 2141-2144; ρ value reported as +1.50. (c) Kirksey, C. H.; Hambright, P. *Inorg. Chem.* **1970**, 9, 958-960; positive ρ values reported. (d) Imai, H.; Nakata, K.; Nakatsubo, A. *Synth. React. Inorg. Met.-Org. Chem.* **1983**, 13, 761-780. (e) Jones, J. G.; Twigg, M. V. *Inorg. Chim. Acta* **1974**, 10, 103-108. All data employed for

correlation with first binding constant. Second binding constant datum for *p*-cyanopyridine omitted from correlation as datum deviates significantly from the otherwise good linear relationship for log K_2 versus pK_{BH^+} .

12. Still, W. C.; Kahn, M.; Mitra, A. *J. Org. Chem.* **1978**, *43*, 2923-2925.
13. (a) Krafft, T. E., Ph.D. Thesis, California Institute of Technology, February 1985. The trans complex was characterized by X-ray crystallography. (b) Ref 1.
14. Measured in $CH_2Cl_2/0.1$ M TBAP and referenced to Fc^+/Fc internal standard.
15. Stewart, W.; Siddell, T. H., III *Chem. Rev.* **1970**, *70*, 517-551.
16. Ochaia, E. "Aromatic Amine Oxides", Mizoguchi, D. O.; Trans.; Elsevier: New York **1967**; p 167.
17. Peters, D. G.; Hayes, J. M. "Chemical Separations and Measurements; Theory and Practice of Analytical Chemistry"; W. B. Saunders: Philadelphia, **1974**; pp 6-37.
18. All IR spectra of the *t*-Bupy series were taken as nujol mulls, except for that of $[19-tBu]^+$ where a solution spectrum was recorded of crude bulk electrolysis material syringed from an electrochemical cell. All spectra of the $O=PPh_3$ series were recorded as nujol mulls.
19. The formal potentials of **8** can be found in Table 2.3. The formal potentials of **20** are as follows: Os(V/IV), +0.19 V; Os(IV/III), -1.35 V; recorded in $CH_2Cl_2/0.1$ M TBAP and referenced to Fc^+/Fc internal standard at 22 °C.
20. The formal potentials of **15** can be found in Table 2.3. The formal potentials of **21** are as follows: Os(V/IV), +0.83 V; Os(IV/III), -0.18

V; Os(III/II), -0.77 V; recorded in CH₂Cl₂/0.1 M TBAP and referenced to Fc⁺/Fc internal standard at 22 °C.

21. This paper was, in part, compiled from the following article:
Anson, F. C.; Collins, T. J.; Gipson, S. L.; Keech, J. T.; Krafft, T. E.;
Peake, G. P. *J. Am. Chem. Soc.*, in press.

Chapter 5

Kinetics and Mechanism of the Isomerization of cis- α and trans PAC Ligand Complexes

Introduction

In Chapters 3 and 4, the structural and thermodynamic differences between *trans* and *cis-α* isomers are discussed. The differences in N-amido bonding and electron delocalization of the non-planar N-amido groups compared to the planar N-amido ligands give rise to the characteristics that distinguish the *cis-α* and *trans* isomers. Another aspect of the isomerization process is the mechanism of interconversion. That is, what are the intimate steps responsible for transforming a *cis-α* isomer into a *trans* isomer and vice versa? Three systems from Chapter 4 are well-suited for mechanistic study. Oxidation of *trans*-Os(η^4 -CHBA-DCB)(O=PPh₃)₂, **8**, by either chemical or electrochemical means produces both the *cis-α* and *trans* cationic complexes, [20]⁺ and [8]⁺. The neutral *cis-α* phosphine oxide compound **20** can be isolated using low temperature techniques. Warming **20** in solution rapidly converts it into *trans* **8**. Finally, the *t*-Bupy complex *cis-α*-Os(η^4 -CHBA-DCB)(*t*-Bupy)₂, **19-*t*Bu**, can be isolated. Heating a solution of **19-*t*Bu** cleanly generates **10-*t*Bu**, the *trans* isomer. These isomerizations can be followed conveniently by UV-vis spectroscopy (Figure 5.1). From the kinetic investigations of these three systems, it is possible to compare (1) the cationic Os(V) ([20]⁺ \rightleftharpoons [8]⁺) and neutral Os(IV) (**20** \rightarrow **8**) isomerization mechanisms, and (2) the *cis-α* \rightarrow *trans* isomerization mechanisms of the Os(IV) phosphine oxide complex (**20** \rightarrow **8**) and the Os(IV) *t*-Bupy complex (**19-*t*Bu** \rightarrow **10-*t*Bu**).

Four isomerization mechanisms, which can account for these processes, are shown in Scheme 5.1. The simplest mechanism is the intramolecular “twisting” mechanism, T, shown in the middle of Scheme 5.1. The auxiliary ligands and the terminal arms of the PAC ligand

exchange coordination sites simultaneously. No bond breaking or bond forming steps are necessary in this concerted mechanism. The other three mechanisms are dissociative "bond rupture" mechanisms. The mechanism shown in the upper half of Scheme 5.1, D_L , is dissociative in the ancillary ligand L. Extrusion of L is followed by the isomerization of the five-coordinate intermediate. Recapture of L yields the final product. The mechanisms shown in the lower half of Scheme 5.1 extrude a phenolate arm of the PAC ligand, after which the five-coordinate intermediate can isomerize. Reassociation of the PAC ligand arm yields the product. The dissociation of the phenolate arm from the osmium can proceed by homolytic Os-O bond cleavage to produce a dangling phenoxy radical arm and an Os(III) center, D_C , or by heterolytic Os-O bond cleavage to generate a phenoxide anion and a cationic Os(IV) center, D_C .

These mechanisms have been considered before in isomerization and racemization processes of octahedral chelate complexes.¹⁻³ Such processes include $\Delta \rightleftharpoons \Lambda$ isomerizations of tris- β -diketonate complexes, cis and trans isomerization of $M(\eta^2-L L)_2X_2$ compounds, and scrambling of the numerous isomeric forms of $M(bzac)_3$ complexes and other such compounds containing unsymmetrical β -diketonate ligands.¹ Isomerization mechanisms can be regarded as two general types of mechanisms: those that involve momentary cleavage of a metal-ligand bond (e.g., the D_L , D_C , and D_C mechanisms) and those that involve no bond cleavage, only a concerted reorganization of the metal coordination sphere (e.g., T).

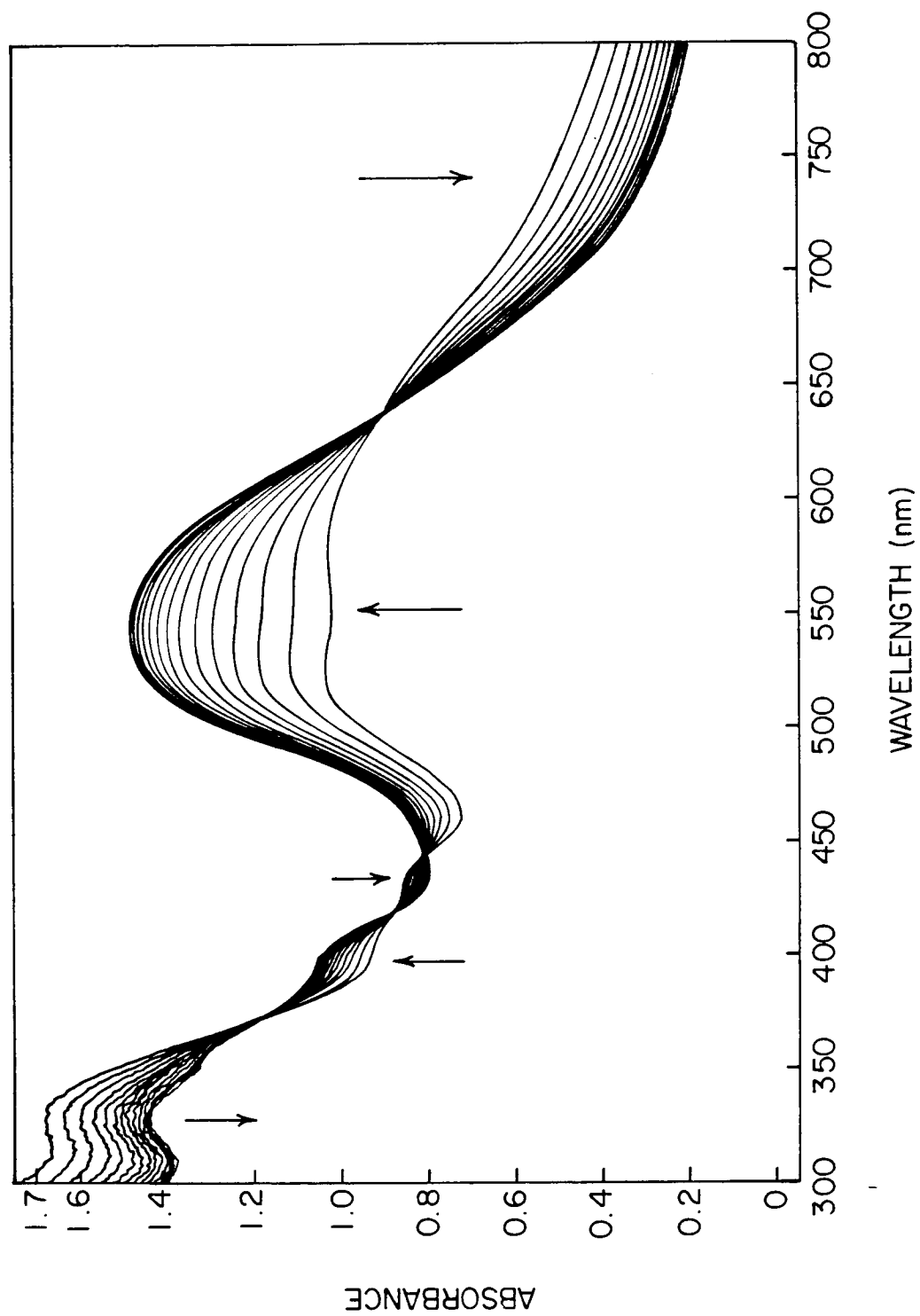
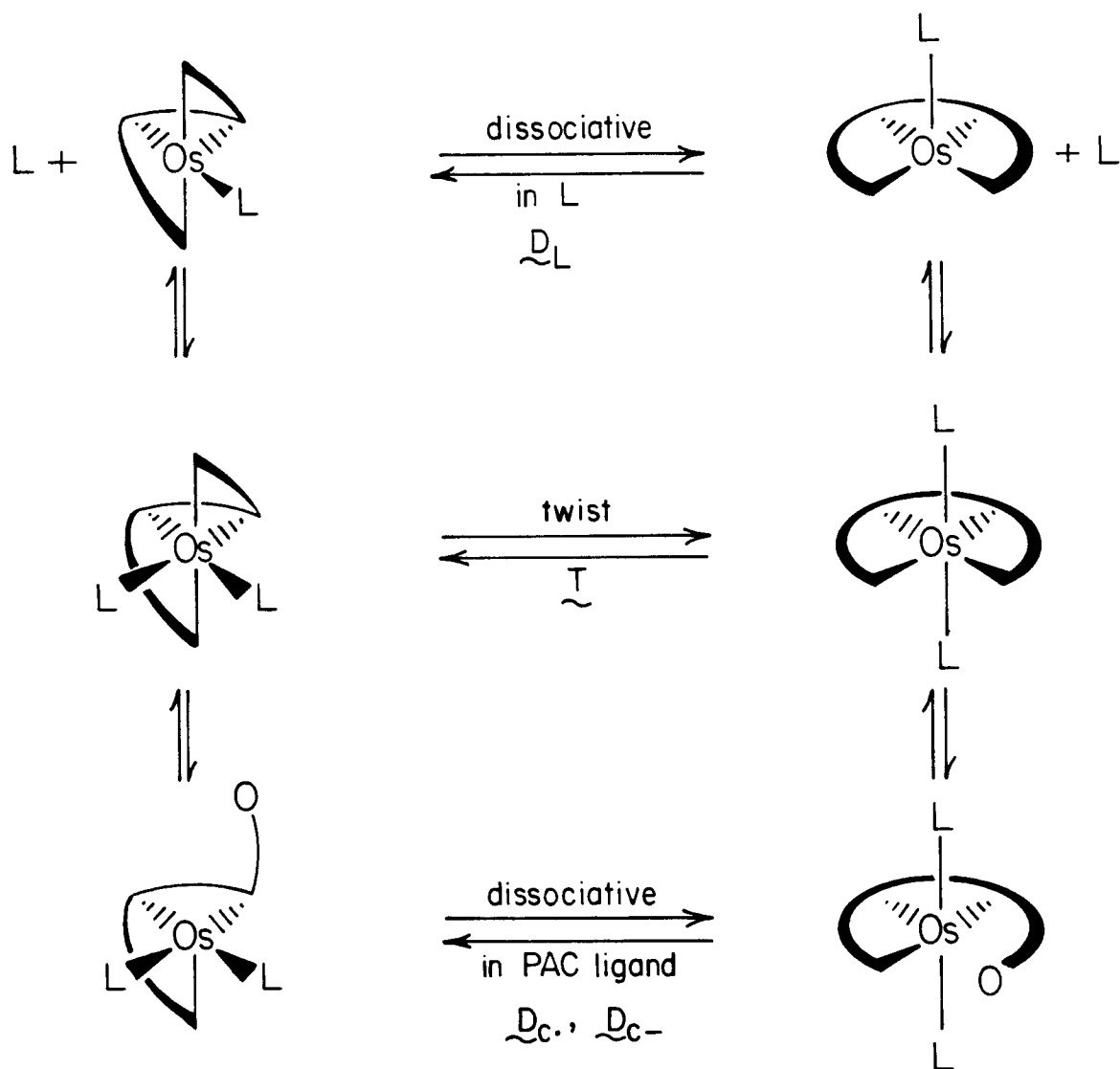


Figure 5.1. UV-vis spectral monitoring of $[20] + 8[8]$ equilibrium in CH_2Cl_2 at 0°C .

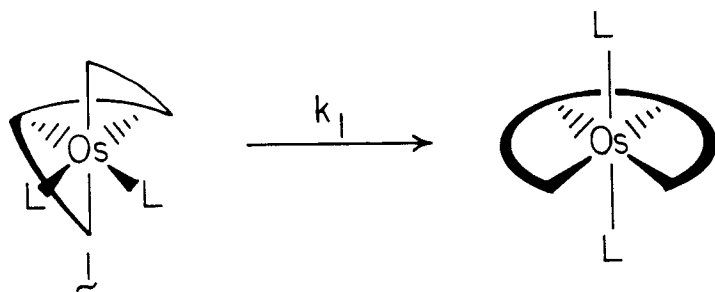
Scheme 5.1. Possible Isomerization Mechanisms.

Results and Discussion

Mechanistic Probes. The isomerization of PAC ligand complexes have thus far involved only *cis-α* and *trans* isomers. No *cis-β* intermediates have been detected in these reactions. If sequential isomerization of each PAC ligand phenolate arm occurs, then a *cis-β* intermediate necessarily must be formed. One might argue that the *cis-β* intermediate is unstable and immediately proceeds to the *cis-α* or *trans* product. This, however, seems unlikely in light of the stable *cis-β* complexes that can be isolated with bipy (11), dppe (13), or two *t*-BuNC ligands (21). Compound 21, in fact, is thermodynamically less stable than its *cis-α* isomer, 15, but isomerizes to 15 only when heated under reflux in *p*-xylene. The absence of *cis-β* isomerization products suggests that the twist mechanism, T, controls the isomerizations. A one-step isomerization can be conceived whereby the ancillary ligands and the phenolate groups of the PAC ligand exchange sites in a concerted T process. Based on this argument, we anticipated at the beginning of this study that the T mechanism controlled the isomerization rather than the D_L , D_C , or D_C - mechanism.

Of the four mechanisms, the D_L mechanism is the most straightforward to probe for. High concentrations of free ligand L can decrease the observed rate by inhibiting the initial step in which L is extruded and the five-coordinate intermediate is formed. This rate suppression, however, is not always observed. Figure 5.2 contains the rate laws for the T and D_L mechanisms. In the T mechanism, the observed rate constant, k_{obs} , equals the reaction rate constant, k_1 . In the D_L mechanism, however, k_{obs} has the complex expression shown. Rates k_2 and k_{-2} describe the equilibrium between bound and unbound L. Rate k_3 describes the

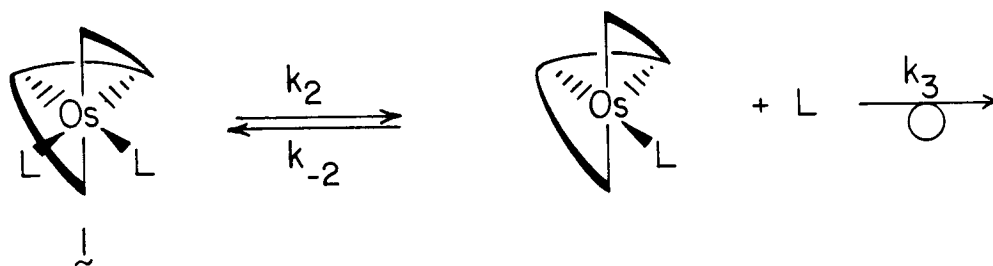
Twist :



$$\frac{-d[\text{axial}]}{dt} = k_1 [\text{axial}]$$

$$k_{\text{obs}} = k_1$$

Dissociative in L :



$$\frac{-d[\text{axial}]}{dt} = \frac{k_2 k_3 [\text{axial}]}{k_3 + k_{-2} [L]}$$

$$k_{\text{obs}} = \frac{k_2 k_3}{k_3 + k_{-2} [L]}$$

Figure 5.2. Rate equations and k_{obs} expressions for T and D_L isomerization mechanisms.

irreversible rate of isomerization of the five-coordinate intermediate. From the denominator of k_{obs} , it is evident that when $k_3 \gg k_{-2} [L]$, no rate suppression will be observed with added concentrations of L. The conclusive test for the D_L mechanism is the addition of labelled ligand, L' , to the isomerizing complex. If the D_L mechanism takes place, incorporation of L' into the product should be detected. Both of these tests for the D_L mechanism were carried out with the three systems that were studied. In the isomerization of the *t*-Bupy complex, neat pyridine- d_5 was used as L' . In the phosphine oxide systems, a 100-fold excess of $O=P(p\text{-tolyl})_3$ was used as L' .

Evidence of the T , D_C , and D_{C-} mechanisms is less definitive than that of the D_L mechanism. Without an exchangeable ligand (such a L), solvent effects, effects of added radical traps, and activation parameters must be used to justify the importance of these mechanisms.

The D_{C-} mechanism invokes a zwitterion intermediate with sufficient charge separation to enable the five-coordinate intermediate to isomerize and then reassociate the phenoxide anion in the product. Depending on the degree of charge separation, varying the solvent polarity should affect the stability of the dipolar intermediate. The following solvents in order of increasing polarity (as indicated by the dielectric constants) were used: benzene ($\epsilon_{25}^\circ\text{C} = 2.3$)^{4a} < dichloromethane ($\epsilon_{25}^\circ\text{C} = 8.9$)^{4b} \approx 1,2-dichloroethane ($\epsilon_{25}^\circ\text{C} = 10.4$)^{4a} < acetonitrile ($\epsilon_{25}^\circ\text{C} = 36.2$).^{4b} The free phenoxide anion should interact with protons. Experiments were run in 100 mM *p*-toluene sulfonic acid in CH_3CN the hope of detecting increased rates. The $\Delta \rightarrow \Lambda$ isomerization of $[\text{Co}(\text{ox})_3]^{3-}$ takes place by anionic oxalate dissociation, D_{C-} , which is acid-catalyzed.¹⁶ Finally, 100 mM TBAP solutions in either dichloromethane or 1,2-

dichloroethane were used to probe rate changes as a function of ionic strength.

The D_C mechanism is the most difficult to probe for. Hydrogen atom sources can be used as radical traps for the phenoxy radical intermediate (e.g., 2-mercaptoethanol and hydroquinone). Positive reactions between these reagents and the osmium complexes would be expected to generate different isomerization products, which would be detected in the kinetic experiments. 2-Mercaptoethanol is commonly used by biologists as a reducing agent to cleave disulfide bonds between cysteine residues.⁵ Reactions of thiols with Mn(acac)₃ produces Mn(acac)₂, acetylacetone and 0.5 equiv of disulfide.^{6a} Similar reactions occur between thiols and Fe(octanoate)₃, producing Fe(oct)₂, octH, and 0.5 equiv of disulfide.^{6b} Unfortunately, thiols can also react as electron-transfer reagents.^{6c} The oxidation of 2-mercaptoethanol is pH-dependent. At pH 11.5, the formal potential for its oxidation is at -0.54 vs. SCE.⁷ The reduction strength of the thiol was sufficient to reduce [8]⁺, [20]⁺, 10-*t*Bu, and 19-*t*Bu to Os(III). This limited the use of 2-mercaptoethanol to the isomerization of 20 → 8.

Reactions proceeding through the intramolecular twist mechanism, T, display solvent-independent rates.^{8a-c} There are discrepancies in the literature about the range of entropies of activation (ΔS^\ddagger) to expect for such a process. In the first reported evidence for a twist mechanism, Ray *et al.* found highly negative entropy factors (-41.5 and -55.3 eu) for the rates of optical inversion of tris-(biguanide)cobalt(III) and tris-(phenylbiguanide)-cobalt(III).³ Similarly, entropy factors of between -119 and -177 eu have been derived from electrochemically measured rate constants for the cis → trans isomerization of [M(CO)₂(DPM)₂]⁺ and

$[M(CO)_2(DEM)_2]^+$ ($M = Cr, Mo, \text{ and } W$; DMP = bis(diphenylphosphino)methane; DEM = bis(diethylphosphino)methane). These entropy factors seem intuitively too negative for a process that involves no association in the transition state. Entropies of activation closer to zero seem more appropriate. In 1H NMR and IR spectroscopic rate measurements of isomerizations proceeding through the T mechanism, entropy factors between -9.8 and -0.44 eu are derived.^{8e,g} The best evidence for a T mechanism is the lack of ligand exchange (L') during isomerization, the lack of evidence for D_C and D_C - mechanisms, and solvent-independent isomerization rates.

Isomerization of *cis*- α 19-*t*Bu \rightarrow *trans* 10-*t*Bu. In Chapter 4, the isolation and characterization of *cis*- α -Os(η^4 -CHBA-DCB)(*t*-Bupy)₂, 19-*t*Bu, are described. In addition to the pure sample of 19-*t*Bu that was isolated, a sample contaminated with the *trans* isomer 10-*t*Bu (2.6 equiv) was collected and used for kinetic rate experiments. All kinetics were first-order in osmium concentration. The temperature range for convenient rate measurements (45 - 70 °C) made it necessary to use 1,2-dichloroethane as the primary solvent medium. The calculated rate constants in various solvent systems and at different temperatures are contained in Table 5.1.

Activation parameters were calculated from the rate constants at temperatures of 35 to 65 °C: $\Delta H^\ddagger = 21.6$ (19) kcal/mol; $\Delta S^\ddagger = -10$ (6) eu. An Eyring plot of these data is shown in Figure 5.4A. These values will be compared to the activation parameters of the other compounds that were investigated (*vide infra*). Rates in many solvent systems were measured at 60 °C. The rate is insensitive to the various solvent conditions

Table 5.1. Measured Rate Constants for $\text{cis-}\alpha \rightarrow \text{trans}$ Isomerization of $\text{Os}(\eta^4\text{-CHBA-DCB})(t\text{-Bupy})_2$.^a

T (°C)	Solvent	$k_{\text{obs}} = k_1 \text{ (s}^{-1}\text{)}$
45	$\text{ClCH}_2\text{CH}_2\text{Cl}$	$6.62(5) \times 10^{-5}$
50	$\text{ClCH}_2\text{CH}_2\text{Cl}$	$1.29(1) \times 10^{-4}$
55	$\text{ClCH}_2\text{CH}_2\text{Cl}$	$2.82(2) \times 10^{-4}$
60	$\text{ClCH}_2\text{CH}_2\text{Cl}$	$4.58(5) \times 10^{-4}$
65	$\text{ClCH}_2\text{CH}_2\text{Cl}$	$5.35(3) \times 10^{-4}$
70	$\text{ClCH}_2\text{CH}_2\text{Cl}$	$8.60(10) \times 10^{-4}$
60	100 mM py/ $\text{ClCH}_2\text{CH}_2\text{Cl}$	$2.18(2) \times 10^{-4}$
60	1.0 M py/ $\text{ClCH}_2\text{CH}_2\text{Cl}$	$1.75(10) \times 10^{-4}$
60	100 mM TBAP/ $\text{ClCH}_2\text{CH}_2\text{Cl}$	$4.17(3) \times 10^{-4}$
60	CH_3CN	$8.78(11) \times 10^{-4}$
60	100 mM $\text{CH}_3\text{C}_6\text{H}_4\text{SO}_3\text{H}/\text{CH}_3\text{CN}$	$4.37(14) \times 10^{-4}$
60	C_6H_6	$3.44(3) \times 10^{-4}$
60	100 mM $p\text{-C}_6\text{H}_4(\text{OH})_2/\text{CH}_3\text{CN}$	$9.3(4) \times 10^{-4}$

^a Values in parentheses are standard deviations in the last digit.

employed. A minor rate increase is observed with increasing solvent polarity: $k(\text{C}_6\text{H}_6) < k(\text{CH}_2\text{Cl}_2) < k(\text{CH}_3\text{CN})$. While this may support a D_C -mechanism, no rate change is seen in 100 mM *p*-toluene sulfonic acid or 100 mM TBAP. A slight rate decrease is observed with increasing pyridine concentration, which might be consistent with the D_L -mechanism. If this is the case, then from the expression for k_obs in Figure 5.2, a plot of $1/k_\text{obs}$ against the concentration of pyridine should be linear. This criterion is not fulfilled. If a D_L -mechanism was present, then liberated pyridine would be expected to interact with the sulfonic acid, which would perturb the rate. As mentioned, however, no rate change is seen in the acidic environment.

A rate measurement was attempted in 2-mercaptoethanol, but the thiol reduced the complex to the Os(III) oxidation state. The formal potential for the Os(IV/III) couple of **19-*t*Bu** is at *ca.* -0.49 V *vs.* SCE and is at *ca.* -0.06 V *vs.* SCE for **10-*t*Bu**. As mentioned, the formal potential for β -mercaptoethanol oxidation is at -0.55 V *vs.* SCE.⁷ Hence, simple reduction of the osmium complexes by the thiol seems reasonable. The rate in hydroquinone is elevated somewhat, but the expected product is observed following the isomerization. From this information, D_C -mechanism cannot be eliminated.

A ligand exchange experiment was conducted to further probe for evidence of the D_L -mechanism. An NMR tube was charged with 1:1 **19-*t*Bu**/**10-*t*Bu** (6 mg) and pyridine- d_5 (1 mL). Thermolysis of the material at 80 °C was intended to induce isomerization. After 10 half-lives (30 min), the ^1H NMR spectrum of the solution revealed little change in the *cis*- α **19-*t*Bu** concentration, but the concentration of *trans* **10-*t*Bu** decreased. Continued thermolysis for 1.25 h at 80 °C decomposed most of the *trans*

isomer, but the *cis-α* isomer remained unchanged. Free *t*-Bupy was also detected. Analytical TLC revealed the reaction products to be **19-*t*Bu**, trace **10-*t*Bu**, **10-H** (the double pyridine-exchange product), and a new complex that may be *trans*-Os(η^4 -CHBA-DCB)(*t*-Bupy)(py) (the single pyridine-exchange product). The same experiment was carried out with genuine **10-*t*Bu** to verify that the exchange occurred with the *trans* isomer. The ^1H NMR spectrum showed free *t*-Bupy, and analytical TLC showed both **10-H** and the presumed single pyridine exchange product. The solution from the isomerization rate measurement in 1.0 M pyridine was examined. Analytical TLC revealed the products to be primarily **10-*t*Bu** and a faint spot with the same R_f as the single pyridine exchange product. Because of the ambiguity introduced from the pyridine exchange with the *trans* isomer, additional experiments would be necessary to determine conclusively whether pyridine exchange occurs only in the *trans* product or if it also exchanges with the *cis-α* starting material in the course of the isomerization reaction. The exchange experiment could be carried out at lower temperatures where pyridine exchange with **10-*t*Bu** does not occur. Based on the available information, the *T* mechanism is favored because of the solvent-independence of the rate data and the slightly negative entropy factor. If *t*-Bupy dissociation precedes isomerization, then a positive entropy factor might be expected.

Isomerization of *cis-α* 20 \rightarrow *trans* 8. In Chapter 4, the isolation and characterization of *cis-α*-Os(η^4 -CHBA-DCB)(O=PPh₃)₂, **20**, are discussed. Besides the pure *cis-α* sample, an additional sample was isolated that was contaminated with *trans* isomer **8** (0.33 equiv). This was used for kinetic rate experiments. Dichloromethane solvent was used in

the variable temperature rate measurements. Calculated rate constants in various solvents and at different temperatures are contained in Table 5.2. All kinetics are first-order in the concentration of osmium.

Activation parameters were calculated from the rate constants at temperatures of 5 to 35 °C: $\Delta H^\ddagger = 21.6 (2) \text{ kcal/mol}$; $\Delta S^\ddagger = +0.3(6) \text{ eu}$. An Eyring plot of these data is shown in Figure 5.4B. The activation parameters will be compared to the parameters of other examined systems. The entropy factor of $+0.3(6)$ seems consistent with the T mechanism. Rates in various solvent conditions were measured at 35 °C. As with the rate constants for the isomerization of 19-*t*Bu to 10-*t*Bu, the rates are insensitive to different solvent systems. Whereas the *t*-Bupy system isomerized faster in polar solvents, the isomerization of 20 into 8 is slightly faster in non-polar solvents: $k(\text{CH}_3\text{CN}) < k(\text{CH}_2\text{Cl}_2) < k(\text{C}_6\text{H}_6)$. This suggests that the D_C mechanism is not important. The rate shows no systematic decrease with increasing concentration of O=PPh₃ up to 2.0 M. This is approximately a 6000-fold excess of phosphine oxide to osmium. In neat 2-mercaptoethanol, the rate is depressed by a factor of only two. The UV-vis spectrum of the product from the isomerization in 2-mercaptoethanol showed it to be trans 8. No reaction between the thiol and 20 had occurred. The decrease in rate may be merely a consequence of the high polarity of 2-mercaptoethanol, just as using polar CH₃CN solvent also depresses the rate. This suggests that the D_C mechanism is not important.

A labelled phosphine oxide, O=P(*p*-tolyl)₃, was used to determine if ligand exchange occurred during isomerization of 20 into 8. A blank was first run on trans 8. After 100-fold excess of the labelled phosphine oxide was stirred with 8 for 3.5 h, the osmium products were isolated. ¹H and

Table 5.2. Measured Rate Constants for cis-a \rightarrow trans Isomerization of
Os(η^4 -CHBA-DCB)(O=PPh₃)₂.^a

T (°C)	Solvent	k _{obs} = k ₁ (s ⁻¹)
5	CH ₂ Cl ₂	7.38(5) x 10 ⁻⁵
10	CH ₂ Cl ₂	1.54(1) x 10 ⁻⁴
15	CH ₂ Cl ₂	2.84(1) x 10 ⁻⁴
20	CH ₂ Cl ₂	5.56(2) x 10 ⁻⁴
25	CH ₂ Cl ₂	1.07(2) x 10 ⁻³
30	CH ₂ Cl ₂	2.01(1) x 10 ⁻³
35	CH ₂ Cl ₂	3.72(2) x 10 ⁻³
35	1 mM OPPh ₃ /CH ₂ Cl ₂	3.60(1) x 10 ⁻³
35	10 mM OPPh ₃ /CH ₂ Cl ₂	3.61(1) x 10 ⁻³
35	50 mM OPPh ₃ /CH ₂ Cl ₂	3.54(1) x 10 ⁻³
35	100 mM OPPh ₃ /CH ₂ Cl ₂	3.37(1) x 10 ⁻³
35	500 mM OPPh ₃ /CH ₂ Cl ₂	3.19(4) x 10 ⁻³
35	1.0 M OPPh ₃ /CH ₂ Cl ₂	2.90(2) x 10 ⁻³
35	1.5 M OPPh ₃ /CH ₂ Cl ₂	3.03(1) x 10 ⁻³
35	2.0 M OPPh ₃ /CH ₂ Cl ₂	2.45(3) x 10 ⁻³
35	100 mM TBAP/CH ₂ Cl ₂	7.19(19) x 10 ⁻³
35	CH ₃ CN	2.98(3) x 10 ⁻³
35	100 mM CH ₃ C ₆ H ₄ SO ₃ H/CH ₃ CN	1.89(19) x 10 ⁻³
35	C ₆ H ₆	6.31(12) x 10 ⁻³
35	100 mM <i>p</i> -C ₆ H ₄ (OH) ₂ /CH ₃ CN	2.62(5) x 10 ⁻³
35	HSCH ₂ CH ₂ OH	1.86(4) x 10 ⁻³

^a Values in parentheses are standard deviations in the last digit.

^{31}P NMR spectroscopies showed no evidence of exchange. A sample of *cis*- α **20** was stirred with 100-fold excess of $\text{OP}(p\text{-tolyl})_3$ and allowed to isomerize to **8** over a period of 3.5 h (10 half-lives). Again, the osmium products were isolated and examined by ^1H and ^{31}P NMR spectroscopies. No evidence of exchange could be detected by either method. From these experiments, the D_L mechanism can be discounted. Based on this negative exchange experiment and the kinetic rate determinations, the T mechanism best describes the isomerization of *cis*- α **20** to **8**.

Thermodynamic Studies of the $[\mathbf{20}]^+ \rightleftharpoons [\mathbf{8}]^+$ Equilibrium. In Chapter 4, a thermodynamic ladder is derived for the equilibrium of *trans* **10-*t*Bu** and *cis*- α **19-*t*Bu** at the Os(V), Os(IV), Os(III), and Os(II) oxidation states. This is accomplished by measuring the equilibrium constant at the Os(V) oxidation state, K^+ , with normal pulse voltammetry (NPV) and then combining this with the formal potentials for the Os(V/IV), Os(IV/III), and Os(III/II) couples of the *cis*- α and *trans* isomers. Prompting this study was the observation that both the $[\text{trans}]^+$ and $[\text{cis-}\alpha]^+$ isomers existed in equilibrium upon controlled-potential electrolysis of neutral *trans* **10-*t*Bu** to the cationic state. A similar isomerization occurs with the $\text{O}=\text{PPh}_3$ complex **8** when it is oxidized by either chemical (vide infra) or electrochemical means.

We wanted to derive the thermodynamic ladder for the $\mathbf{20} \rightleftharpoons \mathbf{8}$ equilibria. Moreover, measurements of K^+ at different temperatures would make it possible to calculate the reaction enthalpy, ΔH° , and entropy, ΔS° , from a van't Hoff plot.

A sample of **8** was bulk electrolyzed to the cationic Os(V) oxidation state. The ratio of the concentration of each isomer, or K^+ , was determined

by NPV. The temperature of the three-compartment electrochemical cell was adjusted by immersing the cell into the reservoir of a refrigerated circulating bath. Equilibrium constants were measured between the temperatures of -2.2 and 30.2 °C (Table 5.3). A smooth progression of K^+ values from 1.74 in favor of the trans isomer at 30.2 °C to 0.140 at -2.2 °C was observed. The van't Hoff plot of these data (Figure 5.3) displays acceptable linearity and has a least-squares correlation of fit (r) of -0.986. From these data, the reaction parameters were calculated: $\Delta H^\circ = +12(3)$ kcal/mol; $\Delta S^\circ = +42(9)$ eu. The enthalpy is consistent with the observed K^+ values; as the temperature decreases, the cis- α isomer, $[20]^+$, is thermodynamically more favored. Apparently, the cis- α isomer must derive more stability from the non-planar N-amido bonding than the trans isomer gains from planar N-amido delocalization stabilization.

From the van't Hoff plot, the calculated value of K^+ at 22 °C is 1.02. By combining this with the formal potentials of **8** (found in Table 2.3) and **20** (found in Chapter 4, ref 19), the equilibrium constants at the Os(IV), K^0 , and Os(III), K^- , oxidation states can be calculated: $K^0 = 6.15 \times 10^4$ in favor of the trans isomer; $K^- = 8.16 \times 10^9$. These equilibrium constants show the same trend that is discussed in Chapter 4 for the equilibrium of **19-*t*Bu** \rightleftharpoons **10-*t*Bu**. As the osmium oxidation state increases, the cis- α isomer is increasingly favored because it is more electron-donating than the trans isomer.

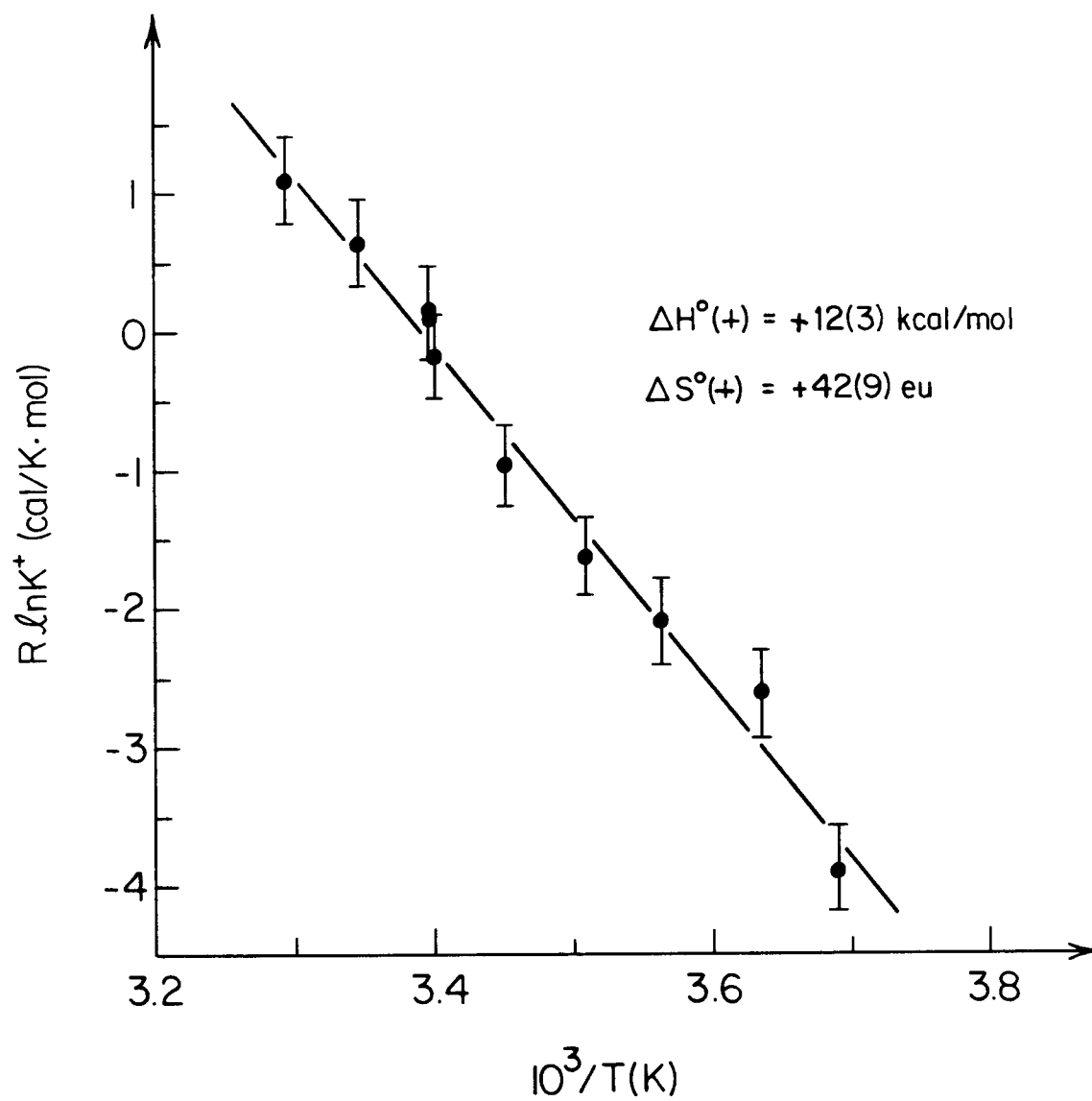


Figure 5.3. van't Hoff plot of $[20]^+ \rightleftharpoons [8]^+$ equilibrium data against $1/T(K)$. Error bars are at 95% confidence level.

Table 5.3. Measured Equilibrium Constants for $\text{cis-}\alpha \rightleftharpoons \text{trans}$ Equilibrium of $[\text{Os}(\eta^4\text{-CHBA-DCB})(\text{O}=\text{PPh}_3)_2]^+.$ ^a

T (°C)	K([trans]/[cis- α])	T (°C)	K([trans]/[cis- α])
30.2	1.74	16.6	0.615
25.9	1.38	12.0	0.438
21.3	1.06	7.5	0.345
21.2	1.05	2.0	0.269
21.0	0.919	-2.2	0.140

^a Measured by normal pulse voltammetry with 100 mM TBAP/ CH_2Cl_2 as solvent. Errors in measurement estimated at $\pm 10\%$.

Isomerization of $\text{trans } [8]^+ \rightleftharpoons \text{cis-}\alpha [20]^+$. Whereas at room temperature the oxidation of **8** produces an equilibrium mixture of $[\text{cis-}\alpha]^+$ and $[\text{trans}]^+$ isomers, at -78°C only $[\text{trans}]^+$ is generated. Low temperatures stop the isomerization process, but clean oxidation of **8** with nitrosonium salts (NO^+) still proceeds. Nitrosonium is a useful oxidant at low temperature.^{8c,9} Because of its insolubility in CH_2Cl_2 , filtration is sufficient to remove excess NO^+ . From a -78°C stock solution of $[8]^+$, an aliquot is removed for each kinetic rate measurement. Because of the reversibility of the cationic isomerization, the observed rate constant, k_{obs} , equals the sum of the forward and reverse rate constants, $k_1 + k_{-1}$, for the equilibrium of $[8]^+$ and $[20]^+$ (see Experimental). The composite rate constants measured in various solvent conditions are compared just as the rate constants for the neutral $20 \rightarrow 8$ and the $19\text{-}t\text{Bu} \rightarrow 10\text{-}t\text{Bu}$ isomerizations have been compared. Composite rate constants are contained in Table 5.4. The variable temperature data have been combined with the equilibrium data to separate the forward and reverse rates (Table

Table 5.4. Measured Composite Rate Constants for $\text{cis-}\alpha \rightleftharpoons \text{trans}$ Equilibrium of $[\text{Os}(\eta^4\text{-CHBA-DCB})(\text{OPPh}_3)_2]^+ \text{ } ^a$

T (°C)	Anion	Solvent	$k_{\text{obs}} = k_1 \text{ (s}^{-1}\text{)}$
0	BF ₄	CH ₂ Cl ₂	1.86(1) x 10 ⁻²
5	BF ₄	CH ₂ Cl ₂	2.75(2) x 10 ⁻²
10	BF ₄	CH ₂ Cl ₂	5.01(4) x 10 ⁻²
15	BF ₄	CH ₂ Cl ₂	8.33(5) x 10 ⁻²
20	BF ₄	CH ₂ Cl ₂	1.26(1) x 10 ⁻¹
0	PF ₆	CH ₂ Cl ₂	1.87(1) x 10 ⁻²
0	BF ₄	1 mM OPPh ₃ /CH ₂ Cl ₂	1.85(1) x 10 ⁻²
0	BF ₄	10 mM OPPh ₃ /CH ₂ Cl ₂	1.92(1) x 10 ⁻²
0	BF ₄	50 mM OPPh ₃ /CH ₂ Cl ₂	1.90(1) x 10 ⁻²
0	BF ₄	100 mM OPPh ₃ /CH ₂ Cl ₂	1.85(1) x 10 ⁻²
0	BF ₄	500 mM OPPh ₃ /CH ₂ Cl ₂	2.10(4) x 10 ⁻²
0	BF ₄	100 mM TBAP/CH ₂ Cl ₂	1.98(2) x 10 ⁻²
0	PF ₆	CH ₃ CN	1.36(3) x 10 ⁻³
0	PF ₆	100 mM CH ₃ C ₆ H ₄ SO ₃ H/CH ₃ CN	1.92(2) x 10 ⁻²

^a Values in parentheses are standard deviations in the last digit.

5.5). All kinetic data have first-order dependence on the concentration of osmium.

Separate activation parameters for the forward and reverse rates are calculated from the composite rate constants ($k_1 + k_{-1}$) and K^+ equilibrium constants (k_1/k_{-1}) at temperatures between 0 and 20 °C. For the forward rate constants ($[20]^+ \rightarrow [8]^+$), $\Delta H^\ddagger = 23.7(6)$ kcal/mol; $\Delta S^\ddagger = +17(2)$ eu. For the reverse rate ($[8]^+ \rightarrow [20]^+$), $\Delta H^\ddagger = 11.5(6)$ kcal/mol and $\Delta S^\ddagger = -25(2)$. Eyring plots of these data are shown in Figures 5.4C and 5.4D. By the principle of microscopic reversibility, the forward and reverse processes should proceed through the same mechanistic path. The difference in the forward and reverse activation parameters seems large for a single mechanism to be in effect. This difference is necessary, though, because the measured reaction parameters ΔH° and ΔS° equal the differences between the forward and reverse rate activation parameters.

The composite rate constants for the isomerization of the BF_4^- and the PF_6^- salts of $[8]^+$ are identical. Thus, no unusual anion effects alter the composite rates (Table 5.4). The rate constants are independent of the concentration of O=PPh_3 up to 500 mM in CH_2Cl_2 . The composite rate constants remain unchanged in both 100 mM TBAP in CH_2Cl_2 and 100 mM sulfonic acid in acetonitrile. The rate decreases slightly in neat acetonitrile, which is opposite of the expected change if a D_C mechanism is present. The consistent insensitivity of these composite rate constants suggests that the T mechanism is predominant. 2-Mercaptoethanol and hydroquinone could not be used in these experiments because both reagents reduce $[8]^+$ back to neutral 8, making it impossible to probe for the D_C mechanism.

The $\text{O}=\text{P}(\textit{p}\text{-tolyl})_3$ exchange experiment was conducted for the $[\mathbf{20}]^+ \rightleftharpoons [\mathbf{8}]^+$ equilibrium system. Cold $[\mathbf{8}]^+$ ($-78\text{ }^\circ\text{C}$) in solution with a 100-fold excess of $\text{O}=\text{P}(\textit{p}\text{-tolyl})_3$ in CH_2Cl_2 was warmed to room temperature rapidly and allowed to isomerize for 2 min. Excess ferrocene was added to reduce the mixture to neutral $\mathbf{8}$ and $\mathbf{20}$, which was subsequently stirred for 3.5 h to allow for complete isomerization back to pure $\mathbf{8}$. The osmium products were isolated and examined by ^1H NMR spectroscopy. Minute signals were seen in the aliphatic region. If they were from bound $\text{O}=\text{P}(\textit{p}\text{-tolyl})_3$, then an upper limit of 3% incorporation could be estimated from the integration. Of the three systems studied, the least rate sensitivity to solvent conditions (including added $\text{O}=\text{PPh}_3$) was observed for the cationic equilibrium of $[\mathbf{8}]^+$ and $[\mathbf{20}]^+$. Thus, we ascribe that the T mechanism controls this equilibrium.

Table 5.5. Derived Forward (k_1) and Reverse (k_{-1}) Rate Constants for $\text{cis-}\alpha \rightleftharpoons \text{trans}$ Equilibrium of $[\text{Os}(\eta^4\text{-CHBA-DCB})(\text{OPPh}_3)_2]^+$.^a

T ($^\circ\text{C}$)	$k_1(\text{s}^{-1})$	$k_{-1}(\text{s}^{-1})$
0	$2.96(2) \times 10^{-3}$	$1.57(10) \times 10^{-2}$
5	$6.06(3) \times 10^{-3}$	$2.14(10) \times 10^{-2}$
10	$1.47(5) \times 10^{-2}$	$3.54(12) \times 10^{-2}$
15	$3.16(10) \times 10^{-2}$	$5.16(16) \times 10^{-2}$
20	$5.91(24) \times 10^{-2}$	$6.7(3) \times 10^{-2}$

^a Values in parentheses are standard deviations in the last digits.

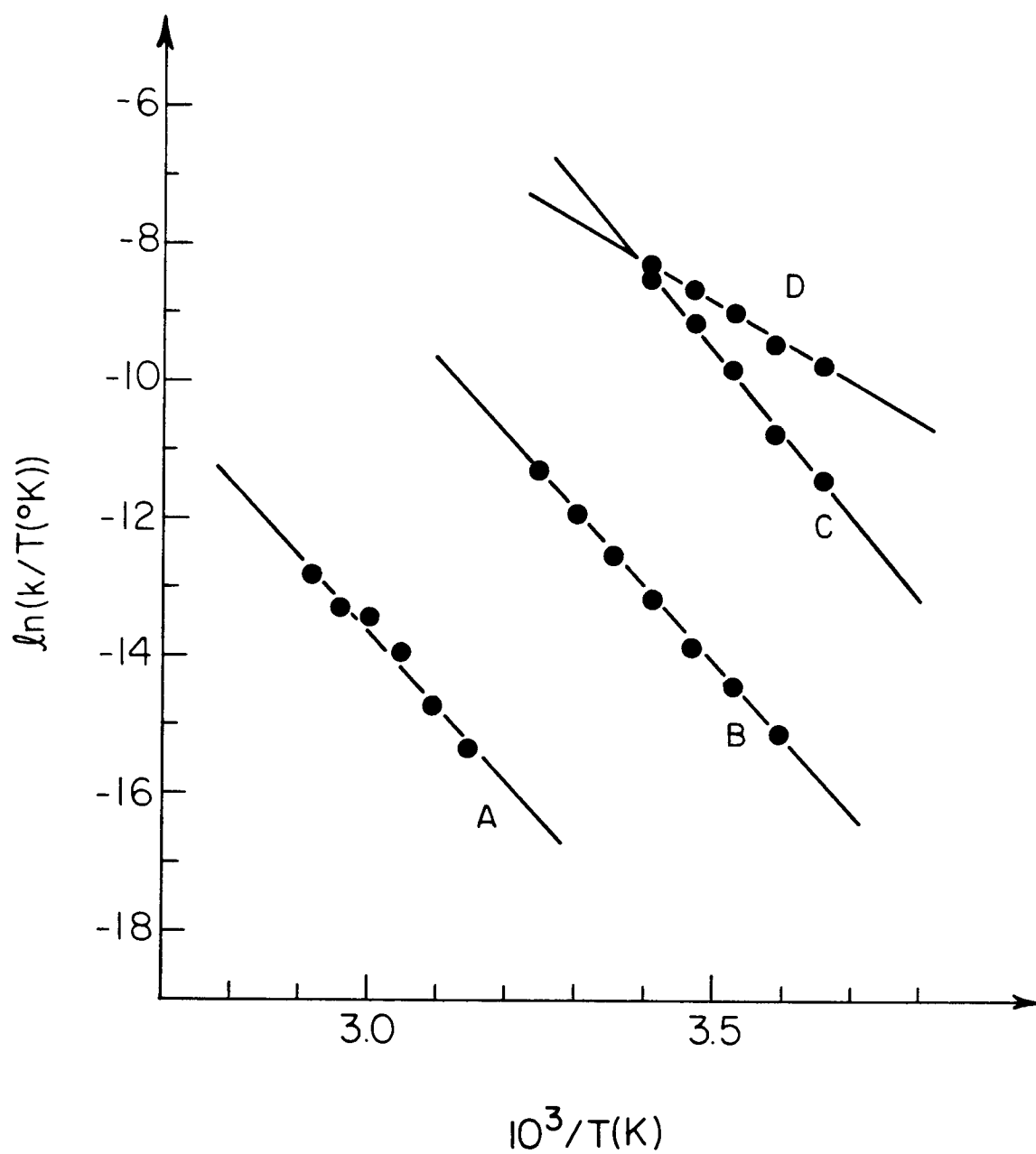


Figure 5.4. Eyring plots of the variable temperature rate data (A) 19-*t*Bu → 10-*t*Bu. (B) 20 → 8. (C) [20]⁺ → [8]⁺. (D) [8]⁺ → [20]⁺.

Conclusions

The three systems examined show little sensitivity to a variety of solvent conditions. Based on kinetic rate measurements and ligand exchange experiments conducted on the three isomerization systems, it is possible to evaluate which mechanisms control these systems. The *cis*- $\alpha \rightarrow$ *trans* isomerization of $\text{Os}(\eta^4\text{-CHBA-DCB})(t\text{-Bupy})_2$, **19-*t*Bu** \rightarrow **10-*t*Bu**, is the slowest isomerization of those examined (Table 5.6). The insensitivity of the rates on solvent conditions suggests that a twist mechanism, T, takes place. The ambiguous results from the ligand exchange experiment, however, raise the possibility that a mechanism invoking *t*-Bupy dissociation, D_L , controls the isomerization. The fact that this is the slowest isomerization of the three systems may indicate that a different mechanism than those present in the other reactions (T) may take place.

The neutral *cis*- $\alpha \rightarrow$ *trans* isomerization of $\text{Os}(\eta^4\text{-CHBA-DCB})(\text{O}=\text{PPh}_3)_2$ (**20** \rightarrow **8**) and the cationic equilibrium of $[\text{Os}(\eta^4\text{-CHBA-DCB})(\text{OPPh}_3)_2]^+$ ($[\text{20}]^+ \rightleftharpoons [\text{8}]^+$) are insensitive to various solvent conditions and show little evidence for the incorporation of external labelled ligand, $\text{O}=\text{P}(p\text{-tolyl})_3$, during isomerization. An intramolecular twist mechanism, T, controls these reactions. This is the simplest of the four possible isomerization mechanisms and explains why no *cis*- β intermediates are observed. At 25 °C, the Os(V) isomerizations are two orders of magnitude faster than the Os(IV) isomerizations. The forward and reverse activation parameters for the cationic equilibria can be derived using variable temperature equilibrium measurements (Table 5.6).

It is interesting that the enthalpies of activation for all three cis \rightarrow trans isomerizations are very close (Table 5.6). If the three isomerizations proceed through the T mechanism and no intermediates are formed during the isomerization, then the similarities in the ΔH^\ddagger parameters suggest that comparable "bond relaxation" must exist in the three different transition states. At 22 °C, the three systems have different isomerization rates, which result from the different entropies of activation (Table 5.6). The trend in ΔS^\ddagger values suggests that the *t*-Bupy system has the tightest transition state ($\Delta S^\ddagger < 0$), and the cationic equilibrium has the loosest transition state ($\Delta S^\ddagger > 0$). The transition states may have trigonal-prismatic symmetry as suggested in the "Bailar Twist" mechanism for octahedral isomerization² or rhombohedral symmetry as in the closely related "Ray and Dutt" isomerization mechanism.³

By combining the Gibbs free energy changes derived in the thermodynamic ladder for $[20]^n \rightleftharpoons [8]^n$ ($n = -1, 0, +1$) equilibria and the rate data for the neutral and cationic isomerization, a reaction profile can be constructed for the phosphine oxide system (Figure 5.5). The energies of the cis- α isomers are arbitrarily made equal to illustrate the trends in ΔG° and ΔG^\ddagger values over different oxidation states. As the osmium becomes increasingly reduced, the ΔG° between the cis- α and trans isomers becomes substantially more negative. The activation barriers, on the other hand, become more positive. Although ΔG^\ddagger for the Os(III) isomerization ($[20]^- \rightleftharpoons [8]^-$) is not known, if the trend continues, then it should be greater than the 21.5 kcal/mol barrier for the Os(IV) isomerization. The trends in Figure 5.5 seem counterintuitive. As the ΔG° values become more negative, it might be assumed that the ΔG^\ddagger barriers would become smaller until a highly exergonic isomerization

Table 5.6. Kinetic Rates and Activation Parameters for Investigated Systems.^a

Process	$k(22\text{ }^{\circ}\text{C})(\text{s}^{-1})^{\text{b}}$	ΔH^{\ddagger}	ΔS^{\ddagger}
19-<i>t</i>Bu → 10-<i>t</i>Bu cis- α trans	$5.03(7) \times 10^{-6}$	21.6(19)	-10(6)
20 → 8 cis- α trans	$7.34(3) \times 10^{-4}$	21.6(2)	+0.3(6)
[20]⁺ → [8]⁺ cis- α trans	$8.17(3) \times 10^{-2}$	23.7(6)	+17(2)
[8]⁺ → [20]⁺ trans cis- α	$8.06(4) \times 10^{-2}$	11.5(6)	-25(2)

^a Values in parentheses are standard deviations in the last digit.

^b Extrapolated to 22 °C from the Arrhenius data.

could proceed rapidly. The observed trend, however, is the reverse of this assumption. This phenomenon accounts for why in CVs we can observe reversible Os(III/II) couples for the cis- α isomers, even though the equilibrium constant for isomerization is as high as 2×10^{15} (Table 4.1).

The opposing trends of the ΔG° and ΔG^{\ddagger} values may result from the T mechanism through which the isomerizations proceed. If the isomerizing bonds in the osmium coordination sphere must pass over filled osmium orbitals, then increased electron-electron repulsions may generate higher ΔG^{\ddagger} barriers. Consistent with this, the Os(V) isomerizations (where the metal is d^3) are faster than the Os(IV) isomerizations (where the metal is d^4). This rate dependence on metal oxidation state is observed in other systems that undergo T isomerizations, where the isomerization rates of 18-electron metal complexes are slower than those of the related oxidized systems, which have 17-electron metal centers.^{8,9}

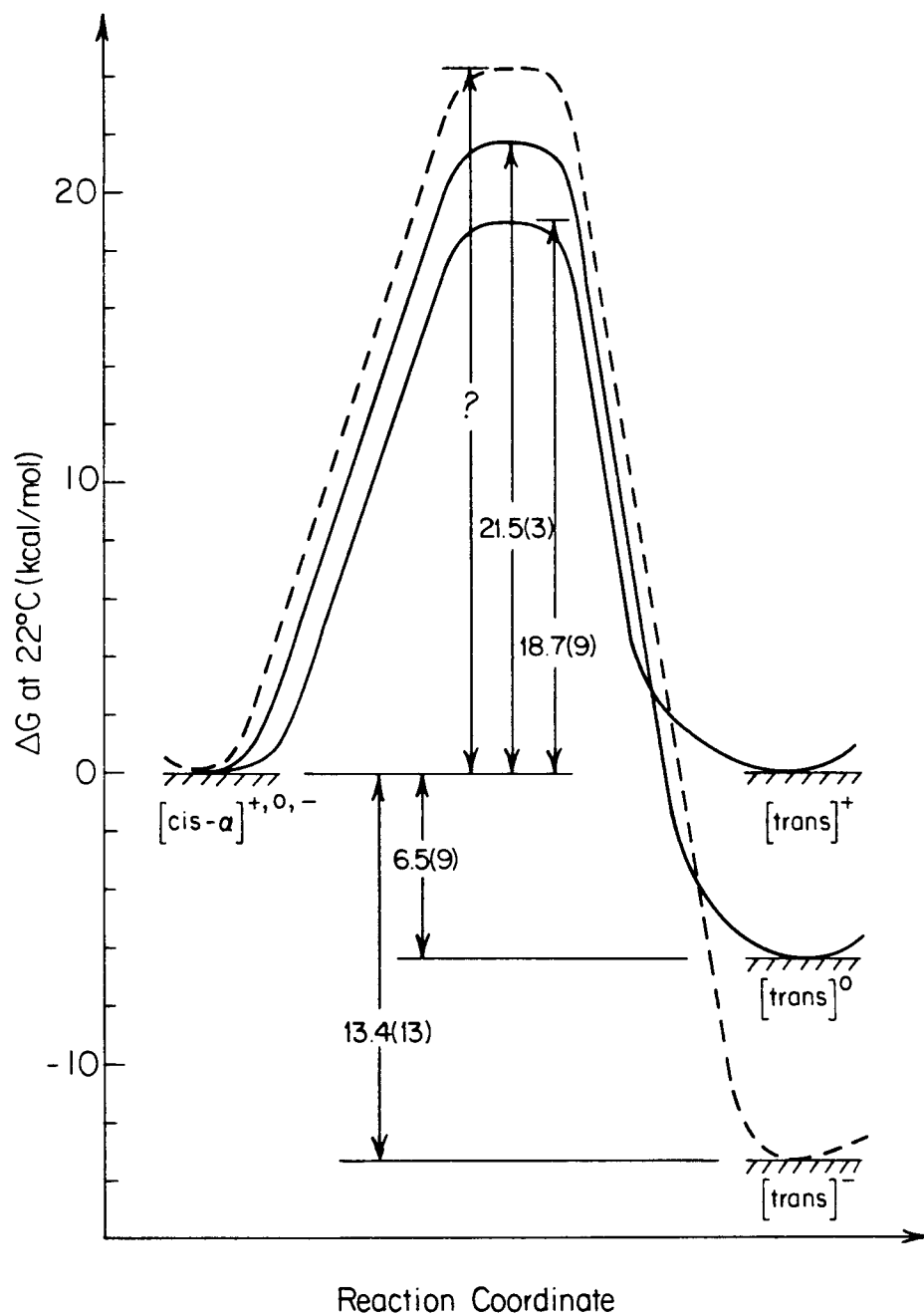


Figure 5.5. Reaction profile for the isomerization of $[\mathbf{20}]^{-,0,+}$ to $[\mathbf{8}]^{-,0,+}$ at 22 °C. Free energies of the cis- α isomers are made equal to demonstrate the positive change in ΔG^\ddagger vs. the negative change in ΔG^0 with increasing reduction of the osmium metal center.

Experimental Section

Materials. Acetonitrile (Mallinckrodt) and dichloromethane (Baker) were distilled from calcium hydride prior to use. Benzene (thiophene free, Aldrich) was washed thrice with conc. H_2SO_4 and then distilled. 1,2-Dichloroethane (Aldrich) was distilled from fresh P_2O_5 . Bromoethane (98%, Aldrich), calcium hydride (Aldrich), chlorobenzene (99%, Aldrich), hydrogen peroxide (30%, Baker), hydroquinone (M.C.B.), magnesium sulfate (Baker), methanol (Baker), nitrosonium hexafluorophosphate (Pfalz and Bauer), nitrosonium tetrafluoroborate (Aldrich), potassium sulfite (M.C.B.), pyridine- d_5 (99% atom D, Aldrich), sulfuric acid (conc., Baker), *p*-toluene sulfonic acid (98%, M.C.B.), and tri-*p*-tolylphosphine (Strem) were used as received. 2-Mercaptoethanol (98%, M.C.B.) was vacuum distilled prior to use. Ferrocene (98%, Aldrich) was sublimed prior to use. A 0.3 M solution of tri-*p*-tolylphosphine oxide in dichloromethane was prepared by reacting a dichloromethane solution of the parent phosphine with aqueous H_2O_2 (30%) for 30 min, washing once with saturated aqueous K_2SO_3 and thrice with distilled water, and drying over MgSO_4 . Molarity was estimated by ^1H NMR spectroscopy. Dry TBAP was provided by Dr. Thomas Guarr. Silica gel used in column chromatography was 60-200 mesh (Davidson).

Physical Measurements. ^1H NMR spectra were recorded at 89.83 MHz on a JEOL FX-90Q or at 399.782 MHz on a JEOL GX-400. ^{31}P

NMR spectra were recorded at 36.28 MHz on a JEOL FX-90Q. Errors were propagated according to the equation

$$\sigma_F^2 = \left[\sum_i \left(\frac{\delta F}{\delta X_i} \right)^2 \sigma_{X_i}^2 \right]^{1/2}$$

where $F = F(x_1, x_2, \dots, x_n)$.¹¹ Errors of ± 5 mV were assumed for E_f .

Syntheses. All reactions were carried out in air unless otherwise noted. The syntheses of *trans*-Os(η^4 -CHBA-DCB)(O=PPh₃)₂, **8**, and *trans*-Os(η^4 -CHBA-DCB)(*t*-Bupy)₂, **10-tBu**, are reported in Chapter 2. The syntheses of *cis*- α -Os(η^4 -CHBA-DCB)(*t*-Bupy)₂, **19-tBu**, and *cis*- α -Os(η^4 -CHBA-DCB)(O=PPh₃)₂, **20**, are reported in Chapter 4.

trans-[Os(η^4 -CHBA-DCB)(O=PPh₃)₂]BF₄, [**8**]⁺. *trans*-Os(η^4 -CHBA-DCB)(O=PPh₃)₂ (11.8 mg, 9.09 μ mol) and excess nitrosonium tetrafluoroborate were added to a round bottom flask (25 mL), which was subsequently sealed with a rubber septum and cooled (-78 °C). Precooled dichloromethane (-78 °C, 10 mL) was syringed into the flask and the mixture was kept cold for 2 h, during which the insoluble nitrosonium salt reacted with the complex to afford a 0.91 mM solution of turquoise product in dichloromethane.

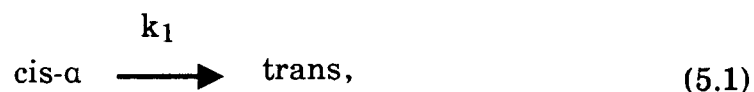
Equilibrium Measurements. Controlled-potential electrolysis was used to oxidize *trans*-[Os(η^4 -CHBA-DCB)(O=PPh₃)₂], **8**, to the [**8**]⁺ and [**20**]⁺ isomers. Compound **8** (12.4 mg, 9.55 μ mol) and TBAP (enough to produce a 0.1 M solution upon CH₂Cl₂ addition) were added to a three-compartment vacuum line electrochemical cell. Working and counter

electrodes were platinum gauze. A silver wire was used as a quasi-reference electrode. After drying the loaded cell *in vacuo* for 12 h, dichloromethane was vacuum transferred into the cell to a predetermined level. Controlled-potential electrolysis was performed with a Princeton Applied Research Model 173 potentiostat equipped with a Model 179 digital coulometer using positive feedback IR-compensation and a Model 175 universal programmer. Current-voltage curves were recorded on a Houston Instruments Model 2000 X-Y recorder. Bulk electrolysis by one Faraday per mole of osmium cleanly generated a mixture of $[8]^+$ and $[20]^+$.

Normal pulse voltammetry was used to measure K^+ for the equilibrium between the $[\text{cis-}\alpha]^+$ and $[\text{trans}]^+$ isomers. It was performed on a Bioanalytical Systems, Inc. BAS-100 Electrochemical Analyzer using a 0.03 cm² platinum disk working electrode. Parameters used were a pulse width of 50 ms, a pulse period of 1 s, and a scan rate of 20 mV/s. The equilibrium constant was taken to be equal to the ratio of wave heights from the two Os(V/IV) reductions. The temperature of the cell was regulated by immersing it into the reservoir of a Neslab Endocal RTE-4 refrigerated circulating bath filled with aqueous ethylene glycol (35% by weight). The recorded cell temperature was actually the reservoir temperature, which was monitored with a thermometer calibrated to 0 °C in a distilled water ice bath. After changing the reservoir temperature, twenty minutes were allowed for the cell to come to thermal equilibrium before taking the measurements. Equilibrium constants were measured between -2.2 and 30.2 °C.

Kinetic Rate Measurements. Kinetic rates for the $\text{cis-}\alpha \rightarrow \text{trans}$ isomerizations of $\text{Os}(\eta^4\text{-CHBA-DCB})(t\text{-Bupy})_2$ and $\text{Os}(\eta^4\text{-CHBA-}$

DCB)(O=PPh₃)₂ , and the cis- $\alpha \rightleftharpoons$ trans equilibrium of [Os(η^4 -CHBA-DCB)(O=PPh₃)₂]⁺ were measured by UV-vis spectroscopy in various solvent systems and at different temperatures. UV-vis spectra were recorded on a Hewlett-Packard HP8450A spectrophotometer equipped with an HP89100A temperature controller and an HP89101A temperature control unit. Solvent (3.0-3.5 mL) was added to a glass cuvette, which was sealed with a rubber septum and brought to thermal equilibrium. The appropriate amount of an osmium reagent was added to the cuvette and automatic data collection was started. First-order conditions were always observed. Data were collected for greater than three half-lives and analyzed by the Kedzy-Swinbourne (K-S) method for first-order rate calculations.^{10a} The K-S analysis eliminates the need for an absorbance reading at infinite time, A_∞ . Given the equation



the absorbance at time t , A_t , equals

$$A_t = (A_o - A_\infty)e^{-k_1 t} + A_\infty, \quad (5.2)$$

where A_o equals the initial absorbance. At a time increment Δ later, the absorbance equals

$$A_{t+\Delta} = (A_o - A_\infty)e^{-k_1(t+\Delta)} + A_\infty. \quad (5.3)$$

The following ratio can be set up

$$\frac{A_\infty - A_t}{A_\infty - A_{t+\Delta}} = e^{-k_1 t} e^{+k_1(t+\Delta)} \quad (5.4)$$

or

$$A_t = e^{k_1 \Delta} A_{t+\Delta} + A_\infty(1 - e^{k_1 \Delta}). \quad (5.5)$$

From the plot of A_t against $A_{t+\Delta}$, the rate constant can be calculated from the slope: $k_1 = [\ln(\text{slope})]/\Delta$. For a reversible first-order equilibrium of B and C, a similar expression can be derived, except the measured rate is actually the sum of the forward and reverse rates. Given the following equilibrium



and the expression relating the absorbance at time t ,

$$A_t = (A_o - A_e)e^{-(k_1 + k_{-1})t} + A_e \quad (5.7)$$

(where A_e is the equilibrium absorbance),^{10b} then relations analogous to those in eqs 5.4 and 5.5 can be derived. These verify that the observed

rates derived from the K-S analyses of reversible reactions equal the sum of the forward (k_1) and reverse (k_{-1}) rate constants.

In all K-S analyses, rates were calculated using Δ time increments of greater than one half-life. If a rate had a large standard deviation, then the calculated A_∞ or A_e values from the K-S analysis were used to plot $\ln(A_\infty - A_t)$ vs. t . Rates determined from these secondary analyses generally had smaller relative errors than those from the initial K-S analyses. Extinction coefficients (ϵ) for all compounds at the wavelengths from which rates were calculated are contained in Table 5.7.

Rate Measurements of the cis- $\alpha \rightarrow$ trans Isomerization of 19-*t*Bu into 10-*t*Bu. Solid material that contained both cis- α 19-*t*Bu and trans 10-*t*Bu isomers (1:2.6 by ^1H NMR; see Chapter 4) was used for kinetic rate determinations. From 1.0 to 1.5 mg of the material were used in a kinetic experiment. Data were collected between 402 and 800 nm. Two isobestic points were observed at 429 and 639 nm wavelengths. Rate constants were calculated from the 468, 576, and 750 nm data and then averaged. The rates had first-order dependence on the concentration of 19-*t*Bu. Activation parameters were determined from rate measurements at temperatures of between 45 and 70 °C in 1,2-dichloroethane. Rates were also measured at 60 °C in 100 mM and 1.0 M pyridine in 1,2-dichloroethane, 100 mM TBAP in 1,2-dichloroethane, acetonitrile, benzene, 100 mM *p*-toluene sulfonic acid in acetonitrile, and 100 mM hydroquinone in acetonitrile.

Rate Measurements of the cis- $\alpha \rightarrow$ trans Isomerization of 20 into 8. Material that contained both cis- α and trans complexes (3:1 by ^1H NMR; see Chapter 4) was used for kinetic rate determinations. From 1.5 to 2.0 mg of the solid were used in a kinetic experiment. Data were collected

between 402 and 800 nm. Two isobestic points were observed at 422 and 629 nm wavelengths. Rate constants were calculated from the 462, 566, and 694 nm data and then averaged. The rates had first-order dependence on the concentration of **20**. Activation parameters were determined from rate measurements at temperatures of between 5 and 35 °C in CH₂Cl₂. Rates were also calculated at 35 °C in 1 mM to 2.0 M OPPh₃ in CH₂Cl₂, 100 mM TBAP in CH₂Cl₂, acetonitrile, benzene, 100 mM *p*-toluene sulfonic acid in acetonitrile, 100 mM hydroquinone in acetonitrile and neat 2-mercaptoethanol.

Rate Measurements of the *cis*-α ⇌ *trans* Equilibrium of [20]⁺ and [8]⁺. An aliquot of the 0.91 mM solution of [8]⁺ (0.2-0.3 mL) was transferred with a cold syringe into the cuvette containing cooled solvent. Data were collected between 300 and 800 nm. Four isobestic points were observed at 369, 422, 442, and 638 nm wavelengths. Because this is a reversible equilibrium reaction, each observed rate constant is actually the sum of the forward (*k*₁) and reverse (*k*₋₁) rate constants. Observed rate constants were calculated from the 344, 544, and 744 nm data and then averaged. The rates had first-order dependence on the concentration of osmium present. Forward and reverse rate constants were separated from the observed rates by combining the data with the equilibrium constants (*K*⁺ = *k*₁/*k*₋₁). Activation parameters were determined for the forward and reverse processes from the separated rates at temperatures of between 0 and 20 °C in CH₂Cl₂. Observed rates were also determined at 0 °C in 1.0 mM to 0.5 M OPPh₃ in CH₂Cl₂, 100 mM TBAP in CH₂Cl₂, acetonitrile, and 100 mM *p*-toluene sulfonic acid in acetonitrile.

Pyridine-d₅ Exchange in 19-*t*Bu → 10-*t*Bu Isomerization. A sample of 1:1 19-*t*Bu and 10-*t*Bu (6 mg, 6 μmol) was added to pyridine-d₅ (1 mL), and the ¹H NMR spectrum was recorded. After heating the tube at 80 °C for 30 min, another ¹H NMR spectrum was recorded that showed a decrease in the trans isomer and a new signal at 1.126 ppm relative to the upfield pyridine-d₅ signal at 7.19 ppm. After continued thermolysis (for a total of 1.75 h at 80 °C), negligible trans 10-*t*Bu was observed in the NMR spectrum, whereas cis-α 19-*t*Bu was still present. The signal at 1.16 had increased and new signals at 8.63 and 7.12 were observed. These were identified to be free *t*-Bupy by adding genuine *t*-Bupy and recording the new spectrum. Analytical TLC of the products (silica gel; 1:1 v/v chlorobenzene/bromoethane eluent) showed cis-α 19-*t*Bu (*R_f* = 0.81), negligible trans 10-*t*Bu (*R_f* = 0.75), a new black compound (*R_f* = 0.58), and the pyridine-exchange product 10-H (*R_f* = 0.50), which was verified by co-spotting the product with authentic 10-H. Thermolysis of pure trans 10-*t*Bu under identical conditions (80 °C, pyridine-d₅ solvent, 1.75 h) also liberated free *t*-Bupy and generated the new uncharacterized compound and 10-H. The new complex may be the mono-substituted product, *trans*-Os(η⁴-CHBA-DCB)(py)(*t*-Bupy). Products from the kinetic run measuring the rate of 19-*t*Bu → 10-*t*Bu isomerization in a 1.0 M pyridine solution in 1,2-dichloroethane (~2400 equiv) at 60 °C were analyzed by TLC. This showed primarily 10-*t*Bu and a faint spot due to the new compound (*R_f* = 0.58).

O = P(*p*-tolyl)₃ Exchange in 8. *trans*-Os(η⁴-CHBA-DCB)(O=PPh₃) (10 mg, 7.7 μmol) was added to the CH₂Cl₂ solution of O=P(*p*-tolyl)₃ (2.6 mL, 100 equiv) and stirred for 3.5 h. All osmium products were precipitated by the addition of methanol and examined by

^1H and ^{31}P NMR spectroscopies. No signals other than those expected for **8** were observed. No methyl protons were detected, and integrations were appropriate for **8**.

O = P(*p*-tolyl) $_3$ Exchange in **20 \rightarrow **8** Isomerization.** A mixture of **20** and **8** (3:1, 21.9 mg, 16.9 μmol) was added to a $\text{O}=\text{P}(\textit{p}\text{-tolyl})_3$ solution (5.7 mL, 100 equiv) and stirred for 3.5 h ($> 10 t_{1/2}$ for the isomerization). The product was precipitated with methanol and passed down a short silica gel plug eluted with CH_2Cl_2 . After recrystallization from $\text{CH}_2\text{Cl}_2/\text{CH}_3\text{OH}$, the product was examined by ^1H and ^{31}P NMR spectroscopies. No evidence for incorporation of $\text{O}=\text{P}(\textit{p}\text{-tolyl})_3$ was observed.

O = P(*p*-tolyl) $_3$ Exchange in $[\textbf{8}]^+ \rightleftharpoons [\textbf{20}]^+$ Equilibrium. A 25 mL round-bottom flask was charged with **8** (26 mg, 20 μmol) and excess nitrosonium hexafluorophosphate and was sealed with a rubber septum. After cooling the flask ($-78\text{ }^\circ\text{C}$), pre-cooled CH_2Cl_2 ($-78\text{ }^\circ\text{C}$, 210 mL) was added and the mixture reacted to form pure $[\textbf{8}]^+$ within 2 h. The solution was transferred into a clean pre-cooled flask to remove the excess NO^+ , and the $\text{O}=\text{P}(\textit{p}\text{-tolyl})_3$ solution was added (6.7 mL, 100 equiv). After warming the solution to room temperature to initiate isomerization, the solution was allowed to set for 2 min and then ferrocene (18 mg, 5 equiv) was added as a CH_2Cl_2 solution to reduce the osmium to a neutral mixture of **8** and **20**. This was allowed to isomerize to **8** (3.5 h) at room temperature. All osmium products were precipitated by the addition of methanol, passed down a short silica gel plug with excess CH_2Cl_2 , and recrystallized from $\text{CH}_2\text{Cl}_2/\text{CH}_3\text{OH}$. The product was examined by ^1H NMR spectroscopy. Minute signals in the aliphatic region were observed; if they had been from bound $\text{O}=\text{P}(\textit{p}\text{-tolyl})_3$, then an upper limit of 3% incorporation would have been established by integration.

Table 5.7. Extinction Coefficients for All Compounds Studied.

Compound	$\lambda(\text{nm})$	$\epsilon(\ell/\text{mol}\cdot\text{cm})$
<i>cis</i> - α -Os(η^4 -CHBA-DCB)(<i>t</i> -Bupy) ₂	468	4.5×10^3
	576	4.5×10^3
	750	5.4×10^2
<i>trans</i> -Os(η^4 -CHBA-DCB)(<i>t</i> -Bupy) ₂	468	2.1×10^3
	576	3.1×10^3
	750	1.7×10^3
<i>cis</i> - α -Os(η^4 -CHBA-DCB)(O = PPh ₃) ₂	462	2.6×10^3
	566	2.0×10^3
	694	7.0×10^2
<i>trans</i> -Os(η^4 -CHBA-DCB)(O = PPh ₃) ₂	462	1.8×10^3
	566	1.5×10^3
	694	1.1×10^3
[<i>cis</i> - α -Os(η^4 -CHBA-DCB)(O = PPh ₃) ₂] ⁺	344	7.6×10^3
	544	7.0×10^3
	744	1.1×10^3
[<i>trans</i> -Os(η^4 -CHBA-DCB)(O = PPh ₃) ₂] ⁺	344	9.0×10^3
	544	4.1×10^3
	744	2.6×10^3

References

1. (a) Serpone, N.; Bickley, D. G. In "Progress in Inorganic Chemistry; Inorganic Reaction Mechanisms", Edwards, J. O., Ed.; Interscience: New York, 1972; Vol. 17, Part II, pp 391-566. (b) *Ibid.*, pp 416-424.
2. Bailar, J. C., Jr. *J. Inorg. Nucl. Chem.* **1958**, *8*, 165-175.
3. (a) Ray, P.; Dutt, N. K. *J. Indian Chem. Soc.* **1943**, *20*, 81-92. (b) Ray, P.; Dutt, N. K. *J. Indian Chem. Soc.* **1941**, *18*, 289-297.
4. (a) "Handbook of Chemistry and Physics"; Weast, R. C., Ed.; CRC Press: Ohio, 1975; pp E55-E56. (b) Gordon, A. J.; Ford, R. A. "The Chemist's Companion"; John Wiley and Sons: New York, 1972; p 5.
5. Stryer, L. "Biochemistry", 2nd ed.; W. H. Freeman: San Francisco, 1981, pp 32-36.
6. (a) Nakaya, T.; Arabori, H.; Imoto, M. *Bull. Chem. Soc. Jpn.* **1970**, *43*, 1888-1889. (b) Wallace, T. J. *J. Org. Chem.* **1966**, *31*, 3071-3074. (c) Cullis, C. F.; Trimm, D. L. *J. Chem. Soc., Faraday Trans. 1* **1968**, *46*, 144-149.
7. Meites, L.; Zuman, P. "Electrochemical Data"; John Wiley and Sons: New York, 1974; Vol. A, Part 1, p 30.
8. (a) Bond, A. M.; Grabaric, B. S.; Grabaric, Z. *Inorg. Chem.* **1978**, *17*, 1013-1019. (b) *Ibid.*, 2153-2157. (c) Bond, A. M.; Colton, R.; McDonald, M. E. *Ibid.*, 2842-2847. (d) Bond, A. M.; Carr, S. W.; Colton, R. *Organometallics* **1984**, *3*, 541-548. (e) Darensbourg, D. *J. Inorg. Chem.* **1979**, *18*, 14-17. (f) Conner, K. A.; Walton, R. A. *Organometallics* **1983**, *2*, 169-171. (g) Datta, S.; Dezube, B.; Kouba, J. K.; Wreford, S. S. *J. Am. Chem. Soc.* **1978**, *100*, 4404-4412.

9. (a) Bond, A. M.; Colton, R.; McCormick, M. J. *Inorg. Chem.* **1977**, *16*, 155-159. (b) Conner, J. A.; Riley, P. I.; Rix, C. J. *J. Chem. Soc., Dalton Trans.* **1977**, 1317-1323. (c) Johnson, B. F. G.; Bhaduri, S.; Connelly, N. G. *J. Organomet. Chem.* **1972**, *40*, C36-C38. (d) Reimann, R. H.; Singleton, E. *Ibid.* **1971** *32*, C44-C46. (e) Robinson, W. R.; Wigley, D. E.; Walton, R. A. *Inorg. Chem.* **1985**, *24*, 918-924.
10. (a) Moore, J. W.; Pearson, R. G. "Kinetics and Mechanism", 3rd ed.; John Wiley and Sons: New York, 1981, p 72. (b) *Ibid.*, p 304.
11. Peters, D. G.; Hayes, J. M. "Chemical Separations and Measurements"; W. B. Saunders: Philadelphia, 1974; pp 6-37.